NUREG/CR-3772
SAND84-0884
R4

Printed November 1984

RELAP5 Assessment: Semiscale Small Break Tests S-UT-1, S-UT-2, S-UT-6, S-UT-7, and S-UT-8

A. C. Peterson

Prepared by
Sandia National Laboratories
Albuquerque, New Mexico 87185 and Livermore, California 94550
for the United States Department of Energy
under Contract DE-AC04-76DP00789

Prepared for
U. S. NUCLEAR REGULATORY COMMISSION

Available from

GPO Sales Program
Division of Technical Information and Document Control
U.S. Nuclear Regulatory Commission
Washington, D.C. 20555

and

National Technical Information Service
Springfield, Virginia 22161

NUREG/CR-3772
SAND84-0884
R-4

RELAP5 ASSESSMENT: SEMISCALE SMALL BREAK TESTS S-UT-1, S-UT-2, S-UT-6, S-UT-7, AND S-UT-8

A. C. Peterson

Date Published: November 1984

Sandia National Laboratories
Albuquerque, NM 87185
Operated by
Sandia Corporation
for the
U. S. Department of Energy

Prepared for
Reactor Systems Research Branch
Division of Accident Evaluation
Office of Nuclear Regulatory Research
U. S. Nuclear Regulatory Commission
Washington, DC 20555
Under Memorandum of Understanding DOE 40-550-75
NRC FIN Nos. A-1205 and A-1374

ABSTRACT

The RELAP5 independent assessment project at Sandia National Laboratories in Albuquerque (SNLA) is part of an overall effort funded by the NRC to evaluate the capability of various system codes to calculate the detailed thermal/hydraulic response of LWRs during accident and off-normal conditions. The RELAP5 computer code is being assessed at SNLA against test data from various integral and separate effects test facilities. As part of the assessment effort, several small break tests with and without upper head injection (UHI) of emergency core coolant (ECC), performed in the Semiscale Mod-2A facility, have been analyzed.

The results show that RELAP5/MOD1 is capable of calculating some aspects of the important phenomena during small breaks both with and without UHI. The times for the system to depressurize to the UHI and/or loop accumulator flow initiation were calculated satisfactorily. The correct trends of the effects of break size and of UHI on the system pressure response were also calculated. The injection rate from the UHI and loop accumulators was not always calculated correctly; the flows cycled on and off because large flow surges caused the accumulator pressures to temporarily decrease below the system pressure. This cycling of the flow had a significant effect on the system response during UHI accumulator flow. When the upper head was liquid-filled from UHI flow, a core liquid level depression was calculated, but not measured, that resulted in a dryout of the core. During UHI flow the calculated densities in the upper plenum and near the top of the core were too high, which also affected the vessel mass distribution. The calculated break flow rates were too large, when the break uncovered later in the transients, contributing to a low liquid level in the vessel and late-time core heatup. Higher late-time core temperatures were calculated than measured both with and without UHI.

Some of the differences between the calculated and measured results can be attributed to uncertainties in the boundary conditions (i.e., break mass flow rate, pump curves, environmental heat losses, bypass flow rate); these uncertainties are large and can significantly affect the results. Since there are also uncertainties in the facility configuration for the S-UT series of tests that are still being addressed, any results for this test series should be considered preliminary until the actual conditions are finally established.

TABLE OF CONTENTS

LIST OF FIGURES

Page

LIST OF TABLES

ACKNOWLEDGEMENTS

I would like to express my appreciation to the following individuals for their efforts in the RELAP5 assessment project: John Orman for modifying and maintaining RELAP5 on the Sandia computer system, Katherine McFadden for graphics support, and Jan Frey for assistance in preparing this report.

1.0 INTRODUCTION

The RELAP5 independent assessment project at Sandia National Laboratories in Albuquerque (SNLA) is part of an overall assessment task funded by the U. S. Nuclear Regulatory Commission (NRC) to determine the capability of various advanced system computer codes to calculate the detailed thermal/hydraulic response of LWRs during accident and off-normal conditions. The RELAP5 computer code [1] is based on a nonhomogeneous and nonequilibrium one-dimensional model for two-phase systems, and has been under development at the Idaho National Engineering Laboratory (INEL) for an extended period, with the first version released in May 1979. The version first used for this assessment project was RELAP5/MOD1/CYCLE14, the latest publicly released version available at the time the project was started. In June 1982, we received the formally-released updates creating cycle 18 together with some unreleased, but recommended, updates then being used at INEL. These changes have been used to create and run a MOD1 version at Sandia we call cycle 18+, which was used as the assessment code for these analyses.

The RELAP5 computer code is being assessed at SNLA against test data from various integral and separate effects test facilities. The assessment test matrix includes five tests from the S-UT series of small break loss-of-coolant experiments [2-10] performed in the Semiscale Mod-2A facility [11,12] at the INEL. These experiments investigated the effects of upper head injection (UHI) of emergency core coolant (ECC) on the system thermal/hydraulic response for 10%, 5%, and 2.5% cold leg breaks. Baseline tests at each break size were performed without UHI, and the tests were then repeated from the same nominal initial conditions with UHI. An additional test was performed in this series that investigated the system response with reduced core bypass flow and modified upper plenum/upper head geometry.

This report describes the results of RELAP5 analyses of 10% cold leg break tests S-UT-1 and S-UT-2 and 5% cold leg break tests S-UT-6, S-UT-7, and S-UT-8. The RELAP5 models used for the analyses are described in Section 2. The individual transient results are presented in Section 3, and the calculations of relative effects and selected sensitivity studies are discussed in Section 4. The overall conclusions and their possible relevance to future RELAP5 computer code development and application are discussed in Section 5. Appendix I provides a brief description of the test facility. The RELAP5 input for each test is contained in Appendix II. RELAP5 calculations using detailed and coarse node steam generators are documented in Appendix III. The additional INEL updates used to create cycle 18+ from cycle 18 of RELAP5/MOD1 are listed in Appendix IV.

2.0 RELAP5 MODELS

The RELAP5 models used for the Semiscale Mod-2A S-UT series of small break calculations are described in this section. The nodalizations used are discussed and a comparison of the calculated and measured steady state conditions used for the initiation of the transient calculations is presented.

2.1 Nodalizations

The Semiscale Mod-2A test facility [11,12] was located at the Idaho National Engineering Laboratory and supported by the NRC. This scaled integral test facility, shown in Figure 2.1.1, was used to investigate thermal and hydraulic phenomena which occur during hypothesized loss-of-coolant accidents and operational transients in a PWR system. The system was scaled to have a core power and system fluid volume 1/1705th of a four-loop PWR, and consisted of two primary coolant loops connected to an electrically-heated core in a pressure vessel which had an external downcomer. Each coolant loop contained an active pump and steam generator. The intact loop had three times the fluid volume and loop mass flow of the broken loop and represented 3 operational loops in a typical 4-loop PWR. The flow paths into and out of the upper head in a full-scale PWR with UHI were simulated in the Mod-2A facility for these tests. Three such flow paths existed: the bypass from the downcomer, the control-rod guide tubes, and the support columns. (A brief description of the Semiscale Mod-2A facility in the S-UT configuration is given in Appendix I.)

The RELAP5 models used in these analyses were obtained from a nodalization developed for the RELAP5 Semiscale Mod-2A S-NC analyses performed previously at SNLA. [13,14] Subsequent to the completion of the S-NC analyses, the steam generator volumes were changed because an error was found by the INEL in the information they had initially provided describing their Mod-2A RELAP5 model [12]. New data provided by the Semiscale Program [15] indicated that the original steam generator volumes were too small by about 15%.

The same basic model was used for each of the tests, except that the UHI system was not used for tests S-UT-1 and S-UT-6 and the broken loop ECC system was not used in tests S-UT-1 and S-UT-2. The basic system nodalization is shown in Figure 2.1.2, on which the various junctions, components, and volumes are identified. This model consists of 210 volumes, 215 junctions and 276 heat structures.

Except for the UHI accumulator line in the upper head, the details of the vessel and external downcomer nodalization are

shown in Figure 2.1.3. The relative elevations of the volume boundaries are shown (for comparison with the facility elevations given in Appendix I). In addition, either the flow area for open piping or the volume for more complex geometry is shown.

The nodalization of the vessel for test S-UT-8 was different from that for the other tests. This difference reflected geometry changes made between the tests. Figure 2.1.4 shows the geometry of the upper plenum and upper head for test S-UT-8 [15]. A valve was installed in the bypass line to adjust the bypass flow, and the elevation of the bypass line discharge into the upper head was decreased from the earlier tests. Six flow holes were drilled into the guide tube just below the upper support plate. The two support columns were to be blocked off; however, instrumentation was removed from the support columns that resulted in a flow path remaining through them from the upper head to the top of the core. The vessel nodalization used for test S-UT-8 included these known changes. The most significant differences were the reduction in the core bypass flow and the flow junction from the guide tube to the top of the upper plenum, modeling the new flow holes in the guide tube. This junction caused the steady state flow in the support columns to be from the upper core to the upper head for this test, whereas the support column flow was from the upper head to the upper core in the other tests.

The details of the intact and broken loop steam generator nodalizations are shown in Figures 2.1.5 and 2.1.6, respectively. The relative elevations of the volumes and either the flow areas or the total fluid volumes are shown. The volume elevations were selected to correspond to the elevations of the baffle plates in the steam generator secondaries. The tubes in each steam generator (6 in the intact loop and 2 in the broken loop) were modeled as a single flow path.

All area changes and elbows in the piping were accounted for in the model. Figure 2.1.7 shows the loss coefficients used in the calculations. These coefficients were either user input, to account for elbow losses, or calculated by RELAP5 using the built-in abrupt area change model. The user input forward and reverse losses are given first; if these losses are different, two values are shown. The losses calculated by RELAP5 are shown in parentheses. These are single-phase losses in the normal direction of flow and may change in two-phase flow. If two values are given, they correspond to different losses for liquid and vapor under two-phase conditions.

For test S-UT-8, a user input loss coefficient of 0.8 was used at the baffle plates in the intact loop steam generator and a loss coefficient of 0.4 was used at the broken loop baffle

plates. These loss coefficients were input, rather than calculated using the abrupt area change model, so they could be combined to have the same total resistance for a steam generator nodalization study. The total surge line resistance was also increased by a factor of 10 for test S-UT-8 based on data in an INEL report [16]. The choking, inertial, and two-velocity models were used at all junctions, and wall friction and thermal nonequilibrium models were used in each volume.

The heat structures of all the major components of the vessel were modeled. These include: pressure vessel, downcomer, support columns, guide tube and bypass line. The core heater rods were also part of the vessel heat structures. The exterior insulation was not explicitly modeled; the residual environmental heat losses from the pressure vessel and downcomer were modeled for tests S-UT-1 and S-UT-2 using a heat transfer coefficient of 15.0 kW/m^2-K on the outside boundary. This value of the heat transfer coefficient was based on data provided by the Semiscale Program [12]. The residual vessel environmental heat losses were not modeled for tests S-UT-6, S-UT-7, and S-UT-8 because band heaters were used to offset environmental heat losses, and we therefore assumed the system was adiabatic.

Heat structures modeling the loop piping were also used in all the calculations. For tests S-UT-1 and S-UT-2 the pipe insulation was not modeled, but residual environmental heat losses were modeled using a heat transfer coefficient of 15.0 kW/m^2-K on the outside boundary of the heat structures, also based on data from the Semiscale Program [12]. For tests S-UT-6, S-UT-7, and S-UT-8, the piping environmental heat losses were not modeled because band heaters were used during the tests to reduce environmental heat losses. For these tests the loop piping walls were assumed to be adiabatic.

The steam generator heat structures represented the U-tubes, shroud, filler pieces, and external walls. Secondary side environmental heat losses from the external walls were modeled for all the calculations since the steam generators did not have band heaters. A heat transfer coefficient of 2.8 kW/m^2-K was applied at the outside boundary of the heat structures. This value of the heat transfer coefficient was based on data reported by the Semiscale Program [12].

The single-phase homologous head and torque curves for the intact and broken loop pumps were based on data supplied by the Semiscale Program [11]. The single-phase data for the broken loop pump were obtained with an orifice installed in the pump discharge instead of the venturi used in most tests in this series. Tests S-UT-1 and S-UT-2 were performed with an orifice in the broken loop pump discharge, whereas tests S-UT-6, S-UT-7,

and S-UT-8 were conducted with a venturi in the broken loop pump discharge. The broken loop pump data are not accurate for tests with the venturi installed, but are the only data available. The intact loop two-phase head and torque multiplier and difference curves were also supplied by the INEL. Since there were no two-phase data for the broken loop pump, the intact loop two-phase curves were used for the broken loop pump as is usually recommended by the INEL.

The cold leg break was modeled with a trip valve connected to a time-dependent volume simulating the pressure boundary condition downstream of the break. The area of the valve depended on the size of the break. The total break areas for the 10% and 5% breaks were 0.233 cm^2 and 0.1123 cm^2, respectively. Subcooled and saturated discharge coefficients were used at the break junction. For the 10% break tests, subcooled and saturated discharge coefficients of 0.85 were used. Limited sensitivity studies (discussed in Section 4.4) indicated they gave the best agreement with the system pressure response. A subcooled coefficient of 0.90 and a saturated coefficient of 0.85 were used for the 5% break calculations; the choice of these coefficients was based on results from INEL calculations [17].

The high pressure injection system (HPIS) was modeled by a time-dependent volume and time-dependent junction connected to the intact loop cold leg. The broken loop HPI system failed in these tests and there was no broken loop HPI flow [5,7].

The loop accumulators were pressurized with nitrogen to about 2.8 MPa and the UHI accumulator to about 8.7 MPa. UHI was terminated in both the relevant tests and the analyses when the specified amounts of coolant were injected into the upper head. For test S-UT-2, check valves were modeled in the UHI surge lines to eliminate calculated unrealistic circulation in the surge line before the initiation of the transient. This recirculation did not appear to significantly affect the overall results; therefore, check valves were not used in the subsequent calculations for test S-UT-7.

Complete input listings for each of the five transient calculations are given in Appendix II.

2.2 Steady State Calculations

Since the initial conditions of each test pair were nominally identical, the same calculated steady state was used for the initiation of corresponding transients with and without UHI. This resulted in some compromise in the initial conditions, particularly in the initial mass in the steam generators. We thought that this difference would not be significant to the overall results and would save some manpower and computer time.

For the steady state calculations, the system pressure and the core power were set at the measured values. The primary pressure was maintained by a time-dependent volume at the top of the pressurizer. The intact loop pump speed was controlled to maintain a specified temperature difference across the core, while the broken loop pump speed was controlled to maintain a specified flow split between the intact and broken loops. The areas of the steam outlet valves were controlled to maintain specified loop cold leg temperatures. Based on the integrated difference between the specified and calculated cold leg temperatures in each loop, the steam outlet valve was opened, if the cold leg temperature was too low, and closed, if the temperature was too high.

The calculated and measured steady state conditions at the initiation of each transient are compared in Table 2.1. The primary pressure, temperatures, and flows were specified by input and maintained by a control system resulting in good agreement between the calculated and measured primary conditions at the initiation of the transients. The forced agreement in the primary side conditions did not result in equally good agreement in the steam generator secondary pressures. In fact, for tests S-UT-1 and S-UT-2, we specified the primary intact loop temperatures at the high side of the measurement uncertainty to improve the agreement with the steam generator secondary pressures.

Assessment calculations for the Semiscale Mod-3 and LOFT facilities had similar problems in matching the primary and secondary conditions simultaneously [18,19,20,21]. Those calculations indicated that using the minimum steam generator tube-to-tube spacing for the characteristic heated equivalent diameter on the secondary side resulted in better agreement for both the primary and secondary conditions.

For these Semiscale Mod-2A calculations, we also intended to use the minimum steam generator tube-to-tube spacing for the heated equivalent diameter. At the completion of these calculations, however, we found that a spacing of 0.00665 m was erroneously used rather than the actual minimum spacing of 0.00955 m. (The spacing used corresponded to the spacing for the Semiscale Type I steam generator used in the Semiscale Mod-3 calculations.) We do not think that this discrepancy significantly affects the results, since the characteristic diameter only appears to a fractional power in the heat transfer correlations.

The largest difference between measured and calculated initial conditions was in the broken loop pump speed. For tests S-UT-1 and S-UT-2, the calculated initial broken loop pump speed was about 10% less than the measured speed; the measured speed for these tests was about 8% above the maximum rated speed. Checking with the INEL, they stated that an orifice was

installed in these tests rather than the venturi nozzle specified in the Experiment Operating Specification (EOS). [2] Since the single-phase curves used for the broken loop pump were developed from data with an orifice installed, we expected good single-phase agreement to be obtained. The source of this difference is not known, but possibly the orifice in the tests was not the same as was used in the calibration. The broken loop pump speed for tests S-UT-6, S-UT-7, and S-UT-8 was about 20% higher than was measured. This difference came from using single-phase curves developed with an orifice in the pump discharge for conditions with a venturi installed.

Another significant difference between calculated and measured initial conditions was the guide tube flow in tests S-UT-6 and S-UT-8. We consider the measured guide tube flow in test S-UT-6 to be in error since the sum of the support column and guide tube flows should equal the bypass flow. (These flows did add to the bypass flow in test S-UT-7, which was run at the same nominal conditions as test S-UT-6.) There are no measurements of the bypass or support column flow for test S-UT-8; however, the Semiscale Program reported in an analysis report that the bypass flow was about 1.5% of the total loop flow. [16] Therefore, we used a bypass flow of about 1.5% (0.22 %/s) in the calculation. Since the flow in the support columns for test S-UT-8 was into the upper head, the bypass flow and the support column flow into the upper head should sum to the guide tube flow out of the upper head. The measured initial guide tube flow was considerably less than the specified bypass flow. The measurement of the guide tube flow indicated the flow reversed at the initiation of the transient, which was not consistent with the flow indicated by the pressure drop measurements in the guide tube. Based on these inconsistencies, we consider the guide tube flow for test S-UT-8 also to be in error.

Table 2.1 Initial Conditions for S-UT Tests

Parameter	S-UT-1	S-UT-2	RELAP	S-UT-6	S-UT-7	RELAP	S-UT-8	RELAP
Core Power (MW)	1.90	1.91	1.91	1.99	1.99	1.99	1.95	1.95
System Pressure (MPa)	15.5	15.5	15.5	15.8	15.6	15.8	15.6	15.5
Intact Loop Cold Leg Temperature (K)	557.9	557.8	559.0	557.0	558.0	557.2	559.5	559.5
Intact Loop ΔT (K)	32.7	32.9	33.0	41.0	41.0	41.0	35.1	35.2
Intact Loop Flow (ℓ/s)	10.7	10.5	11.0	9.4	9.4	8.7	10.3	10.0
Intact Loop Steam Generator Pressure (MPa)	6.03	5.74	5.82	5.70	5.70	5.58	5.71	5.75
Intact Loop Pump Speed (rad/s)	229.9	225.4	227.0	199.0	198.0	196.0	244.0	226.9
Broken Loop Cold Leg Temperature (K)	557.9	557.8	558.0	557.0	559.0	557.0	561.4	561.4
Broken Loop ΔT (K)	31.3	31.8	34.0	40.0	39.0	41.1	33.8	33.3
Broken Loop Flow (ℓ/s)	3.5	3.8	3.4	2.8	2.8	2.6	3.3	3.3
Broken Loop Steam Generator Pressure (MPa)	5.56	5.78	5.69	5.90	5.98	5.71	6.11	6.00
Broken Loop Pump Speed (rad/s)	1725	1714	1541	975	974	1200	1192	1491
Bypass Flow (ℓ/s)	0.43	0.43	0.43	0.37	0.33	0.36	NM*	0.22
Support Column Flow (ℓ/s)	0.10	0.10	0.10	0.09	0.09	0.09	NM*	0.12
Guide Tube Flow (ℓ/s)	0.31	0.31	0.31	0.03	0.26	0.27	0.09	0.34

*Not Measured

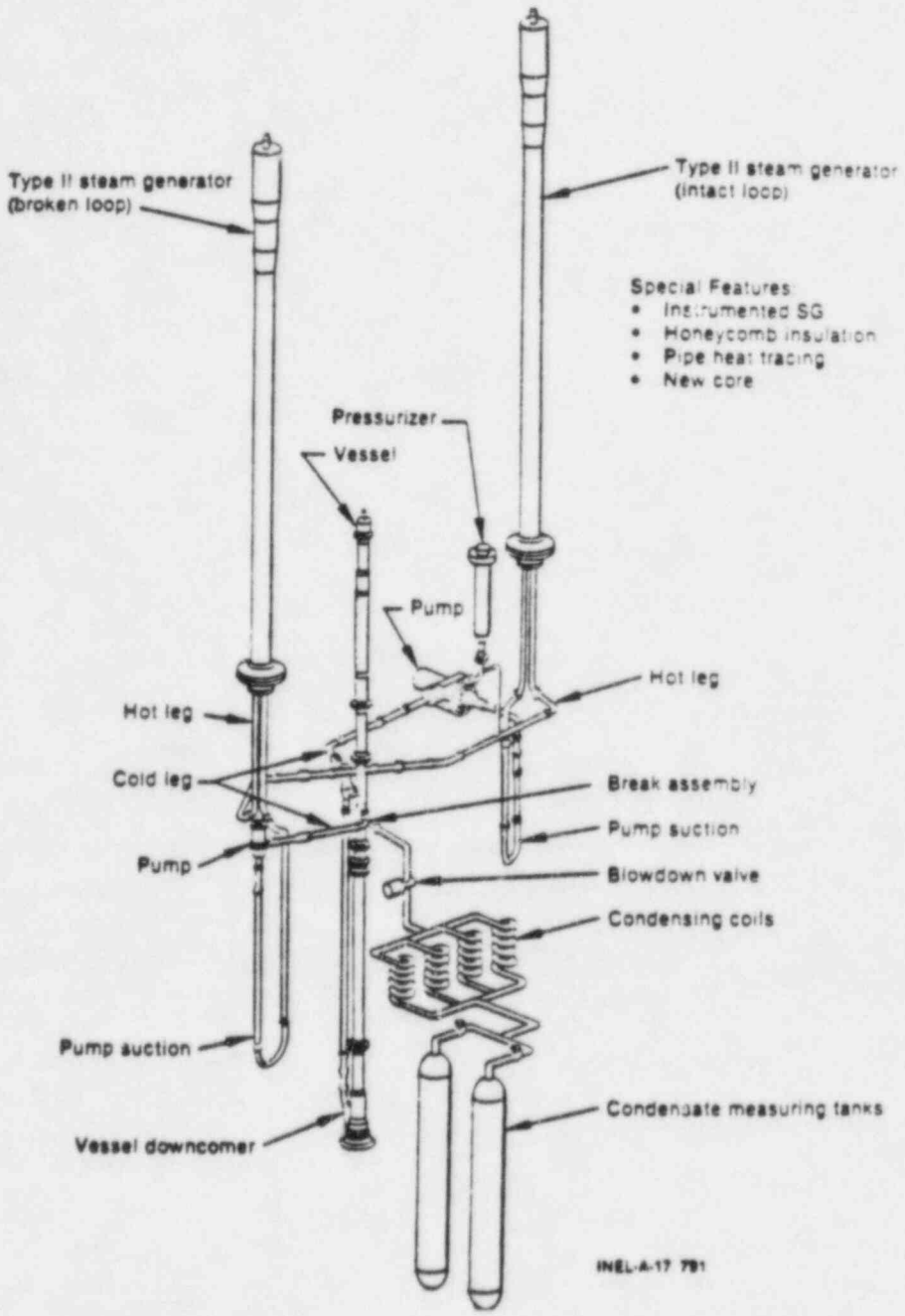

Figure 2.1.1 Isometric View of the Semiscale Mod-2A Facility

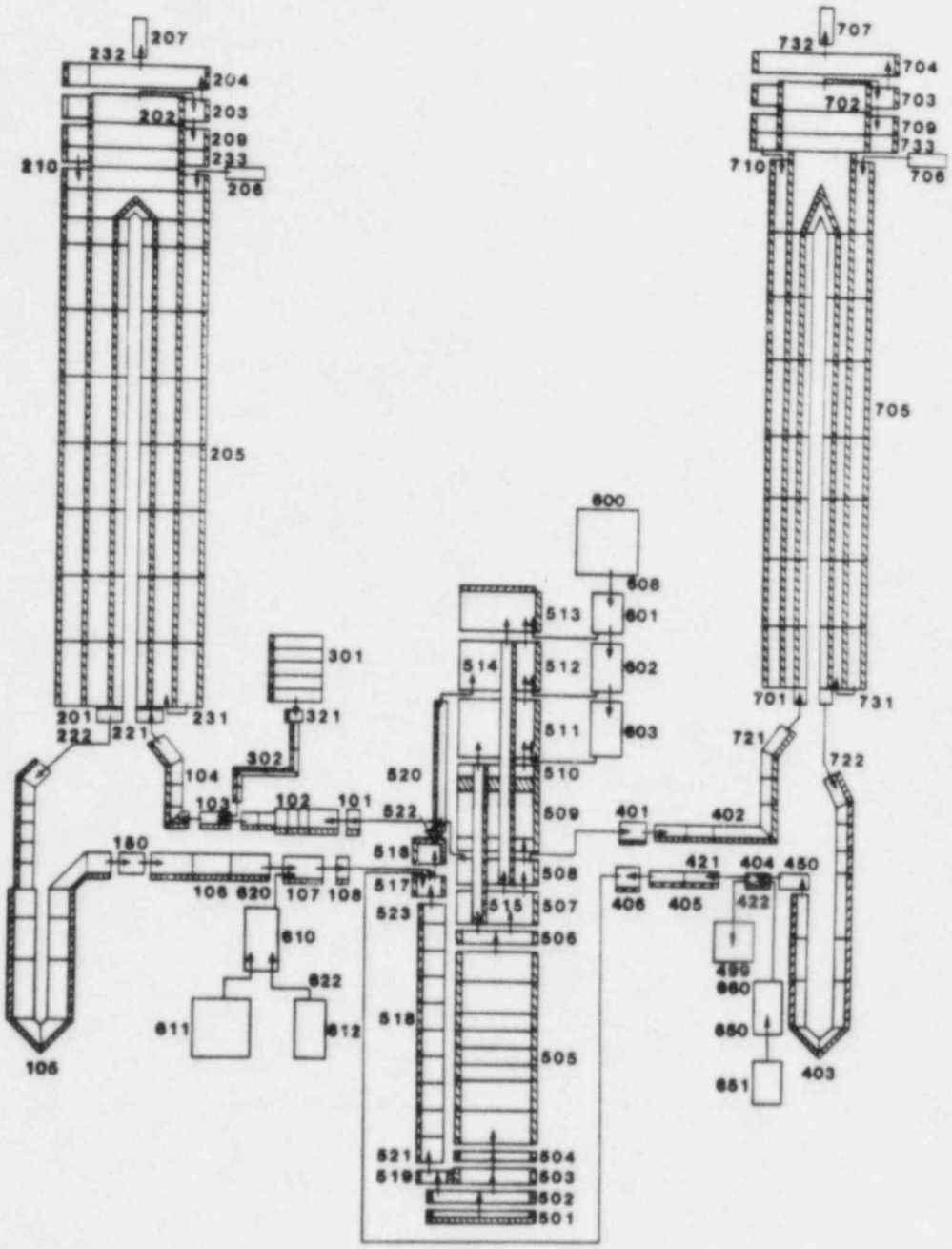

Figure 2.1.2 RELAP5 System Nodalization for Semiscale Mod-2A S-UT Transients

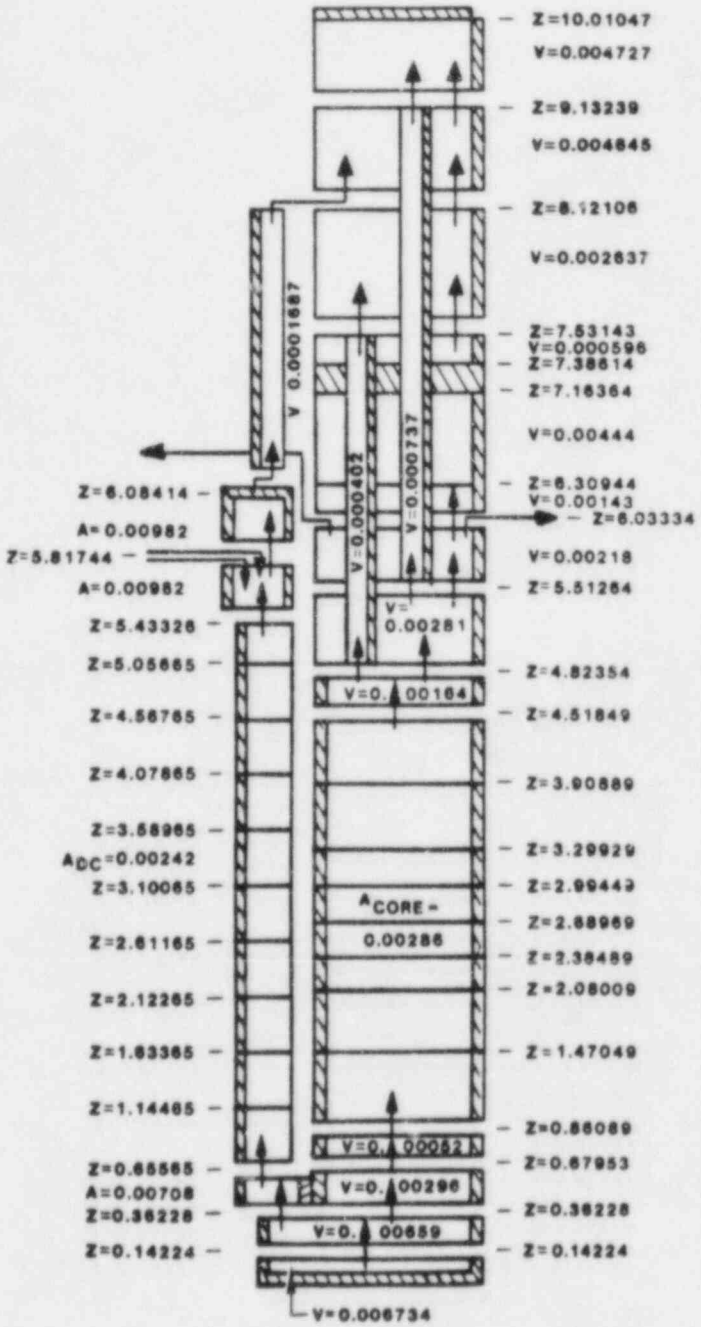

Figure 2.1.3 RELAP5 Vessel Nodalization

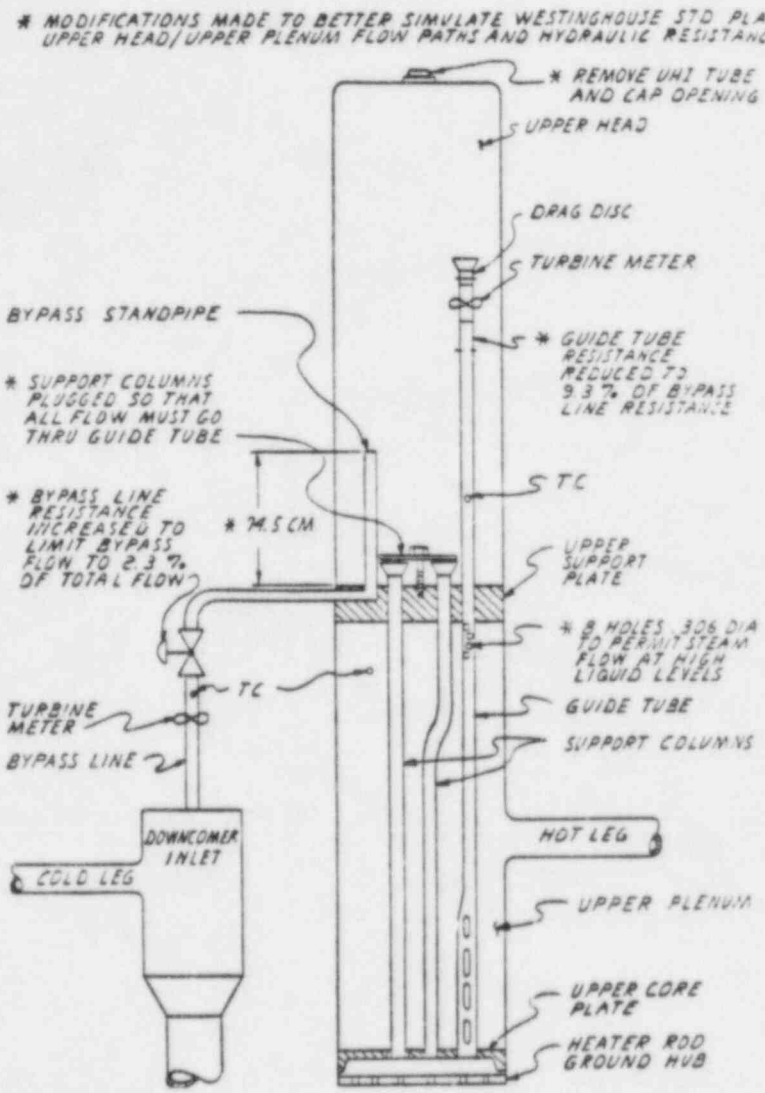

Figure 2.1.4 Upper Head and Upper Plenum Geometry for Test S-UT-8

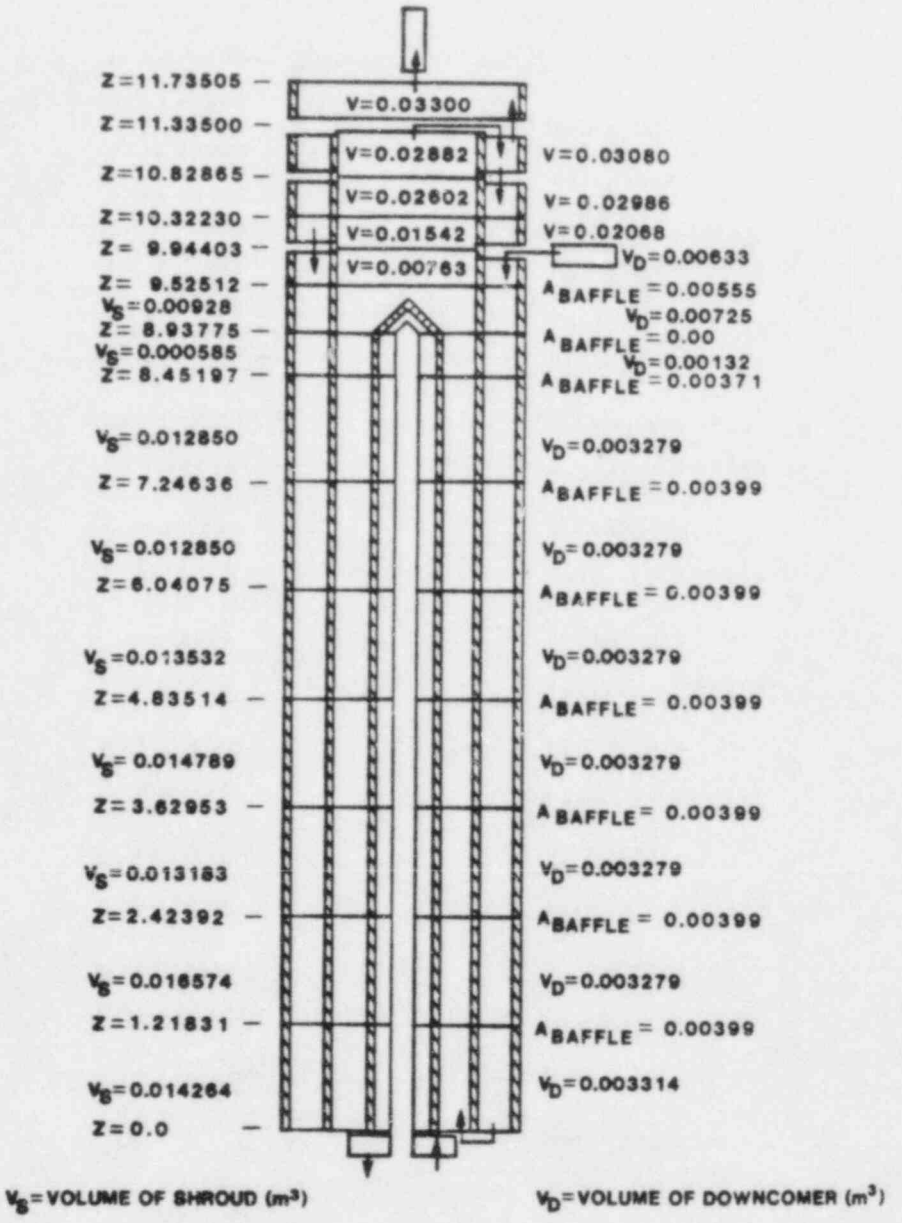

Figure 2.1.5 RELAP5 Intact Loop Steam Generator Nodalization

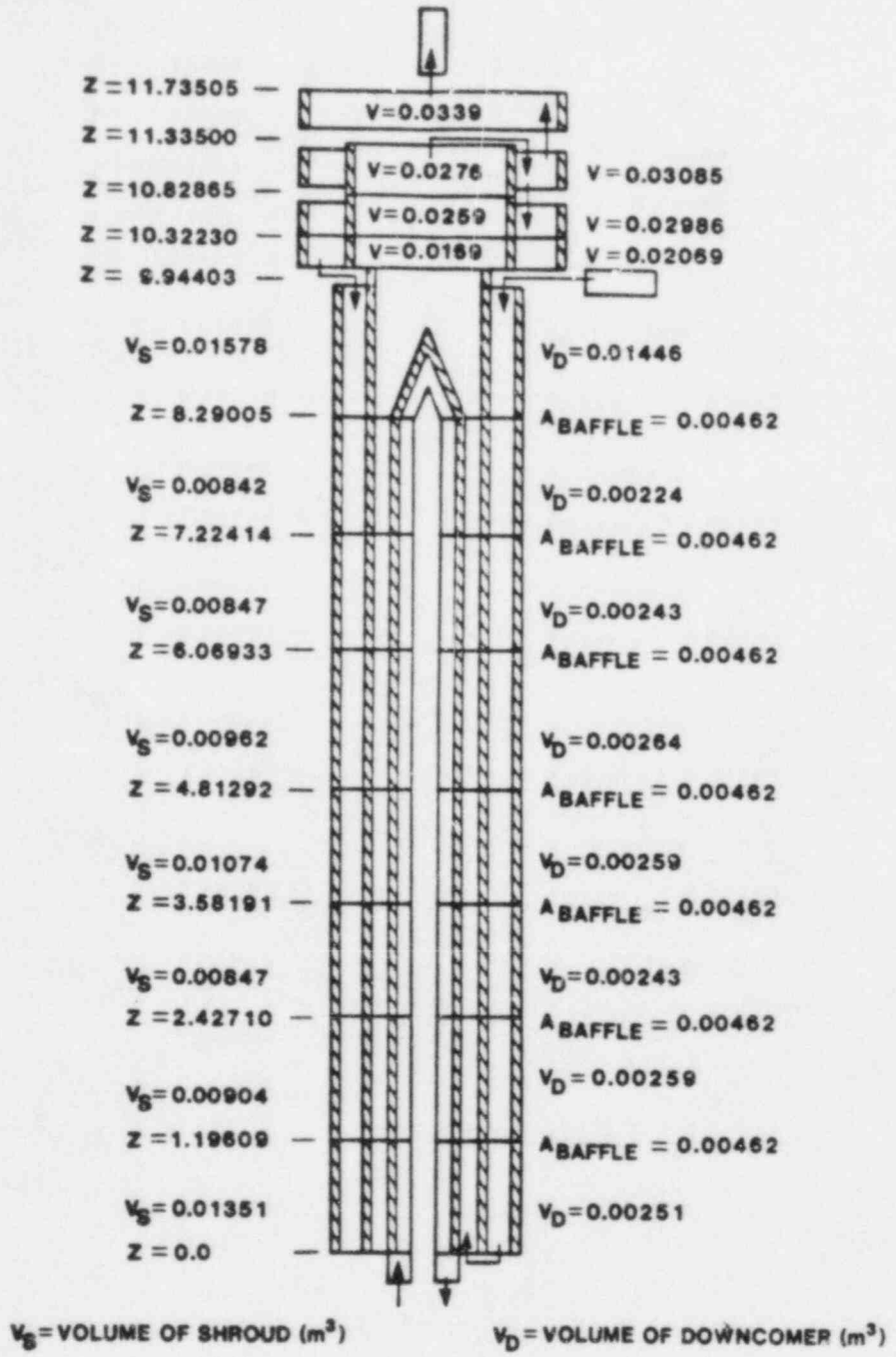

Figure 2.1.6 RELAP5 Broken Loop Steam Generator Nodalization

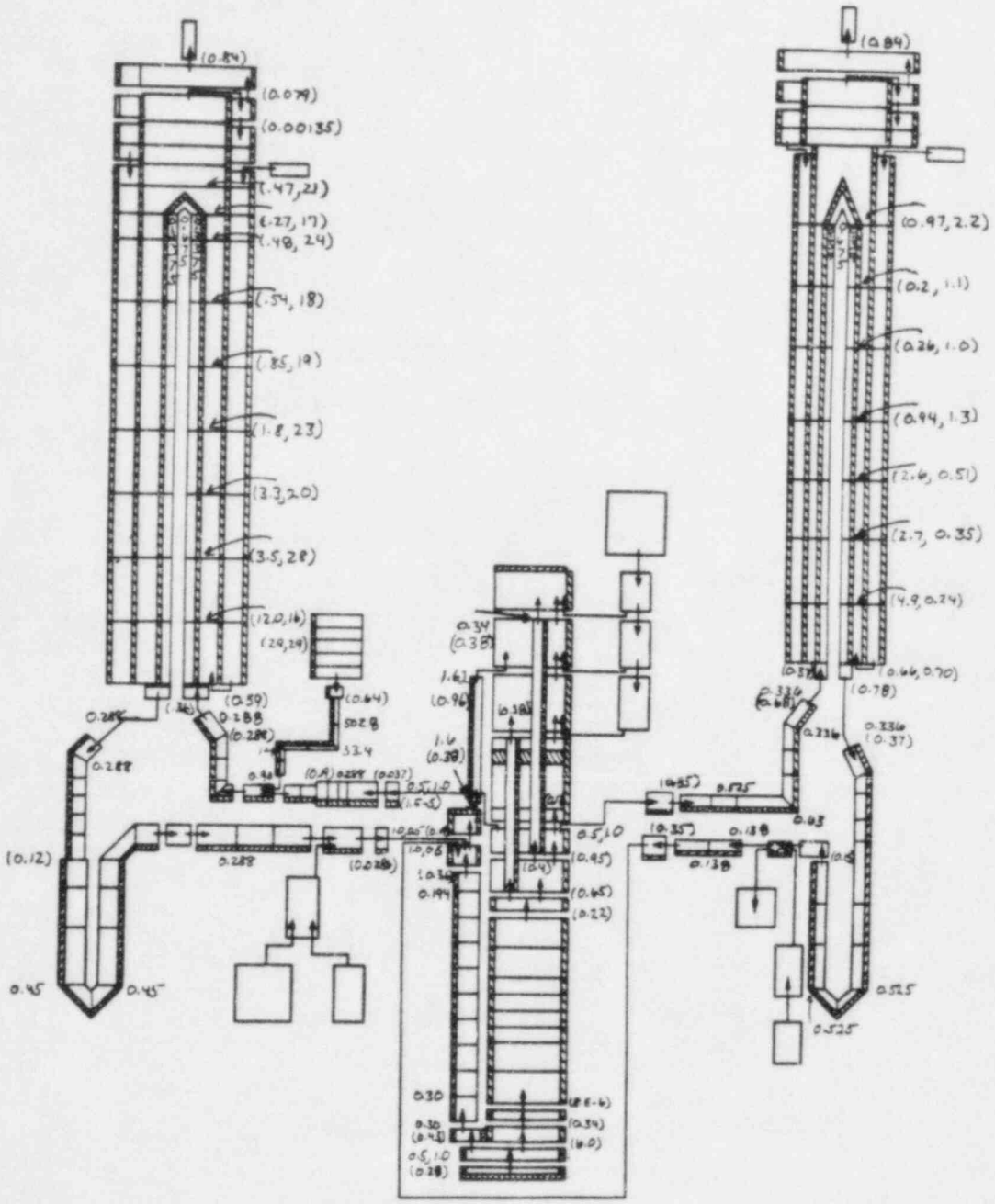

Figure 2.1.7 Loss Coefficients Used in Semiscale Mod-2A Model

3.0 RESULTS

This section compares results from the individual transient calculations with experimental data, and discusses the capability of the RELAP5/MOD1 computer code to calculate the phenomena occurring during small cold leg breaks with and without UHI. Sections 3.1 and 3.2 present the results for 10% cold leg breaks without UHI (test S-UT-1) and with UHI (test S-UT-2), respectively. Sections 3.3 and 3.4 present the results for 5% cold leg breaks without UHI (test S-UT-6) and with UHI (test S-UT-7), respectively. The results for a 5% cold leg break without UHI and with upper head geometry changes that reduced the core bypass flow (test S-UT-8) are presented in Section 3.5.

3.1 Test S-UT-1 (10% Cold Leg Break Without UHI)

Test S-UT-1 was a 10% cold leg break with ECC injection into the intact loop cold leg. The pumps and core power were tripped on low pressurizer pressure (12.4 MPa). The steam generator steam line and feed water valves were also tripped on low pressurizer pressure. Steam generator auxiliary feed water was not used in this test.

The data from test S-UT-1 showed that, after initiation of the break, the system depressurized continuously until the initiation of accumulator flow. The system primarily voided due to flow out the break, and gravity-fed draining of liquid from the higher to the lower elevations in the facility resulted in liquid seals forming in the pump suctions of both loops. These pump suction loop seals blocked the flow of steam through the loops and caused a depression of the liquid level in the core down to the lowest elevation of the pump suctions, resulting in a heatup of the core rods. The eventual clearing of the intact loop pump suction downflow leg, which allowed steam to flow up the upflow leg, resulted in a rapid increase in the vessel liquid level and a rewet of the core. The clearing of the pump suction also provided a path for the steam from the loops to flow directly to the break and thus increased the rate of depressurization. Later in the transient, vessel liquid slowly boiled off and the core liquid level again decreased until the system depressurized to the intact loop accumulator set point and accumulator flow was initiated, which recovered the system. Condensation effects due to the cold accumulator fluid apparently caused oscillations in the system pressure and accumulator flow, which resulted in manometric flow oscillations between the core and downcomer. However, the oscillations in the core liquid level did not adversely affect the cooling of the core.

To provide an initial overall comparison of the calculated and measured results, the chronologies of significant events for test S-UT-1 are summarized in Table 3.1.1. A more rapid initial depressurization was calculated than was measured, resulting in an early trip of the core power and pumps and an early emptying of the pressurizer in the calculation. The first rod dryout in the core, caused by the core level depression, was at 52 s in the test and at 80 s in the calculation. The clearing of the downflow leg in the intact loop pump suction was 46 s earlier in the test than in the calculation, resulting in the core liquid level recovering earlier in the test. The entire core was rewet at 160 s in the test, whereas the rod temperatures were still increasing, due to a low core liquid level, when the calculation was stopped at 590 s.

The transient calculation was terminated at 590 s because there were substantial differences between the calculated and measured results and continuing the calculation would not provide additional assessment of RELAP5's capabilities.

The calculated and measured primary system pressures are shown in Figure 3.1.1. The system rapidly depressurized during the initial 20 s and then, as a result of voids forming in the primary system and a decrease in cooling from the steam generators, the rate of depressurization decreased. The calculated primary pressure was higher than the measured pressure from 20 to 290 s. Two factors contributed to this difference. One was that the initial hot and cold leg temperatures in the calculation were on the high side of the measured temperature uncertainties, which resulted in higher saturation pressures. The second was that the calculated steam generator pressures were higher than measured after 20 s, as shown in Figure 3.1.2. Since the pressures were high, the steam generator secondary temperatures were also high which reduced the primary-to-secondary energy transfer early in the transient, contributing to a slower depressurization. The rate of depressurization of the primary system increased after 250 s in the calculation because the liquid level in the core was very low and the steam generation rate decreased as the core power began to heat up the rods rather than generate steam.

As the system depressurized, voids formed in the hot legs and the core. The calculated and measured densities in the intact loop hot leg are compared in Figure 3.1.3. The decrease in both densities shortly after the initiation of the transient indicates early voiding in the hot legs. After 25 s the measured density was slightly higher than the calculated density, indicating more voiding of the hot leg in the calculation than in the test. The calculated density shows that the hot leg was essentially voided after 300 s, whereas the measured density indicates the presence of some liquid for the entire transient.

Voiding of both the upflow and downflow legs of the primary side of the steam generator tubes also occurred early in both the test and the calculation. Because of the effects of flow on the differential pressure used to calculate the collapsed height of liquid in the tubes in the test, the early voiding cannot be determined accurately. However, it appeared that in the test both the upflow and downflow sides of the tubes were about 50% voided by 30 s and were essentially drained by 60 s. In the calculation the upflow side drained at about 95 s, which was 30 s later than the downflow side. Counter-current flow of steam into the steam generator and liquid (apparently from condensation and hold-up) out of the steam generator delayed the final draining of the upflow side of the steam generator tubes. The drain time of the primary side of the intact loop steam generator tubes affected the calculated collapsed liquid level in the vessel.

The calculated and measured vessel collapsed liquid levels (excluding the upper head) are shown in Figure 3.1.4. The collapsed liquid level dropped below the top of the core at 31 s in the calculation and 38 s in the test. The level continued to decrease in the test to about 1.15 m above the core inlet, the elevation of the bottom of the loop seals, and then increased when the intact loop pump suction cleared and fluid from the intact loop cold leg entered the downcomer and vessel. The level in the calculation decreased to below the core inlet. The large depression of the core level in the calculation was caused by the liquid retained in the upflow side of the steam generator tubes after the downflow side had drained. The hydraulic head created by this liquid exerted an additional pressure on the core liquid, and depressed the level to the lower downcomer distribution annulus. The calculated core inlet flow was negative from 60 to 140 s with vapor flowing up the downcomer. The calculated vessel collapsed level increased and the core was recovered shortly after the intact loop pump suction cleared.

The vessel collapsed liquid level decreased in both the calculation and the test between 160 and 350 s from boiloff of the liquid in the core. The decrease in level was much faster in the calculation than was measured, and the calculated level decreased to below the bottom of the core. The rapid decrease in level in the calculation may indicate potential problems with the interfacial drag model entraining too much liquid.

The initiation of intact loop accumulator flow at 333 s in the test caused an increase in the measured vessel liquid level, as seen in Figure 3.1.4. The initiation of accumulator injection at 327 s in the calculation did not result in a significant increase in the vessel level. The calculated and measured loop accumulator mass flow rates are compared in Figure 3.1.5. Both

the calculated and measured flows cycled on and off. Even though the correct magnitude of the peak flow was usually calculated, the measured period of cycling was shorter than in the calculation, resulting in more ECC being injected and more mass in the vessel at late times in the test. (The negative flow spike, which only persists for one time step, is an artifact of the RELAP5 built-in accumulator check valve logic.)

A cyclic coupling of the accumulator flow to changes in the vapor generation in the core and subsequent changes in the system pressure occurred in the test. Since the calculated collapsed level was below the core inlet when accumulator flow was initiated, a similar coupling did not occur in the calculation. Instead, the cycling of the accumulator flow in the calculation was caused by a surge of liquid out of the accumulator lowering the pressure in the accumulator to below the system pressure, which caused the flow to stop. The system continued to depressurize and, when the accumulator pressure was higher than the system pressure, the flow was initiated again. Such cycling of the accumulator flow also occurred in other assessment calculations, especially for small and intermediate breaks in the LOFT facility [20,21].

The upper head hydraulics did not appear to be significant factors in the vessel hydraulic response for this test. After the initiation of the transient, the flows through the bypass line into the upper head and through the support columns and guide tube out of the upper head continued until about 25 s. At 25 s, the flow in the guide tube reversed in both the calculation and the test, as shown in 3.1.6. (Negative flow in Figure 3.1.6 indicates flow from the upper head into the upper plenum, the flow direction at the start of the transient.) The flow in the bypass line also changed from into the upper head to into the downcomer at about 25 s in both the test and the calculation. The reversal in the guide tube flow in the calculation caused a high quality two-phase mixture to flow into the upper head and the drain of the upper head started soon after. Even though the guide tube density was not measured, we expect a similar change in the guide tube flow to have occurred in the test. There was good agreement in the flow rates until the flow was into the upper head, after which the measured flow rate was significantly higher than the calculated flow rate until 95 s, when both flows were nearly stagnant. The measured flow rate into the upper head may be high after 25 s because the mass flow rate was based on the velocity in the guide tube and the fluid density at the 1.74 m upper head elevation, the top of the guide tube. After the flow reversed and was into the upper head, this density was probably not a good estimate of the density in the guide tube.

The calculated and measured upper head collapsed liquid levels are shown in Figure 3.1.7 and illustrate that the drain of the upper head began at about the same time in both the test and the calculation. After the level dropped below the top of the bypass line, at the 0.89 m elevation in Figure 3.1.7, the flow through the bypass line to the downcomer was mostly high quality steam in the calculation. Even though the bypass line density measurement failed in the test, high-quality steam flow would be expected to have occurred in the test when the bypass line uncovered. The rate of drain of the upper head appeared to increase in the calculation following the uncovery of the top of the bypass line, whereas the rate then decreased in the test. This difference may be a result of combining the two support columns in the RELAP5 model.

Most of the draining of the upper head was through the support columns into the core, due to their larger flow area, lower resistance, and lower elevation. The calculated and measured flows in the support columns are compared in Figure 3.1.8. There are two measurements shown since each of the two support columns in the facility was individually instrumented; these two columns were modeled as a single flow path in the calculation, so the calculated flow should be the sum of the measurements. (Indicated negative flow was from the upper head to the top of the core, which was the direction of flow at the initiation of the transient.) The direction of the measured flows differed at 25 s when the flow in one column was into the upper head and in the other column was out of the upper head. When the top of the bypass line uncovered at 55 s, the calculated flow rate increased significantly; however, a similar increase did not occur in the measurements. In general, the combined measured flow was less than the calculated flow, which contributed to an earlier emptying of the upper head in the calculation than in the test.

As previously mentioned, the upper head behavior did not have a significant effect of the overall vessel response in this non-UHI test. The early voiding in the core is shown in Figure 3.1.9, which compares the calculated and measured densities at the 2.53 m core elevation. Shortly after the initiation of the transient, both the calculated and measured densities decreased. After a brief recovery, both densities dropped at 50 s as substantial voiding occurred at this elevation. The measured density indicated this elevation was essentially steam filled, whereas the calculated density indicated some liquid was still present around 100 s. Both densities increased when the intact loop pump suction leg cleared. The calculated density was higher than measured earlier in the transient, and then lower than measured later in the transient, when the rod heatups were calculated.

The calculated and measured densities at the 1.13 m core elevation and at the core inlet are shown in Figures 3.1.10 and 3.1.11, respectively. As shown in Figure 3.1.10, initial voiding at the 1.13 m core elevation occurred at about 30 s in both the test and the calculation. During the core level depression and subsequent refill, the calculated density was higher than the measured density, indicating more liquid at this elevation, until 240 s when the calculated density rapidly decreased and the core level dropped below this elevation. The calculated liquid level dropped to the core inlet at about 60 s, as shown by the sharp decrease in the core inlet density in Figure 3.1.11. The calculated density at the core inlet then increased when the intact loop pump suction cleared at 118 s; the density decreased again at 310 s, causing the calculation of a late-time rod heatup. The rapid drop in the calculated densities may indicate that other factors than the gradual boiloff of liquid contributed to the drop in density. An increase in the amount of liquid entrained as the level started to decrease could affect the calculated densities. The measured density indicated that the liquid level never dropped to the core inlet during the transient.

The effect of these core fluid densities on the core thermal response is shown in Figures 3.1.12 and 3.1.13. These results are for heater rods at the 2.4 to 3.0 m and 0.0 to 0.6 m elevations in the core, respectively, and indicate the range of calculated and measured results. Two measurements are shown on each figure, which correspond to the highest and lowest temperatures measured in each elevation range. (The initial difference between the calculated and measured temperatures is caused by the measured temperatures being from embedded thermocouples, whereas each calculated temperature is a surface temperature. This difference in location is not significant later in the transient.)

The results at the 2.4 to 3.0 m elevation were representative of the response in most of the core. A rod heatup was measured at about 60 s and a smaller heatup was calculated at around 100 s. The calculated temperatures indicated dryouts and rewets as the calculated volume void fractions fluctuated around 0.96, the dryout criteria in the RELAP5/MOD1 heat transfer logic. Contributing to the lower magnitude of the calculated heatup was that the measured rod dryout and heatup occurred slightly earlier in the transient, when the core power was a little higher. A late-time rod heatup was calculated at most elevations, whereas the late-time measured temperatures remained near the system saturation temperature. The calculated late-time rod heatups were caused by the liquid level incorrectly dropping down into the core.

Figure 3.1.13 shows that, at the bottom of the heated core (0.0 to 0.6 m elevation), brief dryouts and rod heatups were calculated at 90 and 110 s, as well as after 280 s. The measured results indicate the rod cladding temperature remained near the system saturation temperature for most of the transient. After 260 s the measured temperatures were higher than the calculated temperatures, because the measured system pressures (and saturation temperatures) were higher than the calculated pressures.

As discussed earlier, the final clearing of the intact loop pump suction affected the vessel liquid level and thus the rod temperatures. The calculated and measured collapsed liquid levels in the intact loop pump suction are shown in Figure 3.1.14. The collapsed liquid levels are defined as the accumulated height of liquid in the pump suction. (The measured collapsed liquid level was inferred from a differential pressure measurement and a liquid density.) The clearing of each side is indicated by the drop in level to near zero. The calculated downflow and upflow side collapsed liquid levels are both shown, whereas only the measured downflow side is shown. (We think the upflow side data are in error, since they indicate the upflow side cleared shortly after the initiation of the transient.) In the calculation the downflow side cleared about 60 s earlier than the upflow side. A comparison of the calculated and measured downflow side collapsed liquid levels shows that the downflow side cleared at 118 s in the calculation, which was 46 s later than in the test.

The effect of the clearing of the intact loop pump suction on the calculated and measured intact loop cold leg densities on the pump side of the ECC injection location are compared in Figure 3.1.15. The measurements include both a tangential (near the top of the pipe) and a body densitometer measurement, which indicate that the pipe remained nearly filled with liquid until the pump suction cleared at 72 s. After the pump suction downflow leg was cleared, vapor flowed through the loop and cleared the intact loop cold leg. A similar event occurred in the calculation; however, it occurred later because the pump suction cleared later.

The calculated and measured total system mass inventories are compared in Figure 3.1.16. The measured inventories are based on pressure differences in the vertical sections of the system and neglect mass in the horizontal sections, which may cause some of the differences between calculated and measured results early in the transient. The measured total mass decreased rapidly until about 73 s, when the rate of mass loss decreased from 1.3 kg/s to 0.1 kg/s. The change in rate was a result of the intact loop pump suction clearing, providing a direct flow path for vapor to reach the break and for the break

flow to become two-phase. The clearing of the intact loop pump suction later in the calculation than in the test resulted in the break flow becoming two-phase later in the analysis. The calculated system mass continued to decrease, whereas the measured mass remained nearly constant and larger than the calculated total mass. The loss of more mass in the calculation than was measured may indicate that after the break uncovered mostly steam was discharged in the test; however, since RELAP5/MOD1 does not model any stratification effects at the break junction, a lower quality mixture was discharged in the calculation, resulting in a higher mass flow rate.

The calculated and measured (based on combining densitometer and flow measurements) break mass flow rates for test S-UT-1 are compared in Figure 3.1.17. The trends were similar; however, the calculated mass flow was always less than the measured mass flow. The effect of the difference between the calculated and measured break mass flow rate on the total integrated break mass flow is shown in Figure 3.1.18. As expected from the comparison of the break mass flow rates, the calculated total mass flow was much lower than the measured total. The measured total mass flow out of the system at 300 s was about 290 kg. The initial mass in the facility was 155 kg and the only mass flow into the facility before 300 s was the HPI flow of about 0.06 kg/s for a total inflow from HPI of 18 kg. Therefore, based on the measured break flow, about 115 kg more mass left the system than was in it, which indicates a very large uncertainty in the measured break mass flow and that it should only be used for trend analysis.

The calculated and measured densities in the broken loop cold leg on the pump-side and vessel-side of the break are shown in Figures 3.1.19 and 3.1.20, respectively. At both locations the calculated clearing of the pipe was later than was measured. This is attributed to the later clearing of the intact loop pump suction in the calculation than in the test. After the clearing of the pipes on both sides of the break, the average calculated density was higher than the average of the measured density, which could contribute to a higher break mass flow and lower system mass inventory later in the transient.

The calculated and measured collapsed liquid levels in the upflow and downflow legs of the broken loop pump suction are shown in Figure 3.1.21. The downflow leg in the calculation cleared at about 50 s, agreeing with the data; however, it quickly refilled in the calculation but not in the test. The downflow leg started to clear again at 150 s and then gradually refilled in the calculation. Neither leg was cleared late in the calculation, whereas both legs cleared in the test. The fact that the broken loop pump suction did not clear in the calculation did not appear to have a significant effect on the calculated results. Once the intact loop pump suction cleared, there was a flow path for the steam in the loops to reach the break.

A potential cause for the broken loop pump suction not totally clearing in the calculation is shown in Figure 3.1.22. The calculated liquid and vapor velocities at the broken loop pump inlet are shown. The velocities are apparently coupled until 140 s. After 160 s, the liquid velocity was predominantly negative, toward the steam generator, and the vapor velocity was predominantly positive, toward the break. The pump was not rotating and the liquid was decelerating against an adverse pressure gradient. The net mass flow was predominantly out of the pump inlet into the pump suction after 160 s. The flow of liquid backwards through the pump appears to have inhibited the clearing of the broken loop pump suction.

The two-velocity model was used at all junctions in this calculation. The use of this model at the pump junctions for small breaks appeared to have been satisfactory in most of our analyses of the Semiscale Mod-3 small break tests [18]; however, analysis of LOFT large break test L2-5 [19] required a one-velocity model in the pump suction junctions for the loop seals to clear. INEL analyses of the Mod-3 tests with an earlier version of RELAP5/MOD1 also found that the liquid and vapor were not coupled in the pump when a two-velocity model was used. [22] These results may indicate deficiencies in the interphasic momentum transfer in the RELAP5 pump component and that it should be evaluated to determine if the phases should be more tightly coupled.

3.2 Test S-UT-2 (10% Cold Leg Break with UHI)

Test S-UT-2 was a 10% cold leg break with ECC injection into the intact loop cold leg and with UHI. The core power and loop pumps were tripped on low pressurizer pressure (12.4 MPa). The steam generator steam line and feed water valves also tripped closed on low pressurizer pressure. No auxiliary feed water was used in this test.

The overall scenario for test S-UT-2 was similar to that for test S-UT-1. The injection of high pressure accumulator water into the upper head changed the timing of the occurrence of some events; however, the depressurization and core thermal response were similar.

The chronologies of significant events are summarized in Table 3.2.1. The initial system depressurization was more rapid than measured resulting in a slightly earlier trip of the core power and loop pumps in the calculation. However, after the initial depressurization the calculated rate was less than measured, resulting in the initiation of UHI accumulator flow at 23 s in the calculation, which was 8 s later than in the test. The first dryout in the core, caused by the core level depression

from the loop seals, occurred at 57 s in the test and at 84 s in the calculation. The core liquid level recovered and the rods rewet when the downflow legs of the pump suctions cleared both in the test and the calculation. However, a second core heatup later in the transient was calculated that was not measured. UHI flow terminated at 140 s and the upper head drained by 190 s in the test; both events were about 7 s earlier in the test than in the calculation. The calculation was terminated at 560 s because of large differences between calculated and measured core thermal response.

The calculated and measured primary system pressures and intact and broken loop steam generator secondary pressures are compared in Figure 3.2.1. The calculated primary pressure was higher than measured early in the transient because, similar to test S-UT-1, the initial hot and cold leg temperatures and the calculated steam generator secondary pressures and temperatures were higher than measured. During the period of UHI flow (from about 20 s to 150 s), the calculated primary depressurization was faster than measured. For about 100 s after UHI flow was terminated, the calculated primary depressurization was slower than measured. The cause of these differences in the depressurization rates may be due to not calculating the correct clearing of the pump suction. The calculated depressurization rate increased later in the transient when the liquid level dropped down into the core and the steam generation rate in the core decreased, when the core power began heating up the rods rather than generating steam. The calculated steam generator secondary pressures were always higher than measured. As also occurred in the test measurements, the calculated pressure in the intact loop steam generator initially increased more than the broken loop; however, the pressure in both steam generators became equal at about 350 s in the calculation and 500 s in the test.

Due to flow out the break, the system depressurized and voids formed in the vessel and in the hot legs. The calculated and measured broken loop hot leg densities are compared in Figure 3.2.2 and show that in both the test and the calculation voids formed in the hot legs shortly after the initiation of the break. After 25 s the broken loop hot leg was completely voided in the test, whereas some liquid remained until 150 s in the calculation. The density was higher in the calculation, because during UHI flow a relatively high density was calculated in the upper plenum volume connected to the broken loop hot leg, which appeared to delay its draining. At 340 s the measured density increased for a few seconds; this may have been the result of a surge of liquid through the core when the intact loop accumulator flow began.

As voids formed in the loops, voids also formed in the vessel. The calculated and measured vessel collapsed liquid levels are compared in Figure 3.2.3 and show that the collapsed level dropped to the top of the core at about 38 s in both the calculation and the test. The measured level dropped to about 1.0 m above the core inlet and quickly recovered when the broken loop pump suction downflow leg cleared. In the calculation, the UHI flow caused a delay in the clearing of the pump suction and a further depression of the vessel level, which did not increase until the termination of UHI flow and the clearing of the pump suction at 150 s. The vessel collapsed liquid level in the calculation decreased after 250 s down to the core inlet from boiloff of liquid in the core, whereas little boiloff occurred in the test. The measured and calculated effects of the intact loop accumulator injection were similar to those for test S-UT-1.

After the initiation of the transient, flow continued into the vessel upper head through the bypass line and out of the upper head through the guide tube and support columns until about 30 s. At 30 s the flow in the guide tube reversed in both the calculation and the test, as shown in Figure 3.2.4. The reversal in flow resulted in a two-phase mixture flowing in the guide tube in the calculation. Since the guide tube density was not measured, it is not known if the flow was a two-phase mixture or mostly steam in the test. The calculated flow direction oscillated several times during the period of UHI flow, whereas, after the initial change in flow direction, the measured flow was always from the upper plenum into the upper head. At about 150 s, shortly after the completion of UHI flow, the calculated guide tube flow was fairly large and into the upper head and no longer fluctuated, whereas the measured flow dropped to near zero. The calculated guide tube flow decreased to near zero at about 190 s when the upper head drained.

The oscillations in the guide tube flow were caused by surges in the UHI accumulator flow. The calculated and measured UHI mass flow rates are compared (on a short term plot) in Figure 3.2.5, which shows the cycling on and off of the calculated UHI flow after about 90 s, whereas the measured flow did not cycle. The peak magnitudes of the calculated flow surges from the accumulator were about twice as large as the average measured flow. These calculated surges in the accumulator flow reduced the accumulator pressure to below the system pressure and caused the accumulator flow to stop temporarily. The system continued to depressurize and, when the pressure decreased to below the accumulator pressure, accumulator flow started again.

During UHI, flow out of the upper head was through the bypass line to the upper downcomer and through the support columns to the upper core. The calculated and measured support

column mass flow rates are compared in Figure 3.2.6. Two measurements are shown, one for each of the two support columns in the Mod-2A facility; these were combined into one flow path in the RELAP5 model. The measured flows indicate that, between 70 and 140 s, the flow was predominantly up (from the top of the core to the upper head) in one column and down in the other column. The calculated mass flow, which should be the sum of the measured flows, was larger than the combined measured flows and always from the upper head to the top of the core, until the upper head drained.

The upper head was essentially water filled until the termination of UHI flow in both the calculation and the test. Figure 3.2.7 compares the calculated and measured upper head collapsed liquid levels. In both the test and the calculation the upper head started to drain shortly after the termination of UHI. The upper head drained slightly faster in the calculation than the test.

The upper head hydraulics during UHI flow affected the calculated densities in the vessel. The calculated and measured densities 3.42 m above the core inlet are compared in Figure 3.2.8. The measured density indicated this elevation was essentially vapor filled after 50 s even though UHI liquid was entering the core through the support columns. The calculated density indicated liquid, apparently from the UHI flow, was present until about 260 s. The calculated and measured core inlet densities are compared in Figure 3.2.9, which shows that the calculated core liquid level was below the core inlet from 60 to 150 s while the measured density indicated mostly liquid was present for the entire transient. During the 60 s to 150 s time period, the calculated core inlet velocity was negative, and vapor from the core was flowing into the downcomer.

The depression of the core liquid level down to the core inlet during the 60 to 150 s period in the calculation was caused by the hydraulic head in the upper head and support columns on the fluid in the core. This liquid exerted a pressure of up to 37.5 kPa (5.1 m of head) on the core fluid and depressed the core level to below the core inlet. The core level increased when the upper head drained and the associated hydraulic head decreased. While the upper head and support columns were full of liquid in the test, they did not depress the core level. A possible reason for the calculation of the core level depression was that the liquid from the UHI did not drop down into the core as it flowed out of the upper head. A significant amount of the liquid was retained in the upper elevations of the vessel. The calculated densities in the five upper plenum volumes are shown in Figure 3.2.10. (The volume numbers correspond to the volume numbers in the system nodalization shown in Figure 2.1.2) The densities at these elevations remained high until the upper head drained.

UHI affected the vessel liquid level in the calculation, which in turn affected the core thermal response. The calculated and measured rod cladding temperatures at the 3.0 to 3.6 m core elevation are compared in Figure 3.2.11. The measured temperature was near the system saturation temperature for the duration of the transient. The calculated temperature indicated a dryout and rewet at 100 s and a late-time core dryout and heatup at 270 s.

The calculated and measured rod cladding temperatures at a mid-core elevation (2.1 to 2.4 m above the core inlet) are shown in Figure 3.2.12. The data shown correspond to the highest and lowest temperatures measured at this elevation and are similar to other mid-core results. The test results show that the highest temperature on one rod during the transient was 630 K when a dryout occurred at about 60 s, while no dryout or temperature increase occurred on the other rod. After the pump suction cleared and the vessel level increased, the measured temperatures remained near the system saturation. The calculated temperature indicates dryouts and rewets during the 90 to 150 s period, when the core level was depressed and the void fraction fluctuated around 0.96. Because of the rewets, the maximum calculated temperature was not as high as the measured maximum temperature. After 300 s, a late-time core heatup was calculated when the mass in the core was boiled off and the liquid level again dropped down into the core.

In the calculation the hydraulic head on the core fluid from the liquid in the upper head and the support columns which depressed the core liquid level also inhibited the clearing of the pump suction. The calculated and measured intact loop pump suction collapsed liquid levels are shown in Figure 3.2.13. In the test the intact loop suction cleared at 73 s, whereas in the calculation the downflow leg cleared at 95 s and immediately partially refilled. The downflow leg finally cleared at about 150 s due primarily to the flashing of the liquid in it as the system depressurized. The loop seal was cleared, as indicated by the drop in the upside collapsed liquid level, at about 150 s, and the intact loop cold leg was quickly cleared, as shown by the comparison of the calculated and measured intact loop cold leg densities shown in Figure 3.2.14.

The calculated and measured total primary system mass inventories are compared in Figure 3.2.15. The measured inventories are based on pressure differentials in vertical sections of the system and neglect mass in the horizontal sections, which may be the reason for the differences early in the transient. The measured primary mass decreased rapidly to about 50 kg at about 50 s. The rate of mass loss then decreased as the broken loop pump suction cleared and the break flow

became two-phase. After 80 s, the measured mass slowly decreased to 32 kg at 350 s and then started to increase from the intact loop accumulator flow. The calculated system mass decreased to about 18 kg at 450 s. The initiation of accumulator flow at 375 s in the calculation did not result in an increase in the system mass, as occurred in the test; however, it appeared to stop the gradual overall loss of mass. The overall difference in the final mass in the system appears to be primarily caused by the calculated break mass flow rate being higher than occurred in the test after the break uncovered. Since RELAP5 does not model stratification effects, the quality of the mixture discharged at the break was probably lower in the calculation than in the test, resulting in the loss of more mass.

A comparison of the calculated and measured break mass flow rates, shown in Figure 3.2.16, indicates the calculated break mass flow rate was much lower than measured, which is not consistent with the system mass inventories. The measured mass flow was based on combining densitometer and flow measurements. This measurement system was the same as used in test S-UT-1 and, similar to the conclusions from test S-UT-1, this comparison indicates a large uncertainty in the data. This data should only be used for trend analysis.

The mass distribution in the broken loop cold leg is shown in Figures 3.2.17 and 3.2.18. The calculated and measured broken loop pump suction collapsed liquid levels are shown in Figure 3.2.17. The downflow leg in the calculation initially cleared at 55 s, as occurred in the test; however, this leg quickly refilled in the calculation. The final clearing of the downflow leg was at 150 s in the calculation, which was 92 s later than measured. The clearing of the downflow leg was similar to the intact loop downflow leg clearing; liquid in it flashed as the system depressurized and steam flowed back through the steam generators to the upper plenum. When the pump suction cleared at 150 s, the pipe on the pump side of the break also cleared. Figure 3.2.18 compares the densities on the pump side of the break and shows that the pipe was cleared at 70 s in the test and at 150 s in the calculation.

The system mass inventories discussed earlier showed a gradual increase in mass in the test after the initiation of intact loop accumulator flow. The calculated and measured intact loop accumulator flows are compared in Figure 3.2.19. Accumulator flow started at 345 s in the test and the flow cycled with a fairly regular period and peak flow. In the test, accumulator flow appeared to cause an increase in the vapor generation rate in the core and a subsequent increase in the system pressure causing a cycling of the accumulator flow. Accumulator flow

started at 375 s in the calculation and cycled on and off, but the period and peak flow were not uniform. In the calculation, the flow surged out of the accumulator and lowered the pressure in the accumulator to below the system pressure so the flow stopped. Flow began again when the system depressurized to below the accumulator pressure. The total flow from the accumulator in the calculation was much less than in the test and this difference contributed to the calculation of less mass in the system than was measured later in the transient.

3.3 Test S-UT-6 (5% Cold Leg Break Without UHI)

Test S-UT-6 was a 5% cold leg break with ECC injected into the intact and broken loop cold legs. The core power and loop pumps were tripped on low pressurizer pressure (12.6 MPa). The steam line and feed water valves also tripped closed on low pressurizer pressure. The feed water valves closed 24 s after the steam line valves and no auxiliary feed water was used in this test.

The calculated and measured chronologies of significant events for test S-UT-6 are summarized in Table 3.3.1. Due to a slightly faster initial depressurization in the calculation, the core power and loop pumps were tripped slightly earlier in the calculation than in the test. The time of clearing of the intact loop pump suction was about 220 s in both the test and the calculation. The only dryout in the core was due to boiloff of core liquid, rather than to a core level depression caused by the loop seals. The initial dryout was calculated at 465 s, which was 95 s earlier than was measured. Good agreement also occurred in the initiation of flow in the loop accumulators. Only the upper elevations of the core dried out in the test and the entire core was rewet at 1000 s, whereas the entire core dried out and was continuing to heat up when the calculation was terminated.

The calculation was terminated at 800 s, because the calculated response was significantly different from the measurements and we felt that no additional assessment of the capabilities of RELAP5 would be obtained by continuing the transient calculation.

The calculated and measured primary system pressures and intact and broken loop steam generator secondary side pressures are compared in Figure 3.3.1. In both the calculation and the test, the system rapidly depressurized for the initial 50 s. After 50 s, as a result of voids forming in the primary system, the rate of depressurization decreased. In the test, the rate of primary depressurization was coupled to the intact loop steam generator secondary until the intact loop pump suction cleared; shortly after the pump suction cleared, the rate increased. In the calculation, an increase in the system depressurization rate

occurred at about 280 s, which was 60 s after the pump suction cleared, when the break junction flow became mostly steam. The primary and intact loop secondary pressures became equal at 224 s in the test and at 278 s in the calculation. From 280 s to 490 s the rates of depressurization in the calculation and the test were nearly equal; however, at 490 s the calculated rate of depressurization was more rapid than measured, when the core power began to heat up the rods rather than generate steam and the core steam generation rate decreased. The calculated and measured pressures were in agreement again by about 730 s.

As the system depressurized, voids formed in the vessel and the loops. The calculated and measured broken and intact loop hot leg densities are compared in Figures 3.3.2 and 3.3.3, respectively. Middle and bottom measurements were available in the broken loop and tangential (near the top) and bottom measurements were used in the intact loop. Figure 3.3.2 shows that the broken loop hot leg was essentially completely voided at 100 s; however, a few seconds later the bottom (B) measurement indicated the presence of some liquid. An increase in the density occurred in both the test and the calculation at about 250 s when the primary side of the broken loop steam generator drained. The broken loop hot leg emptied again later in both the test and the calculation; however, it drained much earlier in the calculation.

The voiding of the intact loop hot leg is shown in Figure 3.3.3. The tangential (T) measurement and the calculated density indicates that voiding in the intact loop hot leg occurred shortly after the initiation of the transient. The measurements also indicate that the flow was stratified with some liquid remaining in the hot leg for the duration of the test analyzed. The calculation indicates that the hot leg was essentially drained by 300 s. A higher steam flow rate through the core in the test could have retarded the draining of the hot legs.

As the system depressurized the vessel also voided. Figure 3.3.4 compares the calculated and measured vessel collapsed liquid levels. The level decreased to the top of the core at about 70 s in both the test and the calculation. Due to the formation of the loop seals, the core level was depressed to 1.5 m above the core inlet in the calculation and to 2.2 m in the test. The vessel level increased in both the test and the calculation when the intact loop pump suction cleared. The calculated level increased again at 300 s when the broken loop steam generator primary side drained and liquid flowed through the broken hot leg into the vessel. A similar increase in level did not occur in the test; the fluid remained in the broken hot leg until much later in the transient. The collapsed liquid level in both the test and the calculation slowly decreased as the liquid in the core was boiled off. The measured level dropped to

about 1.4 m above the core and then slowly started to increase shortly after the initiation of the loop accumulator flows at 730 s. The calculated level dropped much more rapidly to below the core inlet, before accumulator flows began at about 750 s. The calculated loop accumulator flows cycled similarly to the calculated loop accumulator flows in test S-UT-1 and S-UT-2, while the measured flows did not cycle.

The flows in the guide tube were nearly the same in the test and the calculation with a reversal in flow direction from into the top of the core to into the upper head at about 50 s in both; however, the support column flows were somewhat different. The calculated and measured support columns mass flow rates are compared in Figure 3.3.5. Since each support column was instrumented in this test, two measurements are shown. Both measured flows and the calculated flow were from the upper head to the top of core until the upper head was drained. The calculated mass flow was significantly larger than the sum of the two measured flows, which it should equal. Figure 3.3.6 compares the upper head collapsed liquid levels and shows that the upper head drained at a faster rate in the calculation than the test, which may be a result of combining the two support columns into one flow path in the RELAP5 model.

The voiding in the core is shown in Figure 3.3.7, which compares the calculated and measured densities at the 3.42 m core elevation. The measured density indicates some voiding by 20 s with the density continuing to decrease until about 100 s. From 100 to 560 s the top of the core was partially liquid filled in the test. At 560 s the measured density quickly dropped to a value characteristic of "pure" steam. The calculated density was higher than the measured density until 110 s indicating that, early in the transient, less voids were calculated than were measured. The increases in the calculated density at 210 s and 320 s were a result of the pump suction clearing and the draining of the broken loop steam generator, respectively. After 450 s this elevation was essentially steam filled in the calculation.

The agreement early in the transient between the calculated and measured densities at the 1.73 m core elevation was better than at the higher elevation, as shown in Figure 3.3.8. Except for a large temporary decrease in the calculated density at 290 s, good agreement in the densities was obtained until 460 s, when the calculated density decreased from a value indicating mostly liquid to one indicating a low density mixture. The comparison in densities at the core inlet was better than the early-time agreement at the 1.73 m core elevation, as shown in Figure 3.3.9. The core inlet was liquid filled in both the calculation and the test until 620 s. After 620 s, the calculated density was very low, indicating mostly vapor, whereas the measured density indicated this level was liquid filled for the duration of the transient.

The clad temperature responses at the 3.0 to 3.7 m, 1.5 to 1.8 m and 0.0 to 0.6 m core elevations are shown in Figure 3.3.10 through 3.3.12, respectively. Figure 3.3.10 shows that the measured temperatures at the 3.0 to 3.7 m core elevation followed the system saturation temperature until 560 s. After 560 s, a dryout and rewet was measured on each rod, followed by a prolonged core heatup at 660 s. Several early-time dryout and rewets were calculated between 200 s and 350 s as the void fraction in the adjacent hydraulic volume fluctuated around a value of 0.96. A sustained rod heatup was calculated at 565 s, which was 95 s earlier than was measured. At the 1.5 to 1.8 m and 0.0 to 0.6 m core elevations, the measured rod temperatures followed the system saturation temperature, as shown in Figures 3.3.11 and 3.3.12, respectively. The calculated rod temperatures at these elevations indicated a late-time rod heatup, with the calculated rod temperature above 800 K at the 1.5 m to 1.8 m elevation. The difference between the measured and calculated rod temperatures before the calculated rod heatup resulted from the slight difference in the measured and calculated system pressures. The decrease in the calculated core liquid level to below the core inlet resulted in a temperature increase over the entire core.

The formation of loop seals in the pump suctions slightly depressed the core level early in the transient, and when the pump suction cleared the vessel level increased. The calculated and measured intact loop upside and downside pump suction collapsed liquid levels are compared in Figure 3.3.13. Good agreement in the clearing of the pump suction occurred which caused good agreement in the clearing of the intact loop cold leg. The calculated and measured (tangential and body) densities on the vessel side of the ECC injection nozzle are shown in Figure 3.3.14. The measurements indicate some horizontal stratification after 30 s, due to draining into the vessel, whereas the pipe was essentially water-filled in the calculation until the pump suction was cleared.

The calculated and measured integrated total break mass flows are compared in Figure 3.3.15. Unlike tests S-UT-1 and S-UT-2, the measured integrated mass flow for test S-UT-6 was obtained from a condensing system which should provide accurate data. Excellent agreement was obtained until about 400 s. After 400 s, more mass was calculated to be leaving the system than was measured. A possible cause of the difference is that, in the test, after the horizontal break uncovered and the flow was stratified, a high quality fluid was exiting through the break, whereas a somewhat lower quality mixture was calculated at the break junction.

The calculated and measured densities in the broken loop cold leg on the pump side of the break are compared in Figure 3.3.16. Measured middle and bottom densities are shown, and indicate the pipe was liquid filled until 300 s. After 300 s, the measurements indicate the fluid was stratified with liquid on the bottom of the pipe. The initiation of the broken loop accumulator flow at 750 s in the test caused the broken loop cold leg to began to refill. The calculated density shows the pipe began emptying at 200 s and mostly contained a low-density mixture after 300 s.

The broken loop pump suction upside and downside collapsed liquid levels are compared in Figure 3.3.17. In the test, the downflow leg cleared at 300 s; however, only a brief decrease and nearly immediate recovery in the upside collapsed level occurred. The measured upflow side level started decreasing at about 390 s and the slow rate of decrease indicates it was mostly due to boiloff of the liquid in it, as the system depressurized. The calculated downflow leg also started to decrease at about 300 s, but at 370 s it started to refill and remained full for the remainder of the transient. After the downflow leg refilled, the collapsed level in the upflow leg very slowly decreased, probably from flashing as the system depressurized. An increase in the upflow level was calculated at 750 s after the initiation of broken loop accumulator flow. Since the intact pump suction had cleared, the fact that the broken loop did not clear in the calculation did not appear to have a significant effect on the overall system response.

Similar to test S-UT-1, a possible reason the broken loop pump suction did not clear was that the correct broken loop pump response was not calculated. The calculated liquid and vapor velocities at the broken loop pump outlet are shown in Figure 3.3.18. The vapor and liquid flow were coupled until 340 s. After 360 s, the liquid velocity was predominantly negative, from the pump discharge toward the steam generator, and the vapor velocity was positive, toward the pump inlet. The flow of liquid into the pump suction prevented the clearing of the broken loop pump suction. Again, this may indicate a deficiency in the modeling of the pump component.

3.4 Test S-UT-7 (5% Cold Leg Break With UHI)

Test S-UT-7 was a 5% cold leg break with ECC injected into the intact and broken loop cold legs and UHI. The core power and loop pumps were tripped on low (12.6 MPa) pressurizer pressure. The steam line and feed water valves also closed on low pressurizer pressure. The feed water valves were closed 24 s after the steam valves. Auxiliary feed water to the steam generators was not used in this test.

The calculated and measured chronologies of significant events for test S-UT-7 are summarized in Table 3.4.1. The calculated initial depressurization rate was more rapid than was measured, resulting in the trip of the core power and the loop pumps about 4 s earlier than was measured. The faster initial depressurization in the calculation also resulted in the UHI flow beginning at 18 s in the calculation which was 3 s earlier than measured. The intact loop pump suction cleared at 180 s in the calculation and 220 s in the test. The calculated UHI flow had terminated when the calculation was stopped; however, the upper head was not completely drained.

The calculation terminated at 433 s due to a large spike in the UHI accumulator flow rate and a subsequent code failure. Since the calculated UHI accumulator flow was not similar to the test results and was dominating the system response, we did not attempt to continue this calculation further.

The calculated and measured primary system pressure responses are compared in Figure 3.4.1. The system rapidly depressurized for the first 50 s and then as voids formed in the system the depressurization rate decreased. Good agreement between the calculated and measured pressure occurred between about 25 s to 145 s. The measured pressure continued to decrease with a slight increase in the rate at about 240 s, after the intact loop pump suction cleared. At 145 s, a brief increase in the calculated depressurization rate occurred when a surge in the UHI accumulator flow was calculated. The calculated system pressure remained essentially constant from 175 s to 240 s, when a rapid decrease in pressure was calculated. Another rapid decrease in pressure was calculated at 433 s. These rapid decreases in pressure were caused by large surges in the UHI flow. The larger the surge of UHI flow, the more the pressure dropped.

The calculated UHI accumulator flow is shown in Figure 3.4.2 and cannot be compared with data since the UHI flow instrumentation failed during this test. The calculated UHI flow initiated at 18 s and the flow rate was similar to test S-UT-2 until 140 s when a surge in the flow to above 3.0 kg/s was calculated. The UHI flow then stopped and the only indication of flow again in Figure 3.4.2 is at 433 s, when the calculated UHI flow surged to above 9.3 kg/s. A spike in the UHI flow was also calculated at 240 s; however, it does not appear on the figure because it spiked within the two second period between plot edits.

The pressure in the UHI accumulator is also an indication of UHI flow. The calculated and measured UHI accumulator pressures are compared in Figure 3.4.3. The pressure responses were nearly identical until 145 s, when a step drop in the accumulator pressure was calculated. The step drop in pressure corresponds to a surge in the accumulator flow and a decrease in the accumulator

pressure to below the system pressure, which shut the UHI flow off until the primary system depressurized to below the pressure in the accumulator. Step drops in the pressure were also calculated at 240 and 435 s. The termination of UHI accumulator flow in the test is visible in Figure 3.4.3 at 296 s. The subsequent gradual increase in the measured accumulator pressure was due to heat transfer from the accumulator walls. UHI flow was terminated at 433 s in the calculation and would not have surged again if the calculation were continued because the correct total amount had already been injected.

The initial voiding of the loops and the vessel was similar to the results for test S-UT-6. However, later in the transient, the UHI flow had a large effect on the liquid level in the upper head and the core. The calculated and measured collapsed liquid levels in the upper head are compared in Figure 3.4.4. The calculated collapsed liquid level shows a partial voiding at 100 s with a subsequent refill at 150 s. Complete emptyings of the upper head followed by later refills were calculated between 160 and 240 s, and 320 and 433 s. The large surges in the calculated UHI accumulator flow appear to be due to the cold UHI liquid rapidly condensing the steam in the nearly voided upper head and lowering the pressure. This condensation significantly increased the pressure difference between the upper head and the UHI accumulator, resulting in a surge in UHI flow. The measured upper head liquid level also indicates that nearly all of the upper head was voided at 230 s; however, the measured subsequent refill was not as rapid as was calculated. This may indicate that the calculation of an excessive condensation rate of the upper head steam caused the spikes in the UHI flow.

The rapid refill of the upper head in the calculation affected the liquid level in the core, as indicated by the densities at the 1.73 m core elevation shown in Figure 3.4.5. Relatively good agreement was obtained except at 175 s and 270 s, when the calculated density decreased, indicating vapor at this elevation. The drop in the density resulted from the core level being depressed by the hydraulic head from the fluid in the upper head and support columns. Similar to the calculation for test S-UT-2, when the upper head and support columns were filled with liquid and liquid was held up in the upper plenum, the pressure on the upper core fluid was increased and the core liquid level depressed. The liquid level was not depressed as low in the calculation for test S-UT-7 as for test S-UT-2. The measured density did not indicate such a core level depression when the upper head refilled at 250 s in the test.

The brief depressions of the core liquid level in the calculation resulted in brief rod dryouts and small increases in the rod temperatures. The calculated and measured rod cladding temperatures at the 1.5 to 1.8 m core elevation are shown in Figure 3.4.6. The calculated rod temperature increased at both 175 and

270 s when the vessel liquid level was depressed. The measured temperatures did not increase at these early times. These temperature comparisons were typical of higher elevations in the core, whereas at lower elevations in the core no rod temperature increases were calculated or measured.

3.5 Test S-UT-8 (5% Cold Leg Break Without UHI and With Decreased Core Bypass Flow)

The Semiscale Mod-2A facility was modified for Test S-UT-8 to improve its prototypicality with respect to the current Westinghouse standard plant upper head and upper plenum flow paths and hydraulic resistances, as discussed in Section 2.1. This modification included decreasing the core bypass flow, blocking off the two support columns, and drilling additional holes in the guide tube. However, instrumentation was removed from the support columns and the instrumentation ports were not plugged, which resulted in an unplanned leakage path from the upper head to the top of the core through the support columns. Holes were drilled in the guide tube below the upper support plate to permit steam flow at high liquid levels in the upper plenum. (Figure 2.1.4, discussed earlier, shows the details of the modifications for this test.) These changes in geometry, in combination with the test conditions, caused a depression of the core liquid level down to the core inlet early in the transient, which was somewhat unexpected. Determination of the capability of RELAP5/MOD1 to calculate this result was a primary objective in including this test in our assessment matrix. Since the early core liquid level depression to the core inlet was not calculated, only 375 s of transient were run due to economic considerations.

Even though one of the major changes was to the upper head/upper plenum flows, no comparisons of calculated and measured flows are possible for test S-UT-8 either because the instrumentation failed or because the flow path was not instrumented. The instrumentation failed in the bypass line, and, because of discrepancies between the indicated flow in the guide tube and an associated pressure drop measurement, we consider the measurement in the guide tube to have essentially failed and not be useful for comparison. There was no instrumentation in the support columns, since removal of those flow meters actually provided the unplanned flow path. The lack of measurements for these flows in this test adds considerable uncertainty to the modeling and interpretation of the results. An Experiment Data Report was not issued for test S-UT-8, which also contributes to uncertainty in the instrumentation and conditions for this test. Until the actual initial and boundary conditions are finally established, the results of the comparisons between the calculation and measurements should be considered preliminary.

The calculated and measured chronologies of significant events for test S-UT-8 are summarized in Table 3.5.1. The calculated initial depressurization was more rapid than measured; however, the calculated emptying of the pressurizer at 32 s was only 4 s earlier than measured. The upper head was drained at about 94 s in both the calculation and the test. The first rod dryout in the core, due to the core level depression from the loop seals, was at 163 s in the test, which was 30 s earlier than in the calculation. The calculated clearing of the intact loop pump suction was at 200 s, 40 s earlier than measured.

The calculated and measured primary system and intact loop secondary pressure responses are compared in Figure 3.5.1. The primary pressures were in agreement at 30 s: however, after 30 s, the calculated pressure was higher than measured. A major cause for the calculation of a higher primary pressure after 30 s was the calculation of too high an intact loop steam generator secondary pressure and secondary temperature. The higher steam generator fluid temperature decreased the energy transfer from the primary to the secondary, resulting in a higher primary pressure.

As the system depressurized, voids formed in the primary system. The calculated and measured intact and broken loop hot leg densities are compared in Figure 3.5.2 and 3.5.3, respectively. In the intact loop the test results include top and bottom densitometers measurements, while the broken loop has top and middle measurements. The measurements and calculations in both loops indicated voiding shortly after the initiation of the transient. After 30 s, the measurements in the intact loop indicate the flow was stratified for the duration of the transient analyzed, whereas the calculated density indicates the intact hot leg was drained after 225 s. In the broken loop, the measurements indicate the flow was stratified at 30 s and the hot leg drained by 90 s, while the hot leg drained at 110 s in the calculation. The hot leg of the broken loop partially refilled in both the test and the calculation at 250 s, when the primary side of the broken loop steam generator tubes drained. This fluid drained out of the hot leg by 350 s in both the calculation and the test.

Voiding also occurred in the primary side of the steam generator tubes early in the transient. The calculated and measured collapsed liquid levels in the primary upside and downside of the intact loop steam generator tubes are compared in Figure 3.5.4. The early time response during the test cannot be determined accurately because of the flow effects on the differential pressure measurements used to calculate the collapsed liquid level. However, by 90 s when the intact loop flow was small, some voiding of both sides was indicated in the test. Both legs started to drain at about 90 s; the downflow side was drained by 170 s and

the upflow side by 220 s. This difference in the time of draining of the two sides affected the vessel collapsed liquid level in the test. In the calculation, the upflow leg started to void by 10 s followed shortly by the downflow leg at 30 s. Both sides of the steam generator were about 50% voided in the calculation by 90 s, and the downflow leg drained at 145 s and the upflow leg at 160 s. The main difference in these calculated results was that the upflow leg of the steam generator drained too fast and, therefore, too early in the calculation. The faster draining probably resulted from less condensation in the steam generator and lower steam flows in the intact loop.

Voids also formed early in the vessel. The calculated and measured vessel collapsed liquid levels are shown in Figure 3.5.5. The calculated collapsed level indicates some voiding at the initiation of the transient, whereas, because of flow effects on the measurements, the early-time response in the test could not be evaluated. Later in the transient, from 220 s to 250 s, the measured collapsed level was depressed to below the core inlet. As discussed above, this large core level depression occurred because the downflow side of the steam generator had drained and, while the upflow side was slowly draining, the liquid in the upflow leg created an additional hydraulic head on the core fluid and depressed the core level. A corresponding large core level depression did not occur in the calculation because both sides of the intact loop steam generator drained at about the same time. In both the calculation and the test, the core level increased after the steam generator tubes drained and intact loop pump suction cleared.

The effects of the change in upper head geometry on the upper head flows in the test could not be directly evaluated because of the lack of instrumentation, as previously discussed. An indication of the upper head flows can be obtained from the upper head collapsed liquid levels, shown in Figure 3.5.6. Some voiding of the upper head occurred at about 30 s in both the test and the calculation. After the initiation of voiding, the upper head drained uniformly in the test, whereas, after the initial voiding in the calculation, the upper head did not start to drain until about 60 s; it then drained at a faster rate so that the upper head was empty in both the test and the calculation at about the same time. Due to the lack of instrumentation of the upper head flows, the reasons for this difference could not be identified.

The calculated and measured fluid densities at the 2.53 and 1.73 m core elevations are compared in Figures 3.5.7 and 3.5.8, respectively. The measured liquid level, as indicated by the density, dropped below the 2.53 m core elevation at about 160 s and recovered at 260 s. The calculated liquid level dropped below

the 2.53 m elevation at about 195 s and recovered a few seconds later. Brief depressions of the level were also calculated between 225 s and 275 s. The measured liquid level dropped below the 1.73 m core elevation, as shown by the density in Figure 3.5.17; the calculated liquid level never dropped to that elevation. In the test, the core liquid level was depressed below the core inlet, whereas the calculated liquid level only dropped to the 2.5 m elevation.

The depression of the core liquid level to below the core inlet in the test resulted in an increase in the rod temperatures at the lower elevations in the core. The calculated and measured rod cladding temperatures at the 1.5 to 1.8 m elevation are compared in Figure 3.5.9. Two measurements are shown, which correspond to the highest and lowest temperatures measured in each elevation range. The measured temperature increased to about 680 K, whereas the calculated temperature remained near the system saturation temperature. At the higher elevations in the core, above the 2.53 m elevation, the steam cooling during the core level depression was apparently large enough in the test that no heatup of the rods occurred. A brief rod heatup was calculated at higher core elevations, when the core liquid level dropped to the 2.5 m core elevation. A second rod heatup was measured over most of the core after 400 s, due to boiloff of core liquid, but the transient analysis was not run long enough to determine if an analogous rod heatup would be calculated.

The collapsed liquid levels in the intact loop pump suction are shown in Figure 3.5.10. (The initial difference in the level when the piping was full is mainly caused by the control variable used to calculate the level not being changed to account for a change in the measurement locations for this test. This difference does not affect the evaluation of the time of clearing of the piping.) The downflow pump suction leg in the calculation cleared at 200 s, whereas the downflow leg cleared at 240 s in the test. The earlier clearing of the pump suction downflow leg in the calculation caused the intact loop cold leg piping to also clear earlier, as shown by the intact loop cold leg densities compared in Figure 3.5.11.

The calculated and measured integrated total break mass flow rates are compared in Figure 3.5.12. The initial difference in flow is partially attributed to the time lag in the condensing system used to measure this flow. Between 75 and 120 s, the calculated mass flow rate was lower than measured, resulting in a 6 kg difference at 120 s. The calculated mass flow rate was higher than measured between 120 and 220 s, resulting in good overall agreement when the transient calculation was stopped at 360 s. Figure 3.5.13 shows that the calculated broken loop density was generally higher than the measured density from about 120 to 220 s, causing the higher break mass flow rate in the calculation than in the test during that period.

To determine if the inaccurate calculation of the steam generator secondary pressures was a major contributor to the liquid holdup in the primary side of the steam generator tubes, and the resulting difference in the core liquid level response, the S-UT-8 calculation was repeated using the measured intact and broken loop steam generator secondary pressures as boundary conditions. The resulting calculated and measured primary system pressures are compared in Figure 3.5.14 and show that agreement was improved from that seen for the base calculation, indicating that the conditions in the steam generator secondary do have a strong effect on the calculated primary pressure. The time before the upflow side of the intact loop steam generator tubes cleared was increased by about 10 s; however, this later clearing did not have a significant effect on the core collapsed liquid level. Figure 3.5.15 compares the calculated and measured densities at the 1.73 m core elevation, and shows that, similar to the S-UT-8 results discussed earlier, no significant core voiding was calculated.

When the analysis of test S-UT-8 was initiated, we were not aware of the removal of the instrumentation from the support columns, and the resulting unplanned leakage path. After starting the analysis, information received from the Semiscale Program indicated the leakage path was from the bottom of the upper head to the top of the upper plenum [23] and some calculations were performed using this information. After we had presented preliminary results from those S-UT-8 calculations, further documentation from the Semiscale Program established that the actual flow path was through the support columns [15].

Two calculations were performed using the initial incorrect information on the leakage flow path, which modeled the leakage flow as being from the bottom of the upper head to the top of the upper plenum. One calculation used the basic model of the steam generators discussed in Section 2.1; the second calculation used approximately one half as many nodes for the steam generators. These calculations were performed at the specific request of the NRC to determine the sensitivity of the core thermal response to steam generator noding, because Argonne National Laboratory [24] had performed calculations for a PWR that showed the core peak temperature during small break LOCAs was higher with detailed noding of the steam generators than with coarse noding. The results of these two early calculations are provided in Appendix III to show the effect of steam generator noding on a small break in the Semiscale Mod-2A facility. This study showed there was not a significant effect on most of the results, including the early-time core liquid level depression and the peak rod cladding temperature.

Table 3.1.1 S-UT-1 Sequence of Events

Event	Time (s) Measured	RELAP5
Break Opened	0.0	0.0
HPI Initiated	2.0	2.4
Pressurizer at 12.4 MPa	7.5	5.6
Pressurizer Emptied	30.0	20.3
First Dryout in Core	52.0	80.0
Intact Loop Pump Suction Downflow Leg Cleared	72.0	118.0
Upper Head Drained	95.0	70.0
Broken Loop Pump Suction Downflow Leg Cleared	130.0	---
Entire Core Rewetted	160.0	---
Intact Loop Accumulator Flow Began	333.0	327.0

Table 3.2.1 S-UT-2 Sequence of Events

Event	Time (s) Measured	RELAP5
Break Opened	0.0	0.0
HPI Initiated	2.0	2.5
Pressurizer at 12.4 MPa	7.7	5.0
UHI Began	15.0	23.0
Pressurizer Emptied	28.0	21.0
First Dryout in Core	57.0	84.0
Broken Loop Pump Suction Downflow Leg Cleared	64.0	150.0
Intact Loop Pump Suction Downflow Leg Cleared	73.0	150.0
Entire Core Rewetted	87.0	---
UHI Ended	140.0	147.0
Upper Head Drained	190.0	196.0
Intact Loop Accumulator Flow Began	345.0	375.0

Table 3.3.1 S-UT-6 Sequence of Events

Event	Time (s) Measured	RELAP5
Break Opened	0.0	0.0
Pressurizer at 12.6 MPa	10.3	8.1
Pressurizer Emptied	28.0	23.0
HPI Initiated	35.0	35.0
Upper Head Drained	210.0	150.0
Intact Loop Pump suction Downflow Leg Cleared	220.0	214.0
First Dryout in Core	560.0	465.0
Intact Loop Accumulator Flow Began	730.0	750.0
Broken Loop Accumulator Flow Began	750.0	730.0
Entire Core Rewetted	1000.0	----

Table 3.4.1 S-UT-7 Sequence of Events

Event	Time (s) Measured	RELAP5
Break Opened	0.0	0.0
Pressurizer at 12.6 MPa	8.6	4.7
UHI Began	21.0	18.0
HPI Initiated	34.0	34.0
Pressurizer Emptied	37.0	23.0
Intact Loop Pump Suction Downflow Leg Cleared	220.0	212.0
UHI Ended	296.0	433.0
Upper Head Drained	370.0	---
First Dryout in Core	700.0	200.0
Broken Loop Accumulator Flow Began	738.0	---
Intact Loop Accumulator Flow Began	822.0	---
Entire Core Rewetted	950.0	---

Table 3.5.1 S-UT-8 Sequence of Events

Event	Time (s) Measured	RELAP5
Break Opened	0.0	0.0
Pressurizer at 12.6 MPa	19.0	10.2
HPI Initiated	35.1	35.1
Pressurizer Emptied	36.0	32.0
Upper Head Drained	94.0	93.0
First Dryout in Core	163.0	193.0
Intact Loop Pump Suction downflow Leg Cleared	240.0	200.0
Intact Loop Accumulator Flow Began	520.0	---

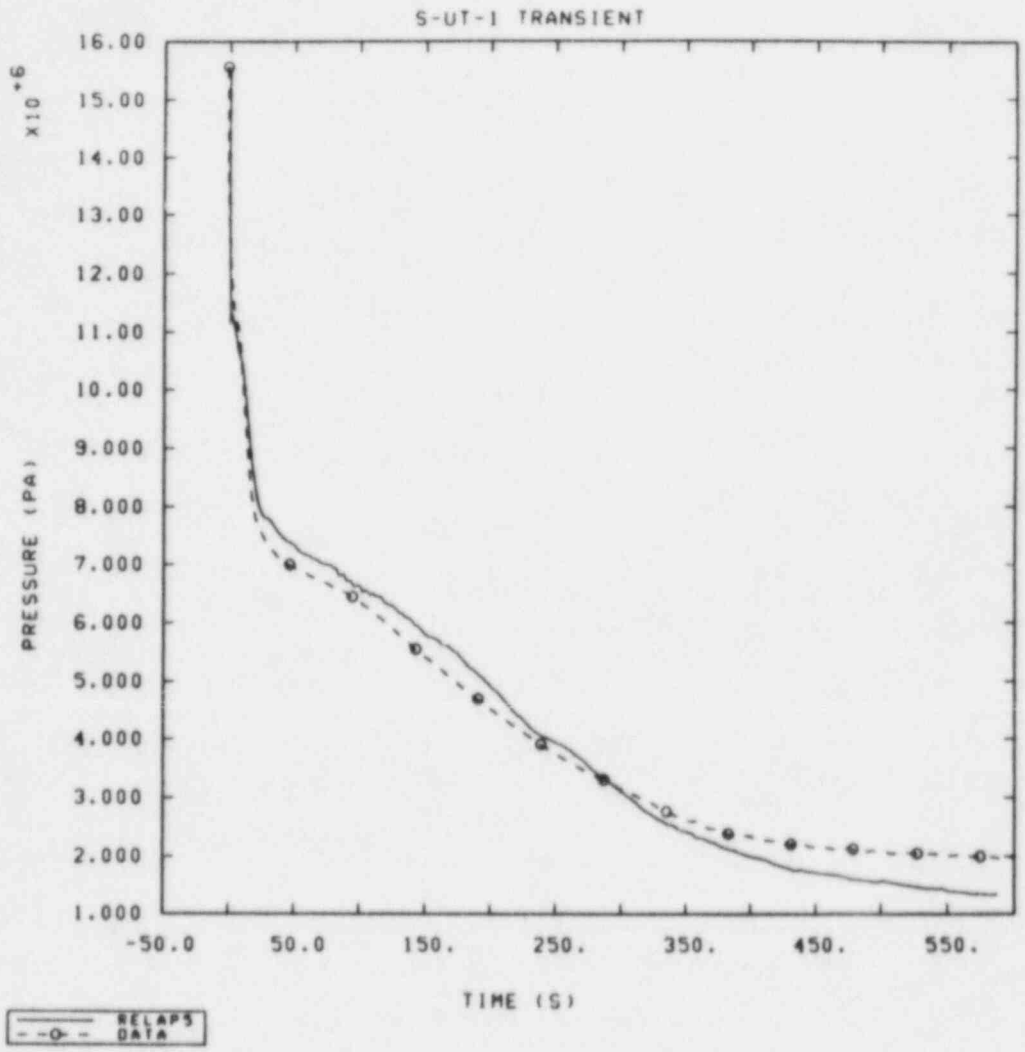

Figure 3.1.1 Comparison of Calculated and Measured Primary System Pressures for Test S-UT-1

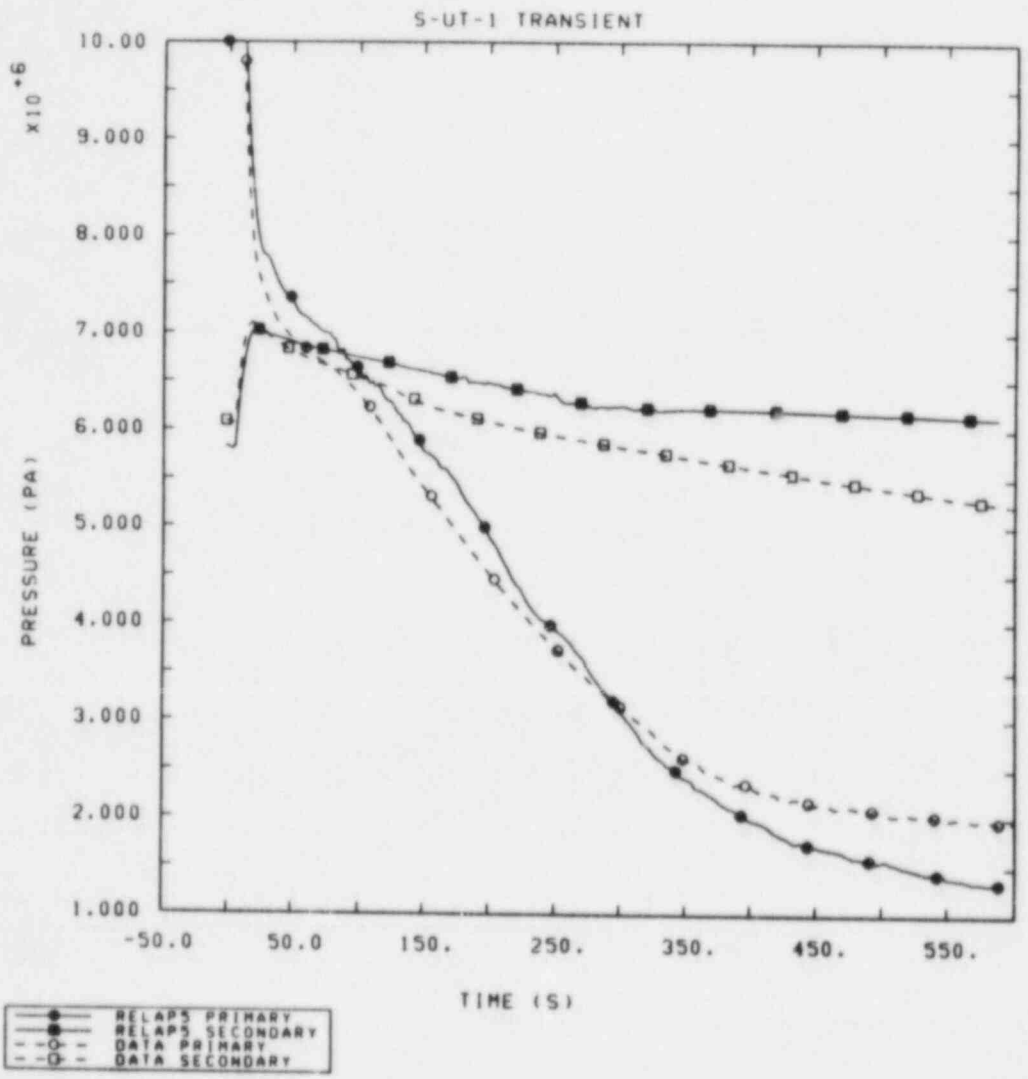

Figure 3.1.2 Comparison of Calculated and Measured Primary and Steam Generator Secondary Pressures for Test S-UT-1

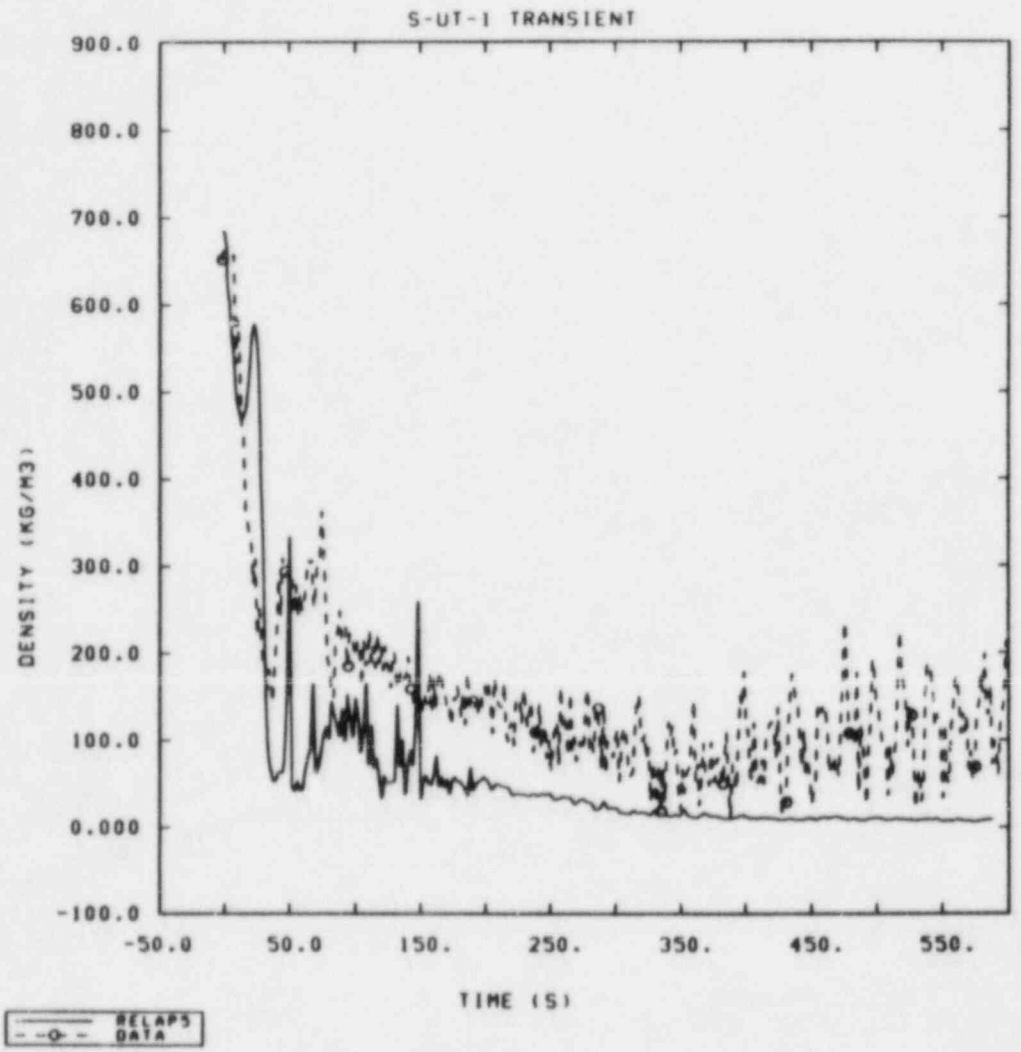

Figure 3.1.3 Comparison of Calculated and Measured Intact Loop Hot Leg Densities for Test S-UT-1

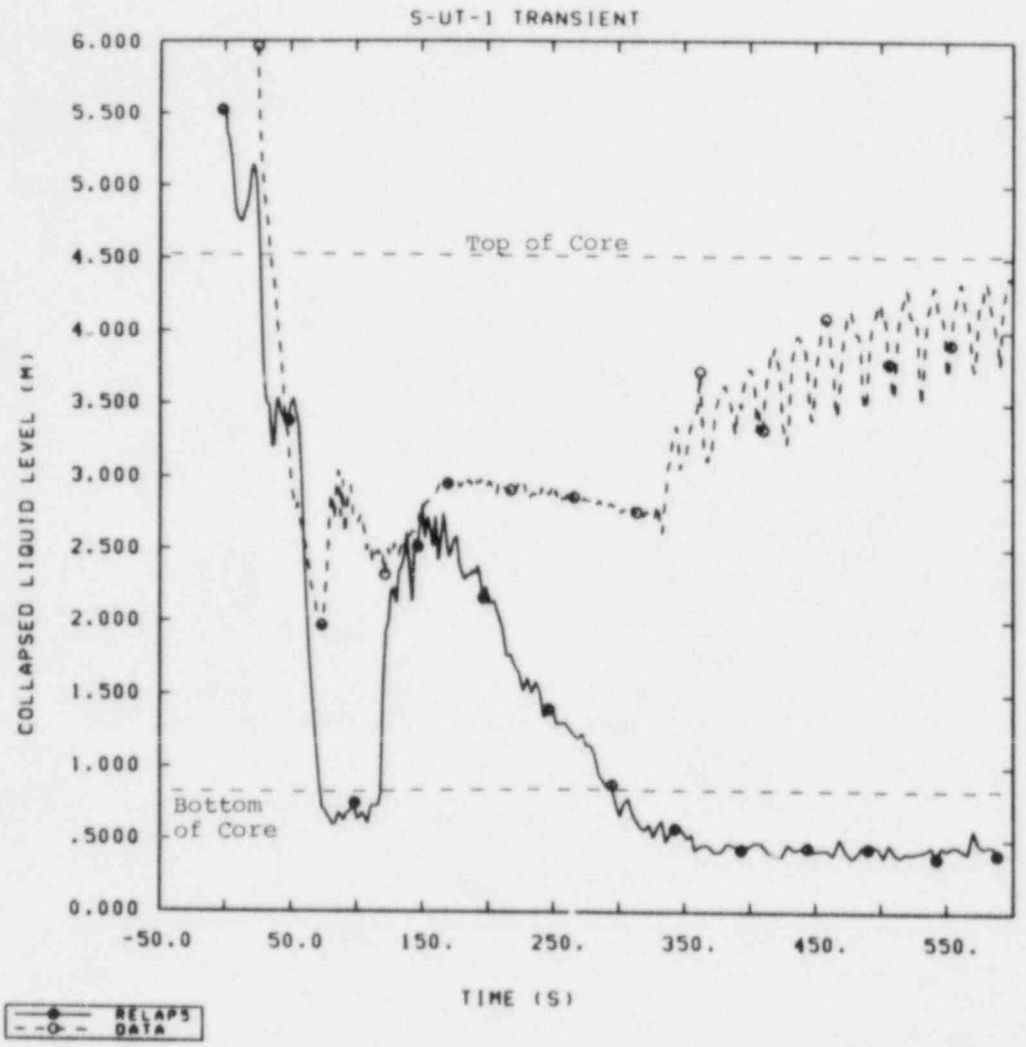

Figure 3.1.4 Comparison of Calculated and Measured Vessel Collapsed Liquid Levels for Test S-UT-1

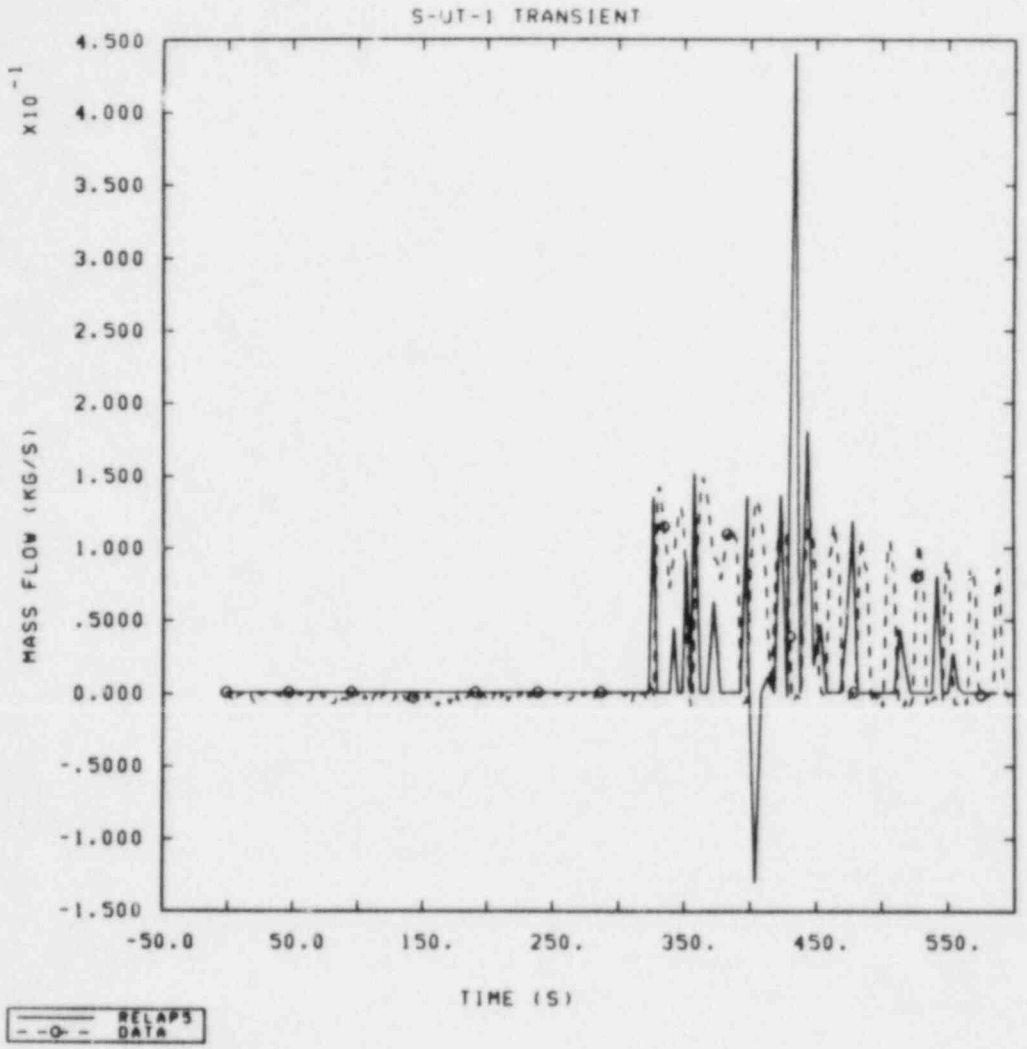

Figure 3.1.5 Comparison of Calculated and Measured Intact Loop Accumulator Mass Flow Rates for Test S-UT-1

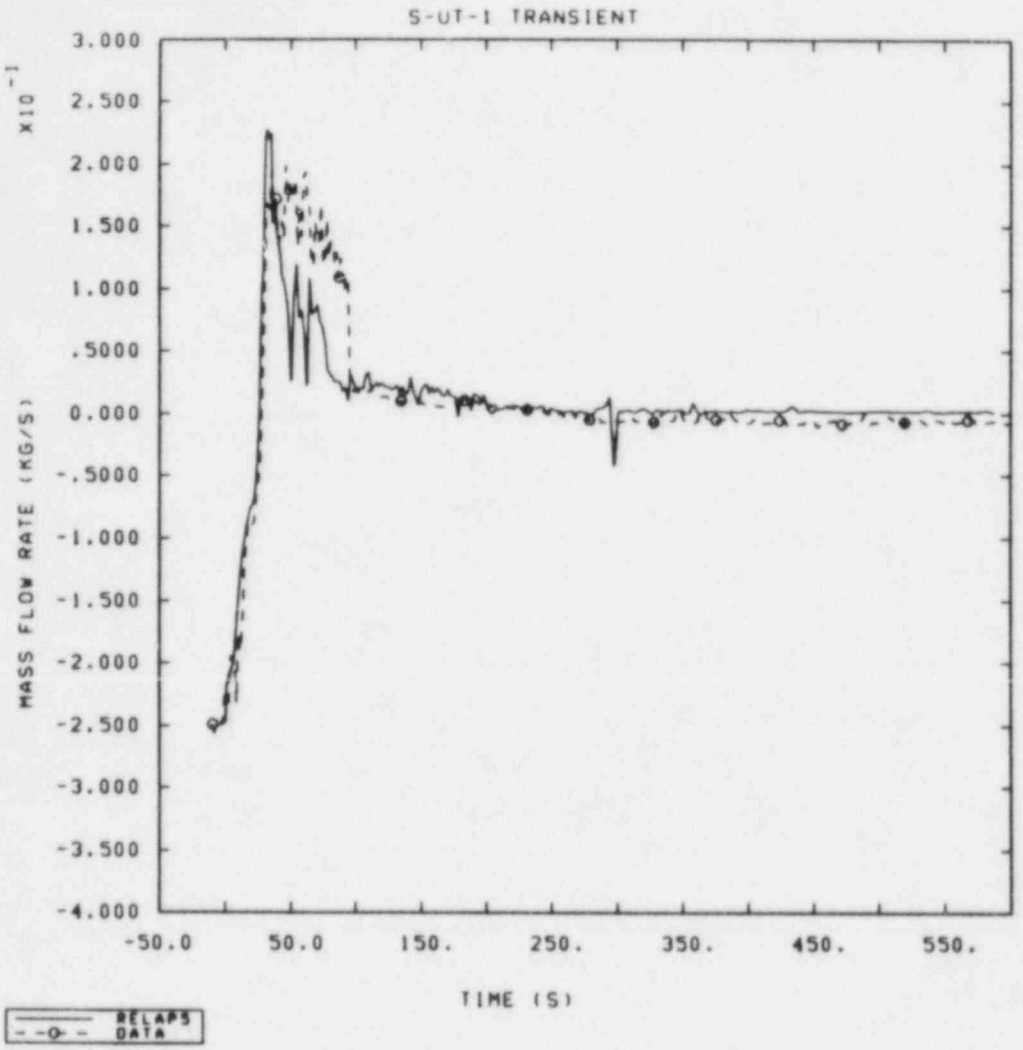

Figure 3.1.6 Comparison of Calculated and Measured Guide Tube Mass Flow Rates for Test S-UT-1

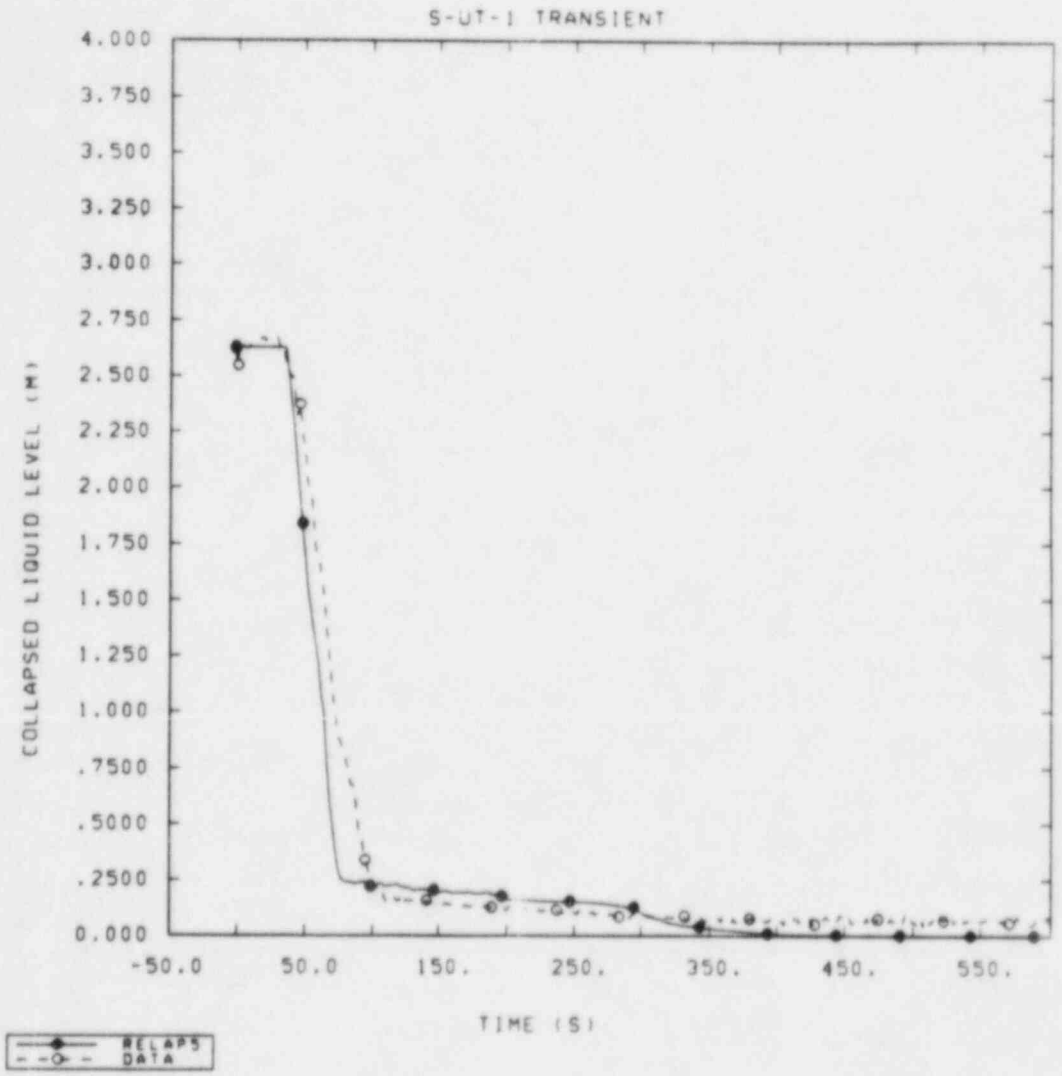

Figure 3.1.7 Comparison of Calculated and Measured Upper Head Collapsed Liquid Levels for Test S-UT-1

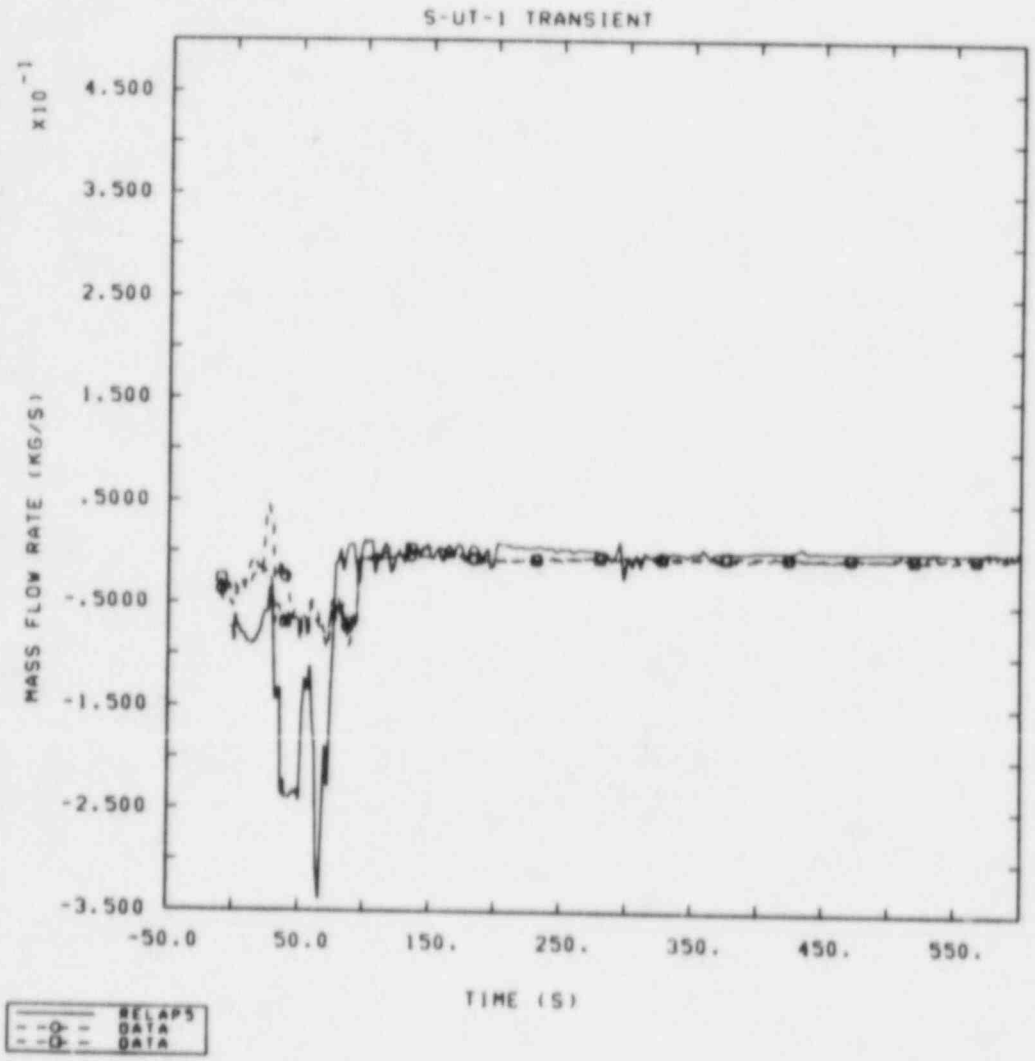

Figure 3.1.8 Comparison of Calculated and Measured Support Column Mass Flow Rates for Test-UT-1

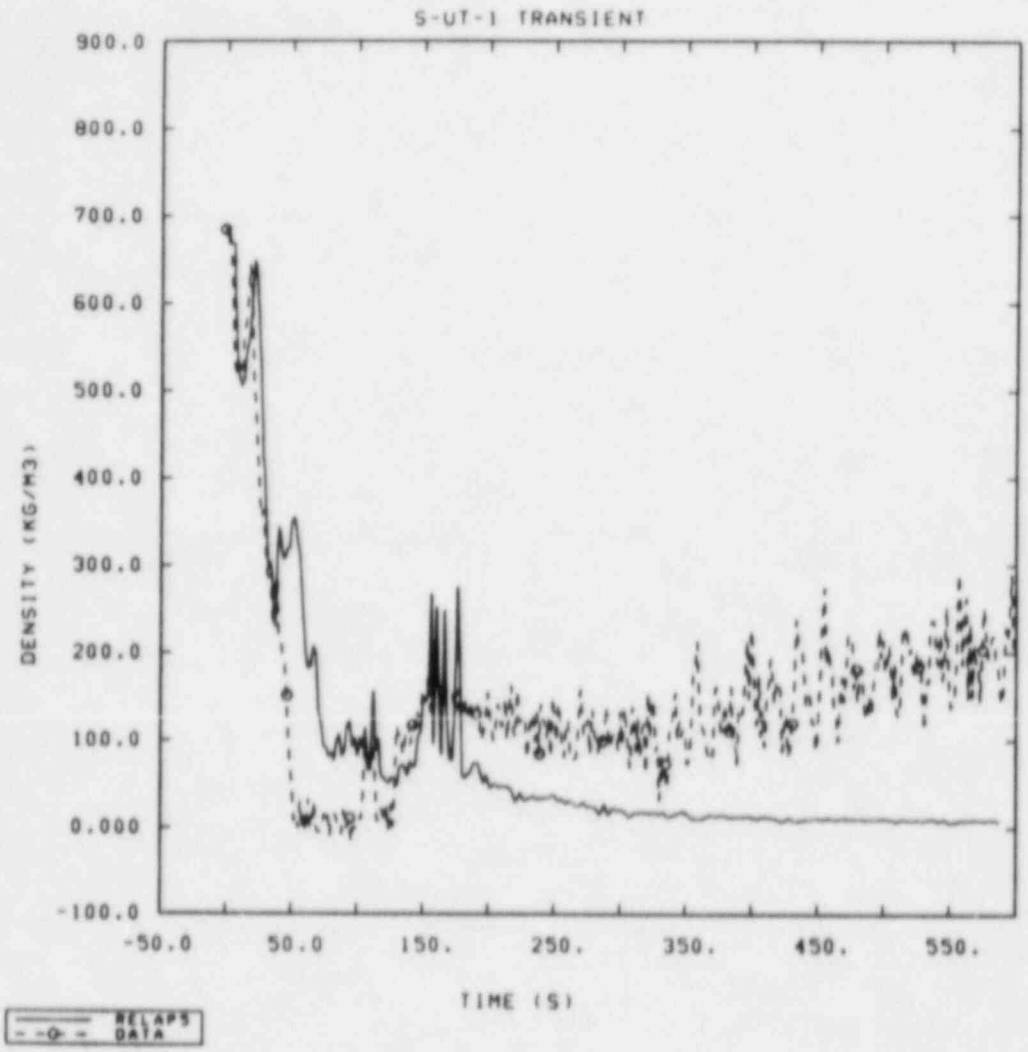

Figure 3.1.9 Comparison of Calculated and Measured Densities at the 2.53 m Core Elevation for Test S-UT-1

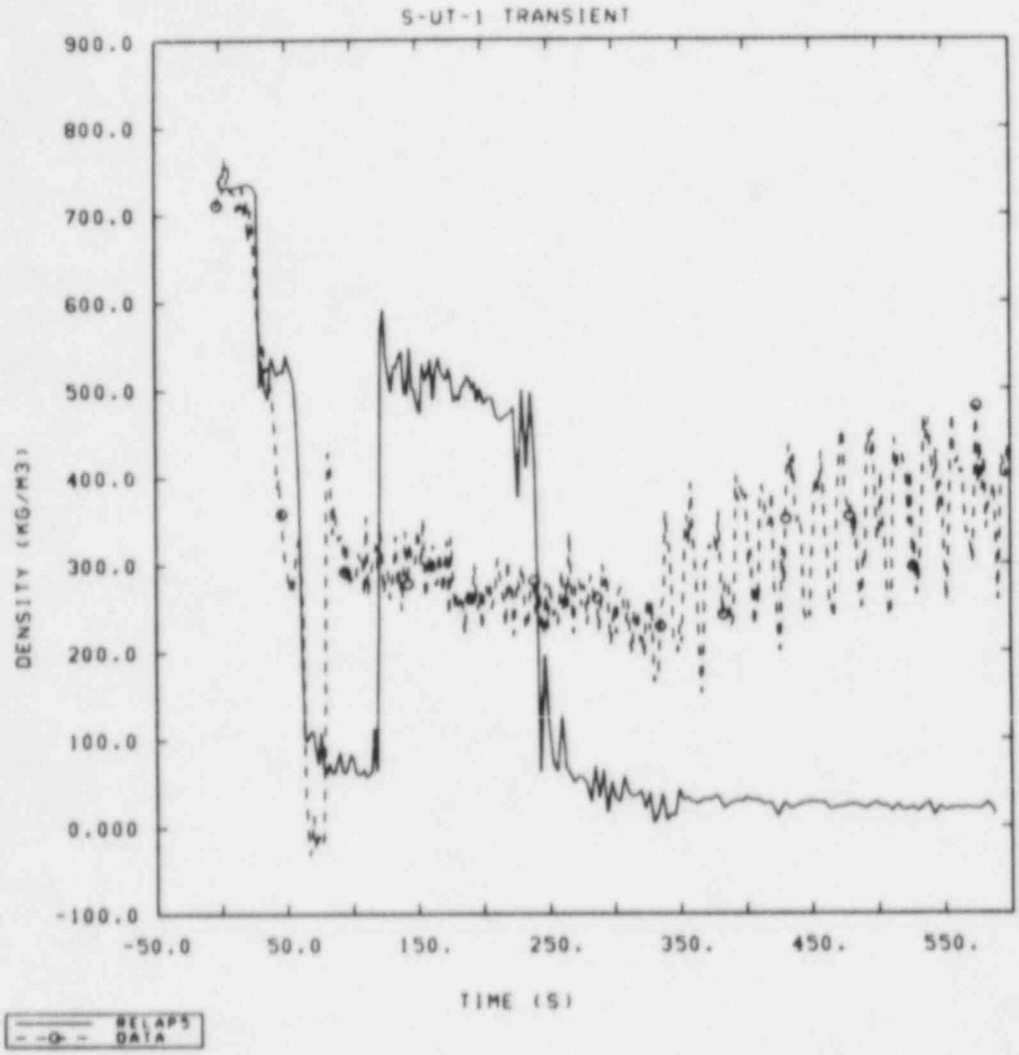

Figure 3.1.10 Comparison of Calculated and Measured Densities at the 1.13 m Core Elevation for Test S-UT-1

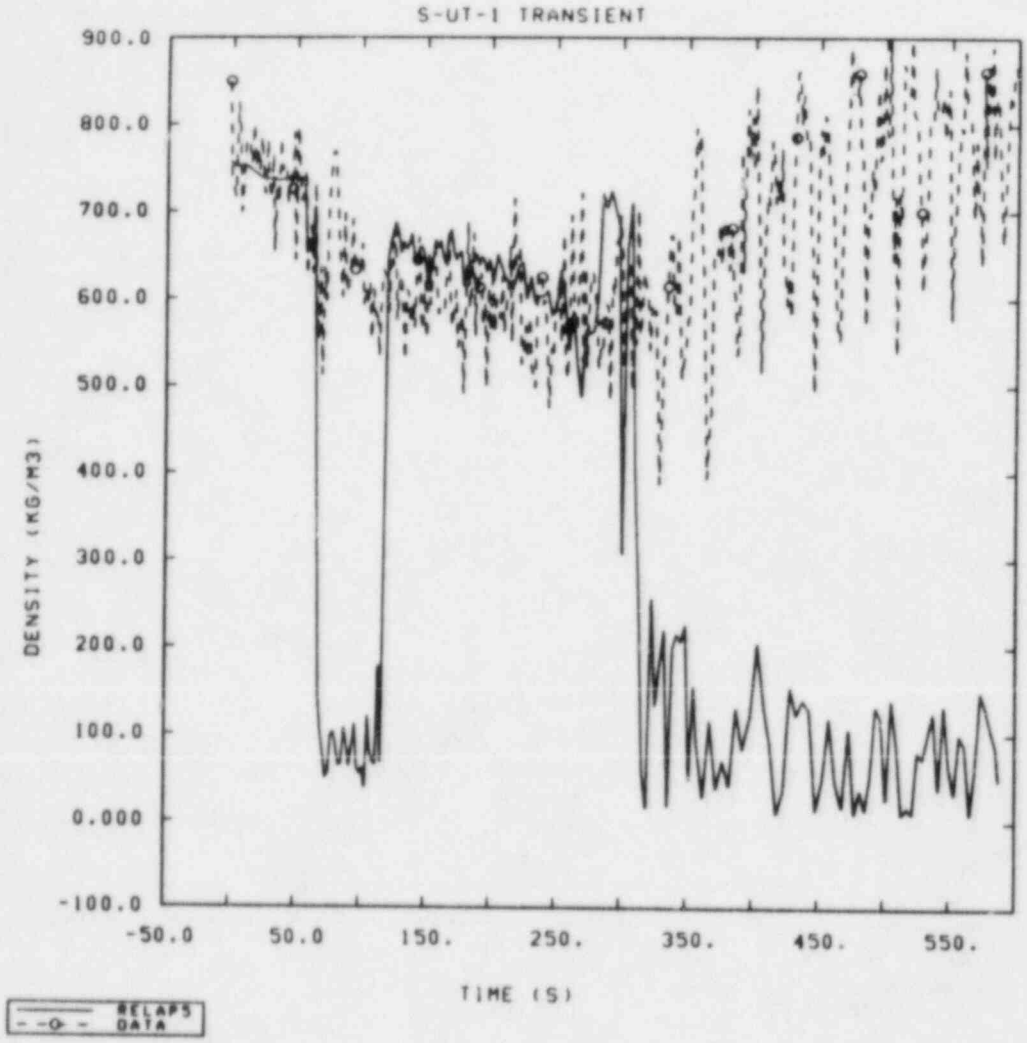

Figure 3.1.11 Comparison of Calculated and Measured Core Inlet Densities for Test S-UT-1

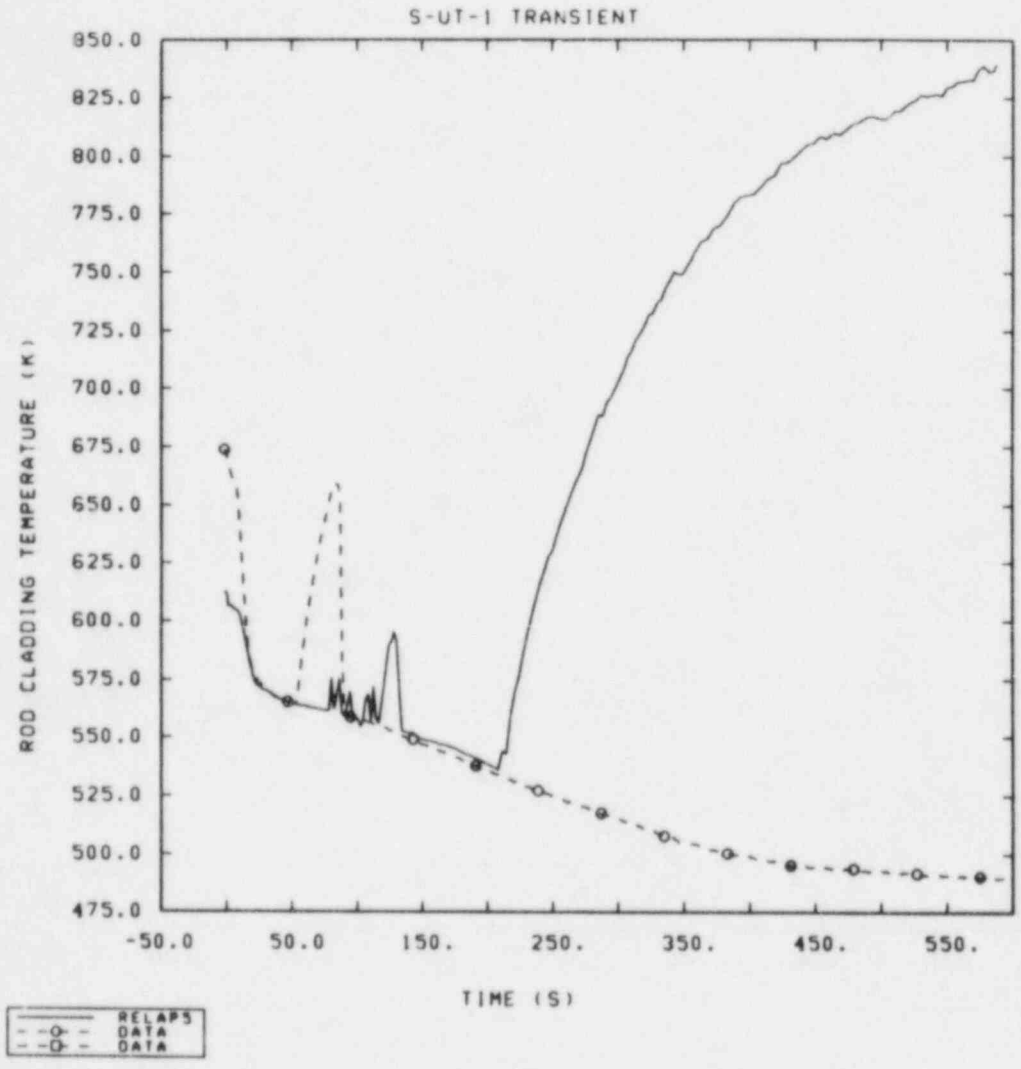

Figure 3.1.12 Comparison of Calculated and Measured Rod Cladding Temperatures at the 2.4 m to 3.0 m Core Elevation for Test S-UT-1

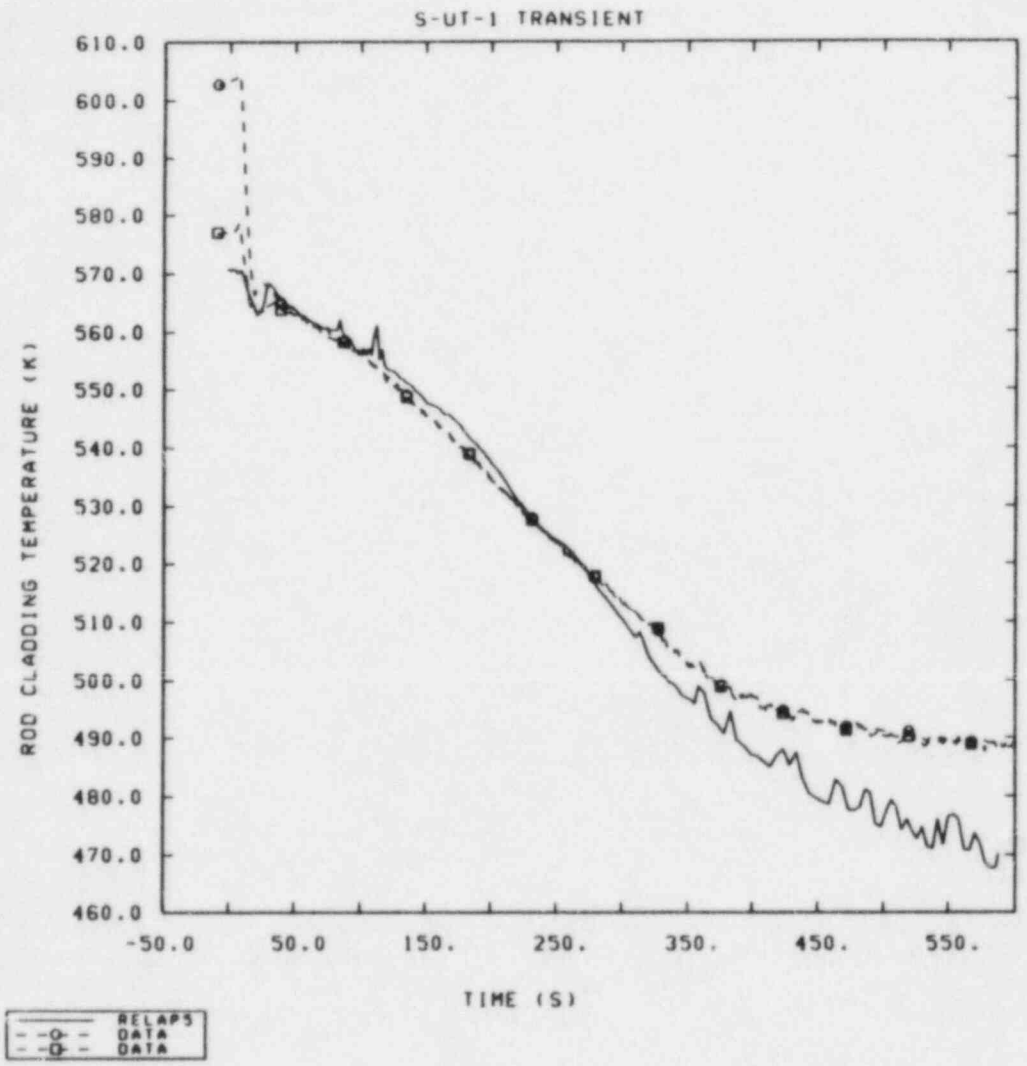

Figure 3.1.13 Comparison of Calculated and Measured Rod Cladding Temperatures at the 0.0 m to 0.6 m Core Elevation for Test S-UT-1

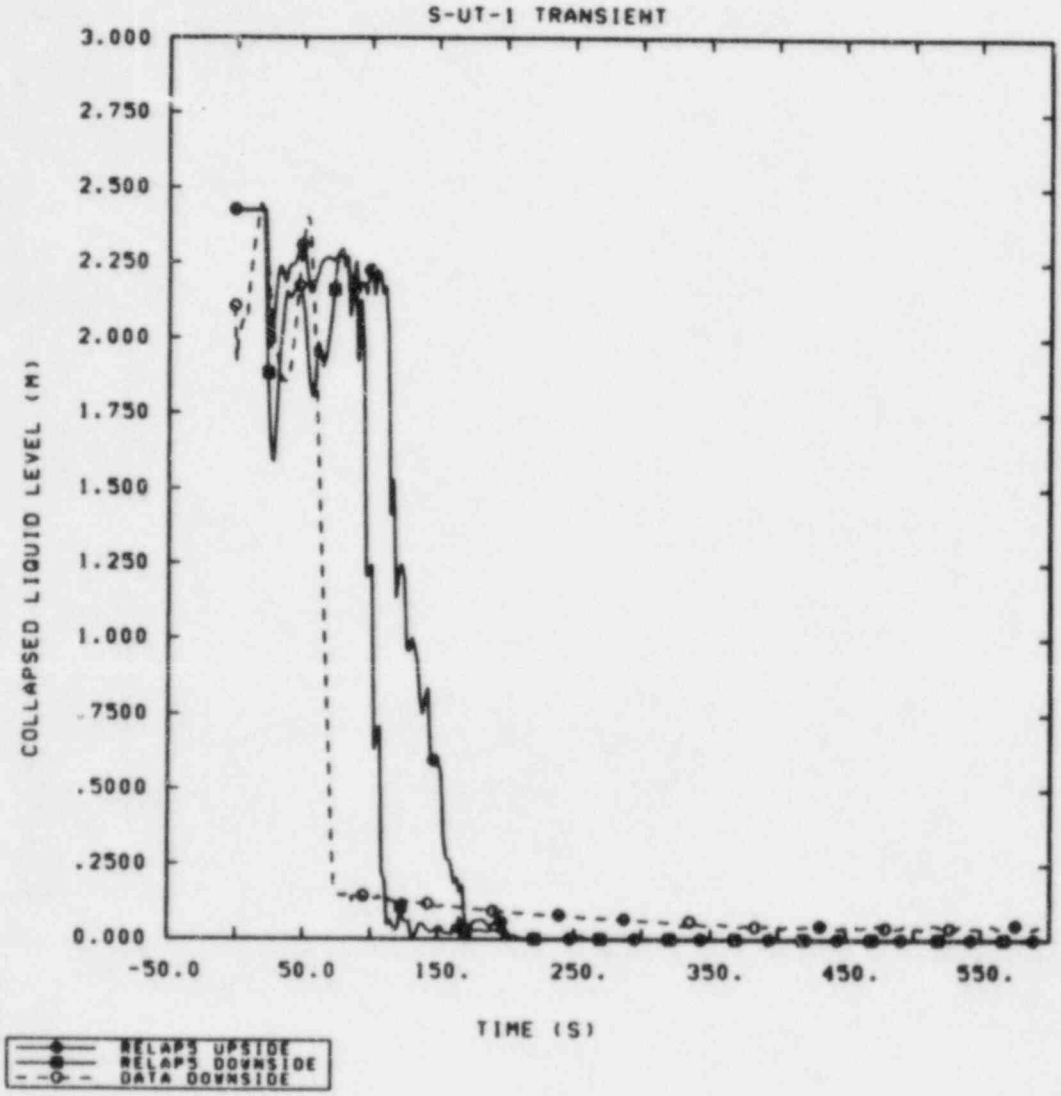

Figure 3.1.14 Comparison of Calculated and Measured Intact Loop Pump Suction Collapsed Liquid Levels for Test S-UT-1

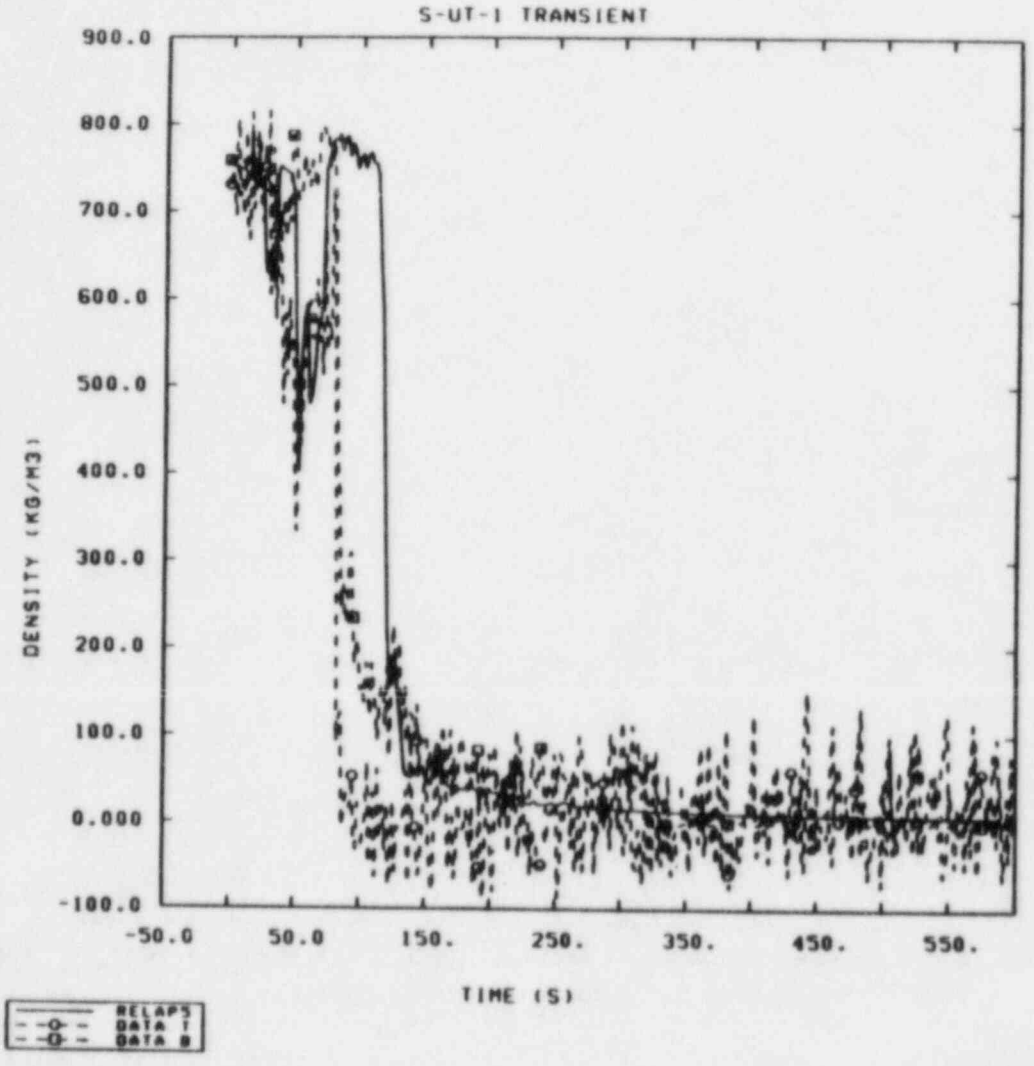

Figure 3.1.15 Comparison of Calculated and Measured Intact Loop Cold Leg Densities (Pump Side of ECC Injection Location) for Test S-UT-1

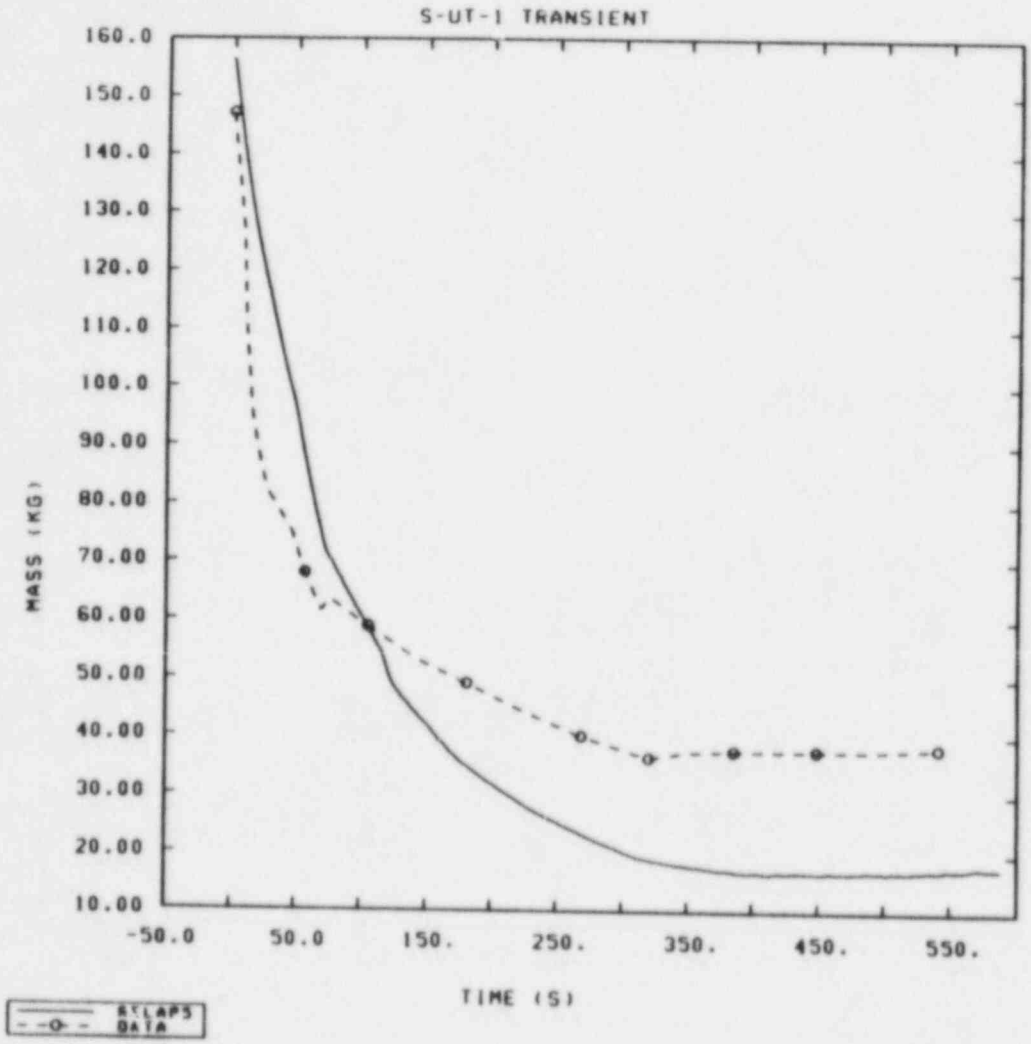

Figure 3.1.16 Comparison of Calculated and Measured Total Primary System Mass Inventories for Test S-UT-1

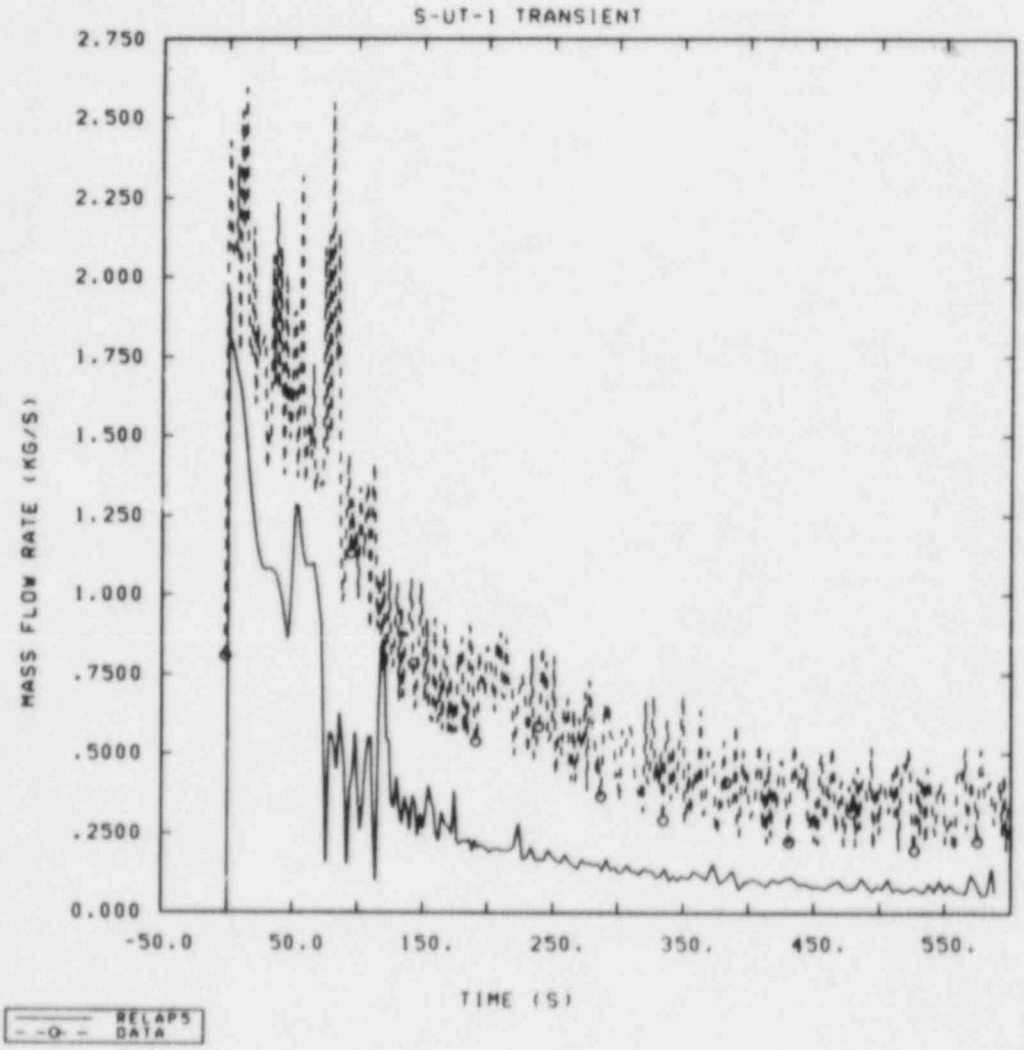

Figure 3.1.17 Comparison of Calculated and Measured Break Mass Flow Rates for Test S-UT-1

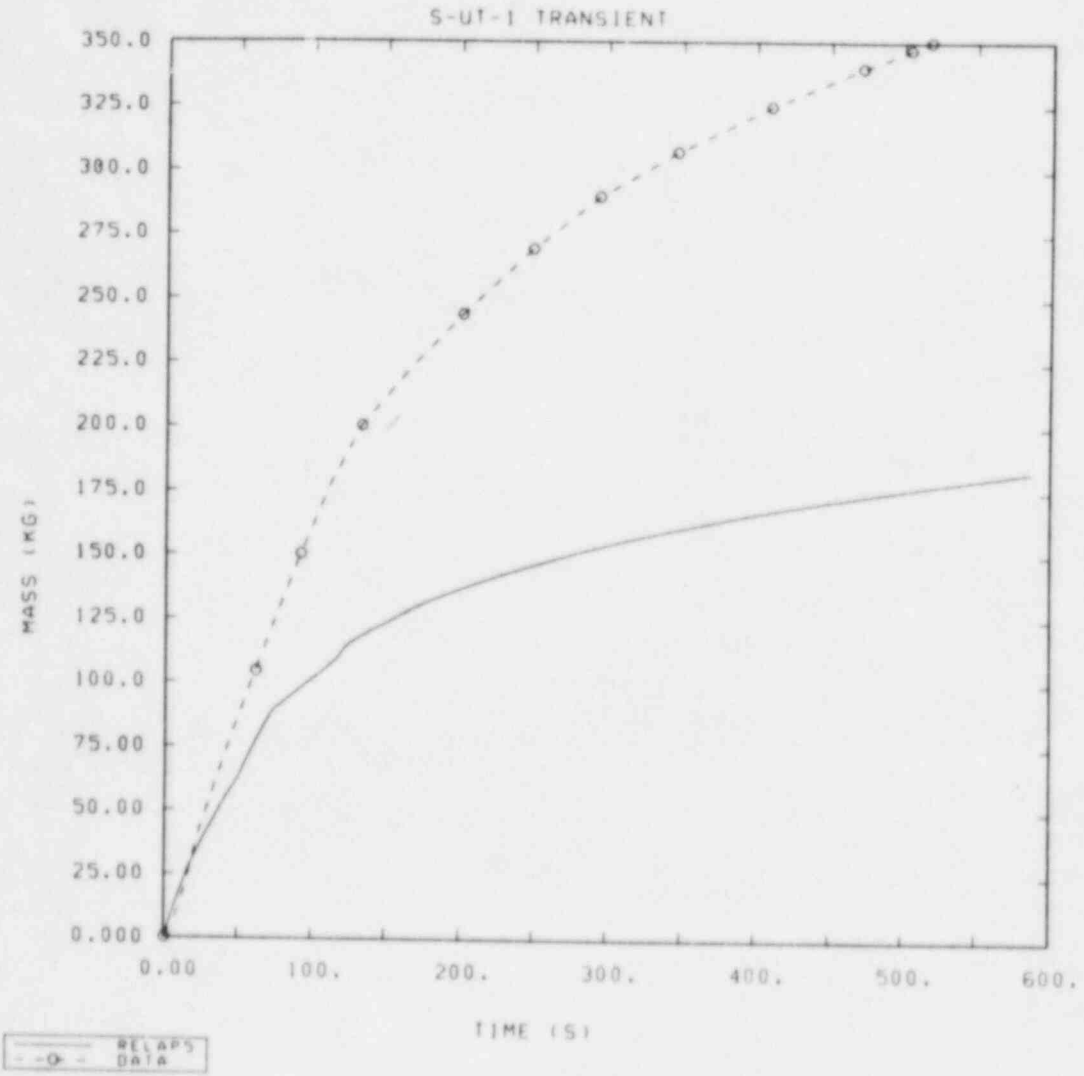

Figure 3.1.18 Comparison of Calculated and Measured Integrated Mass Flows for Test S-UT-1

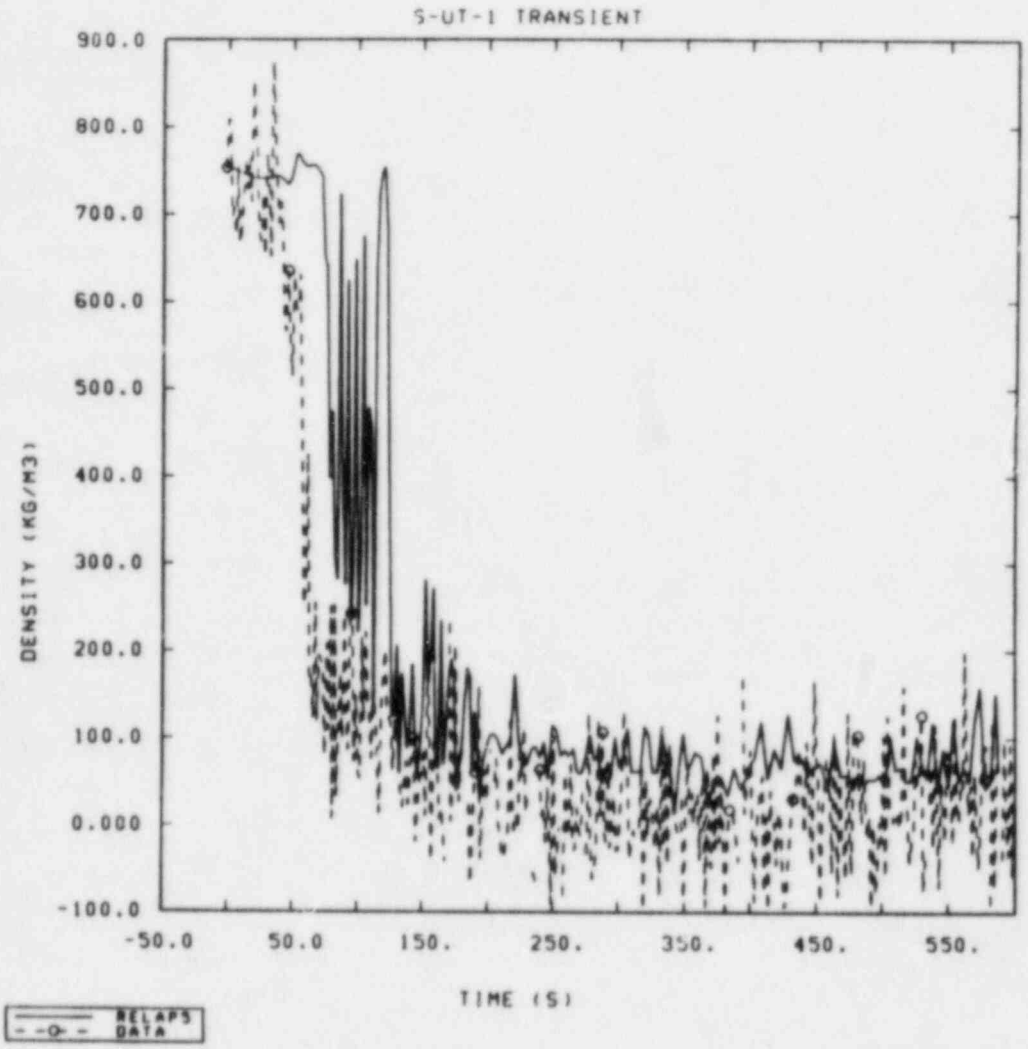

Figure 3.1.19 Comparison of Calculated and Measured Broken Loop Cold Leg Densities (Pump Side of Break) for Test S-UT-1

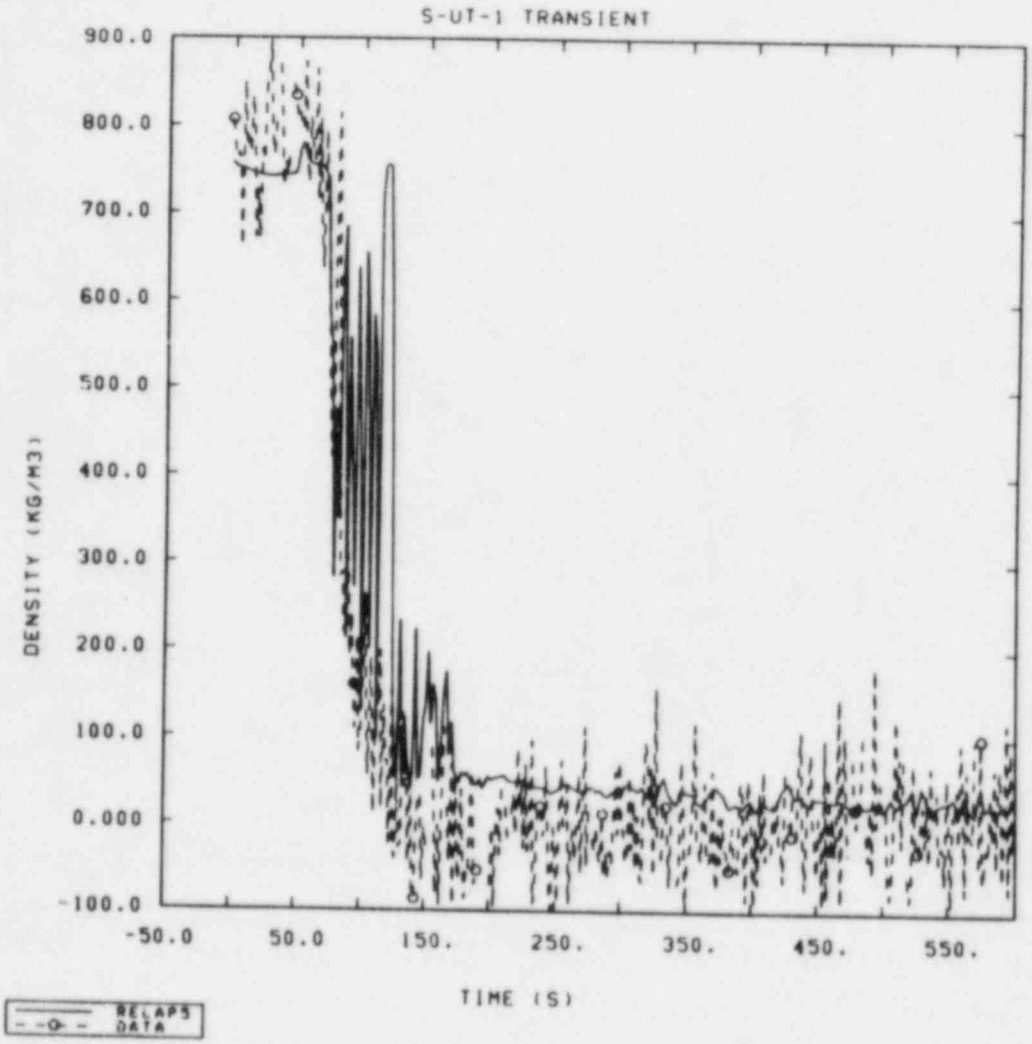

Figure 3.1.20 Comparison of Calculated and Measured Broken Loop Cold Leg Densities (Vessel Side of Break) for Test S-UT-1

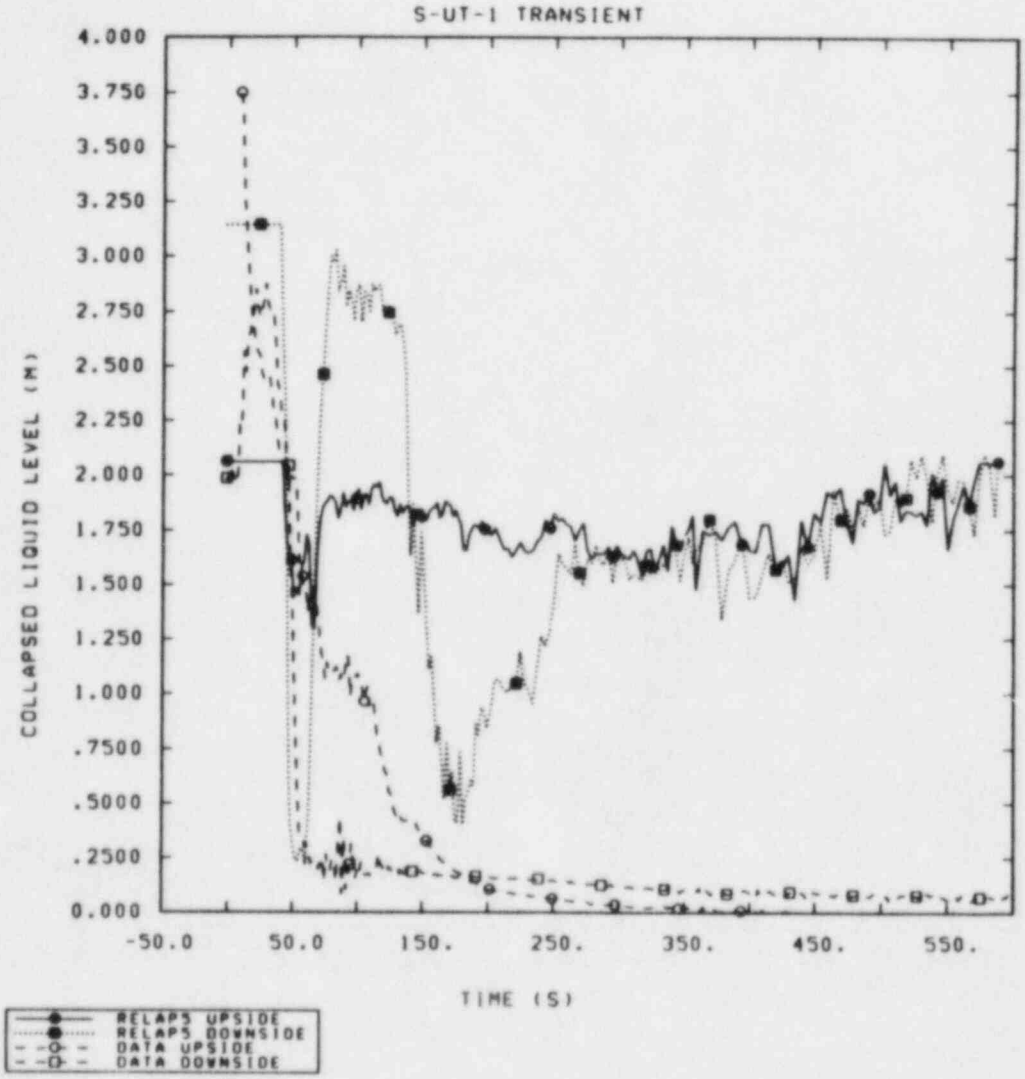

Figure 3.1.21 Comparison of Calculated and Measured Broken Loop Suction Collapsed Liquid Levels for Test S-UT-1

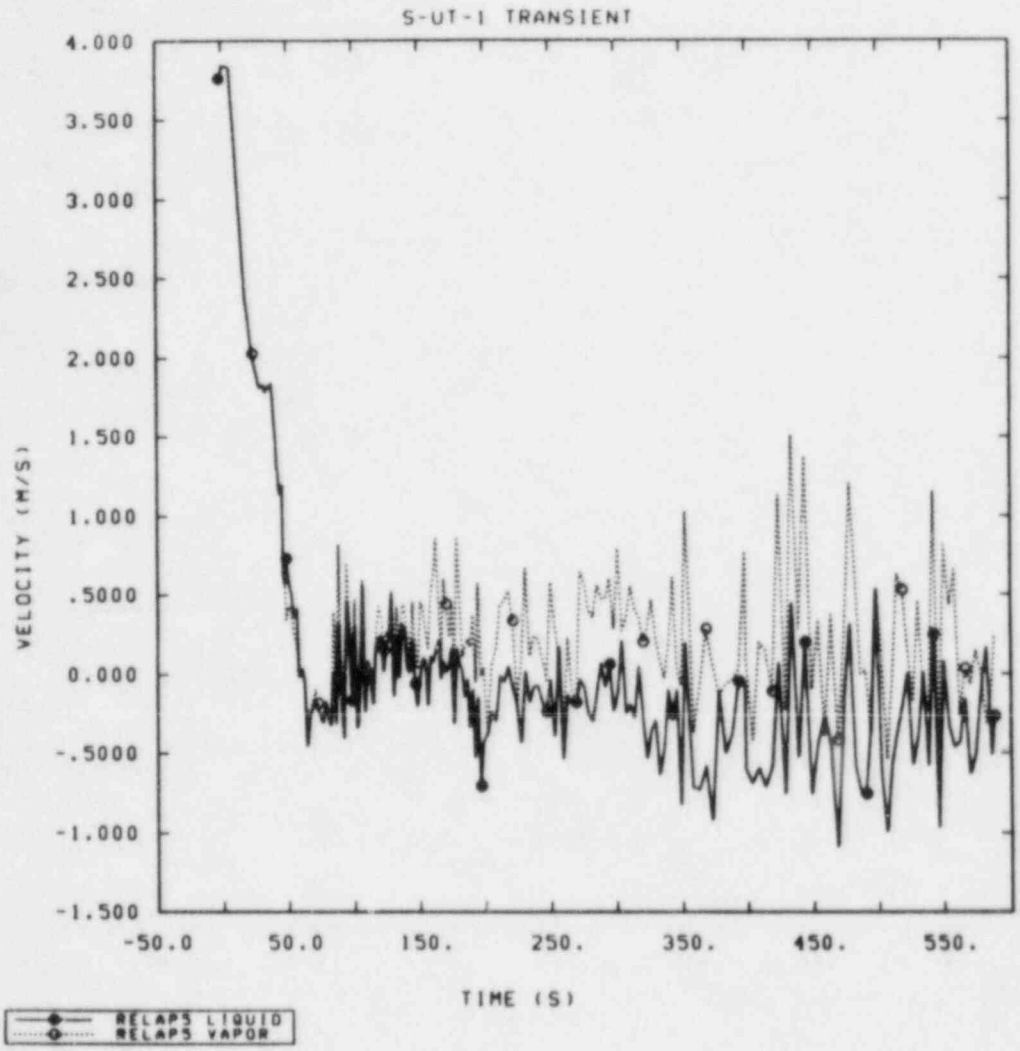

Figure 3.1.22 Calculated Liquid and Vapor Velocities at the Broken Loop Pump Outlet for Test S-UT-1

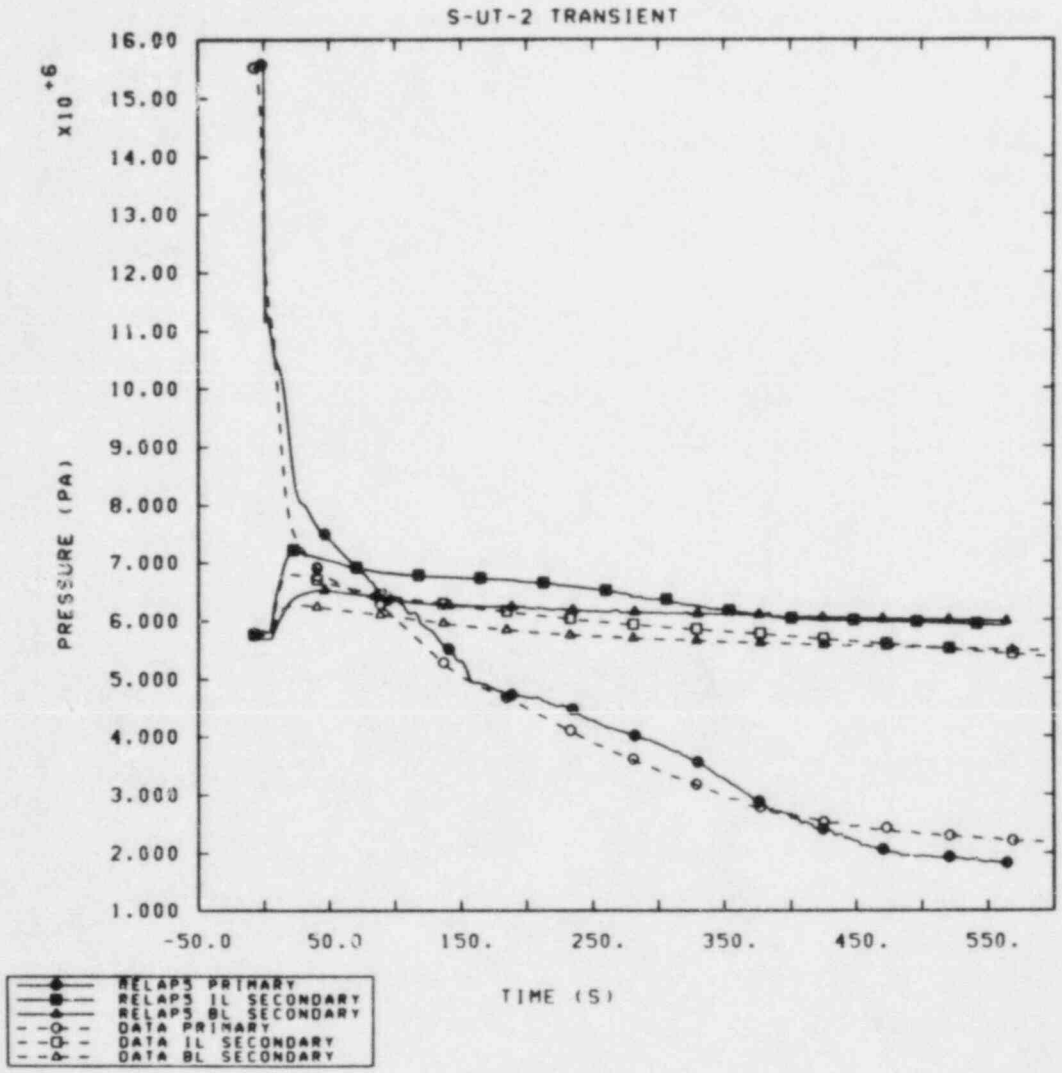

Figure 3.2.1 Comparison of Calculated and Measured Primary and Intact and Broken Loop Steam Generator Secondary Pressures for Test S-UT-2

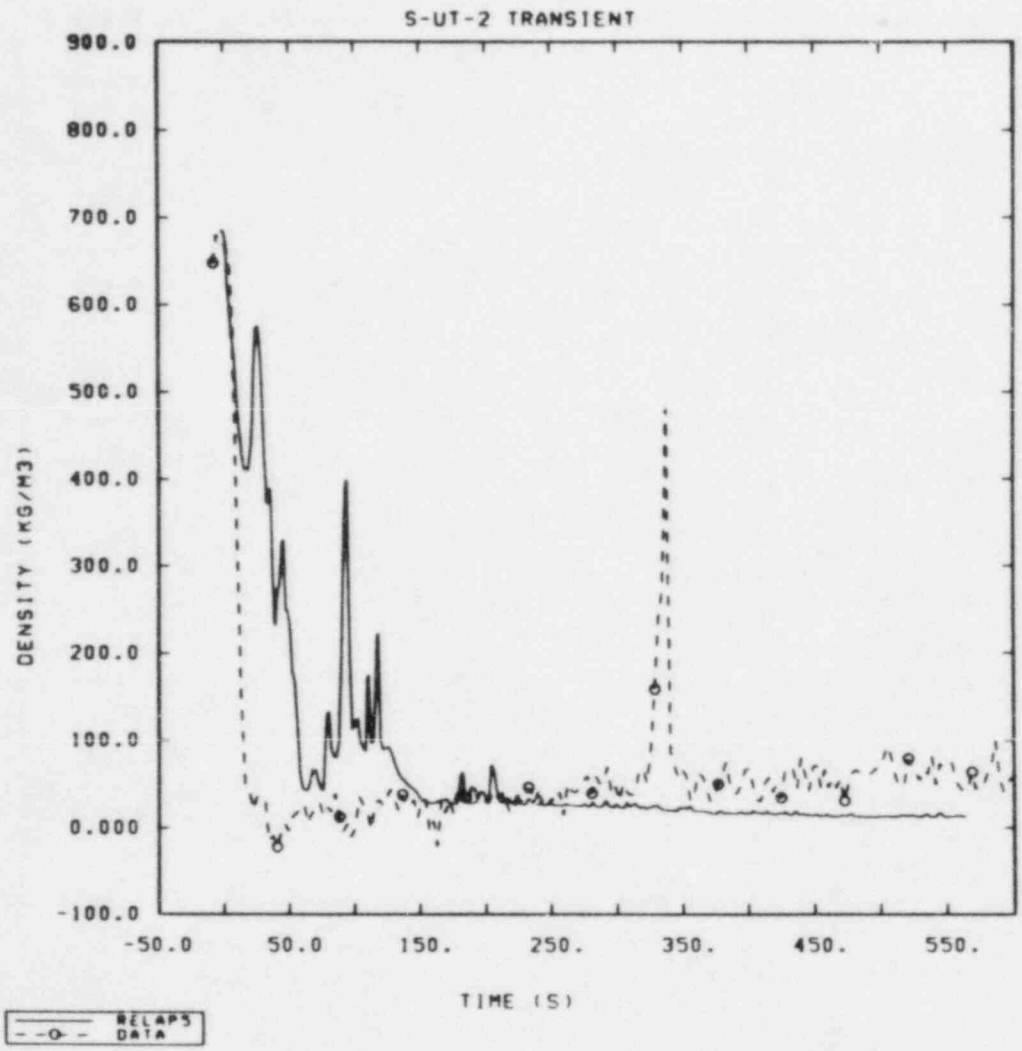

Figure 3.2.2 Comparison of Calculated and Measured Broken Loop Hot Leg Densities for Test S-UT-2

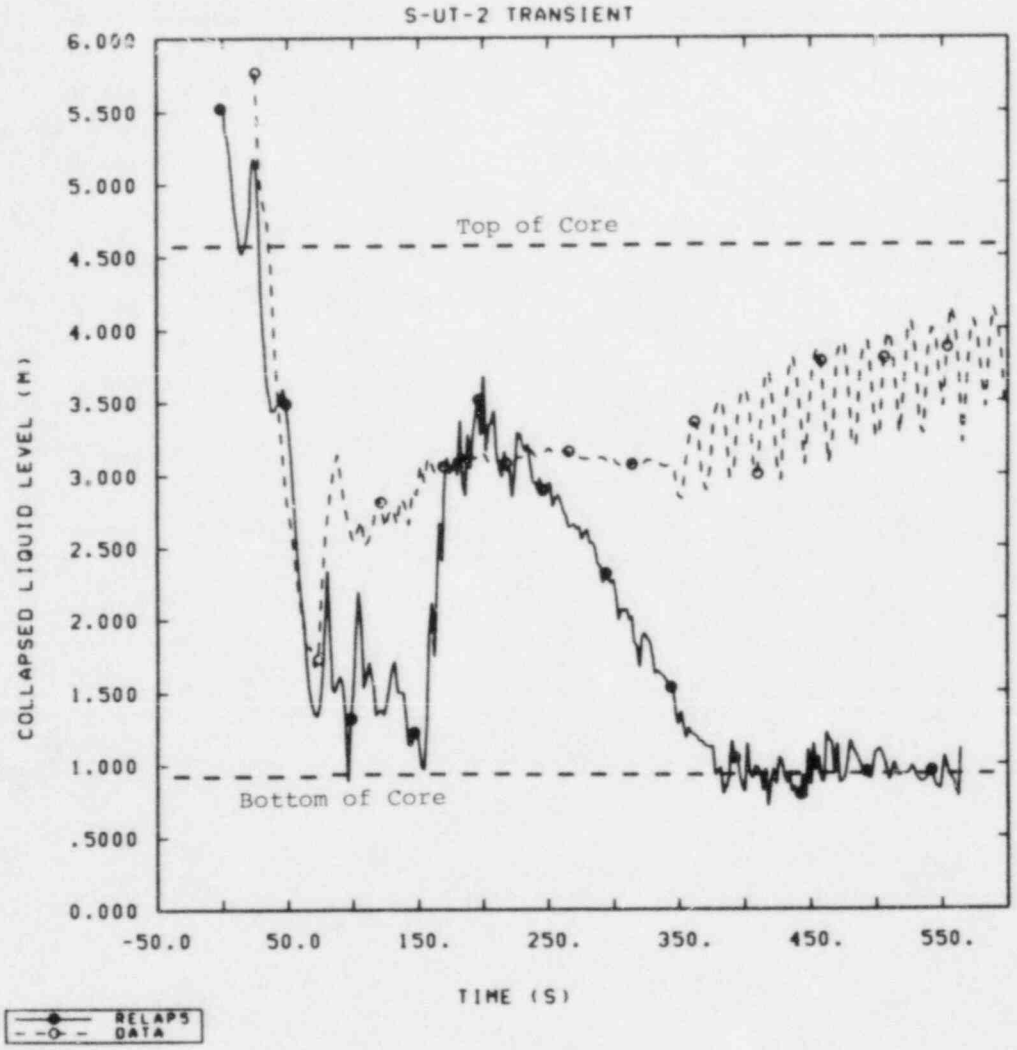

Figure 3.2.3 Comparison of Calculated and Measured Vessel Collapsed Liquid Levels for Test S-UT-2

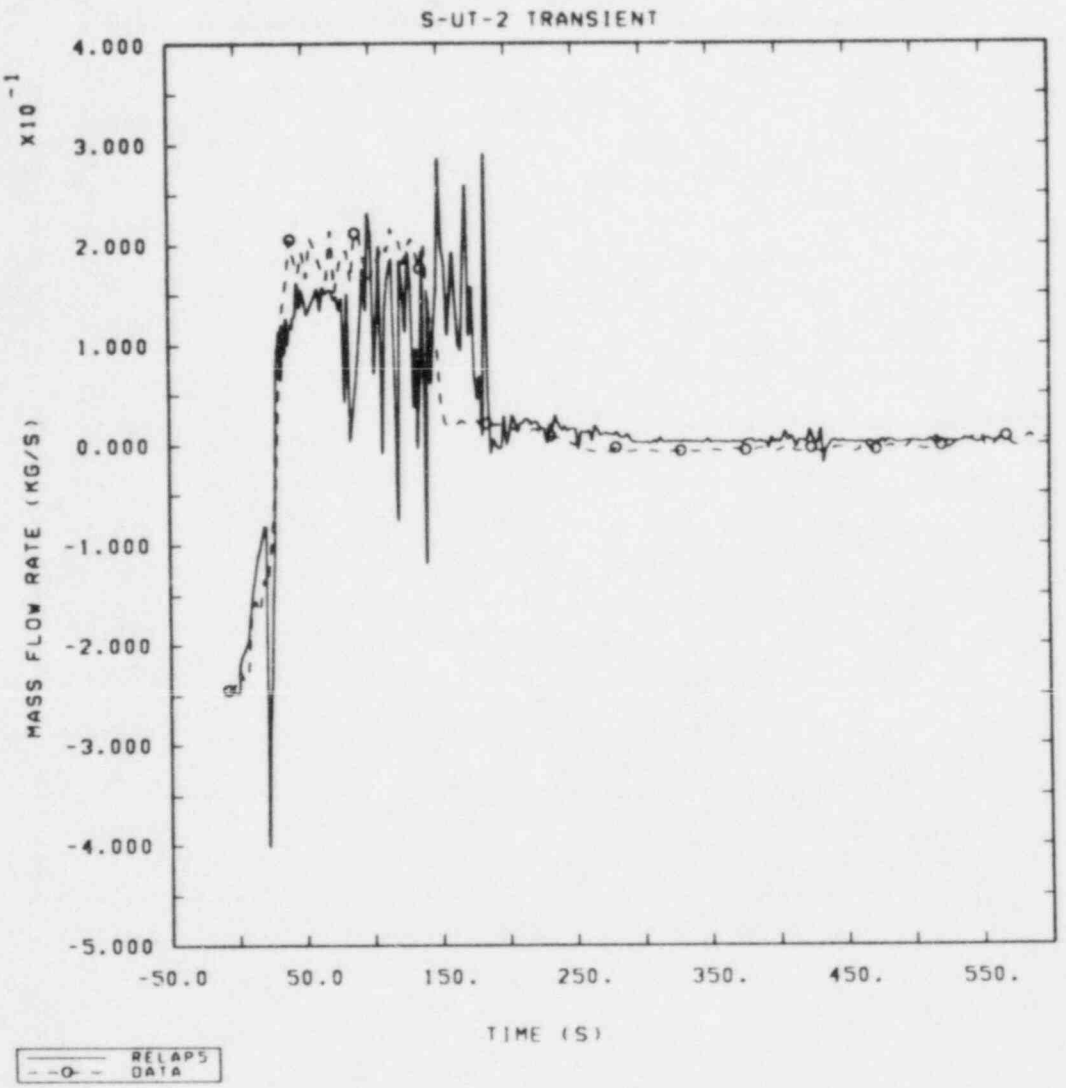

Figure 3.2.4 Comparison of Calculated and Measured Guide Tube Mass Flow Rates for Test S-UT-2

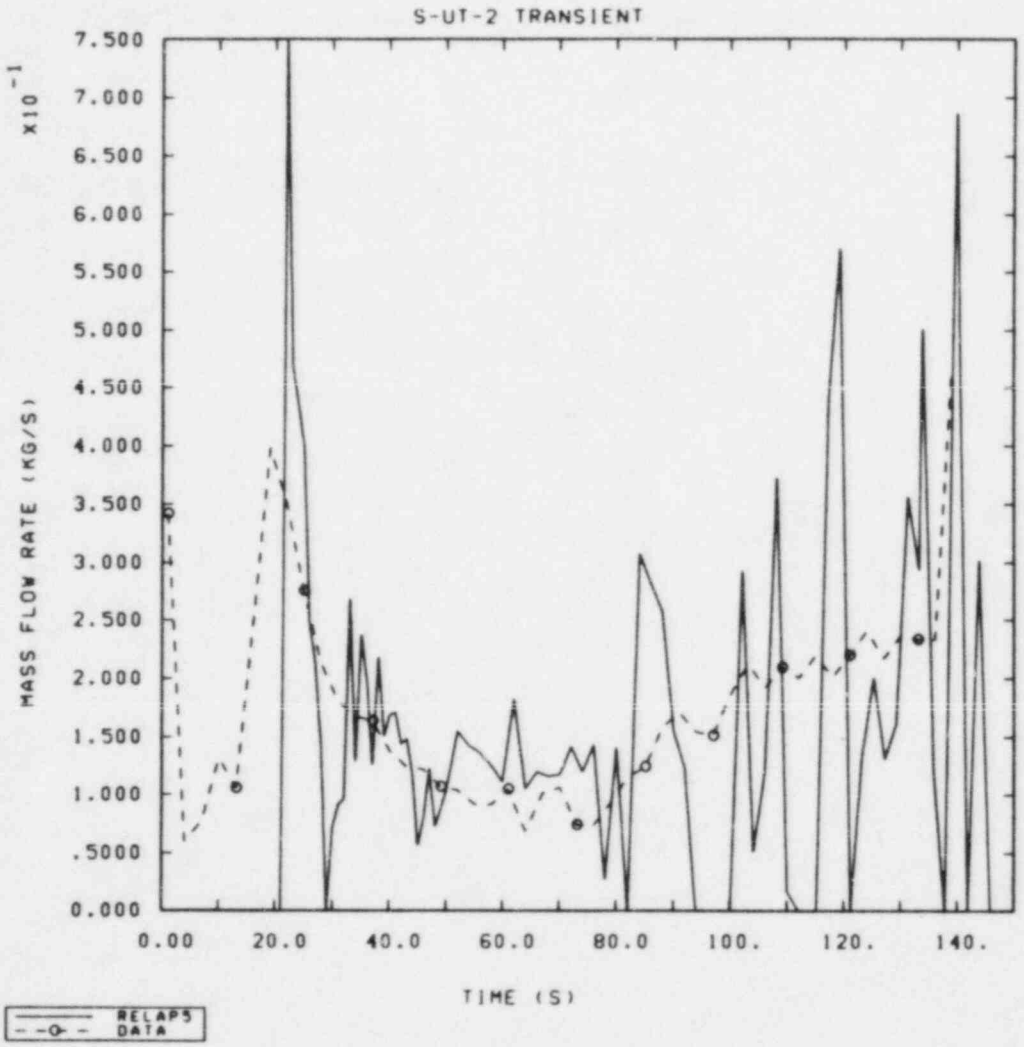

Figure 3.2.5 Comparison of Calculated and Measured UHI Accumulator Mass Flow Rates for Test S-UT-2

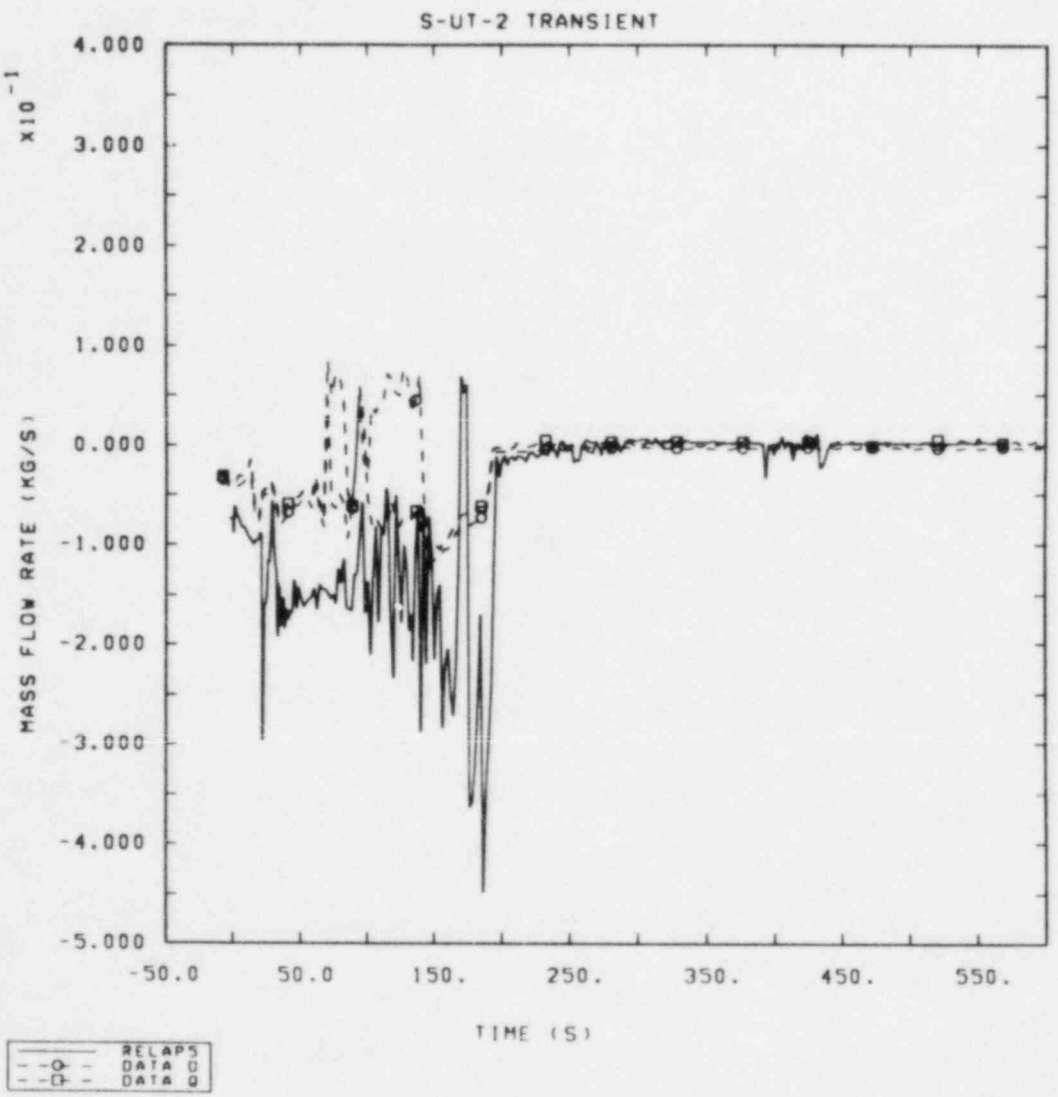

Figure 3.2.6 Comparison of Calculated and Measured Support Column Mass Flow Rates for Test S-UT-2

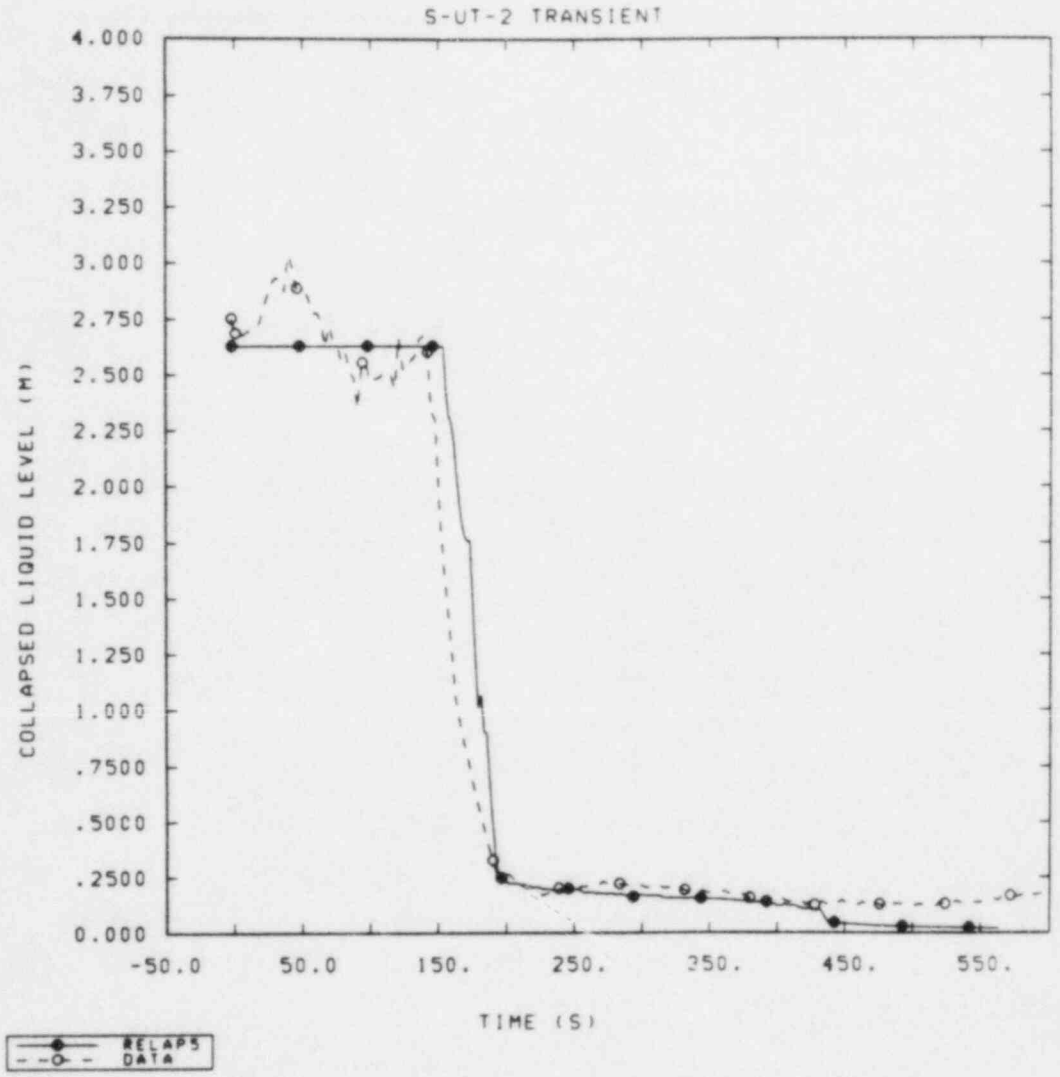

Figure 3.2.7 Comparison of Calculated and Measured Upper Head Collapsed Liquid Levels for Test S-UT-2

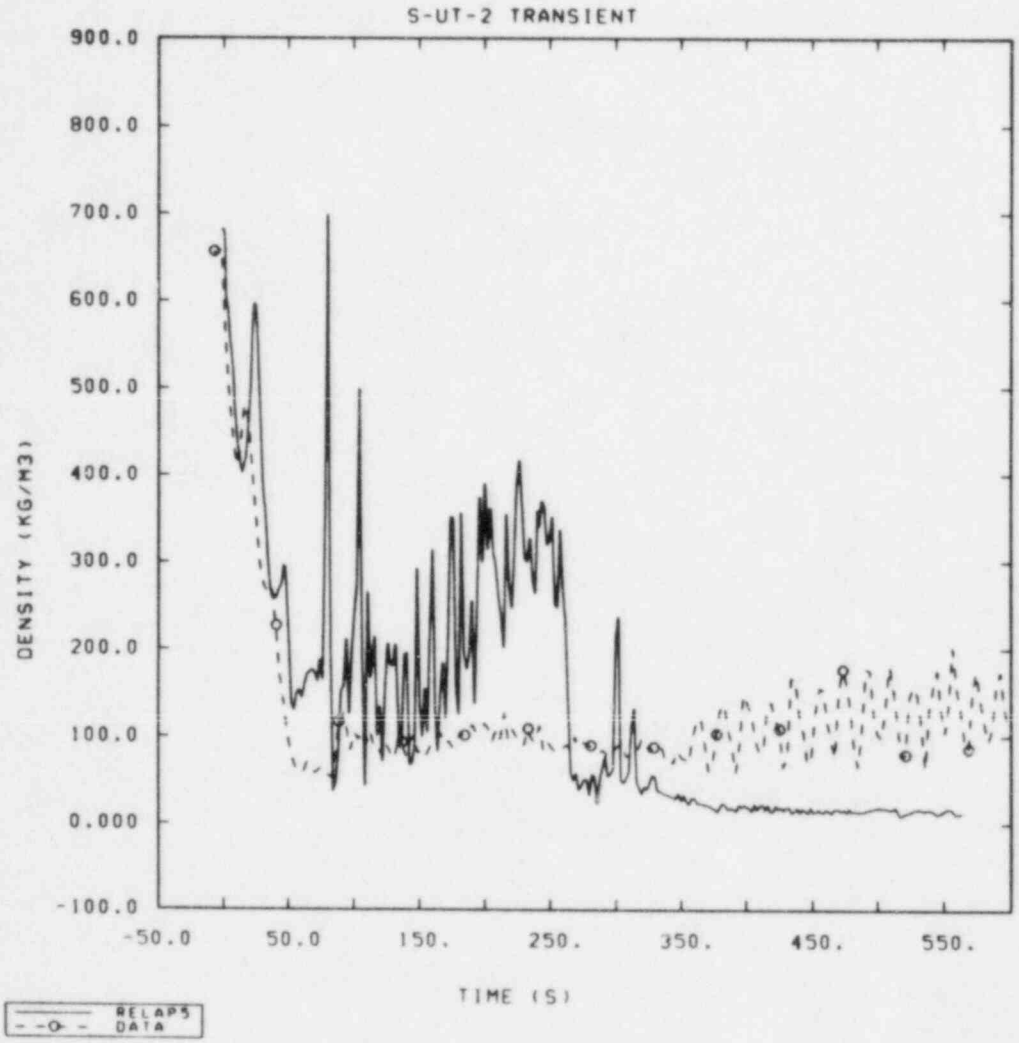

Figure 3.2.8 Comparison of Calculated and Measured Densities at the 3.42 m Core Elevation for Test S-UT-2

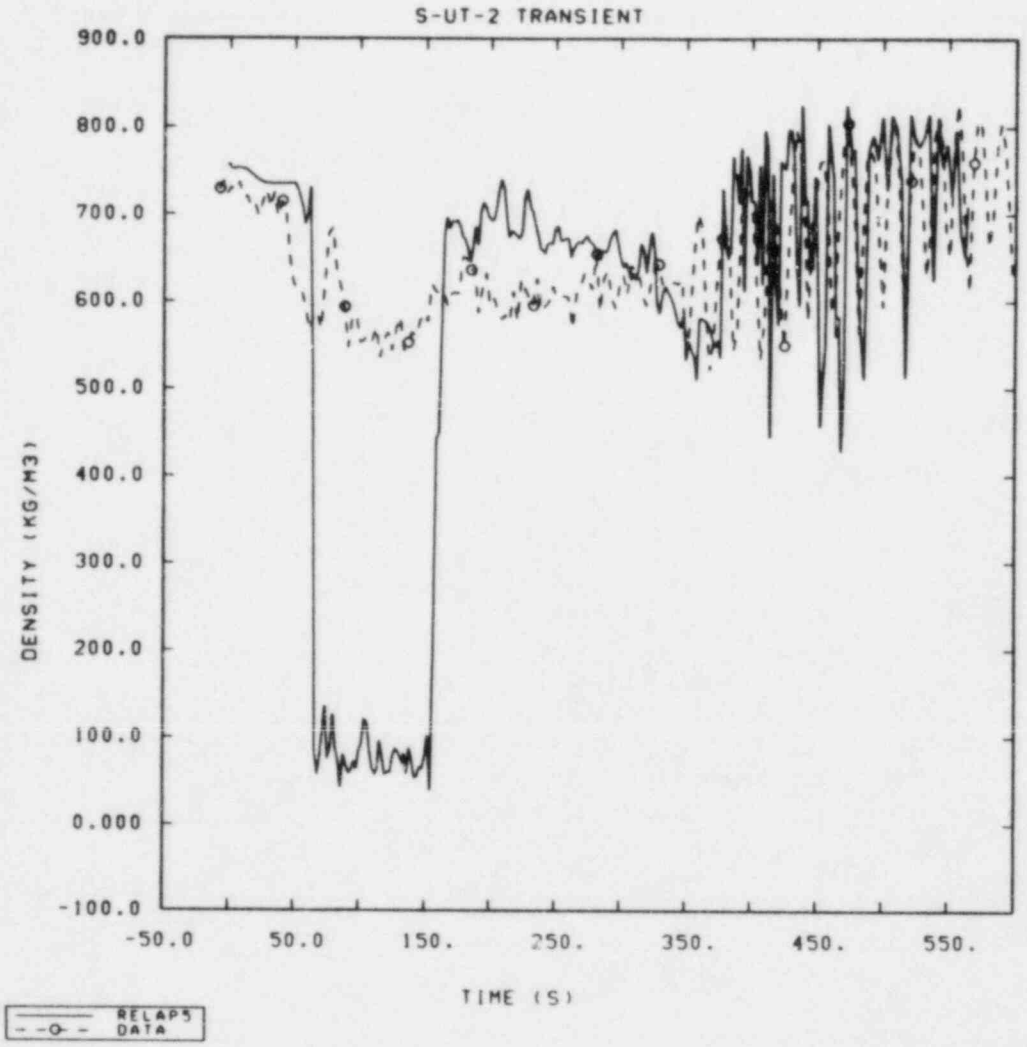

Figure 3.2.9 Comparison of Calculated and Measured Densities at the Core Inlet for Test S-UT-2

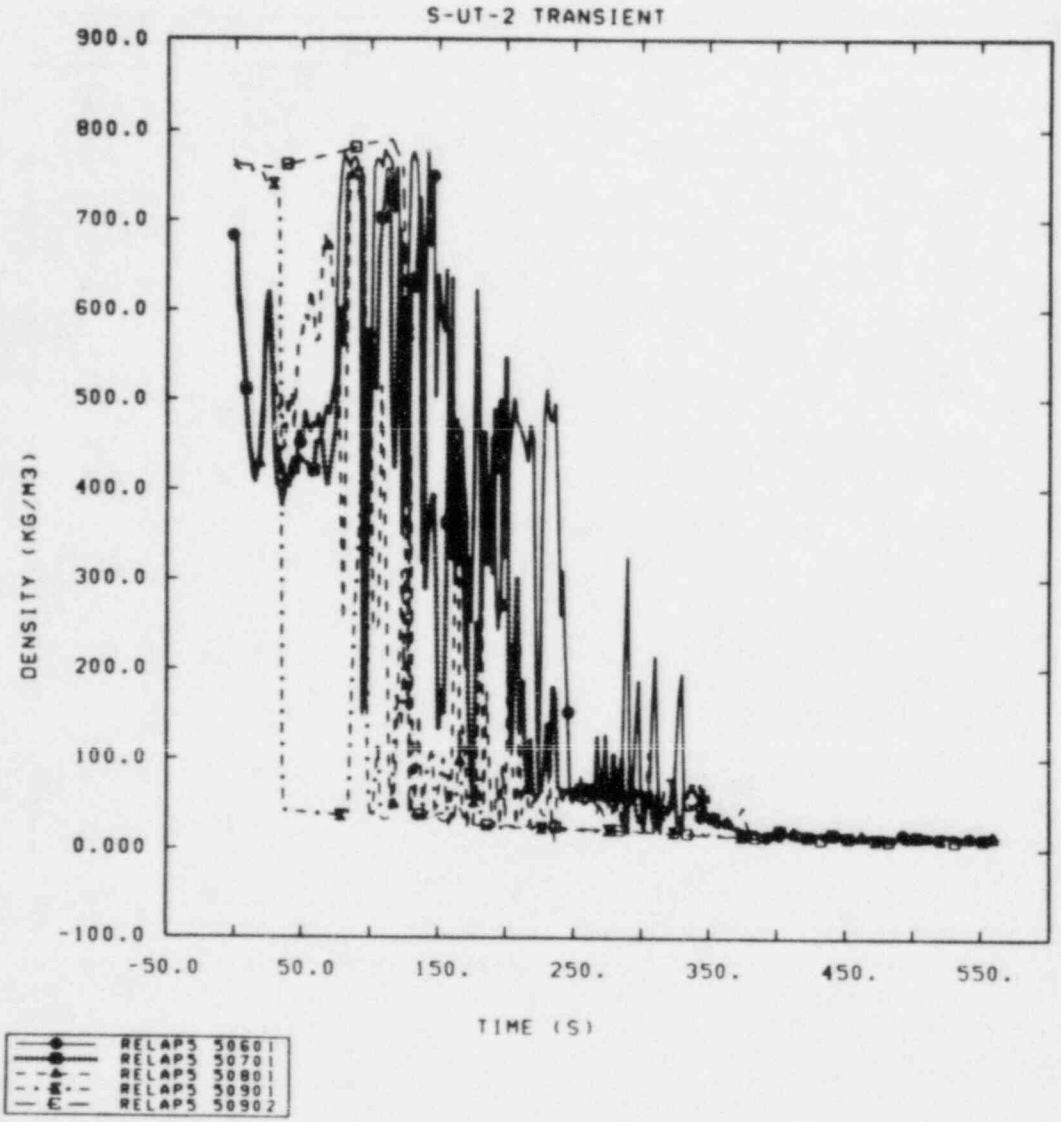

Figure 3.2.10 Calculated Upper Core and Upper Plenum Densities for Test S-UT-2

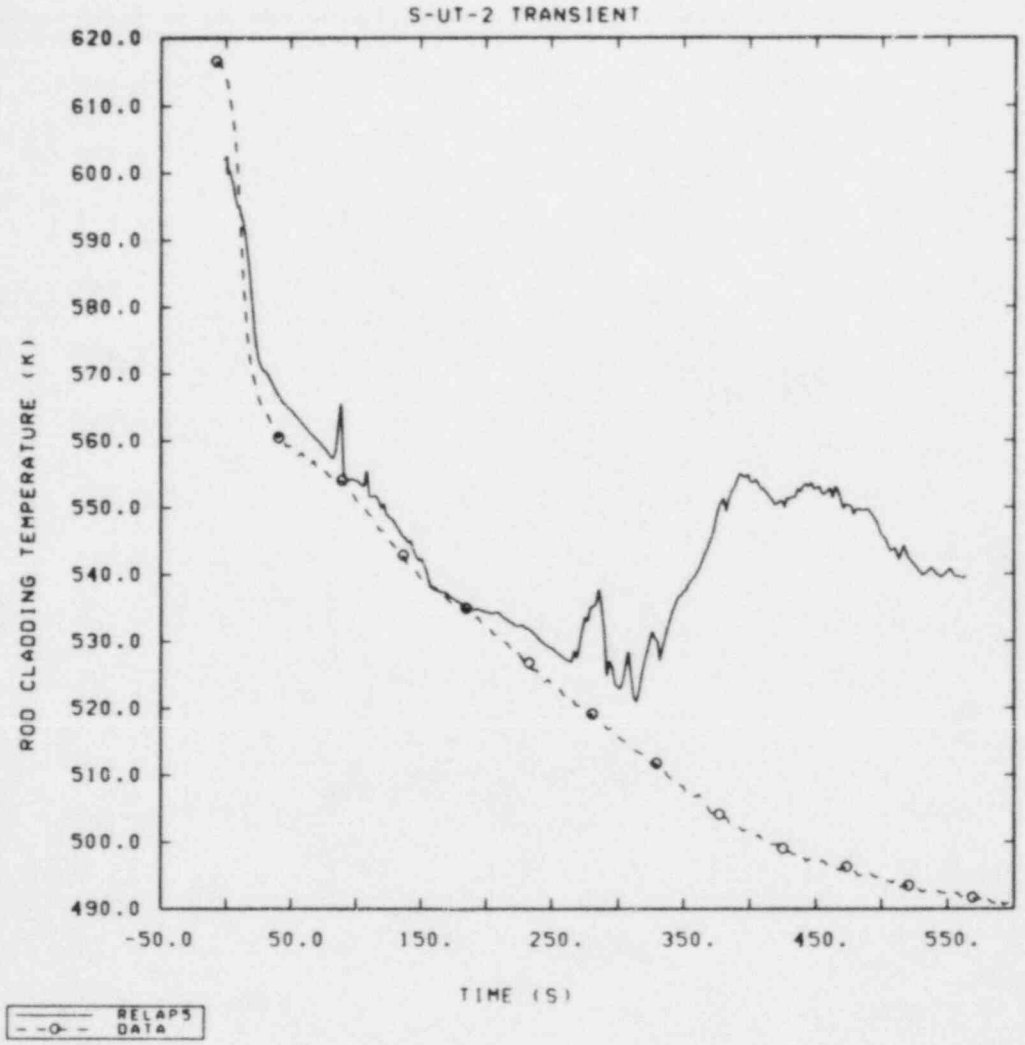

Figure 3.2.11 Comparison of Calculated and Measured Rod Cladding Temperatures at the 3.0 m to 3.6 m Core Elevation for Test S-UT-2

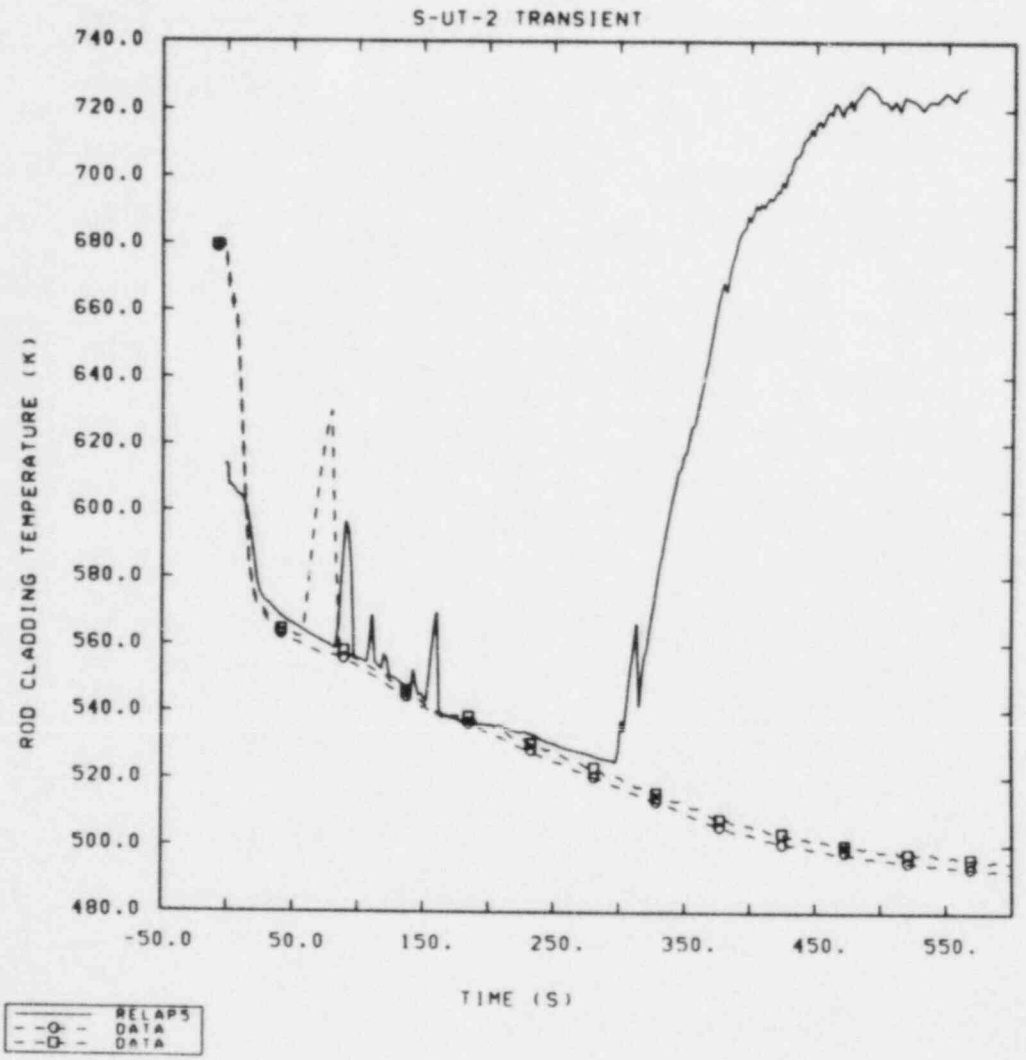

Figure 3.2.12 Comparison of Calculated and Measured Rod Cladding Temperatures at the 2.1 m to 2.4 m Core Elevation for Test S-UT-1

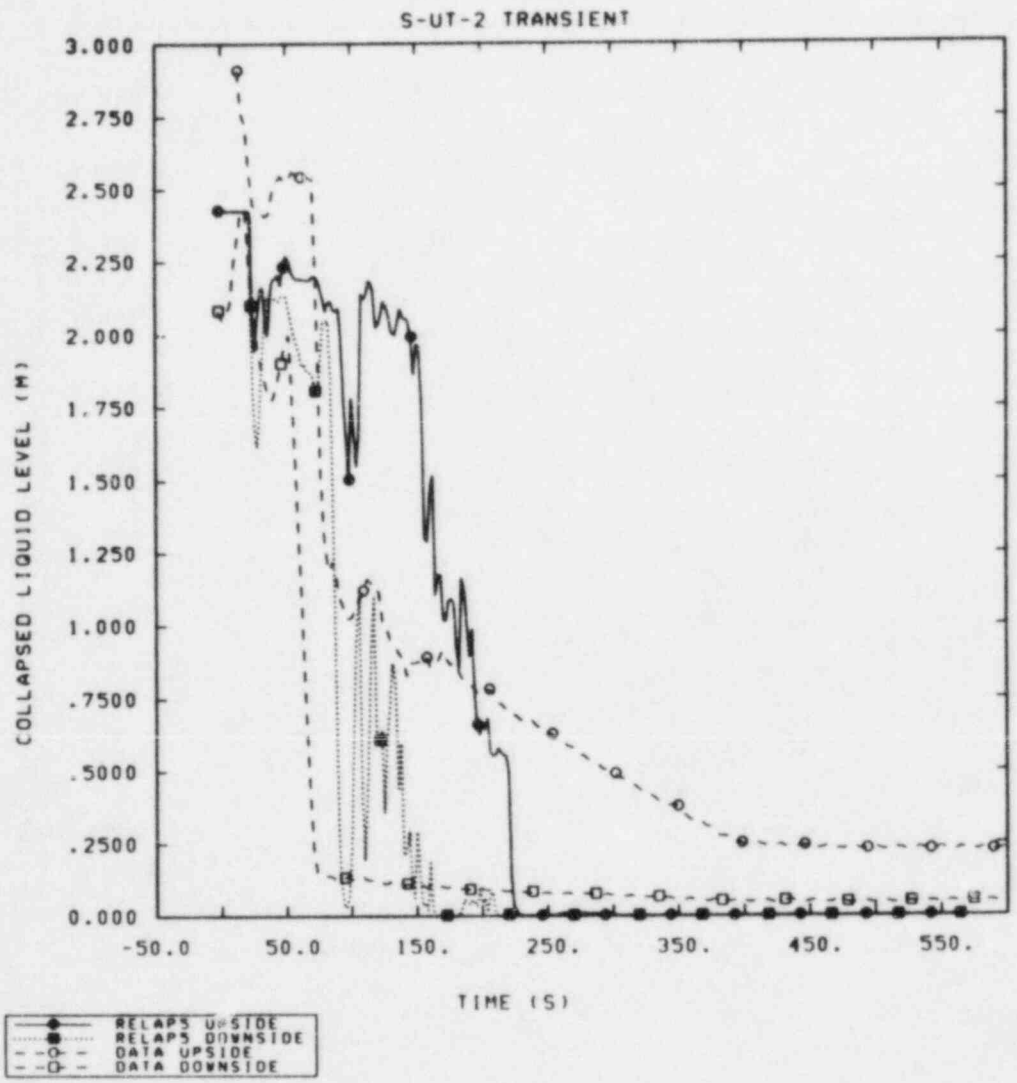

Figure 3.2.13 Comparison of Calculated and Measured Intact Loop Pump Suction Collapsed Liquid Levels for Test S-UT-2

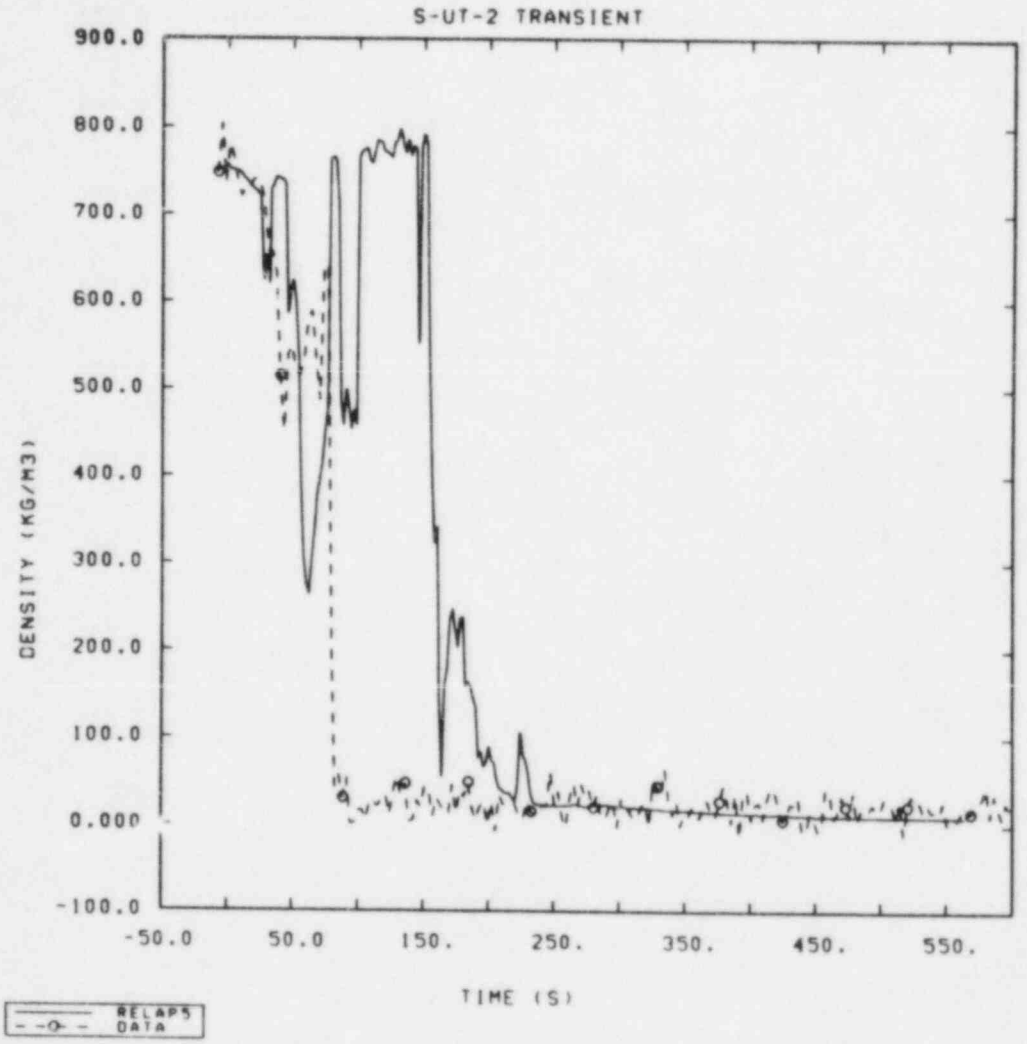

Figure 3.2.14 Comparison of Calculated and Measured Intact Loop Cold Leg Densities for Test S-UT-2

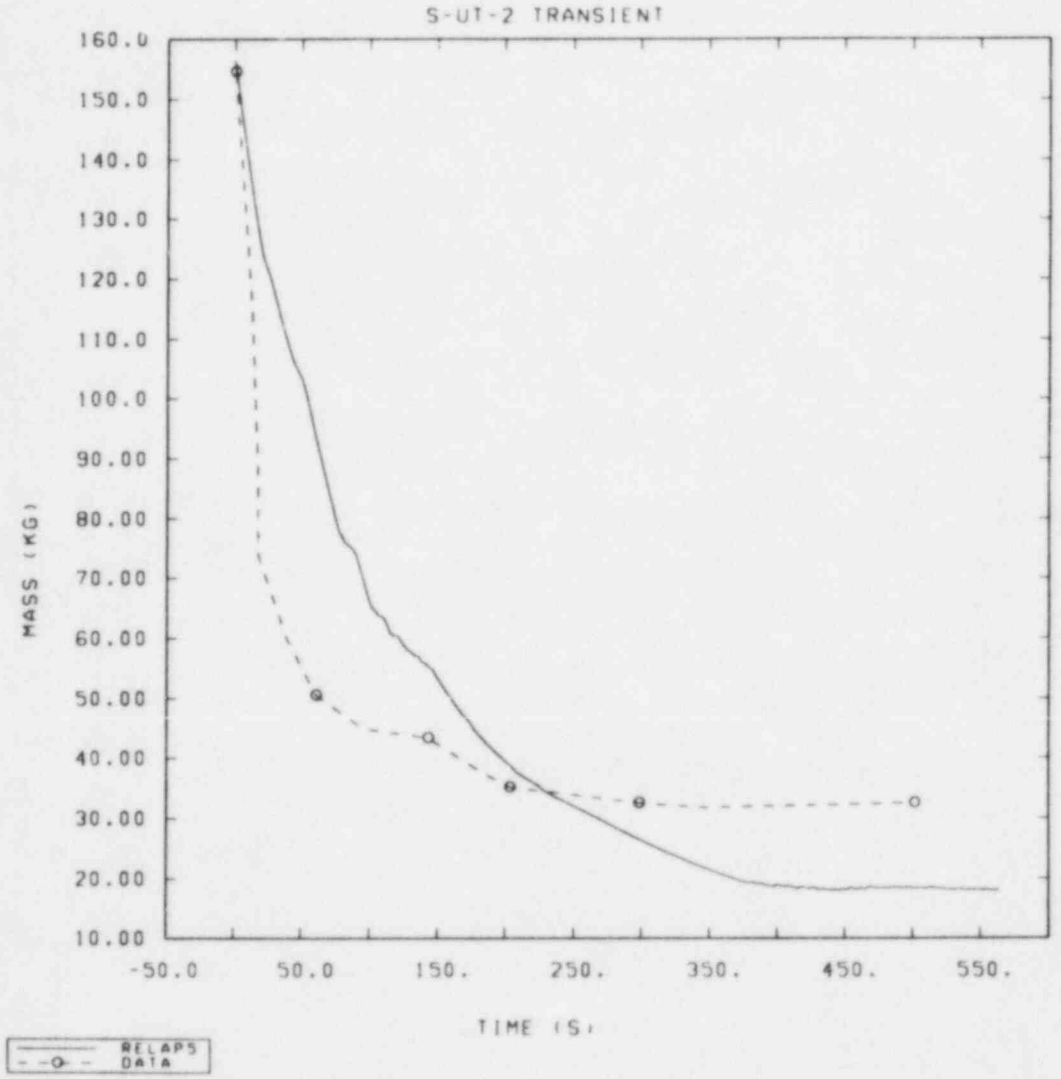

Figure 3.2.15 Comparison of Calculated and Measured Total Primary System Mass Inventories for Test S-UT-2

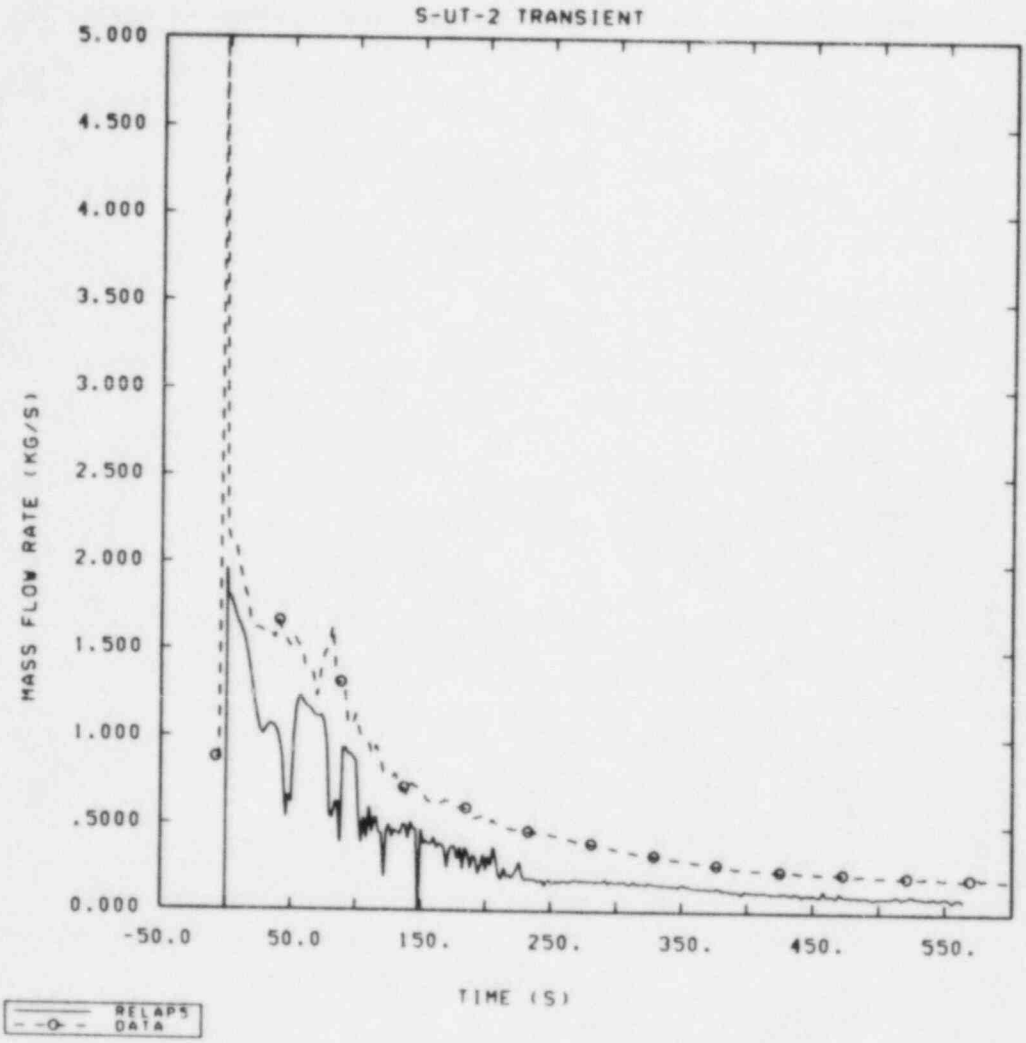

Figure 3.2.16 Comparison of Calculated and Measured Break Mass Flow Rates for Test S-UT-2

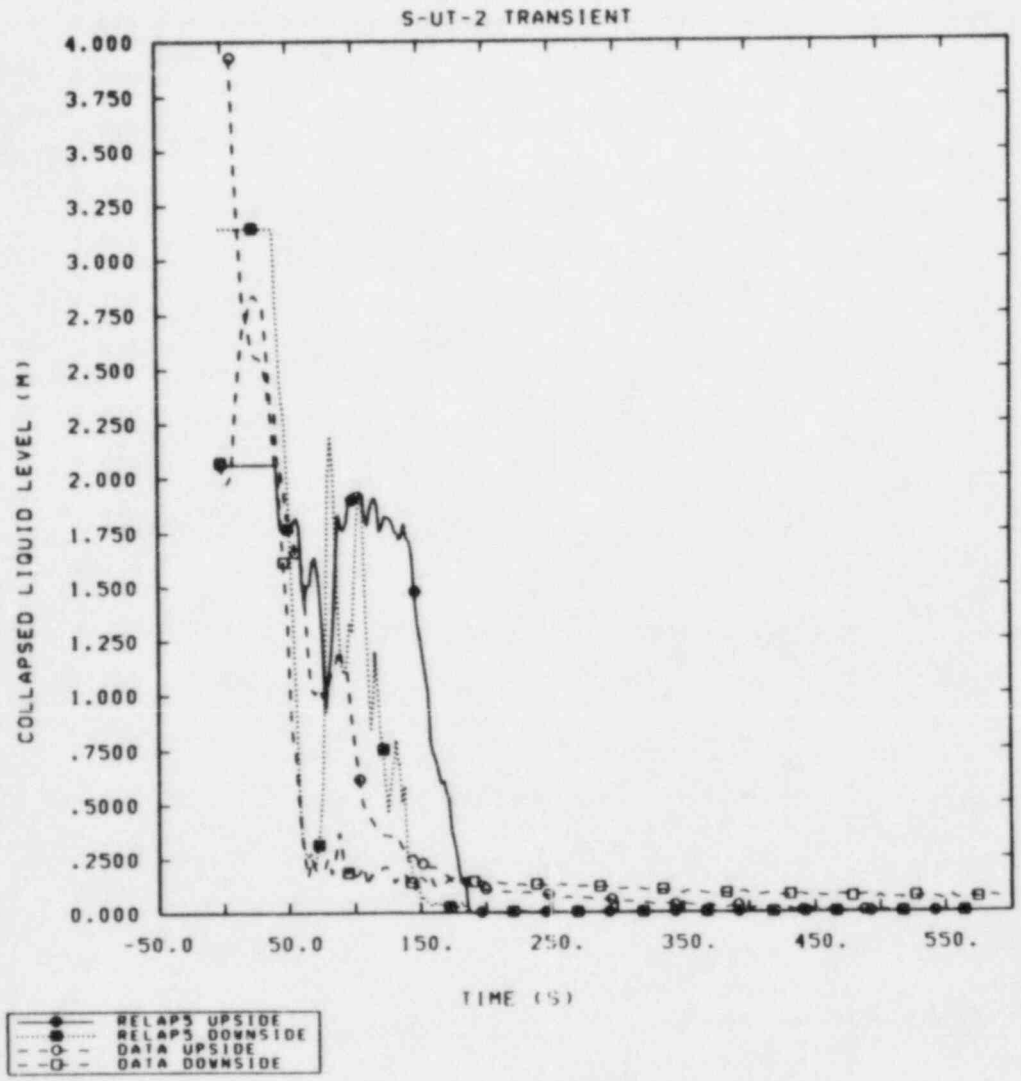

Figure 3.2.17 Comparison of Calculated and Measured Broken Loop Pump Suction Collapsed Liquid Levels for Test S-UT-2

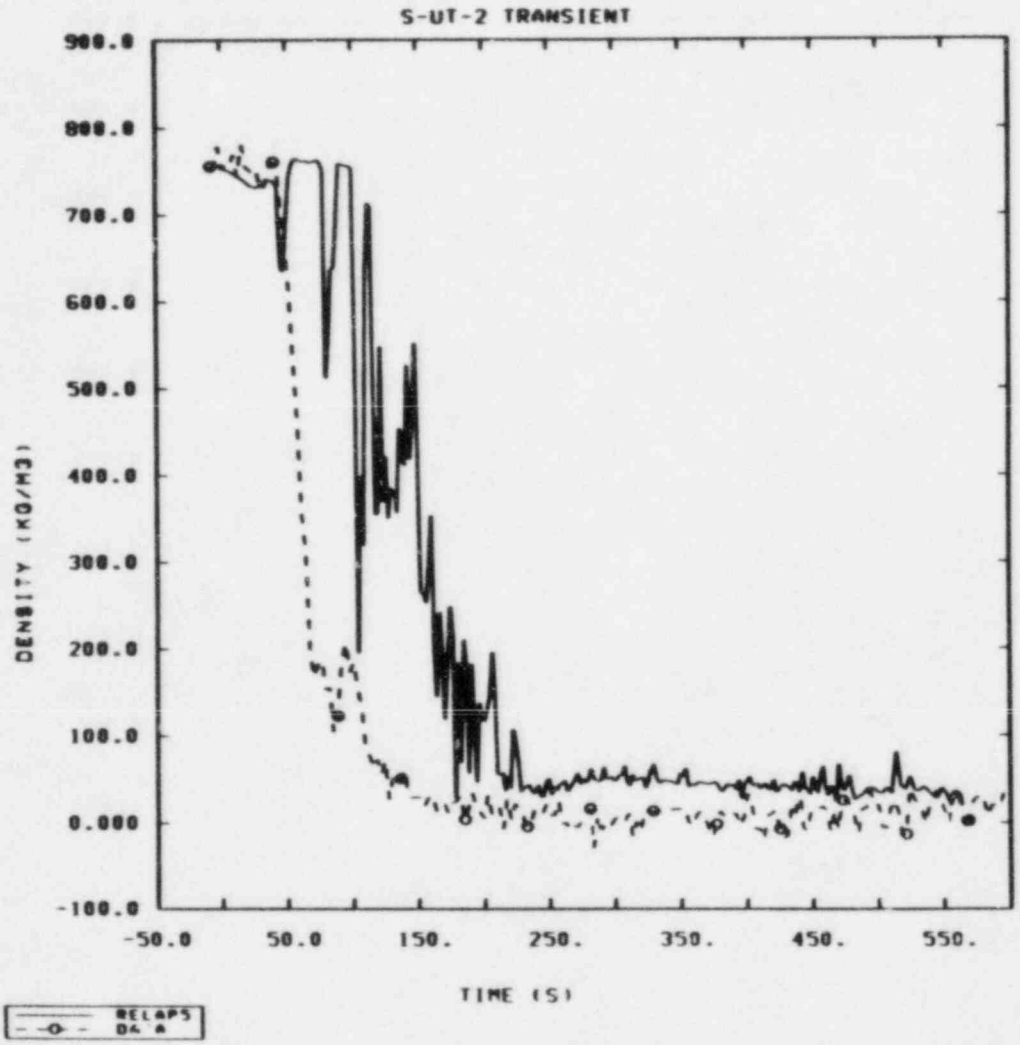

Figure 3.2.18 Comparison of Calculated and Measured Broken Loop Densities (Pump Side of Break) for Test S-UT-2

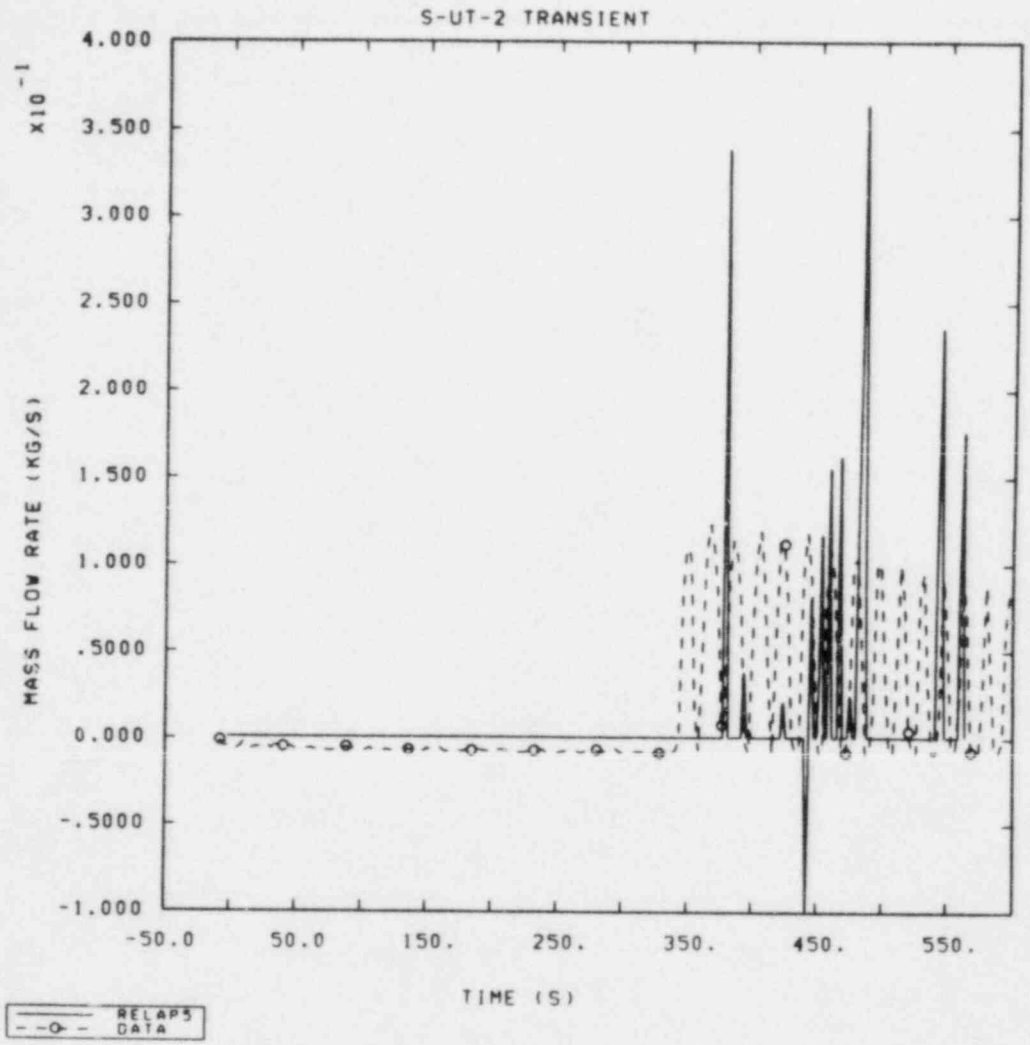

Figure 3.2.19 Comparison of Calculated and Measured Intact Loop Cold Leg Accumulator Flow Rates for Test S-UT-2

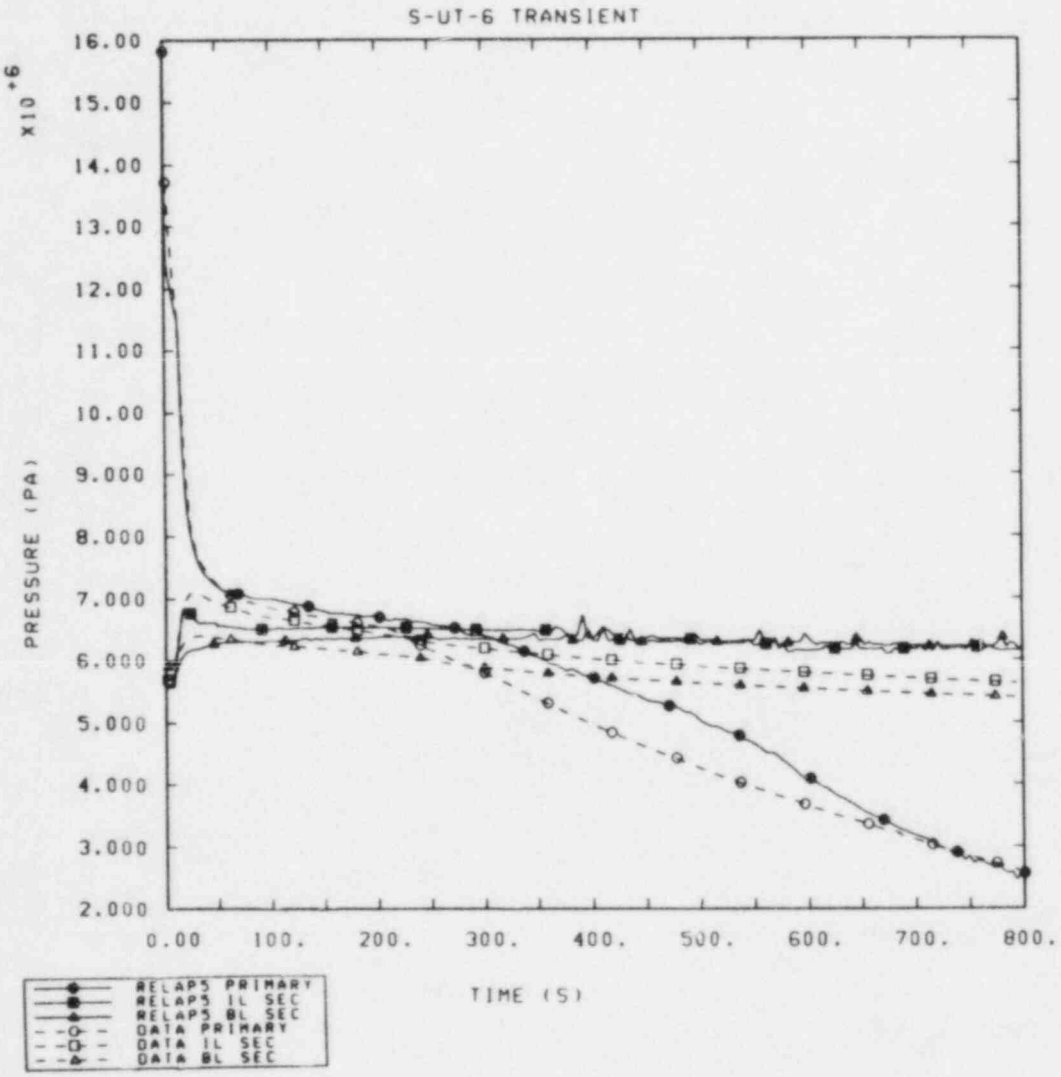

Figure 3.3.1 Comparison of Calculated and Measured Primary and Intact and Broken Loop Steam Generator Secondary Pressures for Test S-UT-6

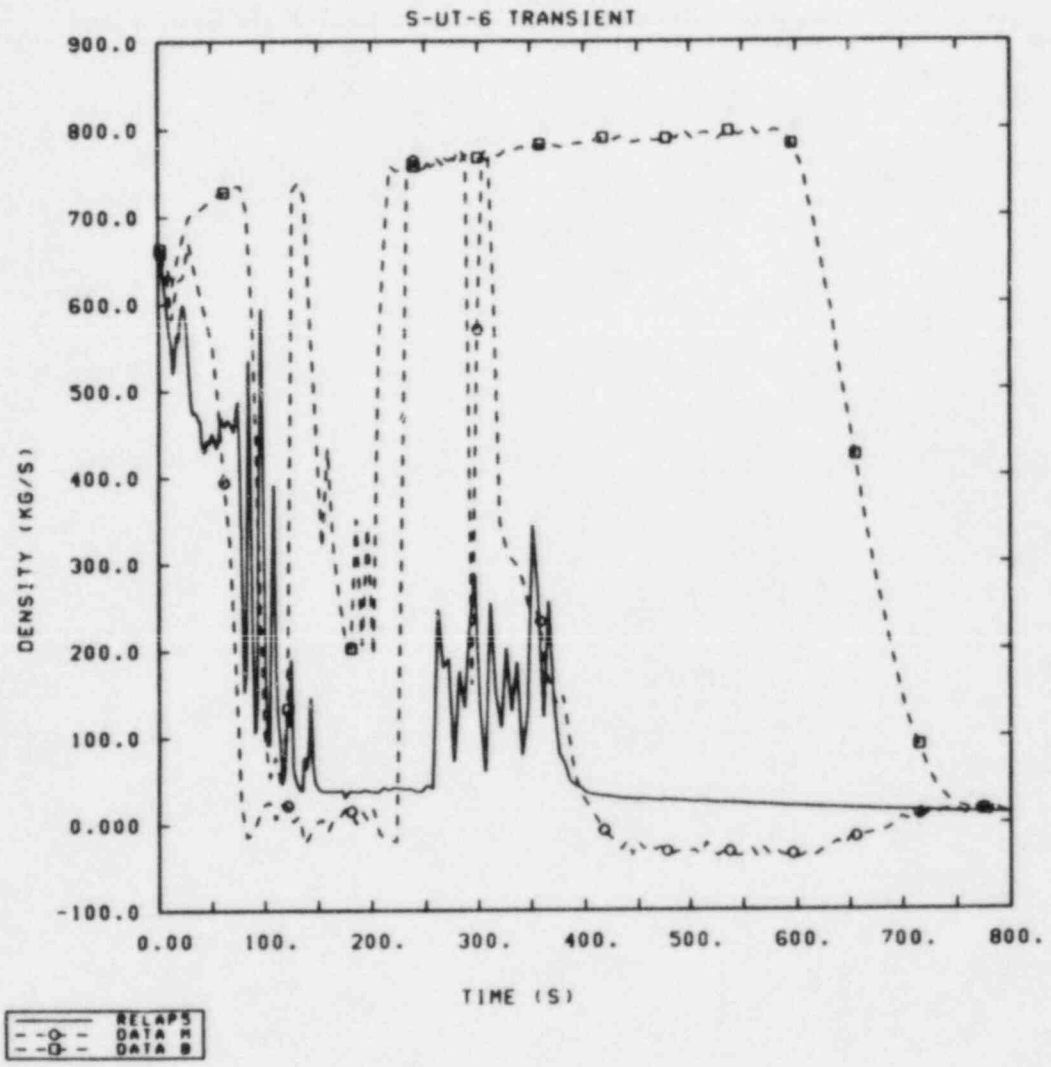

Figure 3.3.2 Comparison of Calculated and Measured Broken Loop Hot Leg Densities for Test S-UT-6

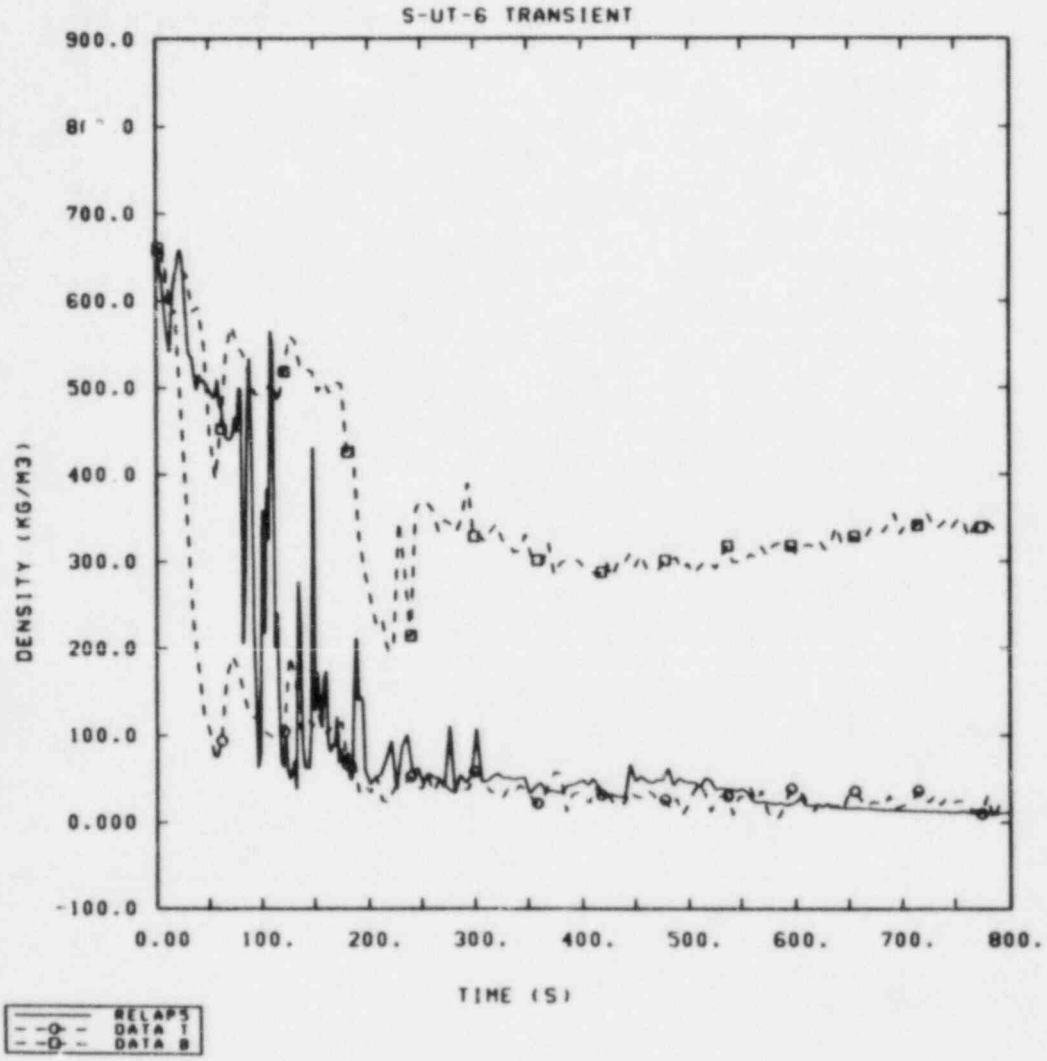

Figure 3.3.3 Comparison of Calculated and Measured Intact Loop Hot Leg Densities for Test S-UT-6

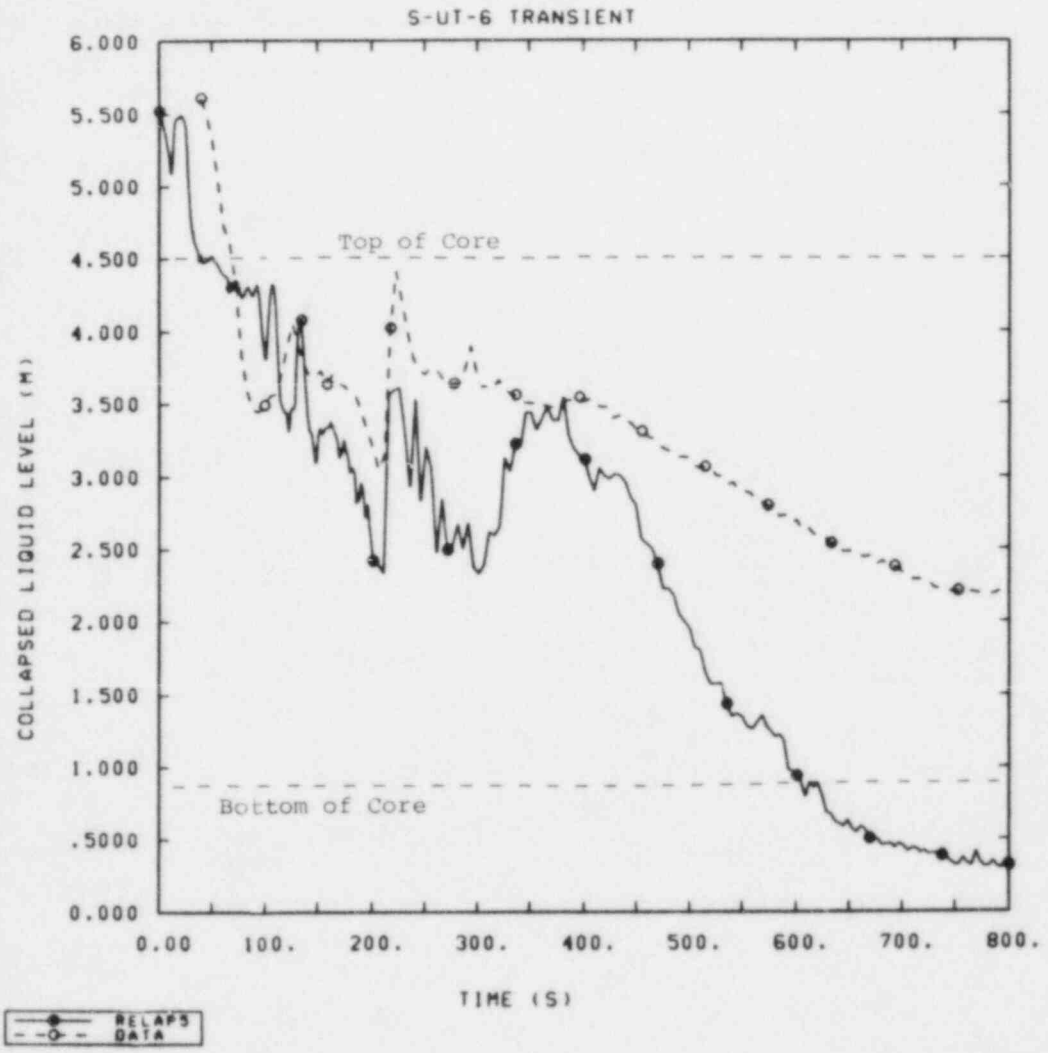

Figure 3.3.4 Comparison of Calculated and Measured Vessel Collapsed Liquid Levels for Test S-UT-6

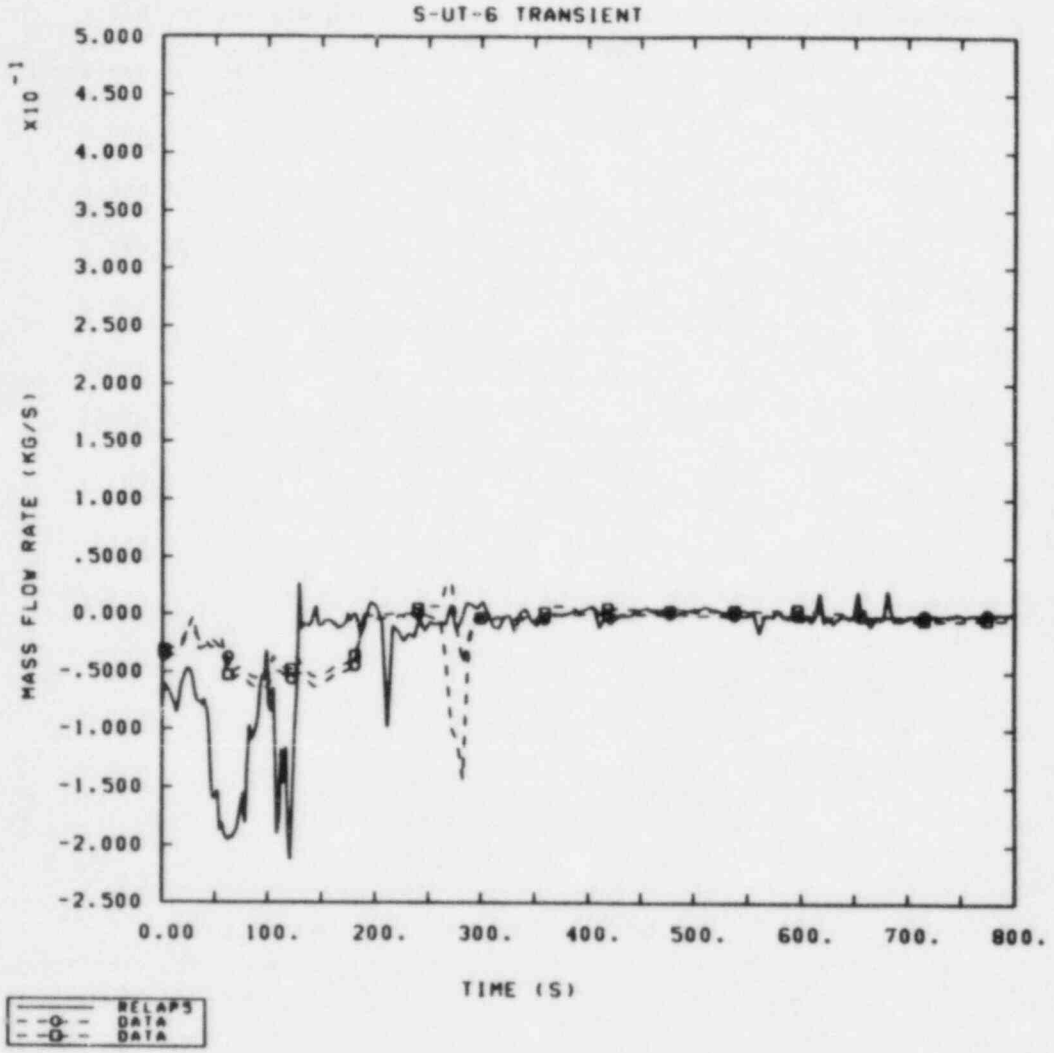

Figure 3.3.5 Comparison of Calculated and Measured Support Column Mass Flows for Test S-UT-6

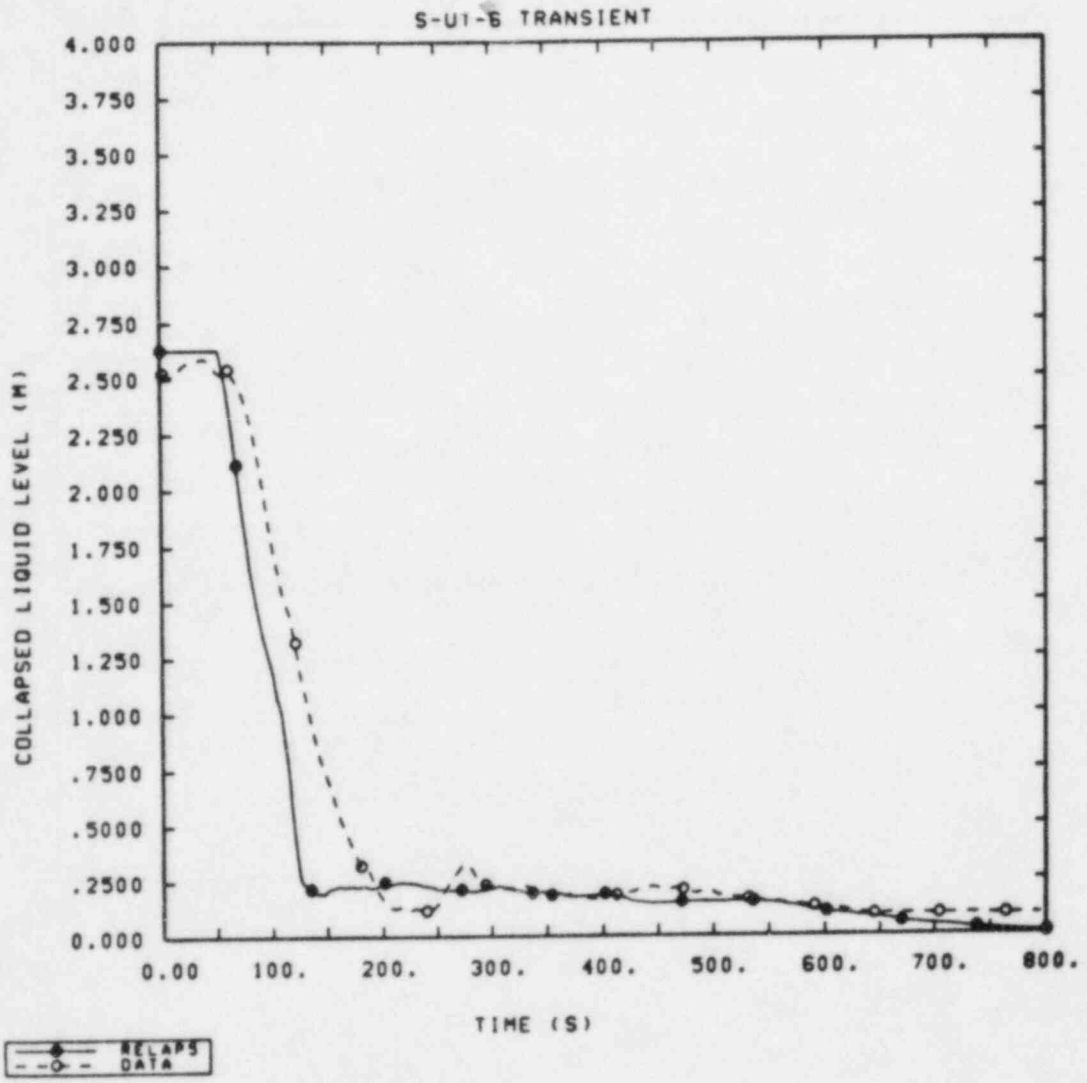

Figure 3.3.6 Comparison of Calculated and Measured Upper Head Collapsed Liquid Levels for Test-UT-6

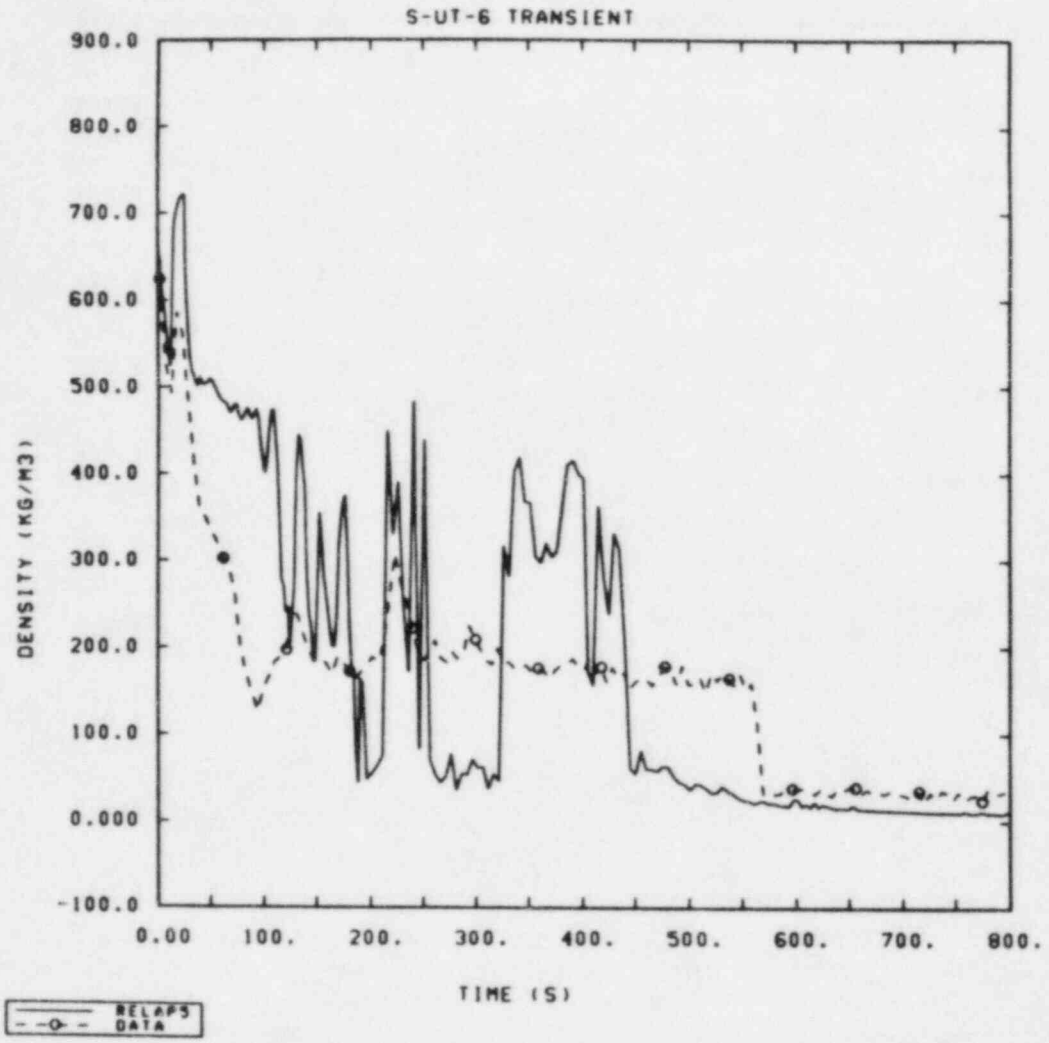

Figure 3.3.7 Comparison of Calculated and Measured Densities at the 3.42 m Core Elevation for Test S-UT-6

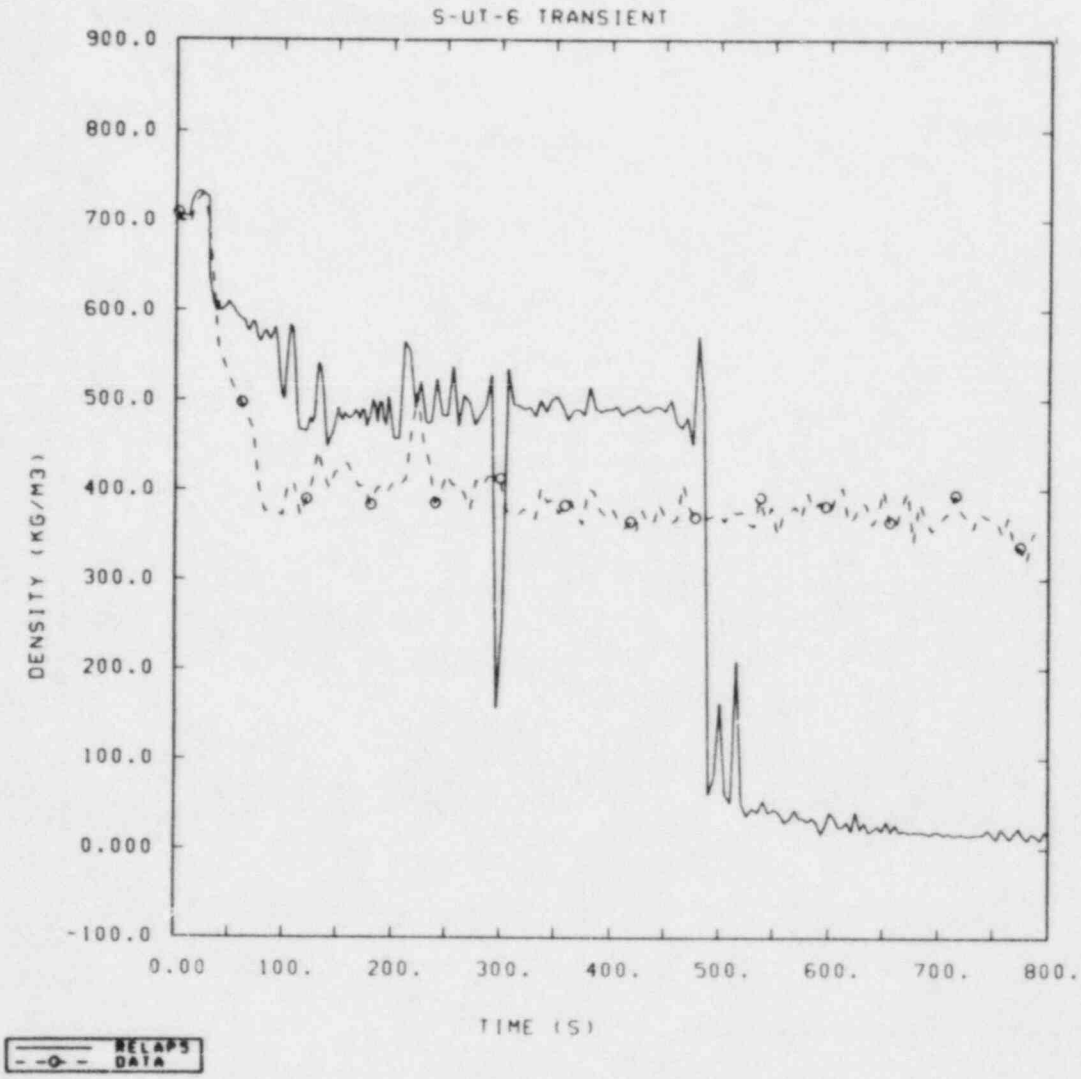

Figure 3.3.8 Comparison of Calculated and Measured Densities at the 1.73 m Core Elevation for Test S-UT-6

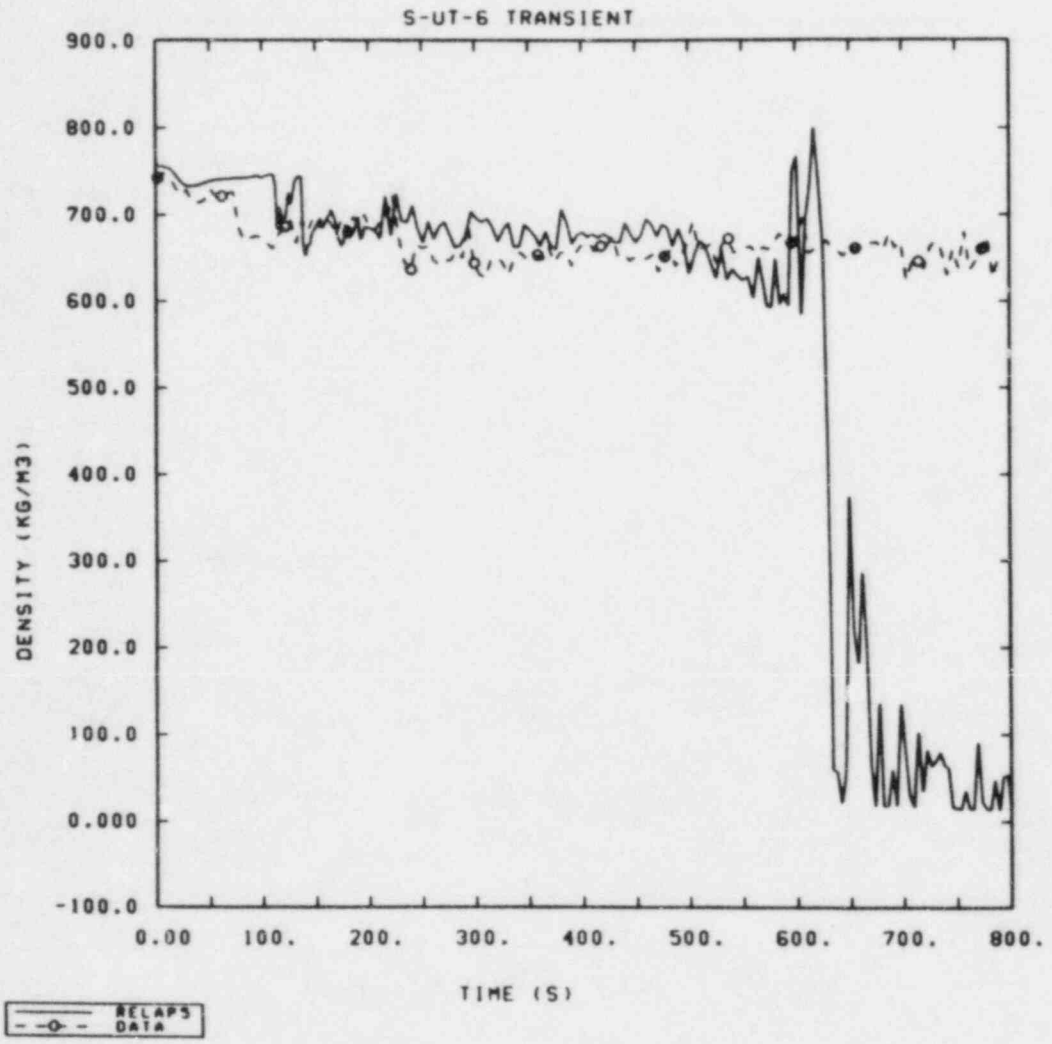

Figure 3.3.9 Comparison of Calculated and Measured Densities at the Core Inlet for Test S-UT-6

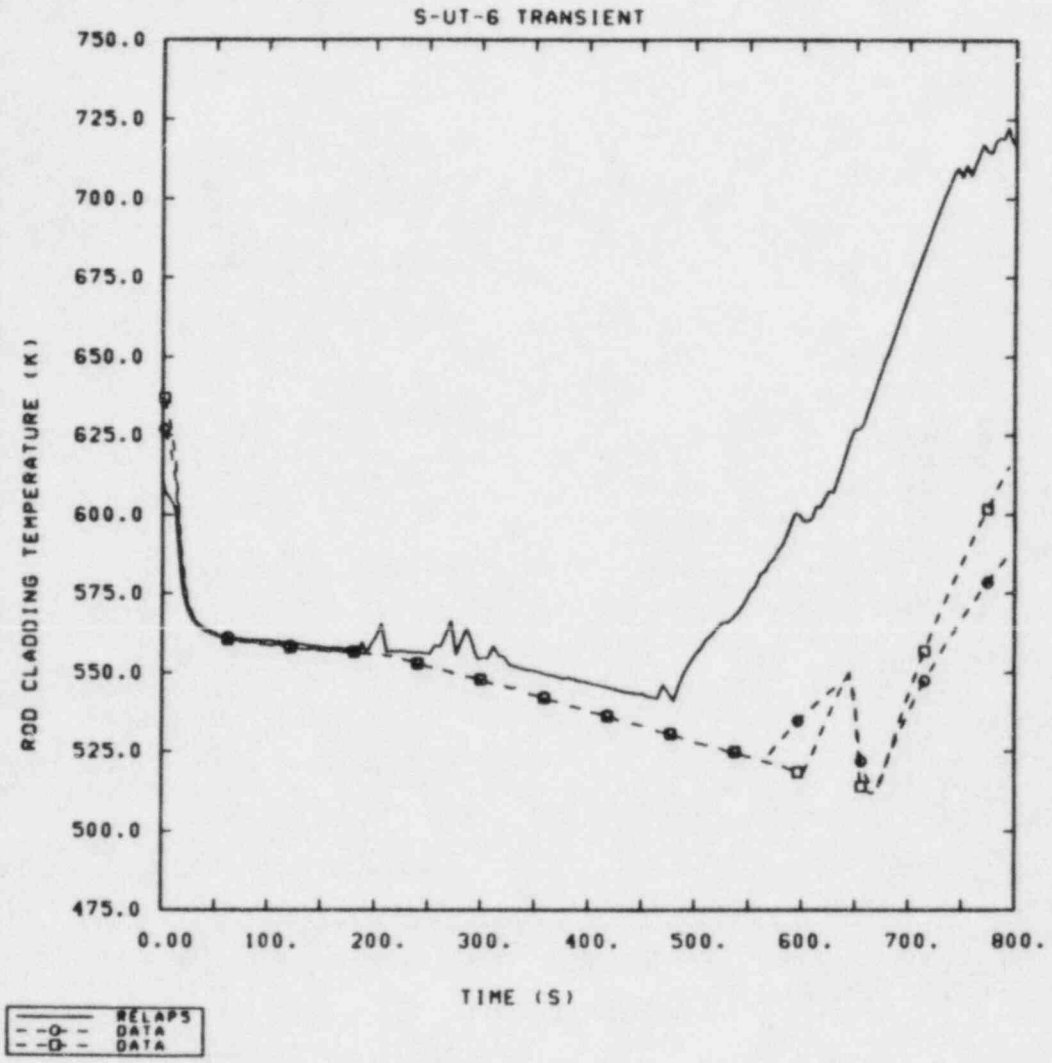

Figure 3.3.10 Comparison of Calculated and Measured Rod Cladding Temperatures at the 3.0 m to 3.6 m Core Elevation for Test S-UT-6

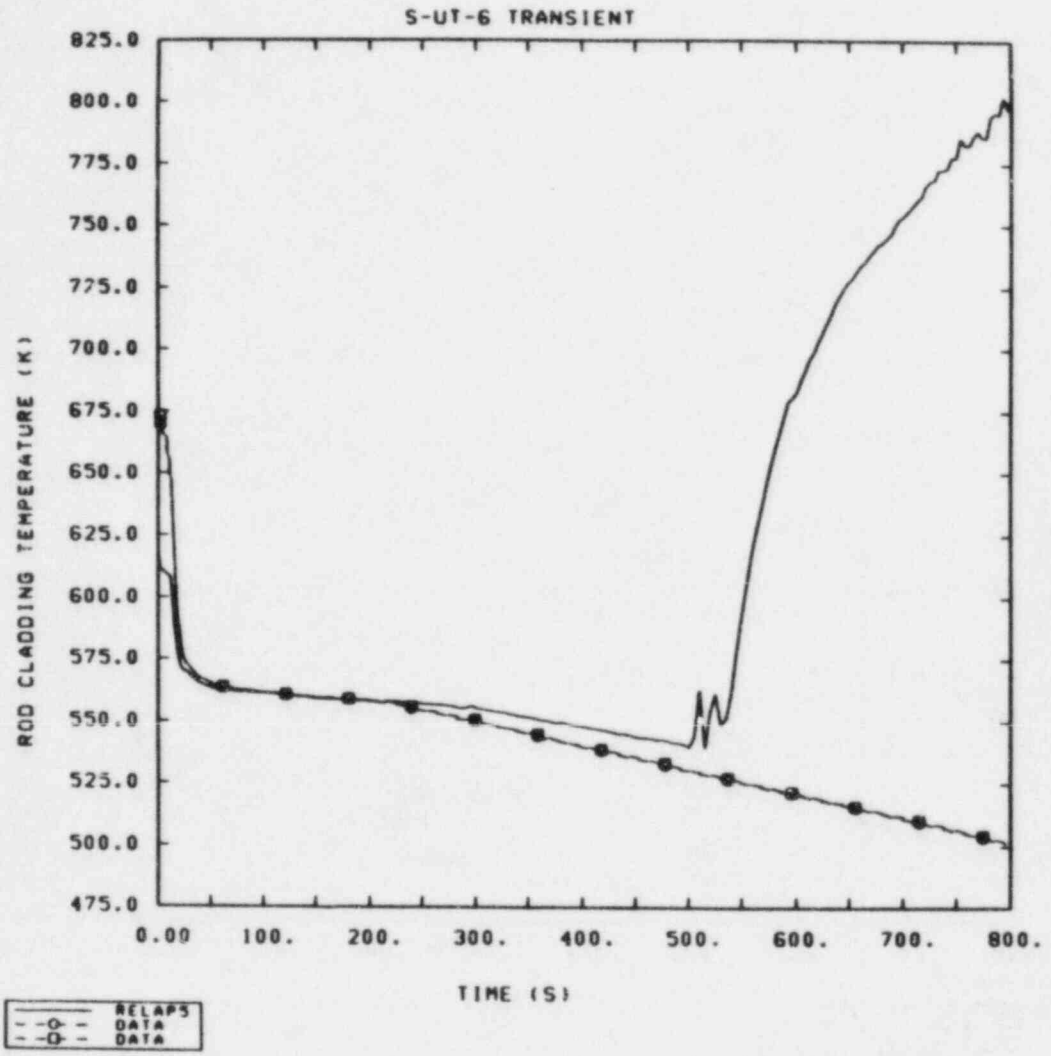

Figure 3.3.11 Comparison of Calculated and Measured Rod Cladding Temperatures at the 1.5 m to 1.8 m Core Elevation for Test S-UT-6

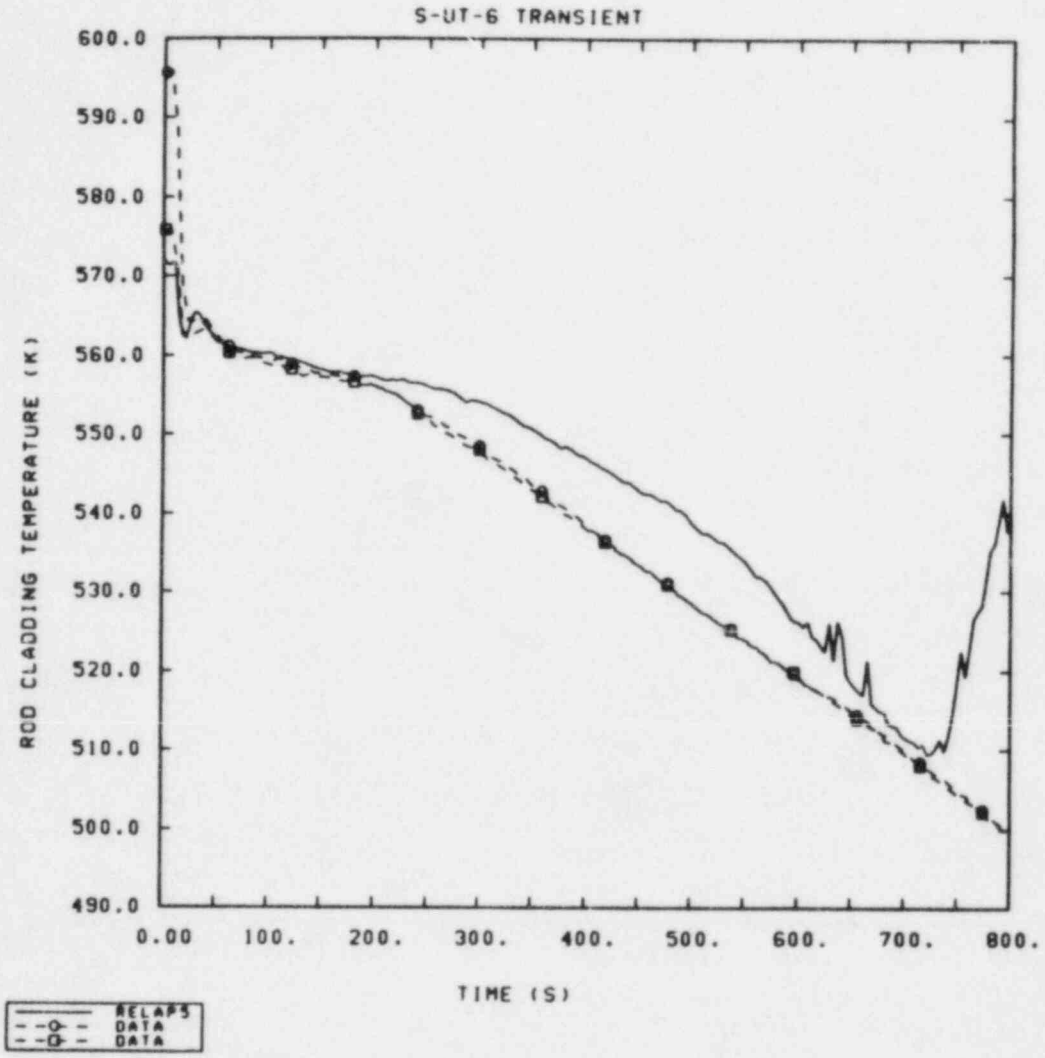

Figure 3.3.12 Comparison of Calculated and Measured Rod Cladding Temperatures at the 0.0 m to 0.6 m Core Elevation for Test S-UT-6

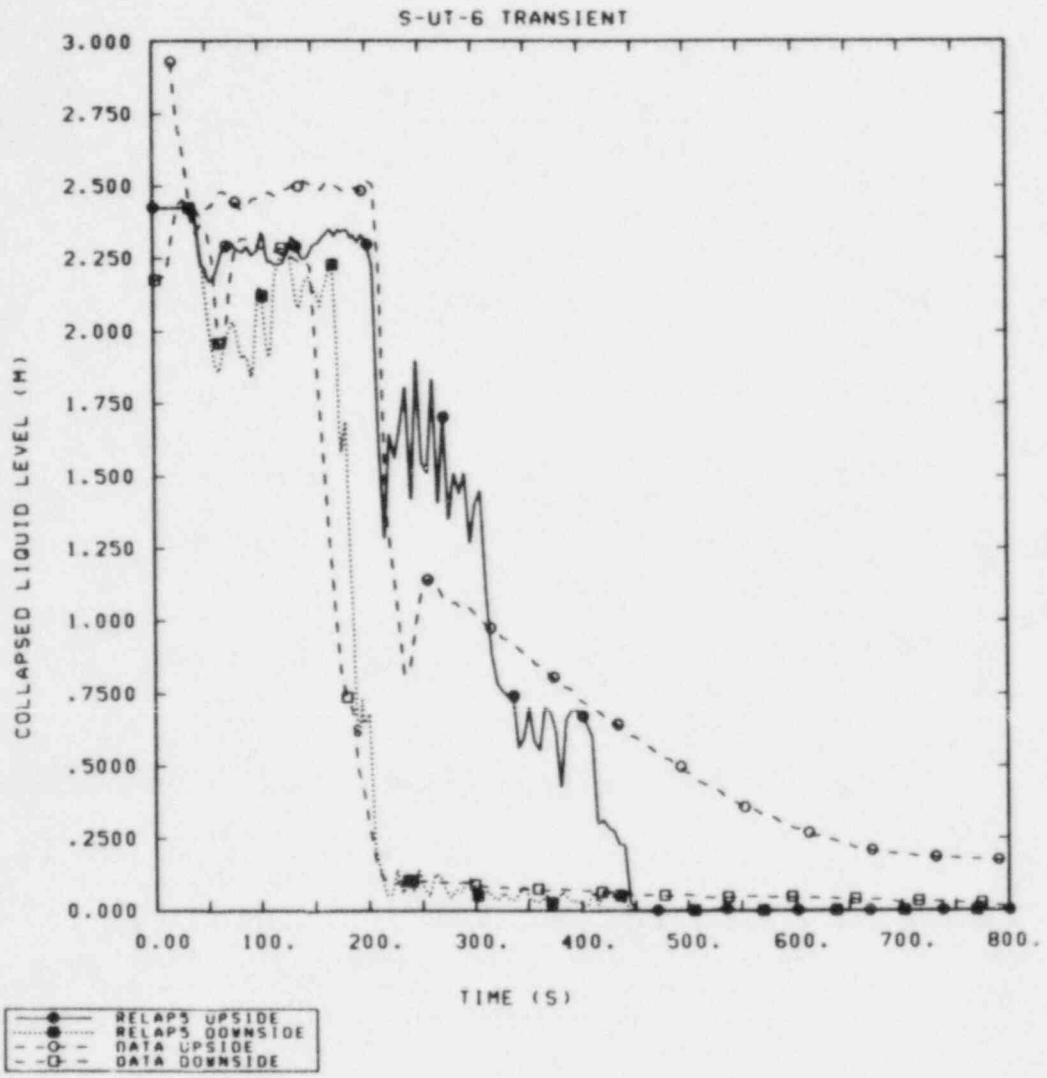

Figure 3.3.13 Comparison of Calculated and Measured Intact Loop Pump Suction Collapsed Liquid Levels for Test S-UT-6

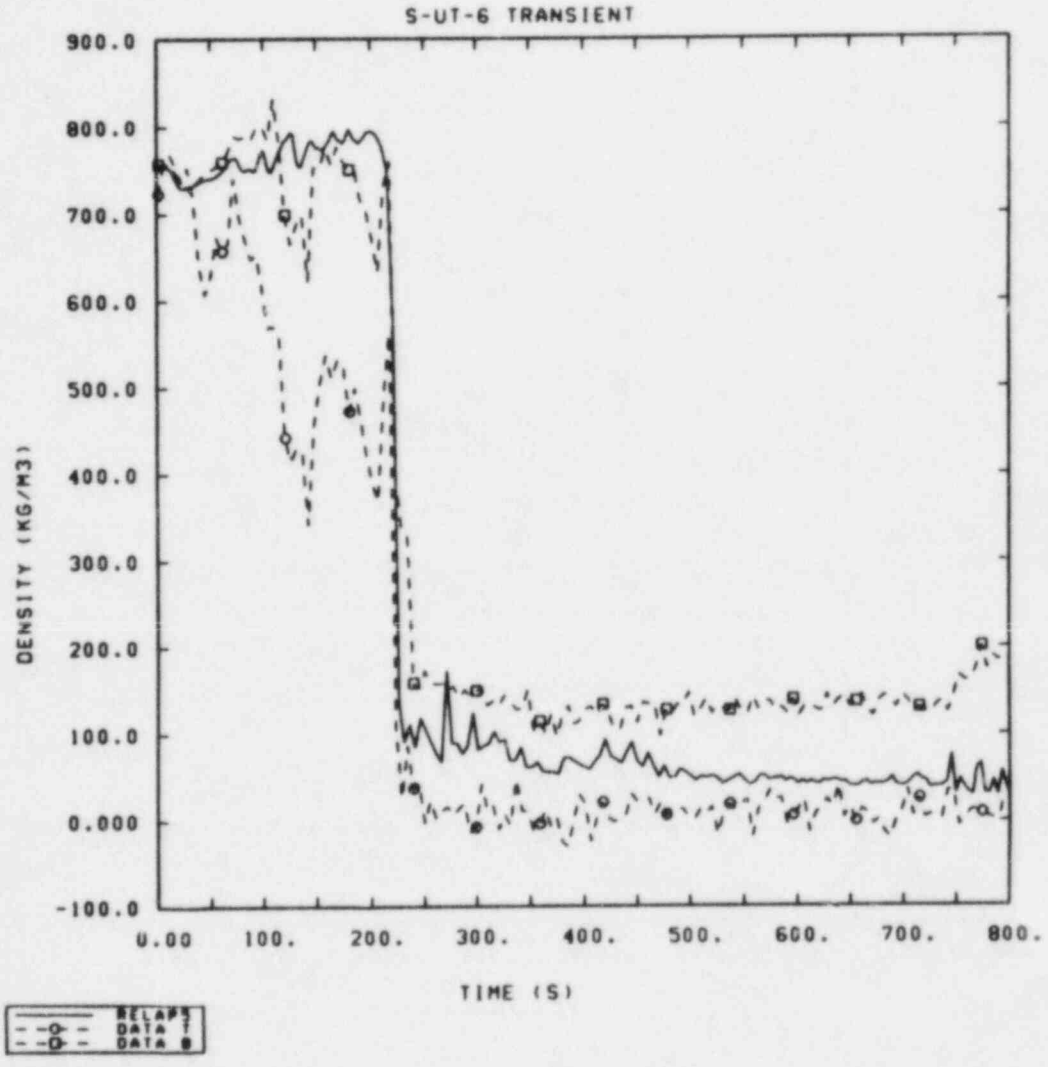

Figure 3.3.14 Comparison of Calculated and Measured Intact Loop Cold Leg Densities for Test S-UT-6

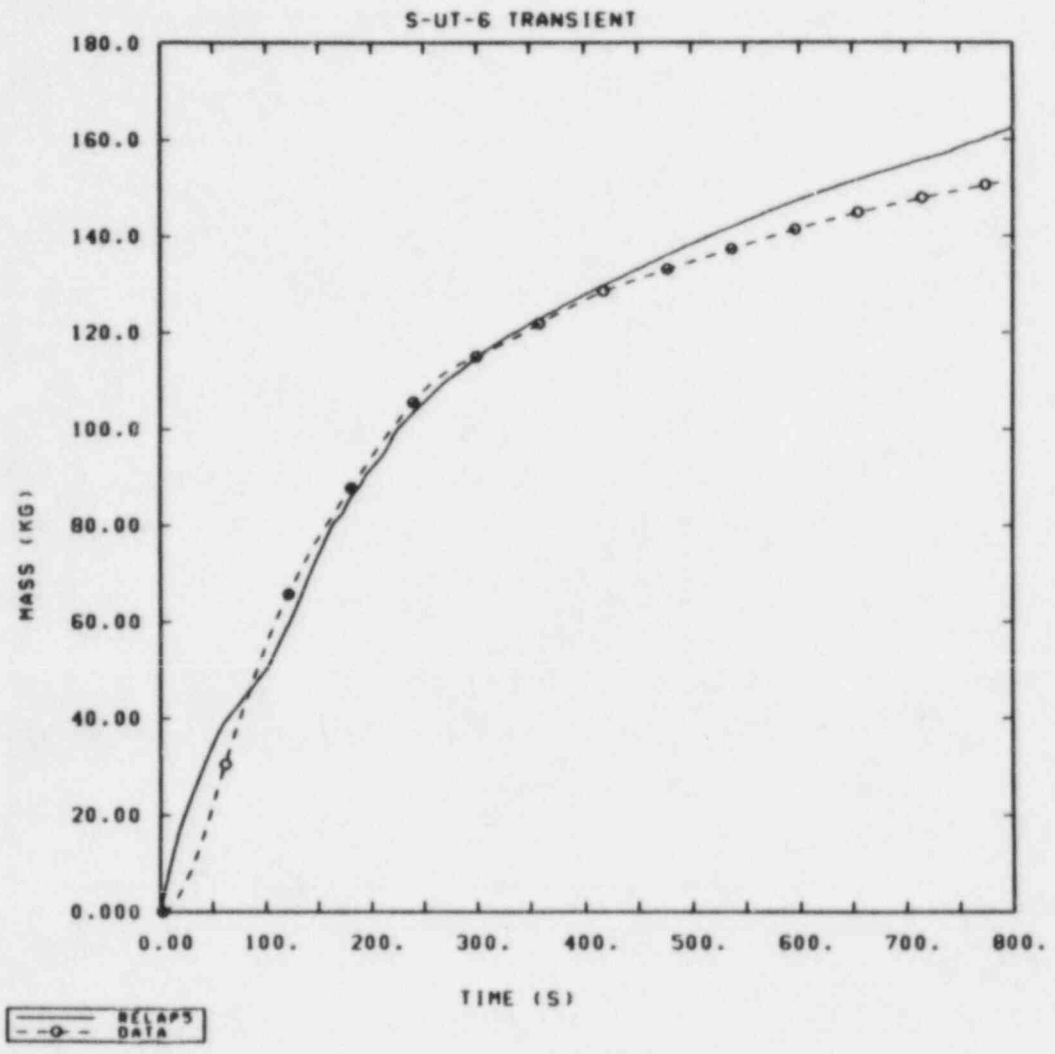

Figure 3.3.15 Comparison of Calculated and Measured Integrated Break Mass Flows for Test S-UT-6

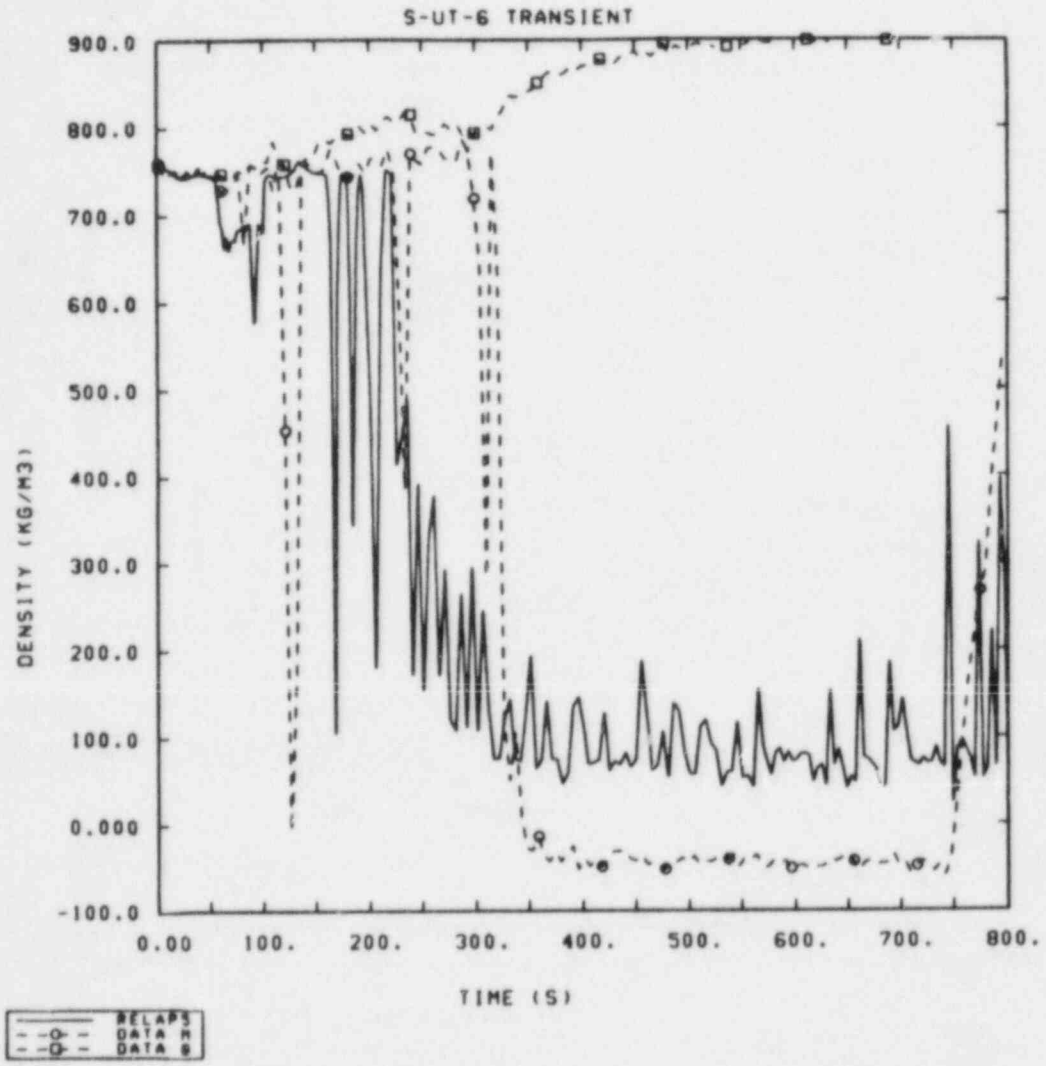

Figure 3.3.16 Comparison of Calculated and Measured Broken Loop Pump Suction Densities (Pump Side of Break) for Test S-UT-6

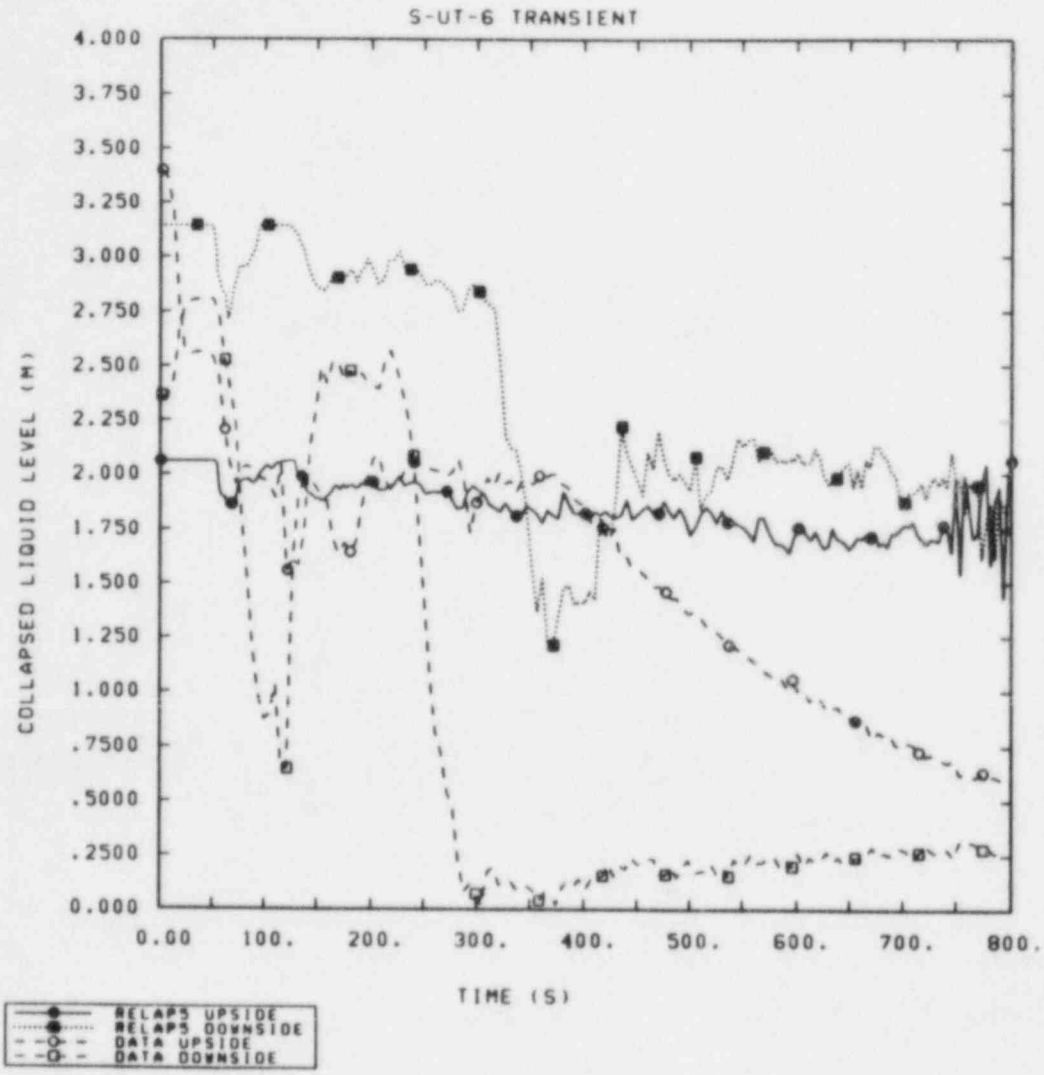

Figure 3.3.17 Comparison of Calculated and Measured Broken Loop Pump Suction Collapsed Liquid Levels for Test S-UT-6

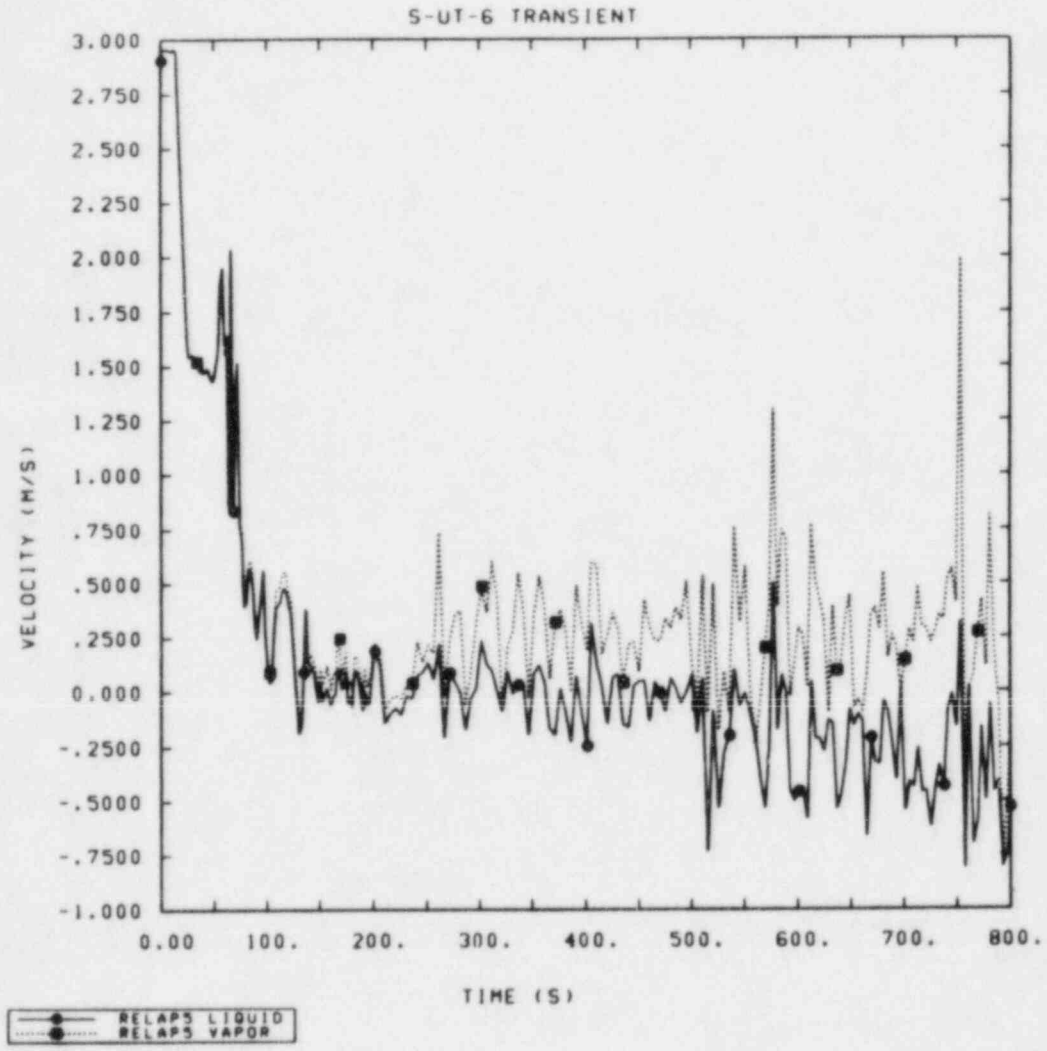

Figure 3.3.18 Calculated Liquid and Vapor Velocities at the Broken Loop Pump Outlet for Test S-UT-6

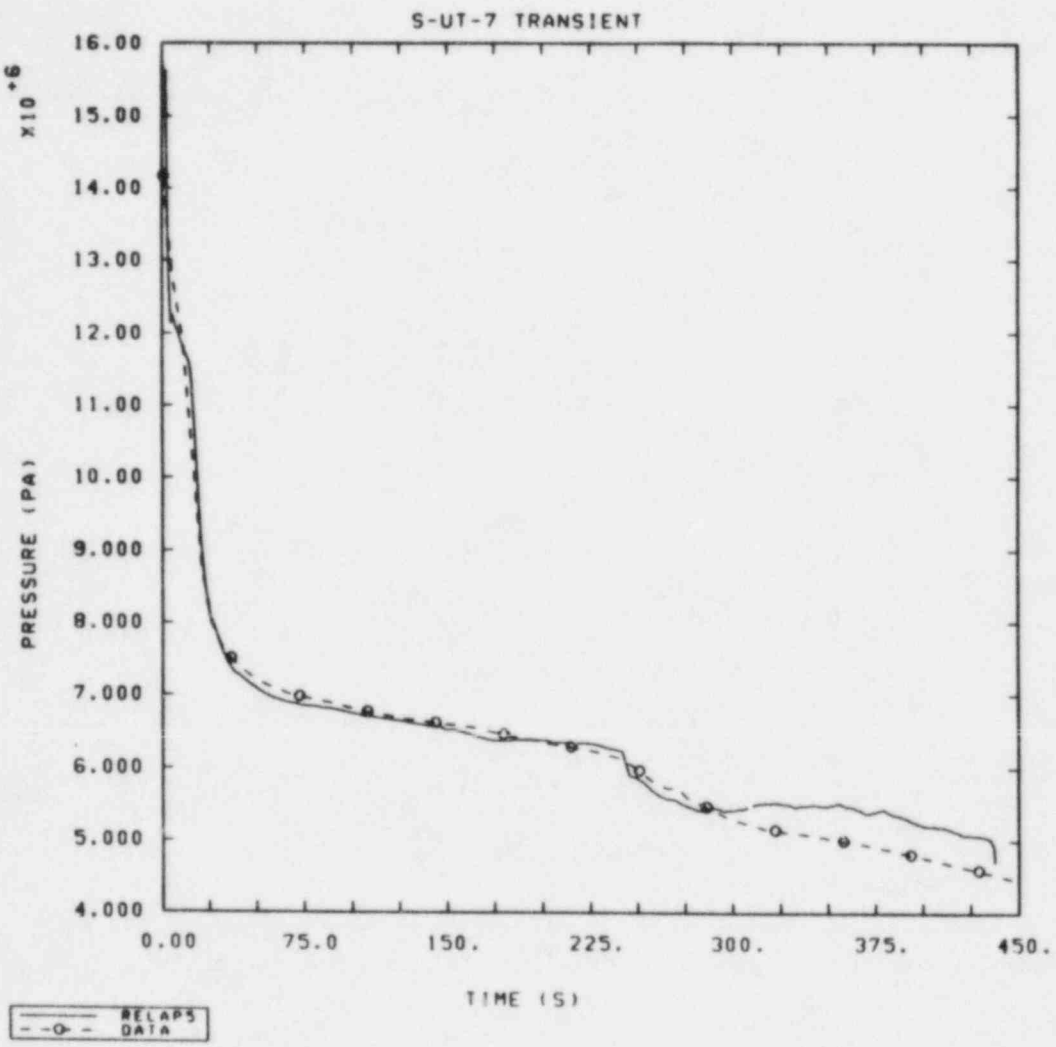

Figure 3.4.1 Comparison of Calculated and Measured Primary System Pressures for Test S-UT-7

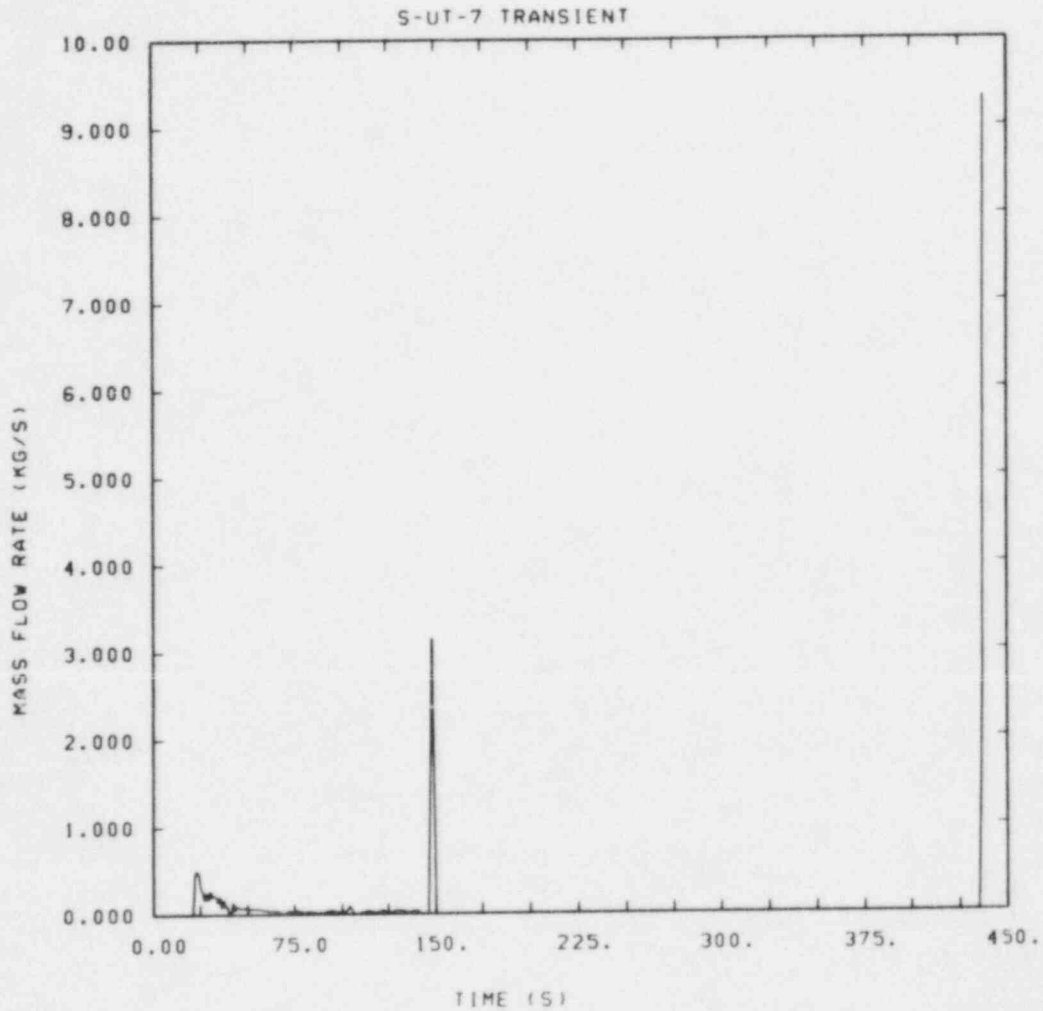

Figure 3.4.2 Calculated UHI Accumulator Mass Flow Rate for Test S-UT-7

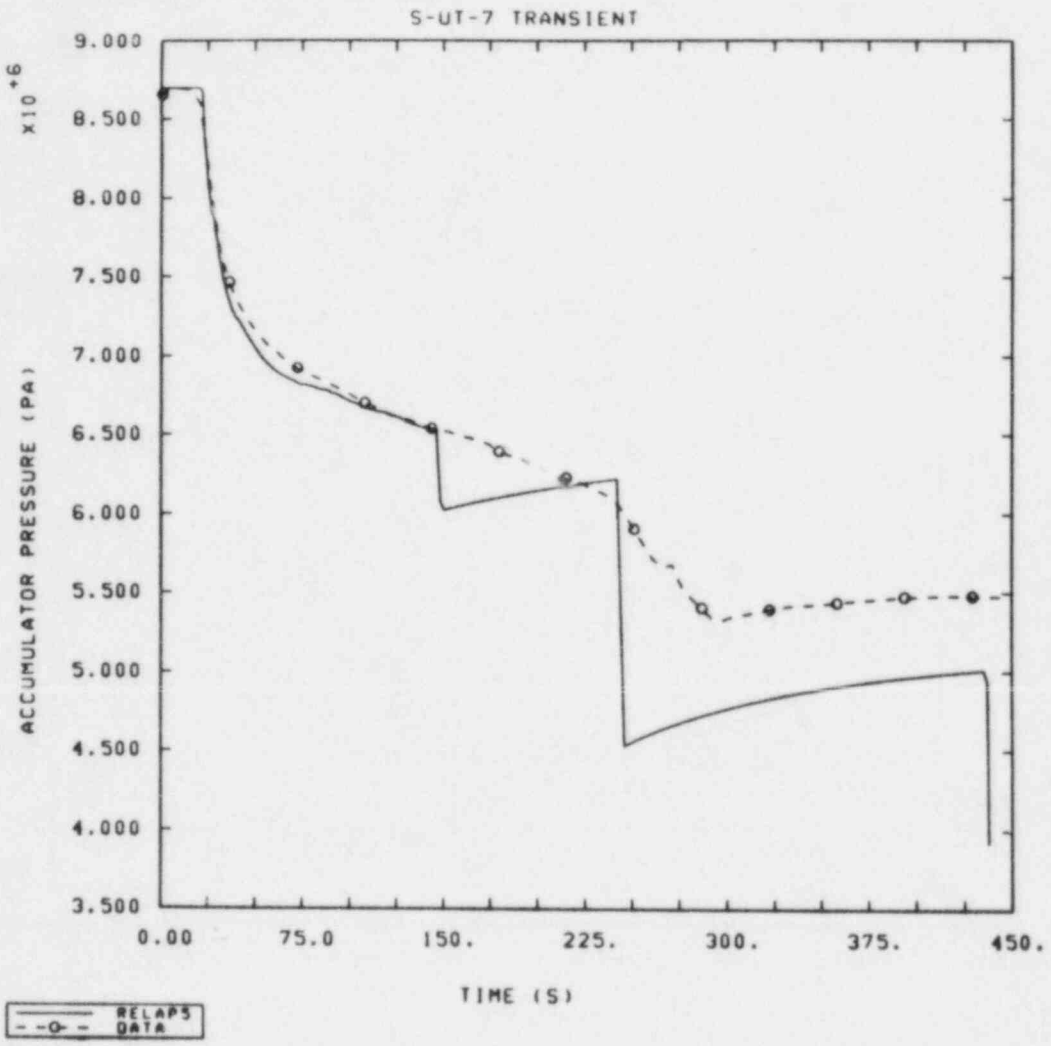

Figure 3.4.3 Comparison of Calculated and Measured UHI Accumulator Pressures for Test S-UT-7

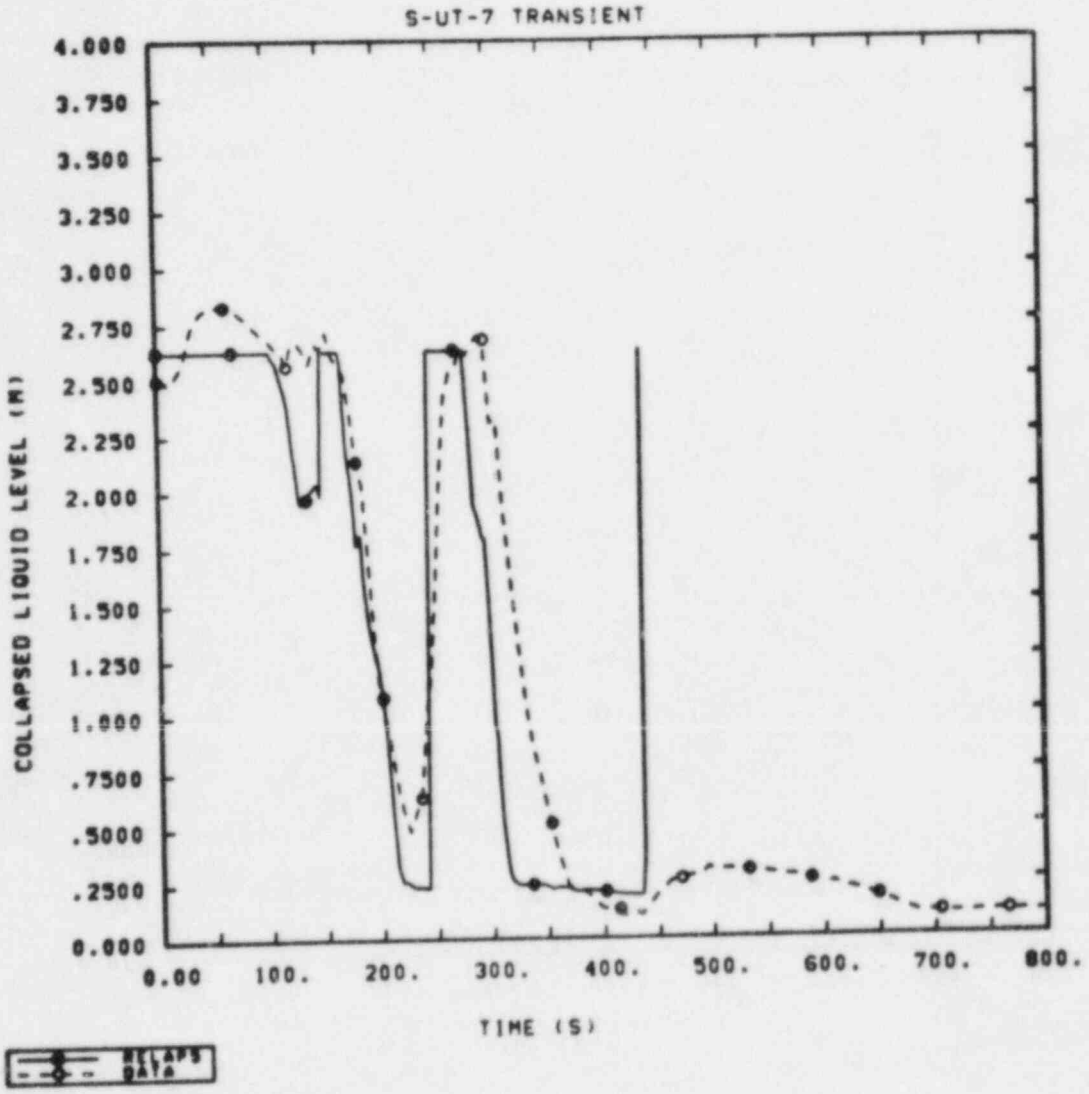

Figure 3.4.4 Comparison of Calculated and Measured Upper Head Collapsed Liquid Levels for Test S-UT-7

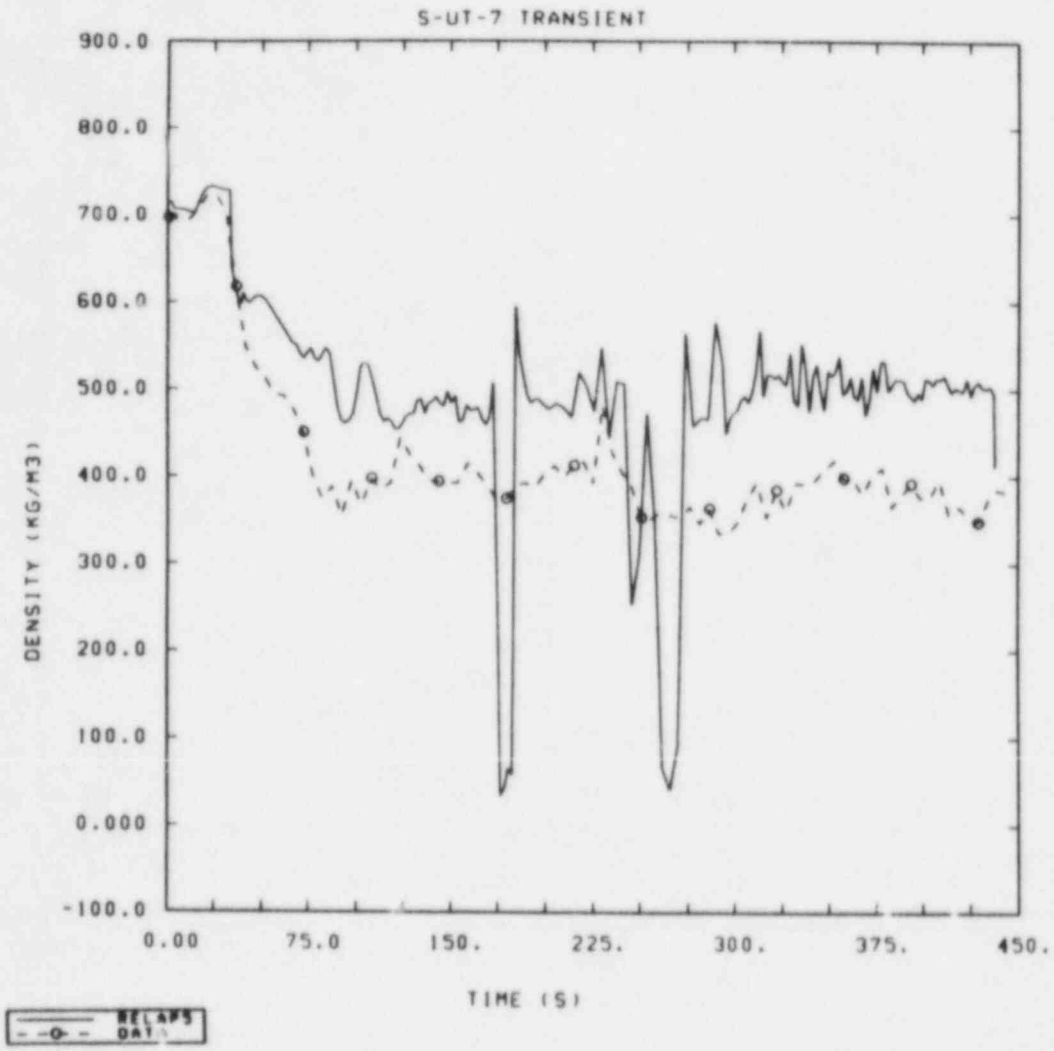

Figure 3.4.5 Comparison of Calculated and Measured Densities at the 1.73 m Core Elevation for Test S-UT-7

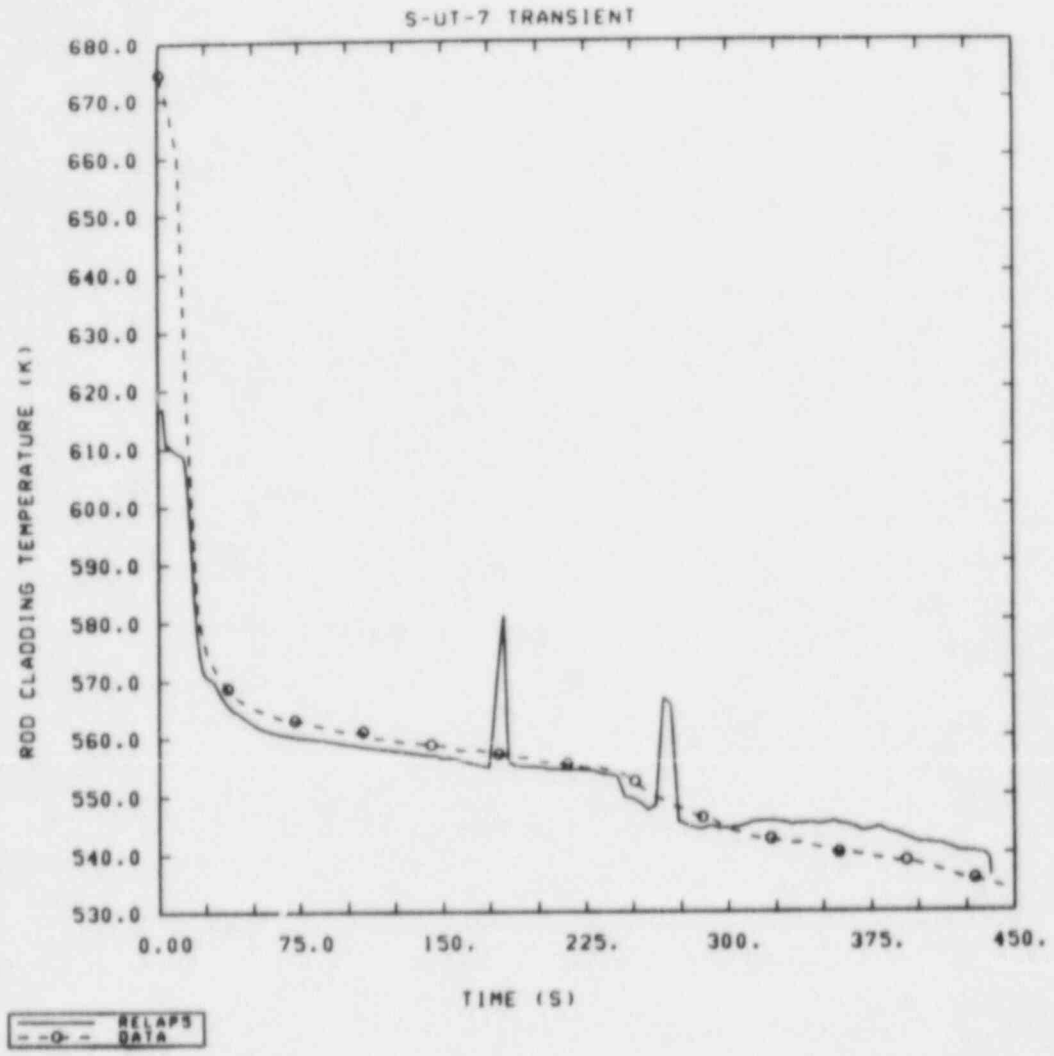

Figure 3.4.6 Comparison of Calculated and Measured Rod Cladding Temperatures at the 1.5 m to 1.8 m Core Elevation for Test S-UT-7

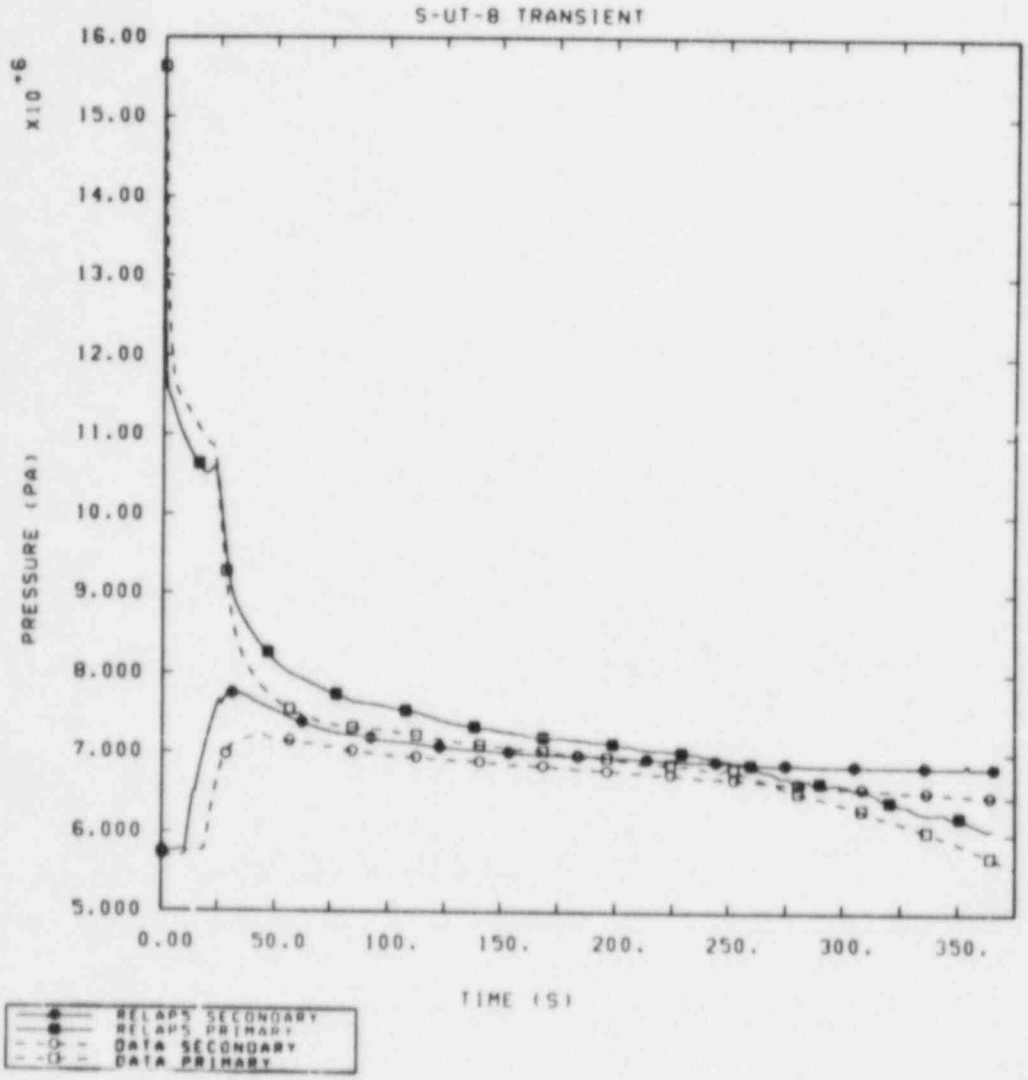

Figure 3.5.1 Comparison of Calculated and Measured Primary and Intact Loop Secondary Pressures for Test S-UT-8

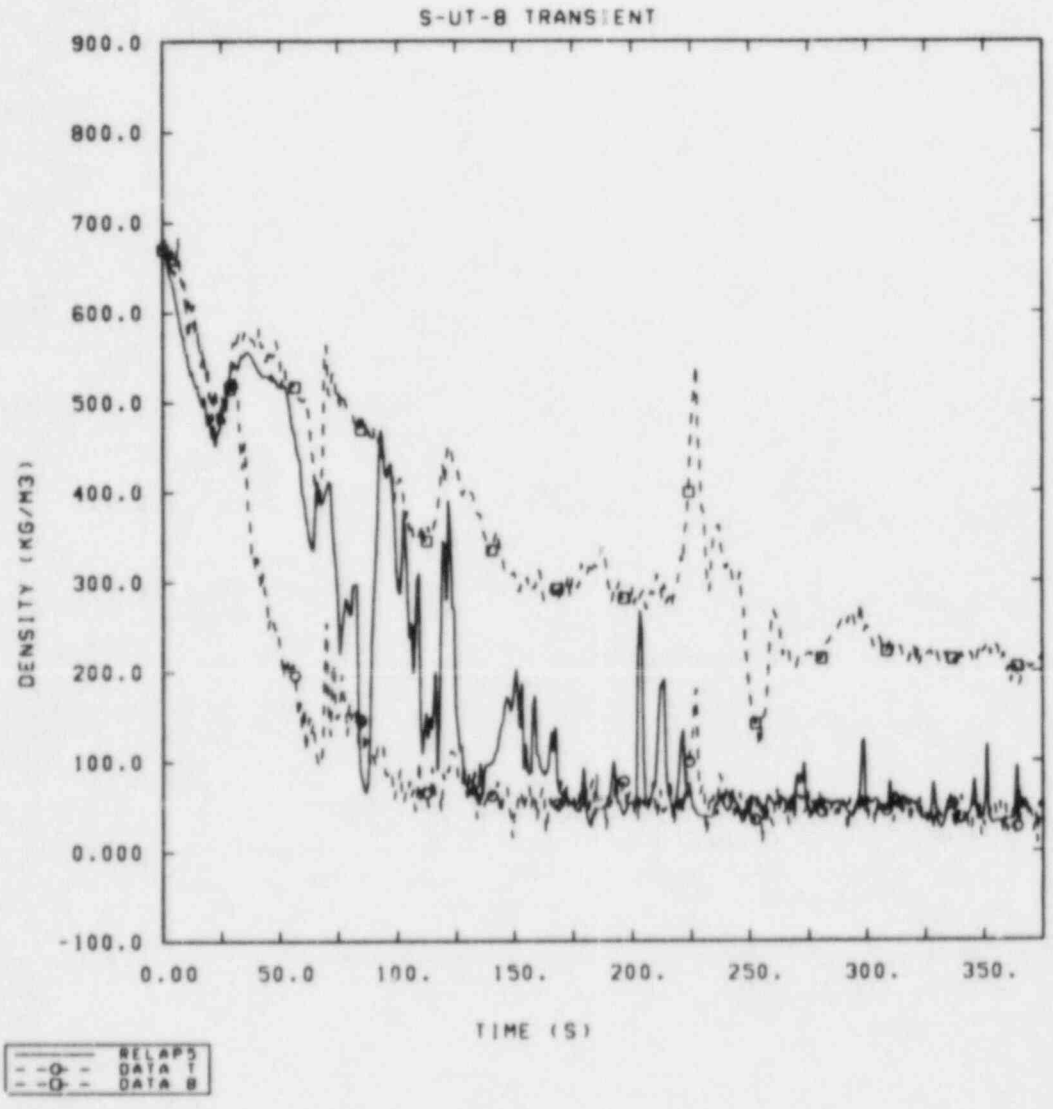

Figure 3.5.2 Comparison of Calculated and Measured Intact Loop Hot Leg Densities for Test S-UT-8

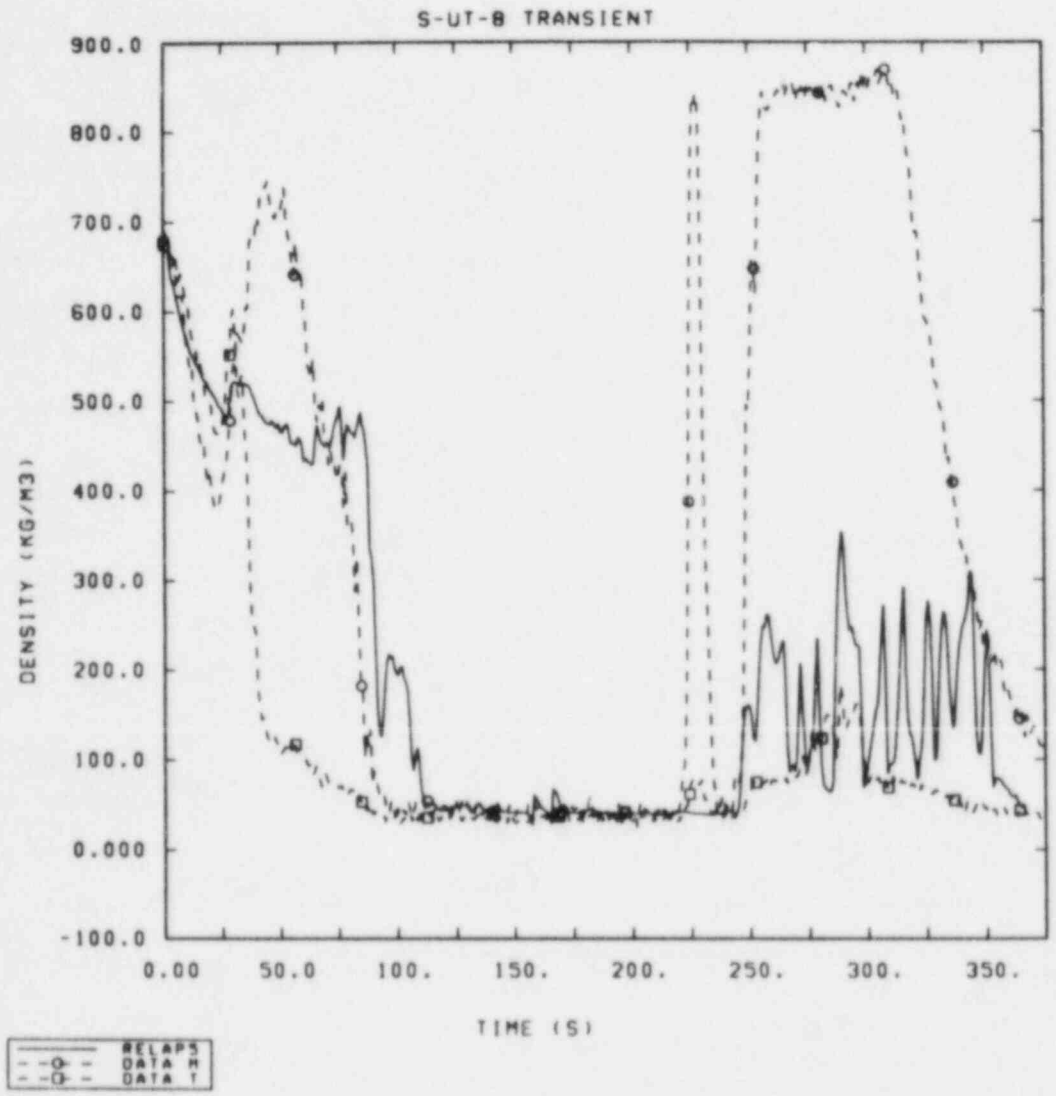

Figure 3.5.3 Comparison of Calculated and Measured Broken Loop Hot Leg Densities for Test S-UT-8

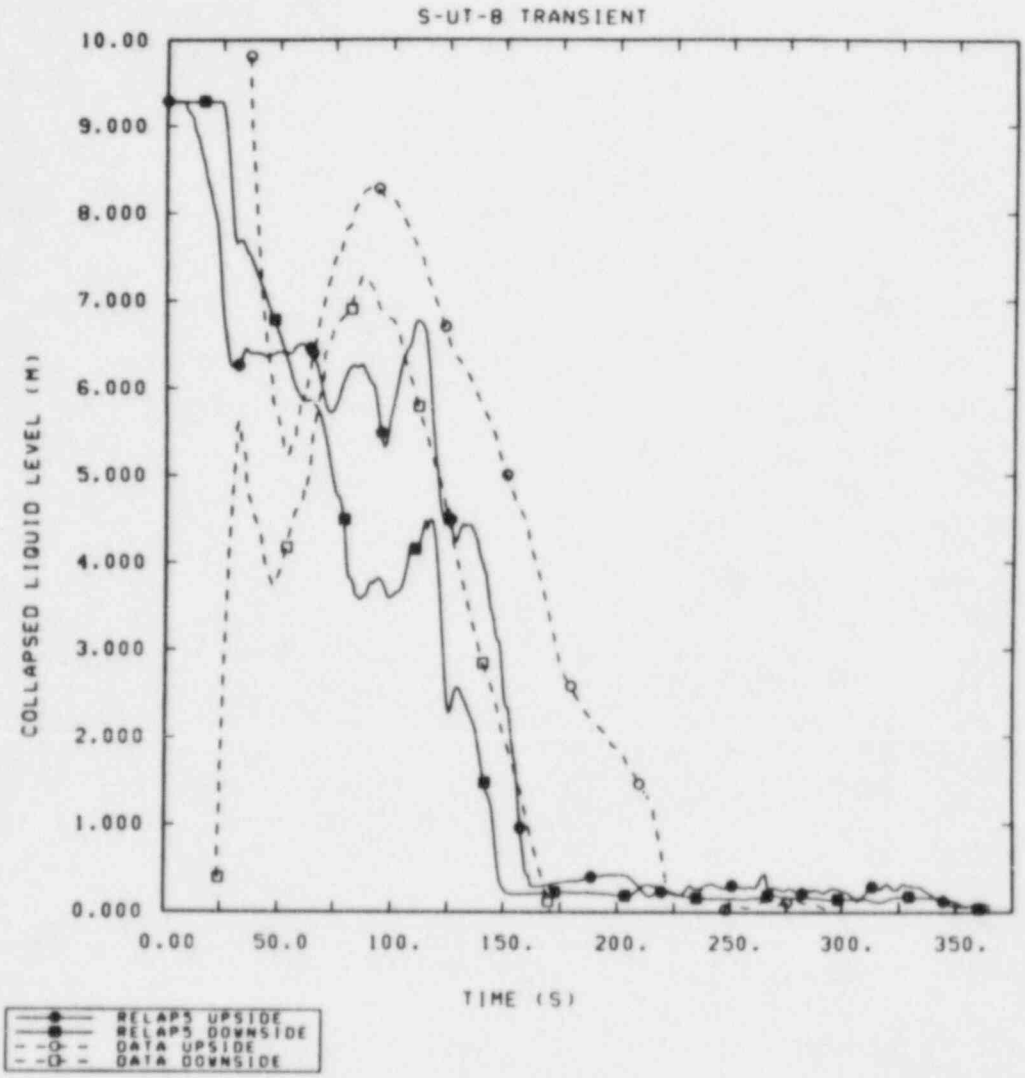

Figure 3.5.4 Comparison of Calculated and Measured Intact Loop Steam Generator Primary Side Collapsed Liquid Levels for Test S-UT-8

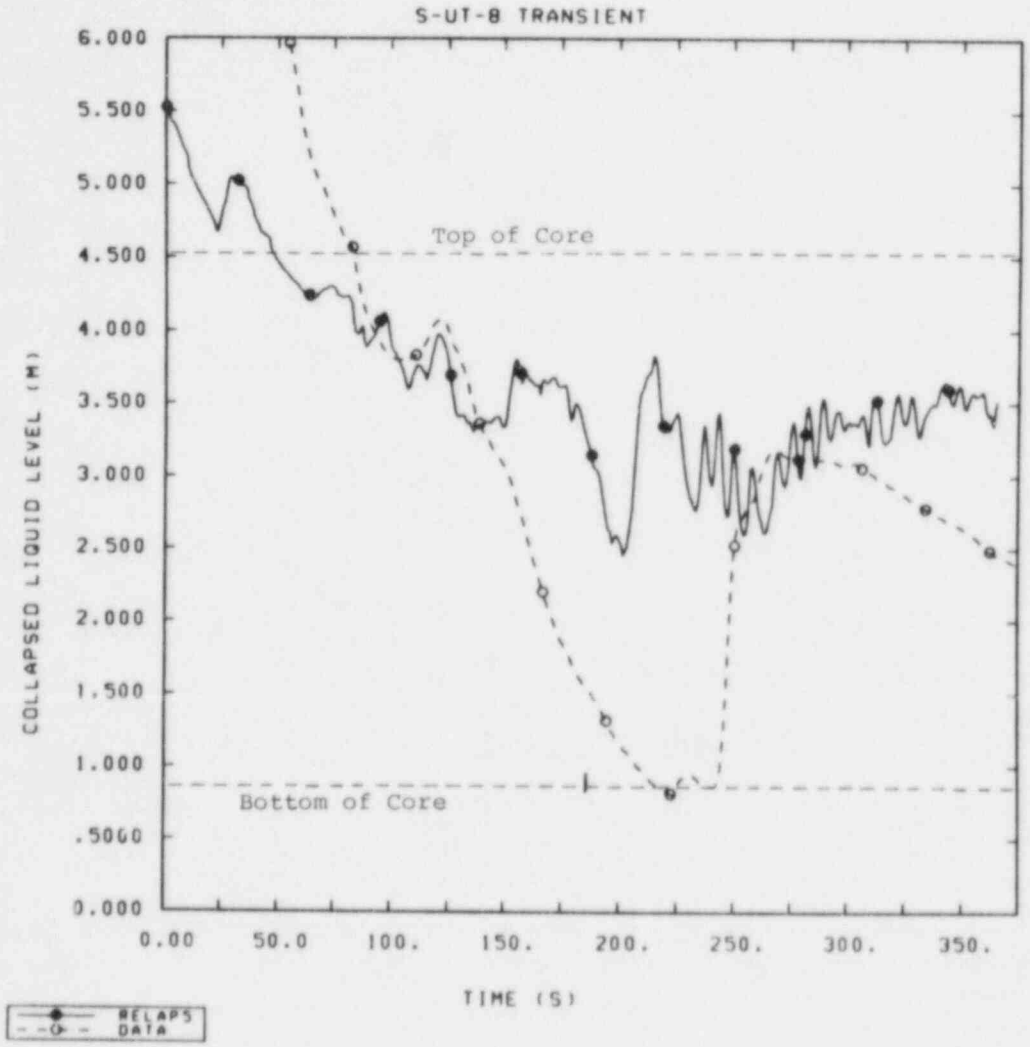

Figure 3.5.5 Comparison of Calculated and Measured Vessel Collapsed Liquid Levels for Test S-UT-8

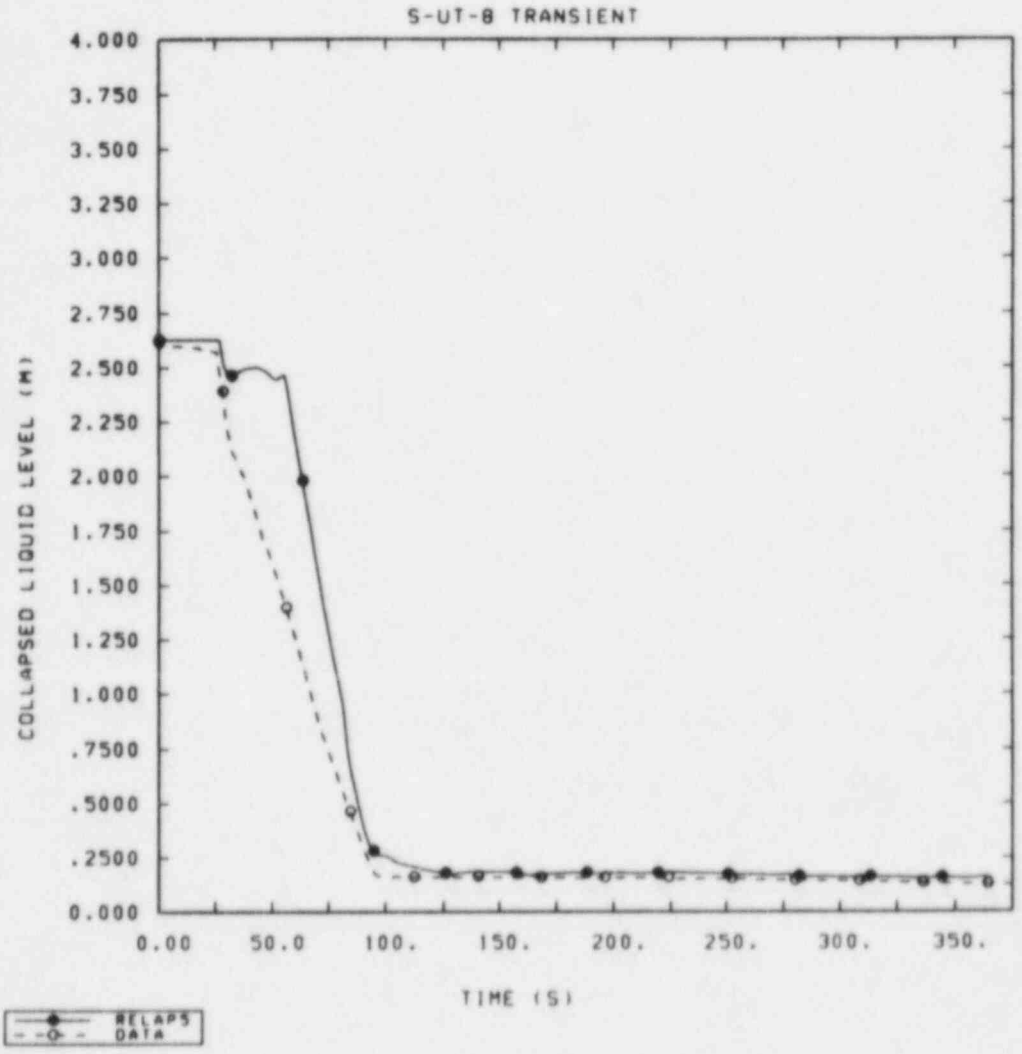

Figure 3.5.6 Comparison of Calculated and Measured Upper Head Collapsed Liquid Levels for Test S-UT-8

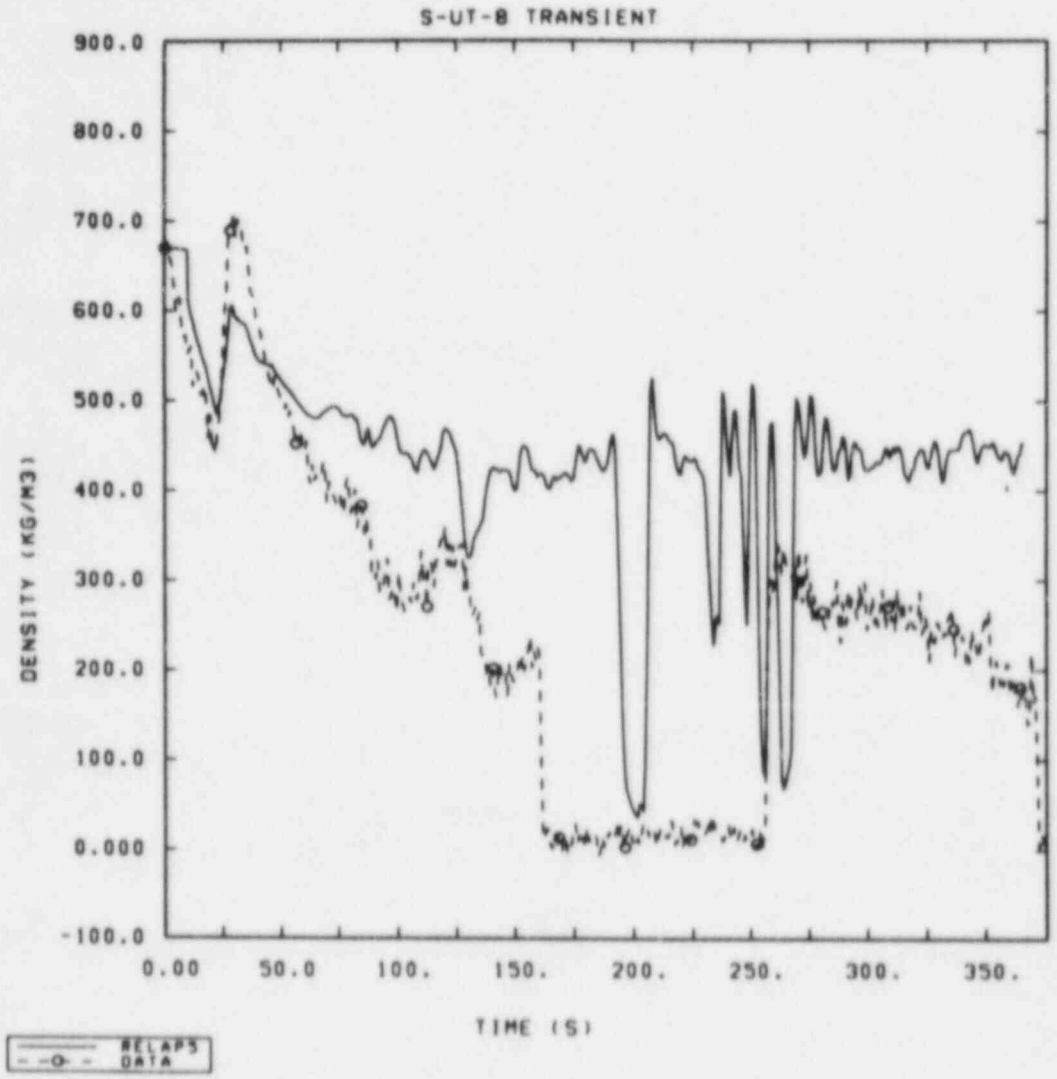

Figure 3.5.7 Comparison of Calculated and Measured Densities at the 2.53 m Core Elevation for Test S-UT-8

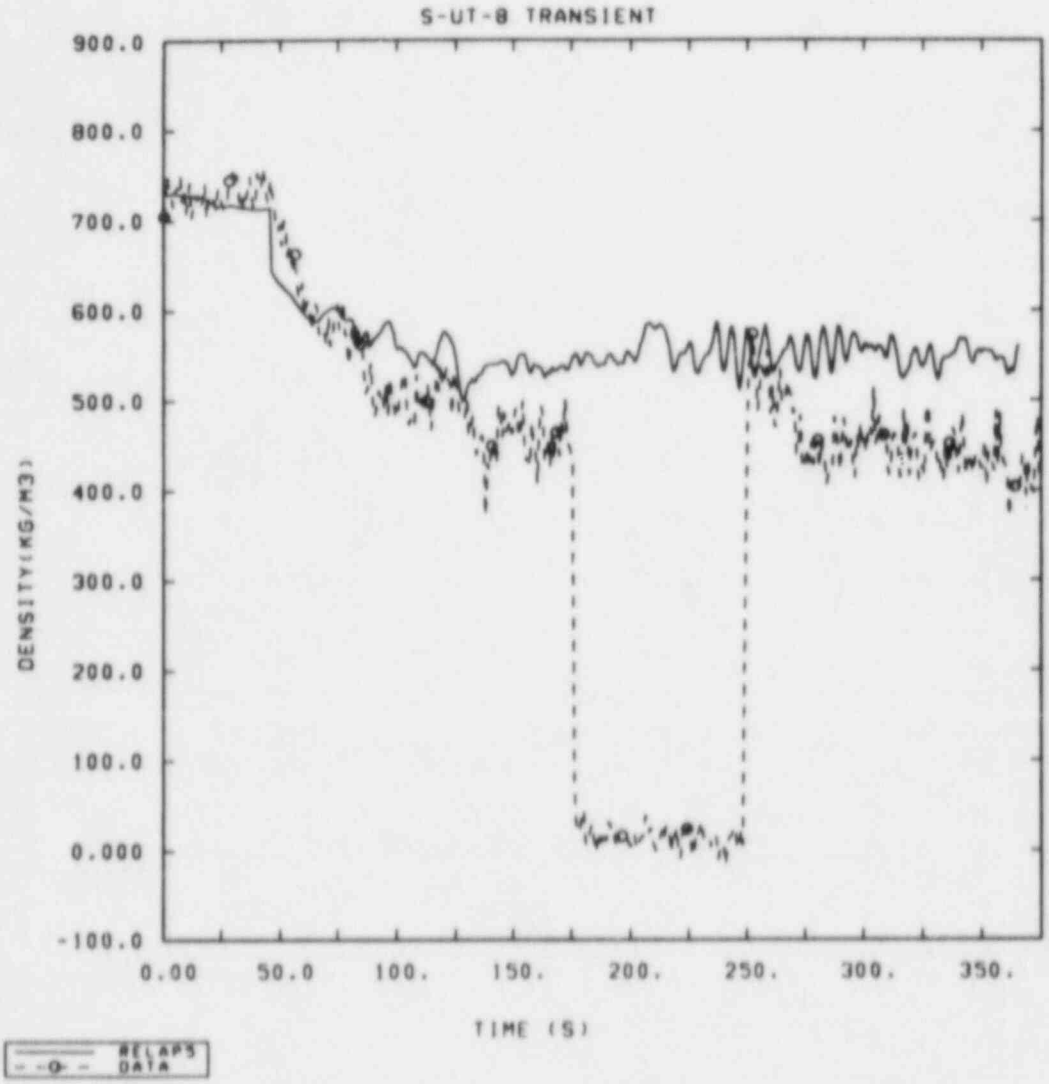

Figure 3.5.8 Comparison of Calculated and Measured Densities at the 1.73 m Core Elevation for Test S-UT-8

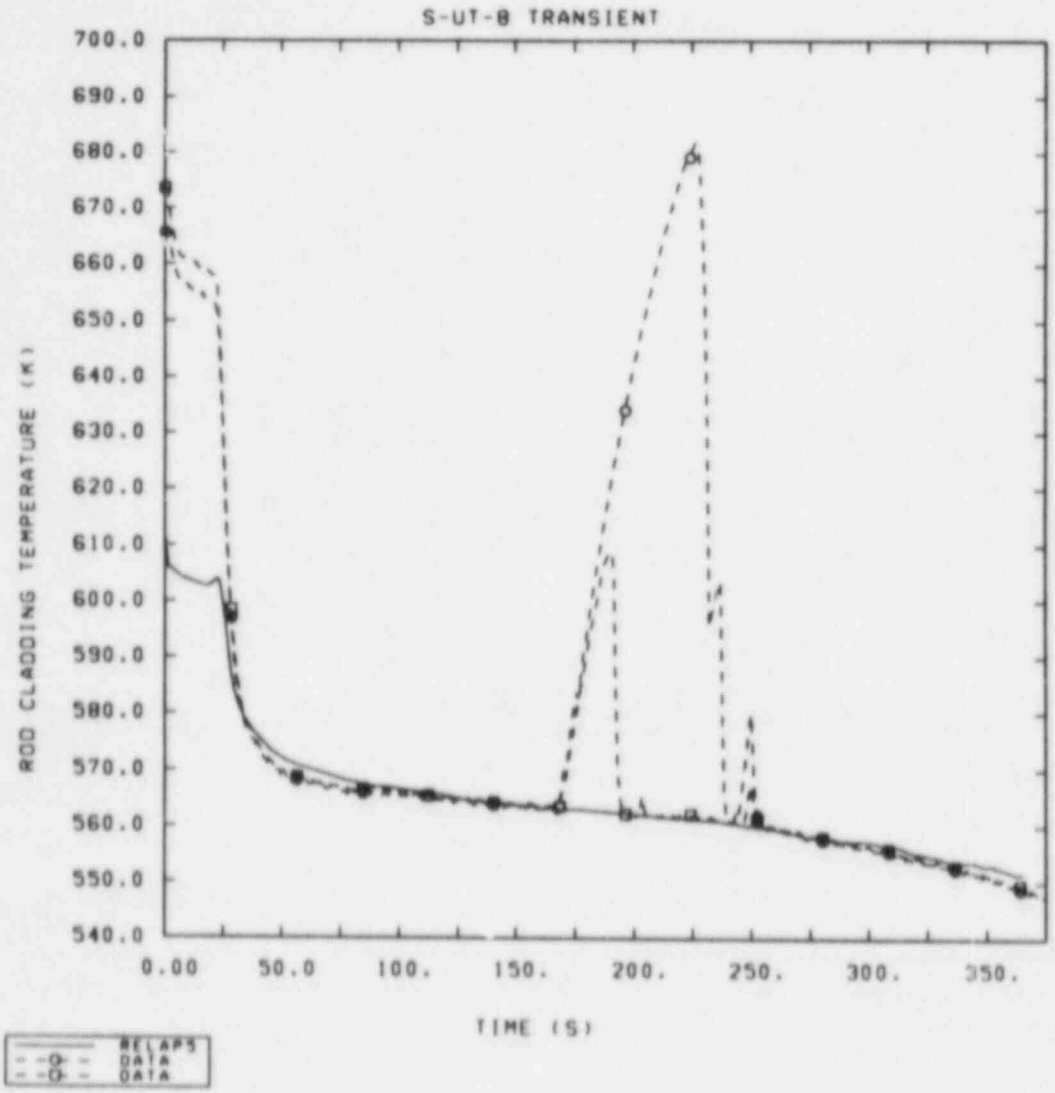

Figure 3.5.9 Comparison of Calculated and Measured Rod Cladding Temperatures at the 1.5 m to 1.8 m Core Elevation for Test S-UT-8

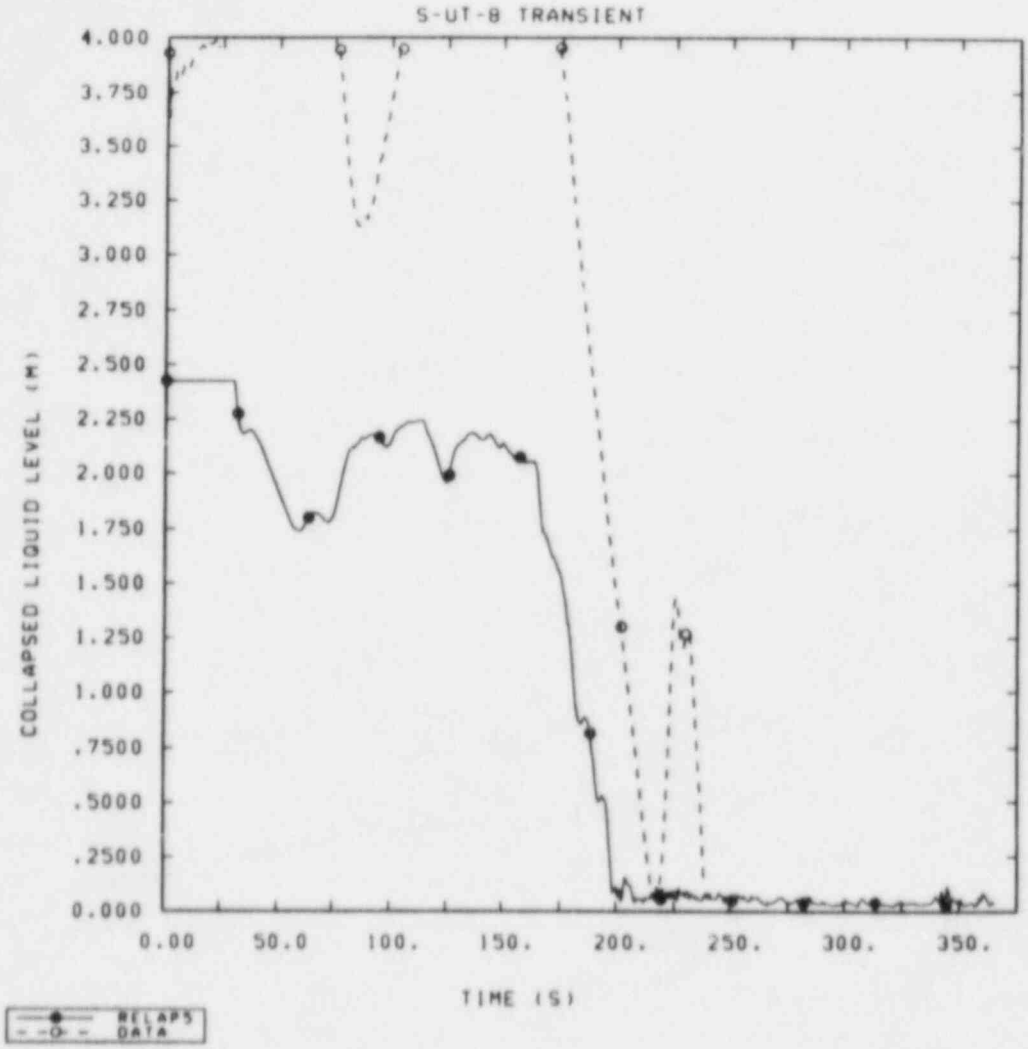

Figure 3.5.10 Comparison of Calculated and Measured Intact Loop Pump Suction Collapsed Liquid Levels for Test S-UT-8

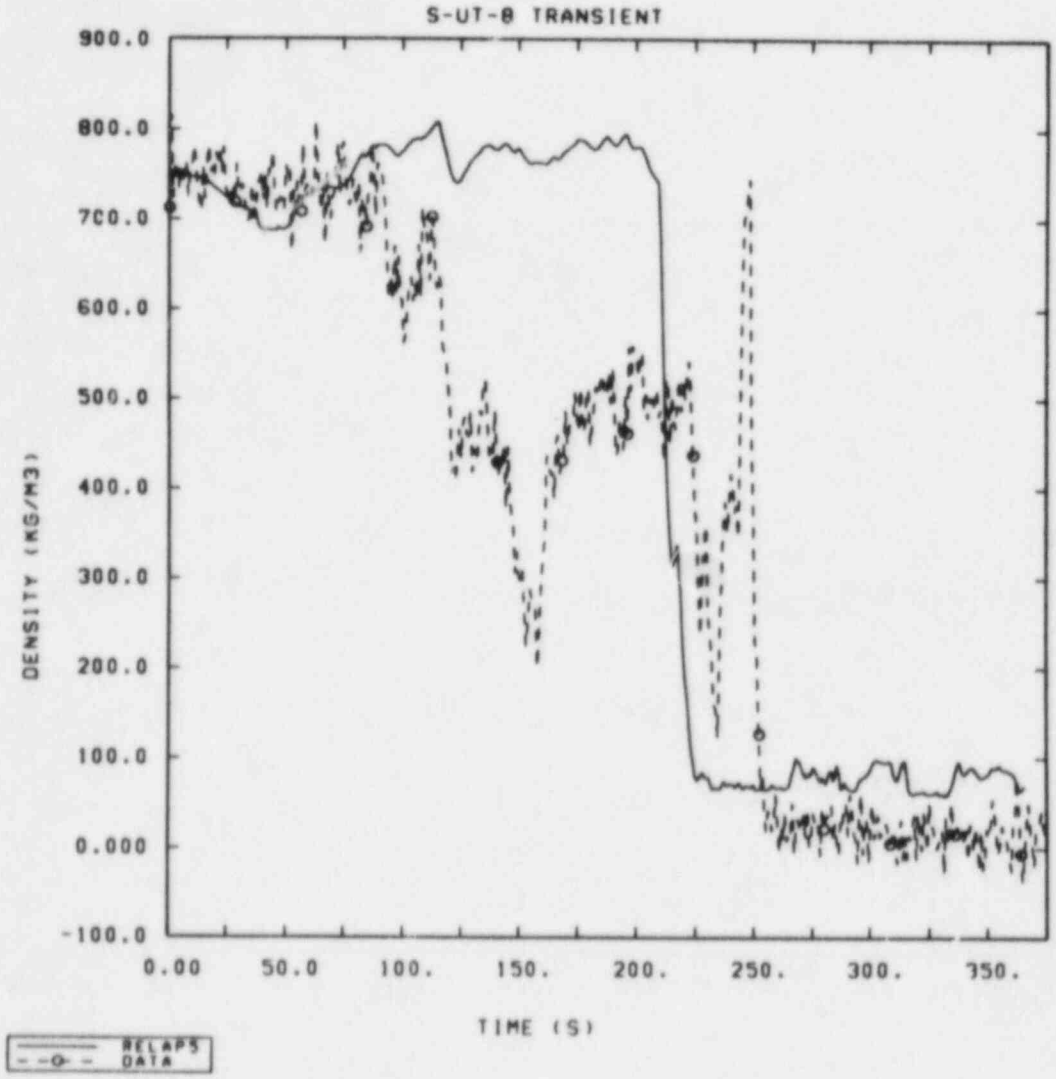

Figure 3.5.11 Comparison of Calculated and Measured Intact Loop Cold Leg Densities for Test S-UT-8

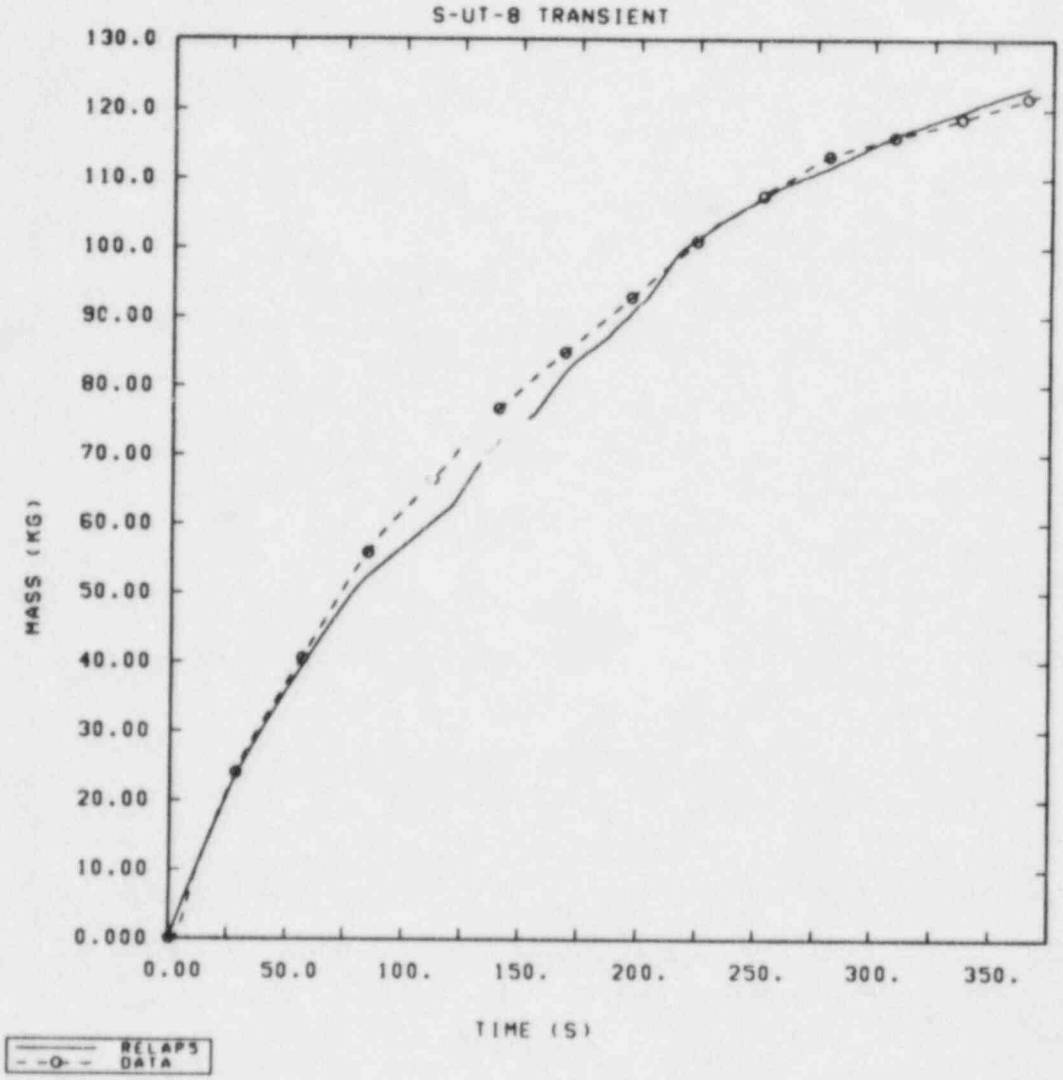

Figure 3.5.12 Comparison of Calculated and Measured Integrated Mass Flows for Test S-UT-8

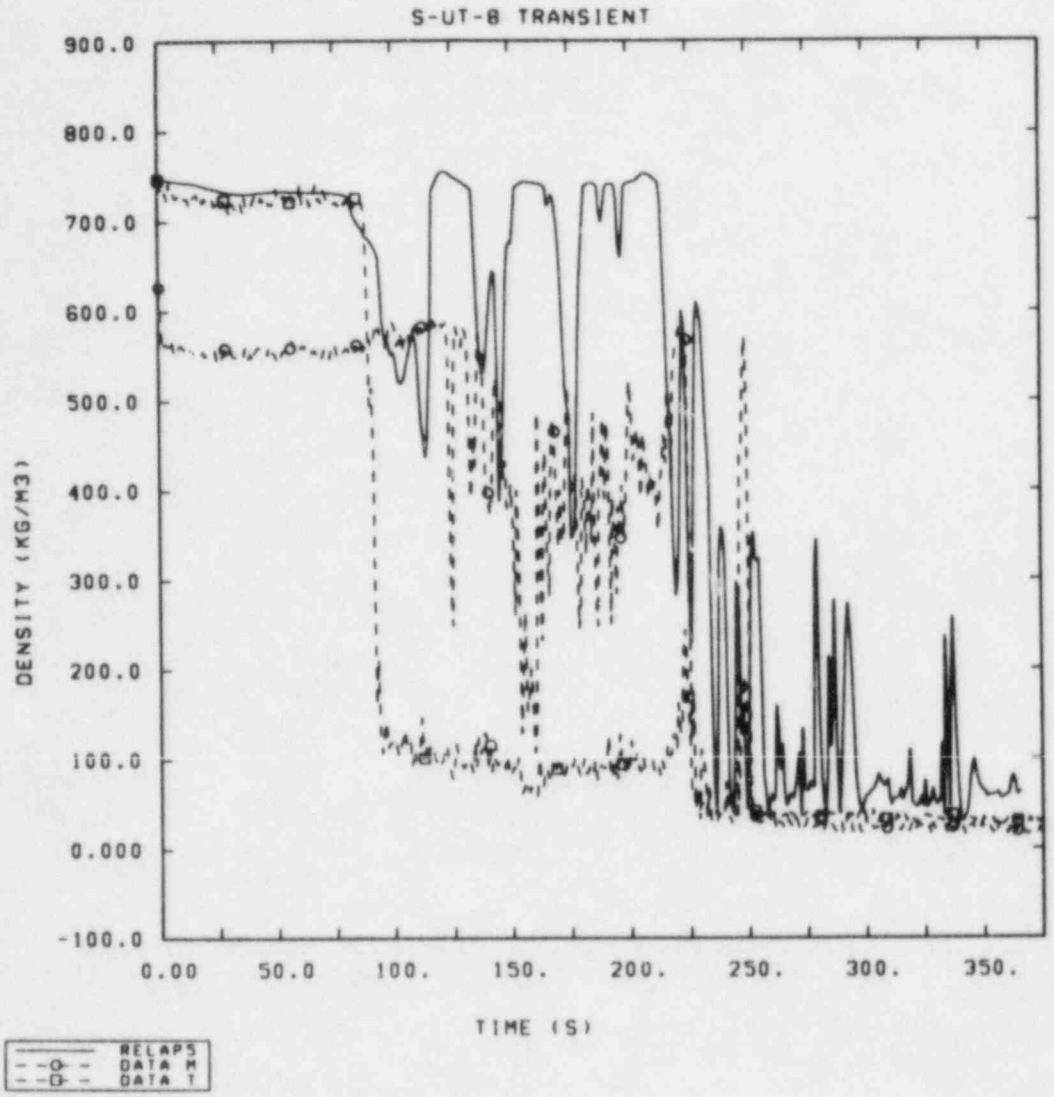

Figure 3.5.13 Comparison of Calculated and Measured Broken Loop Cold Leg Densities for Test S-UT-8

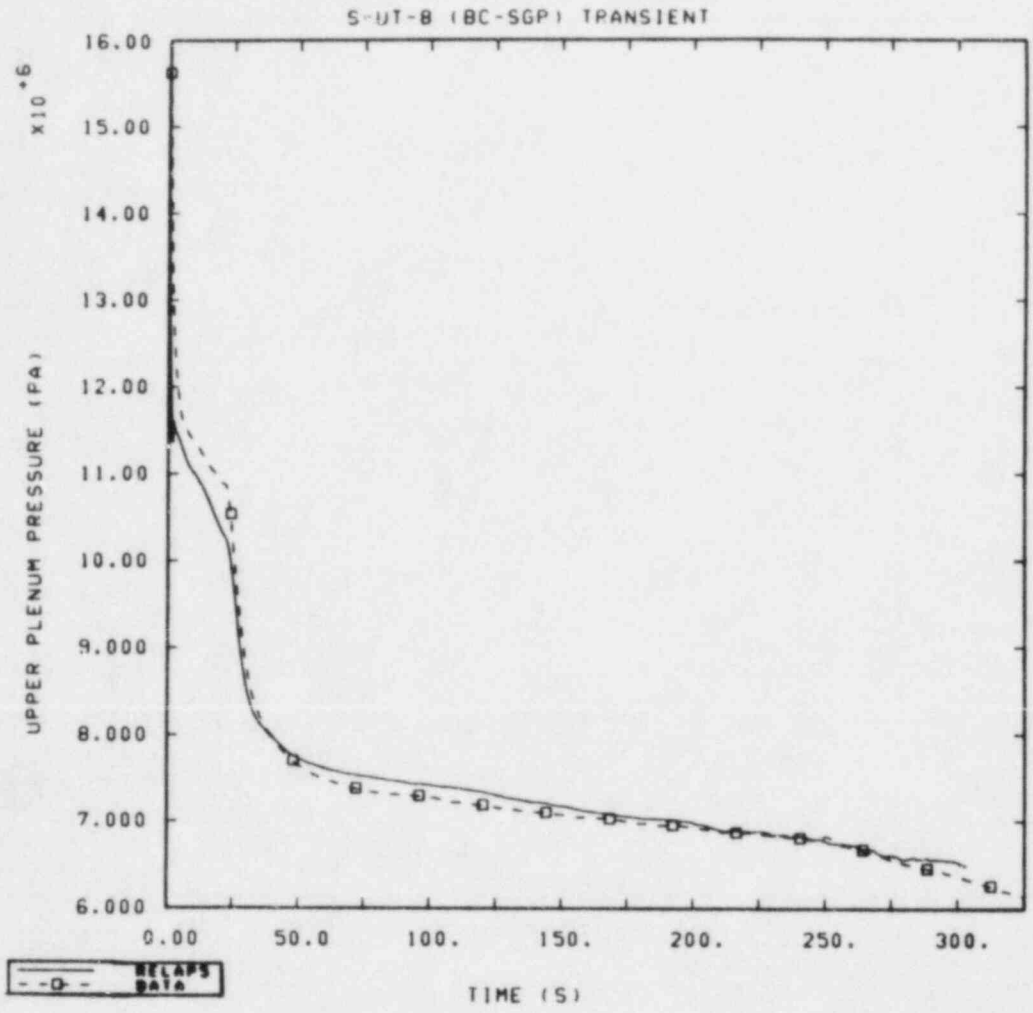

Figure 3.5.14 Comparison of Calculated (Using Steam Generator Secondary Pressures as Boundary Conditions) and Measured Primary Pressures for Test S-UT-8

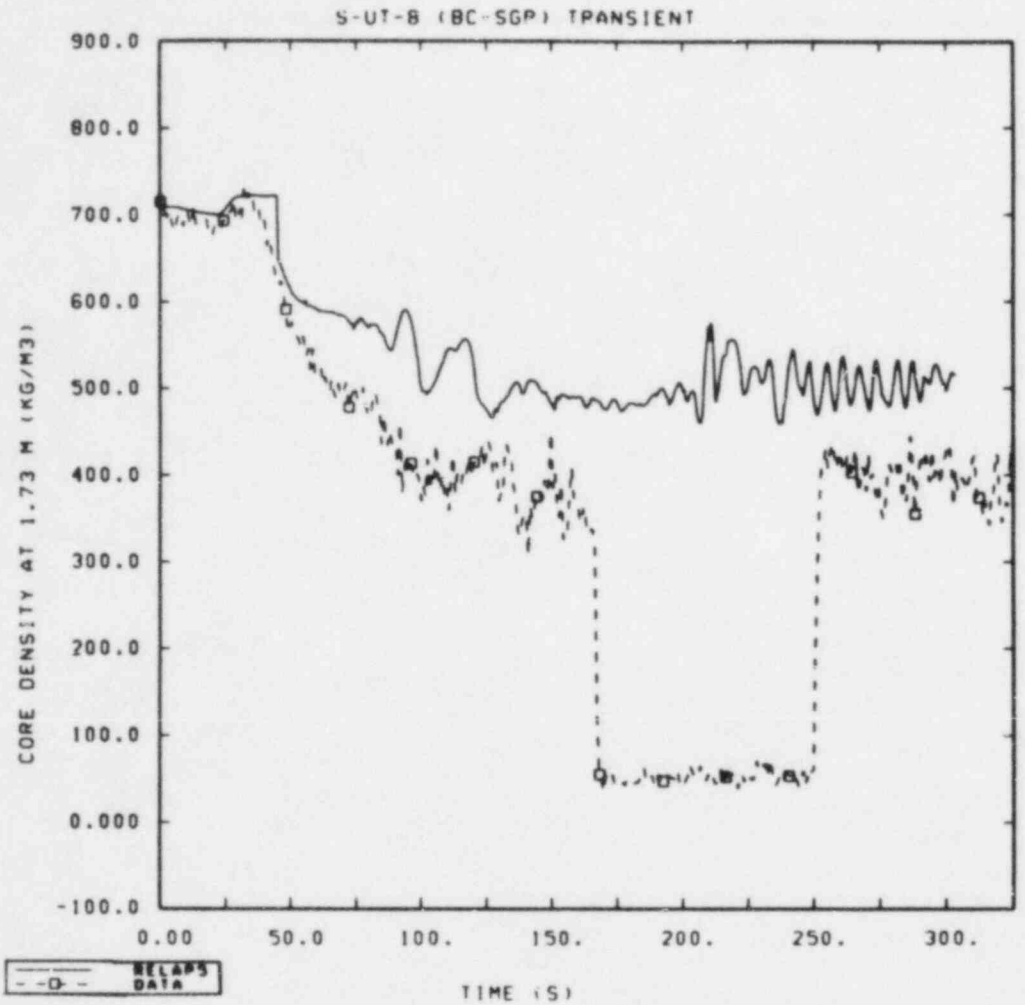

Figure 3.5.15 Comparison of Calculated (Using Steam Generator Secondary Pressures as Boundary Conditions) and Measured Densities at the 1.73 m Core Elevation for Test S-UT-8

4.0 DISCUSSION

The relative effects of UHI and break size on the calculated and measured system response during small cold leg breaks are discussed in Sections 4.1 and 4.2, respectively. The effects of changes in the upper head geometry and of a decrease in the core bypass flow are presented in Section 4.3. A brief discussion of the comparisons of these results with results from other RELAP5 assessment calculations performed at SNLA is presented in Section 4.4. The results of some limited sensitivity studies on the input model for test S-UT-1, the initial analysis performed, are presented in Section 4.5. The run time statistics for these five calculations are discussed in Section 4.6. For reference, calculated and measured key parameters for each test are summarized in Table 4.1.

4.1 Effect of UHI During Small Cold Leg Breaks

The effect of UHI on the system response for small cold leg breaks was evaluated by comparing selected results from test S-UT-1 with results from S-UT-2, and test S-UT-6 with S-UT-7. Since most of the trends were similar and the 10% break calculation with UHI (test S-UT-2) was run for a longer transient time than test S-UT-7, more results will be shown for the 10% break tests S-UT-1/S-UT-2 than for the 5% break tests S-UT-6/S-UT-7. The primary pressures for both the 5% and the 10% cold leg breaks are compared in Figure 4.1.1. During the period of UHI flow, the system depressurization was faster with UHI than without UHI in both the calculations and the tests. After the termination of UHI flow, the depressurization rate decreased and the measured primary pressure was slightly higher with UHI. The overall final difference in primary pressure was less in the tests than in the calculations.

The primary and intact loop secondary pressures for 10% cold leg breaks with and without UHI are compared in Figure 4.1.2. The comparison of the primary and secondary pressure responses in these tests indicates that the coupling between the primary and secondary systems was weak both with and without UHI. The calculated results also indicate the coupling was weak and that there were no significant differences resulting from UHI.

The calculated and measured vessel collapsed liquid levels for the 10% break tests with and without UHI are compared in Figure 4.1.3. The measured levels indicate that the major phenomena occurred at the same time with and without UHI, whereas the calculated levels indicate the major phenomena occurred about 100 s later with UHI. The test results show a 0.3 m lower minimum collapsed liquid level was measured with UHI, while the calculated minimum level was lower without UHI. The calculated collapsed

liquid level was higher with UHI because liquid was held up in the upper plenum, which increased the total vessel collapsed liquid level. Oscillations in level were measured in both tests after the initiation of intact loop accumulator flow, but were not calculated for either test. The source of these oscillations was discussed in Section 3.1. The calculated minimum vessel collapsed liquid level both with and without UHI was lower than was measured and the increase in level due to loop seal clearing was later in the transient. The calculated core levels were depressed to below the core inlet both with and without UHI and a rod heatup occurred later in the transients.

As expected, the most significant effects of UHI were in the upper head. The calculated and measured upper head collapsed liquid levels for both size breaks are compared in Figure 4.1.4. The UHI delayed the draining of the upper head by about 100 s in the 10% break test, and slightly longer in the calculation. For the 10% break with UHI, the upper head was liquid filled until the termination of UHI flow, when the upper head drained. For the 5% break, voiding and refill of the upper head occurred during UHI flow. The trend of the effect of UHI was calculated for both break sizes, but the rate of draining of the upper head was faster in each calculation than in the tests.

The calculated and measured rod cladding temperatures at the 2.4 to 3.0 m core elevation for the 10% breaks are compared in Figure 4.1.5. Measured temperatures in both tests indicated smaller dryouts and rewets at about 80 s; the calculated temperatures indicated smaller dryouts and rewets slightly later. A late-time core heatup was calculated with and without UHI, and was not measured in either test. For the late-time core heatup, the peak temperature was higher without UHI. The calculations thus indicated an effect of UHI on the rod temperatures, whereas there was no effect measured in the test, since there were no prolonged core dryouts.

The intact loop pump suction cleared before the broken loop pump suction in the 10% cold leg break tests and calculations. The intact loop upside and downside collapsed liquid levels are compared in Figure 4.1.6. The intact loop downflow side cleared at essentially the same time with and without UHI in the tests. In the RELAP5 calculations with UHI, the intact loop pump suction cleared 47 s later than without UHI. The cause of the later clearing of the pump suction in the calculation with UHI was due to an increase in the hydraulic pressure on the upper core fluid from the liquid in the upper head and support columns.

The broken loop pump suction collapsed liquid levels for the 10% break tests are compared in Figure 4.1.7. The test results were very similar in the time of clearing of the pump suction. The calculated results were not similar. For the calculation without UHI, test S-UT-1, neither the downflow nor the upflow leg cleared even though both legs cleared in the test.

The effects of UHI on the integrated total break mass flow for 10% and 5% breaks are shown in Figure 4.1.8. The large difference between the calculated and measured total mass loss for the 10% break is the result of the uncertainty in the measured masses, discussed previously. The trend of the 5% and 10% data was similar, with a higher total mass flow out the break with UHI. This trend was calculated; however, the difference in the calculated mass loss between UHI and no UHI was less than was measured. The total break mass flow was larger with UHI because the subcooling upstream of the break was greater during UHI flow.

4.2 Effect of Break Size for 10% and 5% Cold Leg Breaks (Tests S-UT-1 and S-UT-6)

The effect of the relative size of a small cold leg break was evaluated by comparing calculated and measured results for the two break sizes without UHI; similar trends occurred with UHI. The scenarios for the initial 500 s were similar for both break sizes; however, key events occurred later for the smaller break size due to a lower break flow and slower depressurization. A major difference in the test results was that a late-time core heatup occurred for the 5% break.

The effect of break size on the rate of depressurization is shown in Figure 4.2.1. The major effect, as expected, was a faster depressurization with the larger break size. The 10% break (test S-UT-1) depressurized to the loop accumulator pressure at 333 s and the 5% break (test S-UT-6) at 730 s. The calculated pressure reached the accumulator pressure at about the same time as measured for both tests; however, the correct depressurization rates were not always calculated during the transient.

The effect of break size on the vessel collapsed liquid level is shown in Figure 4.2.2. The test results show that the early depression of the vessel liquid level, before the loop seals cleared, was lower for the 10% break; however, later in the transient, the level was lower for the 5% break due to boiloff of liquid before the system pressure decreased to below the loop accumulator pressure and accumulator flow began. The calculated collapsed levels show that the early depression of the core level was also lower for the 10% break; however, the calculated difference in levels was larger than measured. The calculated level for both size breaks dropped later in the transient due to boiloff of liquid and a late-time core heatup was calculated for both size breaks, whereas a late-time core heatup was only measured for the 5% break.

The upper head collapsed liquid levels are shown in Figure 4.2.3. The measured levels show that the upper head drained earlier with the larger break, as expected. The calculated liquid levels also show that the upper head drained earlier for the 10%

break. For both break sizes, the upper head was calculated to drain at a faster rate than was measured. The correct trend was calculated; however, the overall agreement was better for the 10% break than for the 5% break.

The effect of the core liquid level on the calculated and measured rod cladding temperatures at the 3.0 to 3.6 m core elevation is shown in Figure 4.2.4. A rod dryout and rewet was measured in the 10% break when the core level was briefly depressed at about 75 s. For the 5% break, a late-time rod heatup was measured before accumulator flow was initiated. The calculated response for the 10% break resulted in several early rod dryouts and rewets; however, a late-time core heatup was also calculated that was not measured. The calculated results for the 5% break also had several dryouts and rewets between 200 and 300 s and a late-time core heatup. The calculated rod temperatures when the calculations were stopped were much higher than the measured temperatures.

The calculated and measured system masses for the 10% and 5% breaks are compared in Figure 4.2.5. The measured mass for test S-UT-1 was determined from system pressure drop measurements and there is a large uncertainty in this technique. The measured mass for S-UT-6 was determined from a balance of the inflows and outflows from the system. The measured mass for the 10% break was less than for the 5% break, until 370 s when, due to the flow from the intact loop accumulator, the total system mass for the 10% break increased above the mass for the 5% break. The calculated system mass for the 10% break decreased to about 17 kg at 325 s when the intact loop accumulator flow was initiated. The calculated mass for the 5% break had decreased to about this same magnitude when accumulator flow began at 733 s. It appears the system was recovering in the 10% break calculation and the total calculated system mass for the 10% break would be larger than for the 5% break after about 650 s if the calculation had been continued. The general trend of the effect of break size on the total system mass was thus calculated correctly; however, due to the uncertainty in the measured total mass for the 10% break, it could not be determined if the magnitude of the difference was calculated accurately.

4.3 Effect of Upper Head Geometry for a 5% Cold Leg Break (Tests S-UT-6 and S-UT-8)

As previously discussed, there were some geometry changes and differences in initial conditions between tests S-UT-6 and S-UT-8; however, the change in the amount of bypass flow was the dominant difference between the tests. To indicate the capability of RELAP5 to calculate the effect of these changes, comparisons between

selected results for tests S-UT-6 and S-UT-8 were made. The calculated and measured primary system pressures are compared in Figure 4.3.1 and show that the calculated and measured pressures for test S-UT-8 were higher than for test S-UT-6 in the initial 300 s of the transient. This difference resulted from a higher pressurizer surge line resistance in test S-UT-8. The calculated results follow the trend of the measurements and it appears that, if the S-UT-8 calculation were continued, the pressure would be lower later in the transient than for test S-UT-6, similar to the data.

The most significant effect of the changes on the test results was on the core collapsed liquid level. The calculated and measured core collapsed liquid levels are compared in Figure 4.3.2. The measured level for test S-UT-8 decreased to the core inlet, uncovering the entire core, whereas the level for test S-UT-6 dropped only to about the 2.5 m core level. The calculated results were about the same for both tests, with the minimum level being 1.6 m above the core inlet. As discussed in Section 3.5, the reason the large core level depression was not calculated for test S-UT-8 was apparently because the upflow side of the intact loop steam generator tubes drained too early.

The effect of the changes in geometry and the amount of bypass flow on the draining of the upper head are shown in Figure 4.3.3. In both the calculations and tests, the upper head drained earlier for test S-UT-8 than for test S-UT-6, indicating the correct effects of the changes in geometry on the upper head hydraulics were calculated qualitatively, although the measured difference in draining between the tests was larger than the calculated difference.

An important difference in the results between tests S-UT-6 and S-UT-8 was the time the primary upflow side of the intact loop steam generator tubes drained of liquid. The draining of the tubes for both tests is indicated by the upflow side collapsed liquid levels shown in Figure 4.3.4. The measured levels show that liquid remained in the tubes until 220 s in test S-UT-8, whereas the tubes had drained by 180 s in test S-UT-6. The calculated levels show that the tubes drained about 10 s earlier for test S-UT-8 than for test S-UT-6. The difference in the time the primary side of the intact loop steam generator tubes drained of liquid caused a more severe core liquid level depression during test S-UT-8 than during test S-UT-6, and this difference was not calculated correctly.

The effect on the rod clad temperatures of the core liquid level is shown in Figure 4.3.5. The calculated and measured rod cladding temperatures at about 1.8 m above the core inlet are compared. The early depression of the core level in test S-UT-8

resulted in a temperature increase, whereas for test S-UT-6 an early temperature increase was not measured. The calculated results show that an early-time temperature increase was not calculated for either test. Miscalculating the effect of the change in geometry on the core liquid level resulted in an incorrect calculation of the early-time rod temperature for test S-UT-8. A late-time rod heatup was measured for test S-UT-8; however, the S-UT-8 calculation was not run for enough transient time to determine if an analogous rod heatup would be calculated, but, based on previous calculations for this test series, it probably would be. A late-time rod heatup was calculated at this elevation for test S-UT-6 that was not measured, although other regions of the core did experience a late-time heatup in the test.

Both of these tests were conducted with the same size break. The calculated and measured integrated break flows are compared in Figure 4.3.6. The measured integrated break flows show that some differences occurred early in the tests; however, by 700 s the total mass flow from the system was the same for both tests. The calculated integrated break flows also indicate some differences between 50 and 100 s with more mass flow from the system for test S-UT-8 than for test S-UT-6, similar to the measured results. By about 330 seconds, both calculations and test data had approximately the same mass loss.

4.4 Comparison of S-UT Results With Other RELAP5 Assessment Results

Some of the results from the S-UT series were similar to results from other RELAP5 assessment calculations performed at SNLA. These similarities will be briefly discussed to provide an overall indication of the capabilities of RELAP5.

The oscillations in the accumulator flow that were calculated for tests S-UT-1, S-UT-2, and S-UT-7, which were caused by a large surge in the flow from the accumulator dropping the accumulator pressure to below the system pressure, also occurred in other assessment calculations. Similar oscillations in the accumulator flow were calculated for small and intermediate breaks in the LOFT facility. [20,21] Several attempts were made to determine the cause of this problem for the intermediate break calculation, but the cause could not be identified. Problems with the accumulator component were also identified in calculations for large breaks in the LOBI facility. [25]

The experimental conditions for 2.5% cold leg breaks previously performed in the Semiscale Mod-3 facility [18] were somewhat similar to the conditions for the S-UT series, and some similar results were calculated. The calculated steam generator secondary pressure was higher than measured for these S-UT tests,

when there was no auxiliary feed water to the steam generators. The results from those Semiscale Mod-3 small break analyses also calculated too high a steam generator secondary pressure when there was no auxiliary feed water flow. (With no auxiliary feed water flow, the temperature of the secondary side of the steam generator was nearly uniform at the saturation temperature.)

Another result that was the same for the Semiscale Mod-3 and Mod-2A small breaks was the calculation of sudden late-time drops in the core densities. The calculated core densities were higher than measured early in the transient and then as the core liquid boiled off they rapidly decreased and were lower than measured. There was not a smooth, gradual change in the density as would be expected when the liquid was boiling off.

When the horizontal break uncovered, the calculated break mass flow rate for the S-UT series was higher than measured, because a two-phase mixture continued to flow out the break rather than only steam, since RELAP5/MOD1 does not model break stratification effects. A higher break mass flow rate was also calculated when the break uncovered during those small breaks tests with early pump trip in the Semiscale Mod-3 facility.

In summary, many of the significant phenomena that were identified in these analyses have also been calculated for tests in other facilities.

4.5 Sensitivity Studies

Test S-UT-1 was the first analysis performed, and a limited number of sensitivity studies were run to investigate the effect of various modeling methods on the calculated results. The studies included:

1. the use of one horizontal volume or two forty-five degree inclined volumes for the pump suctions to determine if noding affected the time of clearing of the pump suctions,

2. injecting HPI into one volume or splitting the flow equally into an upstream and downstream volume at the injection point to determine the effect of HPI on the intact loop cold leg temperatures,

3. modeling the communicative cold leg break as one junction with the full break size from one volume, and modeling the break with two junctions, each one half of the break area, from an upstream and downstream volume at the break location, to determine if communicative breaks need to be modeled as connected to two different volumes,

4. changing the noncondensible gas,

5. changing the subcooled discharge coefficient from 0.85 to 0.70, and

6. changing the saturated discharge coefficient from 0.85 to 0.65.

The only sensitivity studies which will be discussed in any detail will be the changes in the discharge coefficients and the change in the noncondensible gas, since the other studies did not indicate any significant effect on the calculated results.

Changing the noncondensible gas, which is the gas that pressurizes the accumulators, from air to nitrogen resulted in large differences in the clearing of the broken loop pump suction. The reason for this is not clearly understood at this time. INEL has suggested that the most probable cause is a RELAP5/MOD1 coding error in loading the pressure solution matrix for the accumulator. In our calculation there was a pressure imbalance in the first time step, because the pressure in the accumulator surge line was erroneously input as being significantly lower than the pressure in the accumulator. This imbalance occurred in the first time step when the ECC system was added to the model and the steady state calculation was being continued for an additional two seconds before the initiation of the transient. The RELAP5 Development Team [26] identified that, once the accumulator model has been activated, the error in the pressure solution matrix of the accumulator could possibly propagate through the whole system, although it should be significant only near the accumulator junctions. To clearly resolve this result, the calculations should be repeated with the accumulator model corrected.

The effects of the break discharge coefficients on the system mass and pressure for test S-UT-1 were studied in an attempt to obtain better agreement with the system data, since there was a large uncertainty in the measured break flow. The values of the coefficients were selected to give better agreement with the estimates of the system mass later in the transient. The integrated mass flows for the base case with saturated and subcooled coefficients of 0.85, a case using a subcooled coefficient of 0.70 and a saturated coefficient of 0.85, and a case using a subcooled coefficient of 0.85 and a saturated coefficient of 0.65 are compared in Figure 4.5.1. Even though less mass had left the system, the comparisons with the broken loop densities and with the time the break saturated were not as good with a subcooled discharge coefficient of 0.70 as with the original base case value of 0.85.

The long term results with the saturated discharge coefficient of 0.65 were that about 10 kg more mass remained in the system than for a coefficient of 0.85. The results with this lower saturated coefficient agreed better with the core thermal response, since a late-time core heatup was not calculated. The agreement with the system pressure, however, was not as good with the lower discharge coefficients, as shown in Figure 4.4.2. The pressure was higher with the lower coefficients than for the base case. At 337 s, when the calculation with a saturated coefficient of 0.65 was terminated, the calculated pressure was 4.0 MPa, which was 1.5 MPa above the pressure of the accumulator. The intact loop accumulator flow initiated at 333 s in the test and at 327 s in the base calculation. Since the overall pressure agreement was better with subcooled and saturated discharge coefficients of 0.85, these coefficients were used for the final calculations for the 10% break tests.

4.6 Computational Speed

A summary of the run time statistics for each of the transients is provided in Table 4.6.1. The Courant limit check dominated control of the time step for tests S-UT-1 and S-UT-2 (the 10% breaks), while mass error controlled more often in tests S-UT-6 and S-UT-7 (5% breaks). For the S-UT-8 calculation, a 5% break, the Courant limit again dominated the time step control.

The accumulated CPU times on our Cray-1S computer for the final transient calculations are shown in Figures 4.6.1 and 4.6.2. The results for the 10% breaks (tests S-UT-1 and S-UT-2) shown in Figure 4.6.1 illustrate that, except during UHI injection for test S-UT-2, the average CPU per problem time was about 6 to 1. During UHI injection, which was from 23 to 147 s, the average ratio was about 19 to 1. The step increases seemed to occur during periods when the UHI accumulator flow was cycling on and off; however, the time step was mainly controlled by the mass error criterion in the core bypass line. Later in the S-UT-2 calculation the time step was mostly controlled by the Courant limit in the intact loop hot leg piping and at the broken loop pump outlet. Courant limits in the intact loop hot leg piping and the primary side of the intact loop steam generator mainly controlled the time step later in the S-UT-1 calculation.

The accumulated CPU time for the 5% breaks (tests S-UT-6, S-UT-7 and S-UT-8) are shown in Figure 4.6.2. The two tests without UHI, S-UT-6 and S-UT-8, both ran at about a ratio of CPU per problem time of 4.5 to 1 throughout the transients. The controlling volumes for tests S-UT-6 and S-UT-8 were the intact loop hot leg piping and the broken loop pump suction. Test S-UT-7 ran at an overall ratio of 6.2 to 1. Step increases in CPU time per problem time for test S-UT-7 occurred at about 190 s and 290 s, when spikes in the UHI accumulator flow occurred. During these periods, the time step was mostly controlled by the mass error criterion in the UHI surge line and the core bypass line.

Table 4.1 Summary of Key Parameters for S-UT Parameters

	S-UT-1		S-UT-2		S-UT-6		S-UT-7		S-UT-8	
	EXP	CALC	EXP	CALC	EXP	CALC	EXP	CALC[1]	EXP	CALC[2]
Minimum Vessel Collapsed Liquid Level (m) (Referenced to Core Inlet)	1.15	-0.51	0.86	-0.10	1.15	-0.54	1.61	1.40	0.00	1.57
Time of Minimum Vessel Collapsed Liquid Level (s)	74	424	72	454	780	800	800	265	230	201
Peak Rod Clad Temperature (K)	658	839+	630	745+	658	868+	570	581	825	NO
Time of Initiation of Core Uncovery (s)[3]	38	31	38	31	71	75	72	52	85	47
Time of HPI Initiation (s)	2.0	2.4	2.0	2.5	35.1	35.1[4]	35.1	35.1[4]	35.1	35.1[4]
Time of IL Accumulator Injection (s)	333	327	345	375	730	750	822	NO	520	NO
IL SG Peak Pressure (MPa)	7.09	7.03	6.80	7.20	7.08	6.80	7.06	6.74	7.22	7.73
BL SG Peak Pressure (MPa)	6.01	6.39	6.26	6.52	6.40	6.51	6.34	6.23	6.78	6.84
Time of IL SG Peak Pressure (s)	17	25	20	21	28	18	29	23	29	43
Time of BL SG Peak Pressure (s)	17	45	22	46	32	411	28	78	43	72
Time IL Secondary-Primary Pressure Equalization (s)	78	91	71	75	225	278	208	229	263	249
Time BL Secondary-Primary Pressure Equalization (s)	134	126	102	95	278	311	253	242	275	278
Time IL Pump Suction Down Flow Leg Clearance (s)	72	118	73	150	220	214	220	212	240	200
Time BL Pump Suction Down Flow Leg Clearance (s)	130	NO	64	150	305	NO	300	NO	NA	NO

(1) Transient Calculation Stopped at 423 s
(2) Transient Calculation Stopped at 360 s
(3) Collapsed Liquid Level Below Top of Core From Initiation of Uncovery Until Transient Terminated
(4) Correct Because Forced Trip on Time
NA Not Available
NO Did Not Occur During Transient

Table 4.6.1 Execution Statistics for Tests S-UT-1, S-UT-2, S-UT-6, S-UT-7, and S-UT-8

	S-UT-1	S-UT-2	S-UT-6	S-UT-7	S-UT-8
Problem Time (s)	589.5	565.4	800.0	437.6	365.6
CRAY-1 CPU Time (s)	3746.0	5615.0	3742.0	2693.0	1590.0
Total Cycles	19627	28417	19872	13984	8170
Repeated Time Steps	3151	2645	4581	2947	1530
% Repeated Time Steps	16	9	23	21	18
% Controlled by Quality Check	24	25	27	15	20
% Controlled by Mass Error Check	21	24	34	53	27
% Controlled by Property Check	8	10	7	3	3
% Controlled by Courant Limit Check	47	41	32	29	50
Grind Time (s) (CPU/volume-cycle)	.00094	.00094	.00091	.00092	.00093

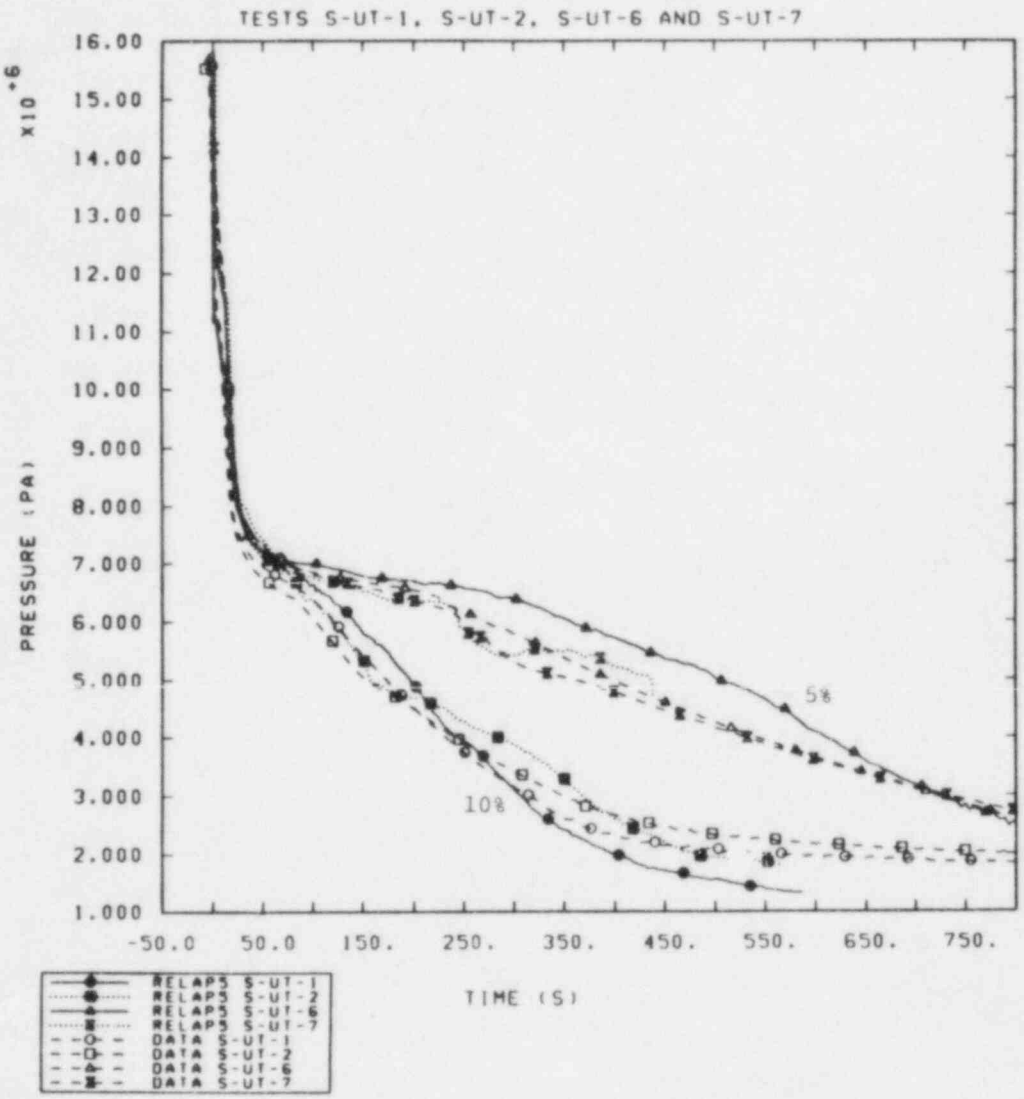

Figure 4.1.1 Effect of UHI on Primary Pressure for 10% and 5% Cold Leg Breaks

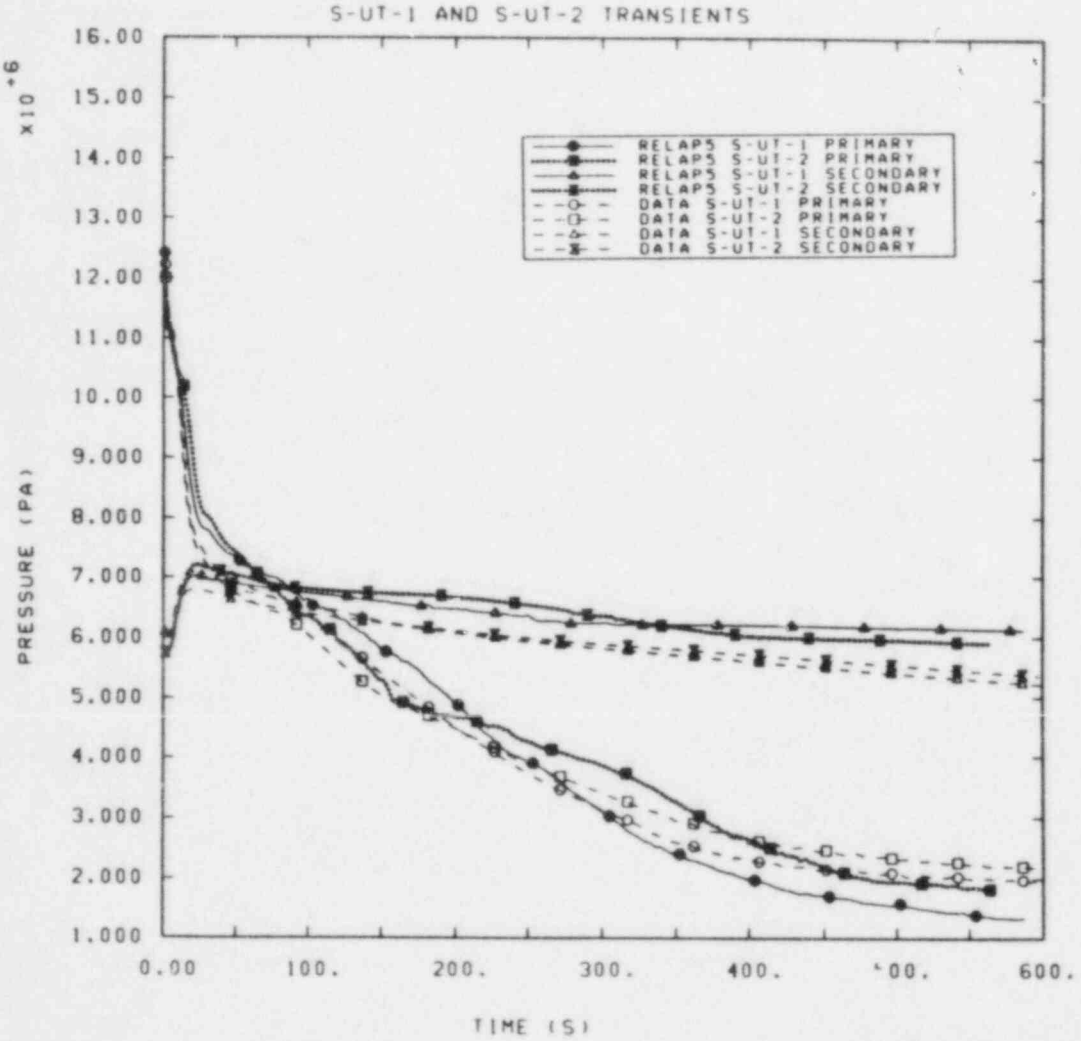

Figure 4.1.2 Effect of UHI on Primary and Intact Loop Steam Generator Secondary Pressures for 10% Cold Leg Break

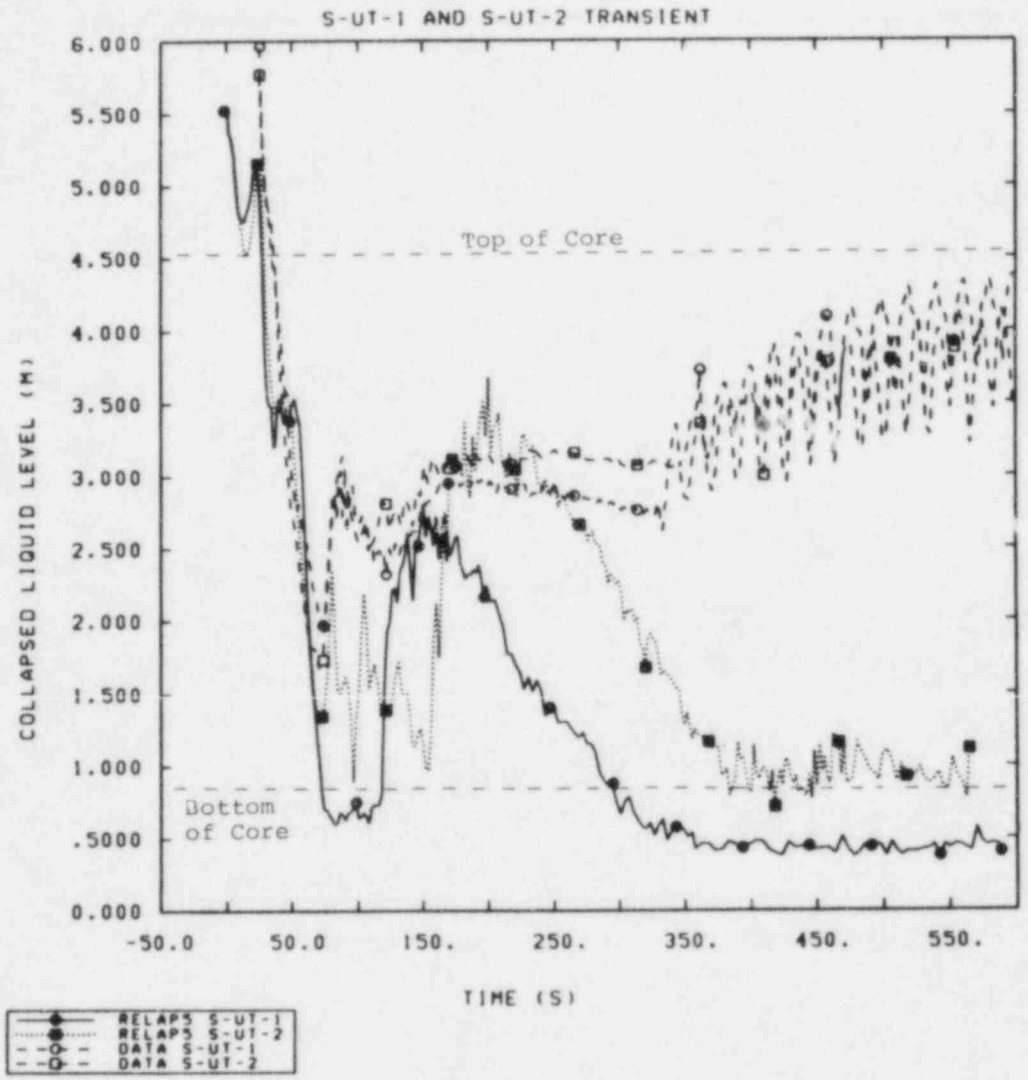

Figure 4.1.3 Effect of UHI on the Vessel Collapsed Liquid Level for 10% Cold Leg Breaks

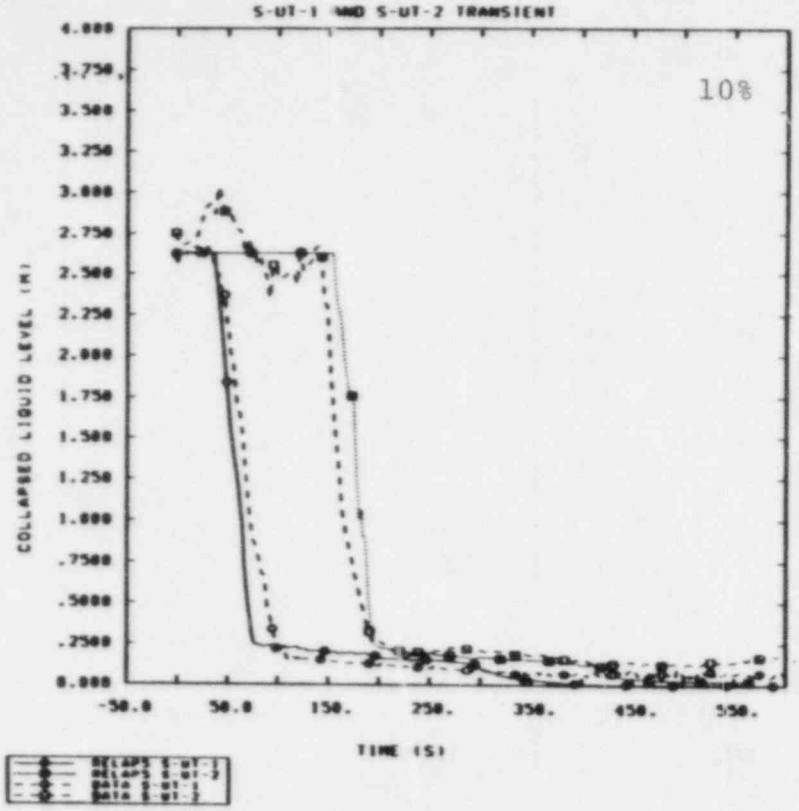

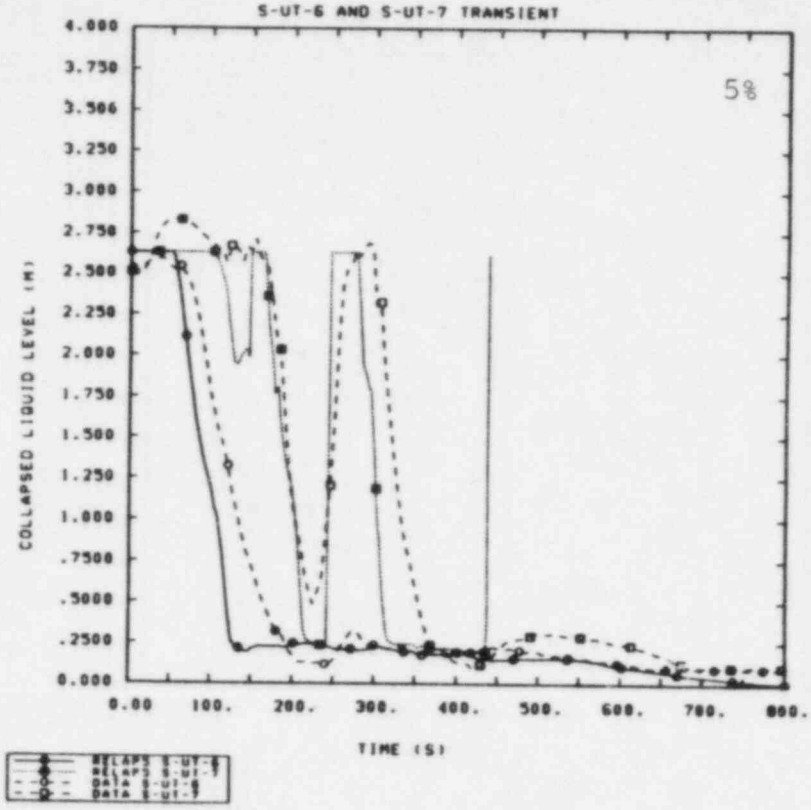

Figure 4.1.4 Effect of UHI on the Upper Head Collapsed Liquid Level for 10% and 5% Cold Leg Breaks

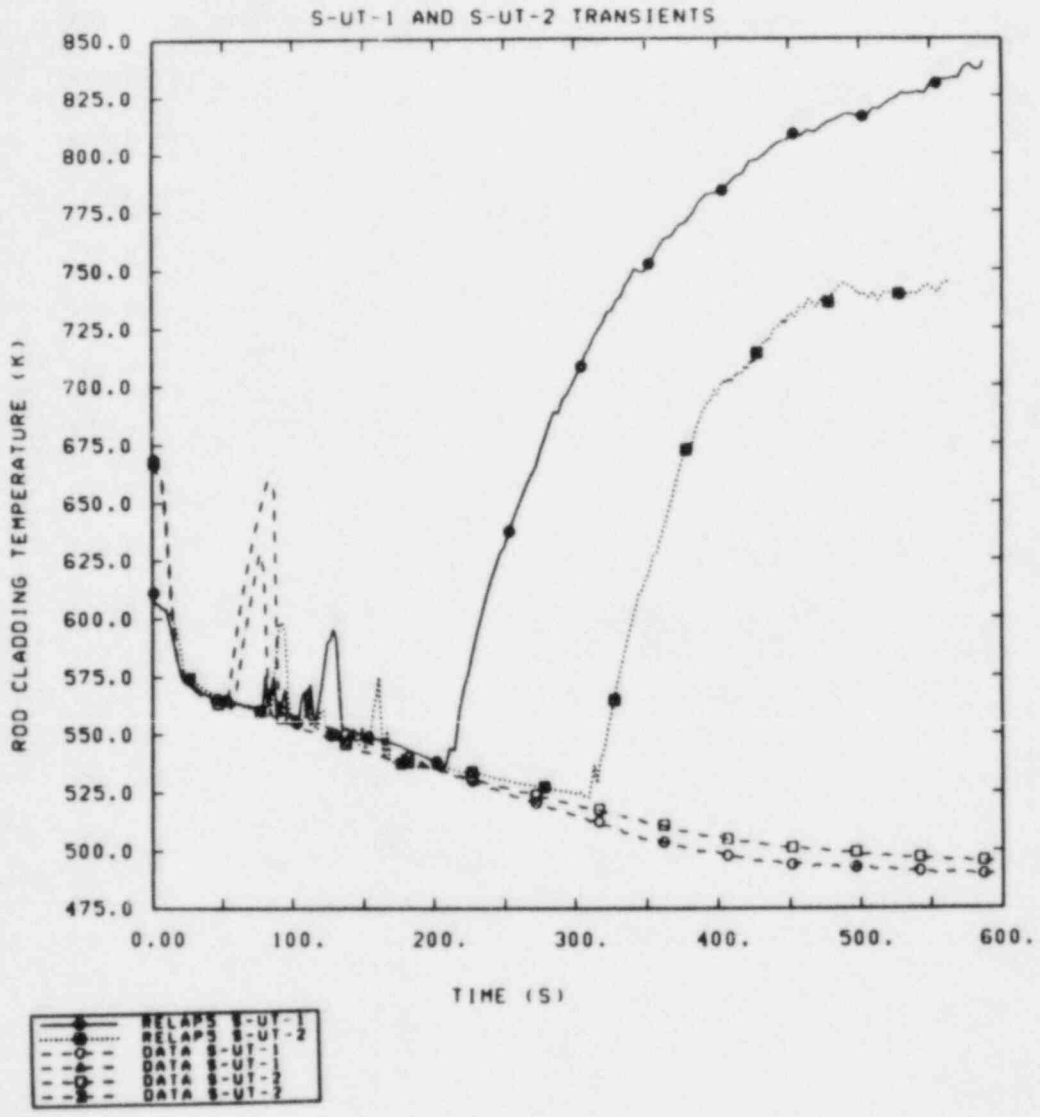

Figure 4.1.5 Effect of UHI on the Rod Cladding Temperature at the 2.4 m to 3.0 m Core Elevation for a 10% Cold Leg Break

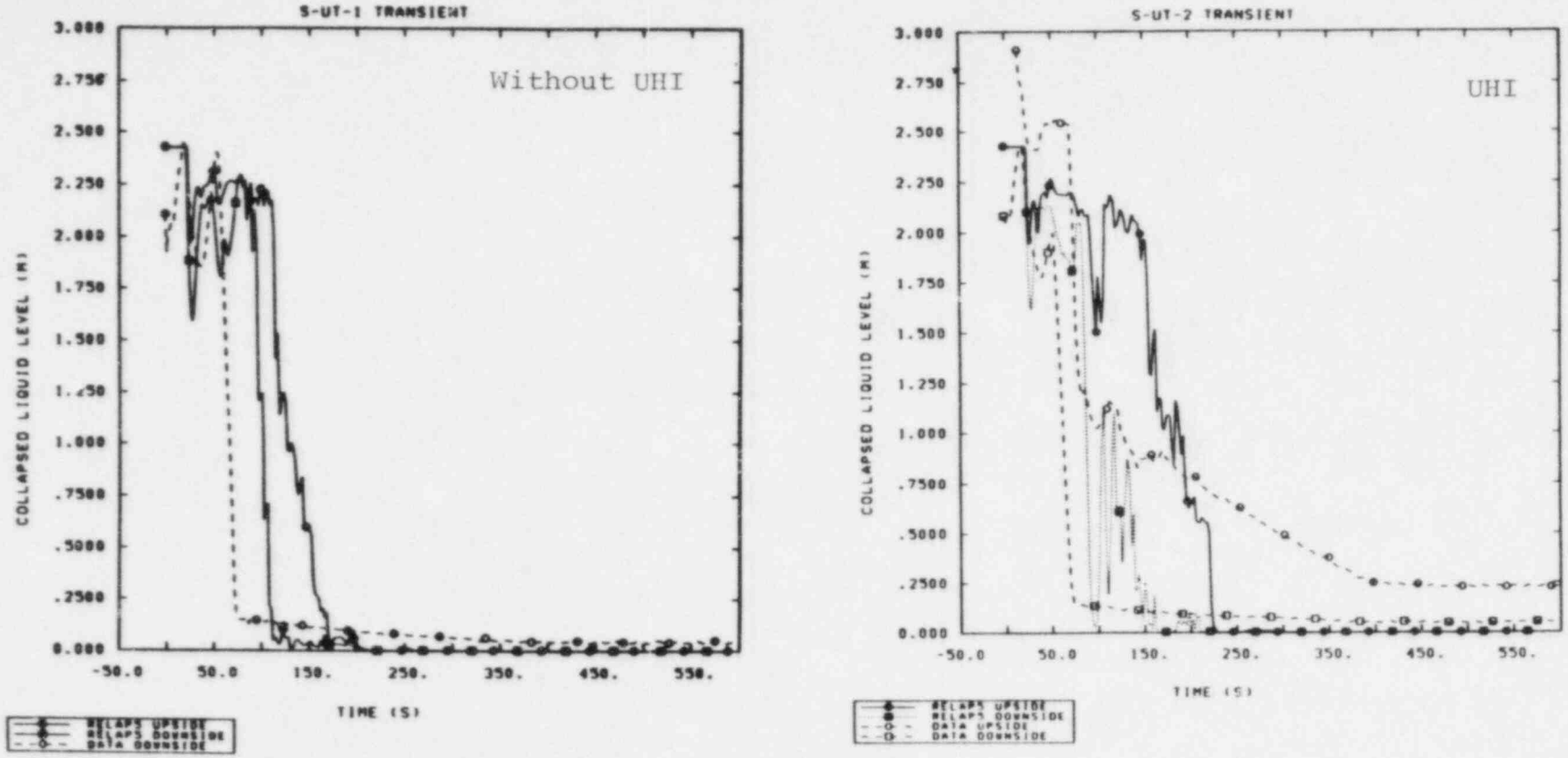

Figure 4.1.6 Effect of UHI on the Intact Loop Pump Suction Collapsed Liquid Levels for a 10% Cold Leg Break

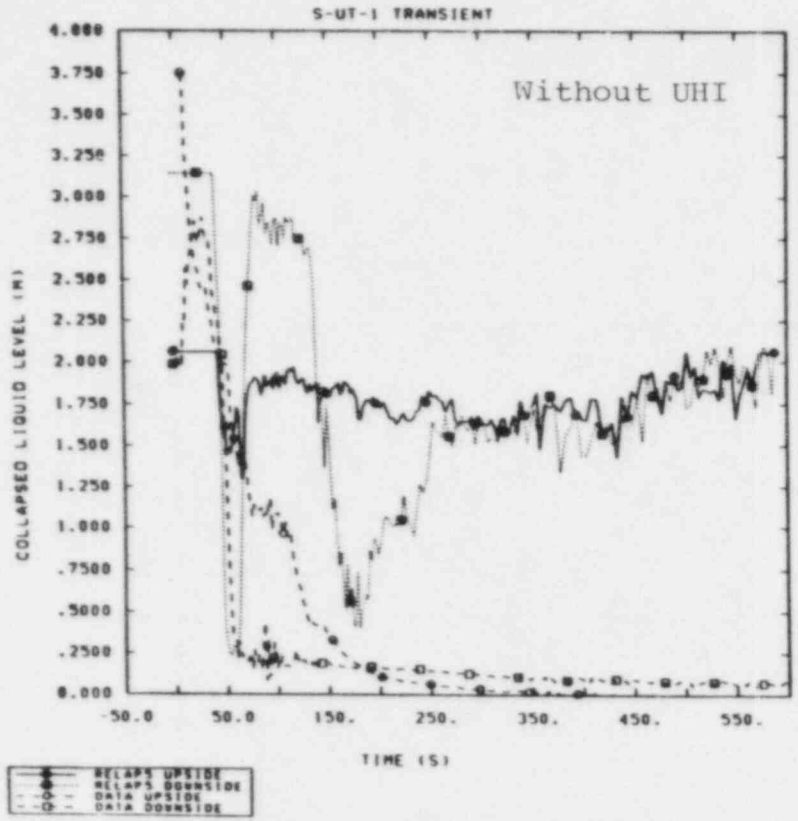

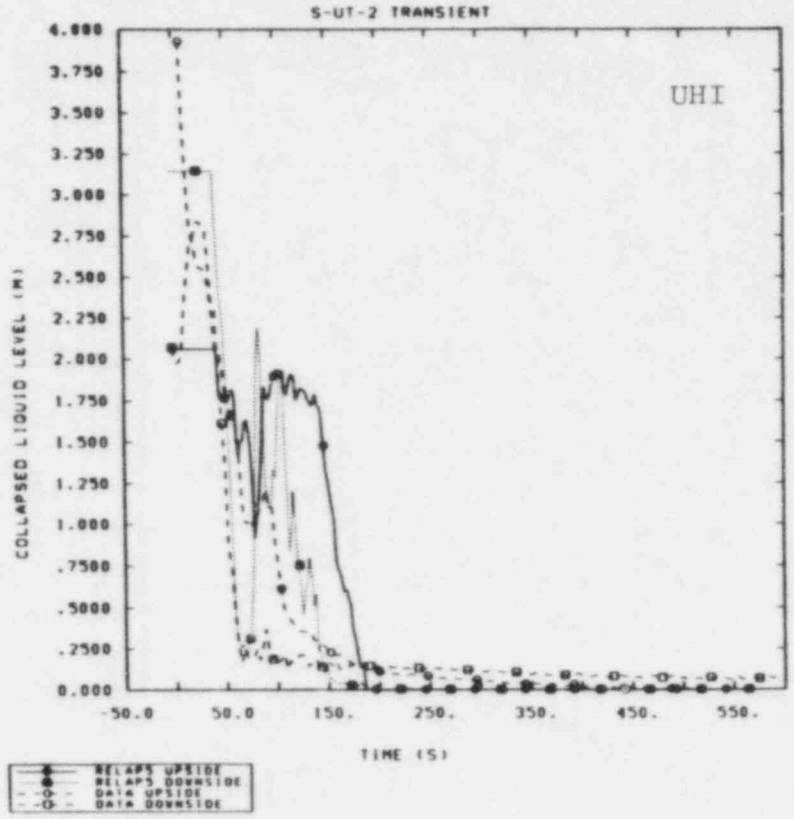

Figure 4.1.7 Effect of UHI on the Intact Loop Pump Suction Collapsed Liquid Levels for a 10% Cold Leg Break

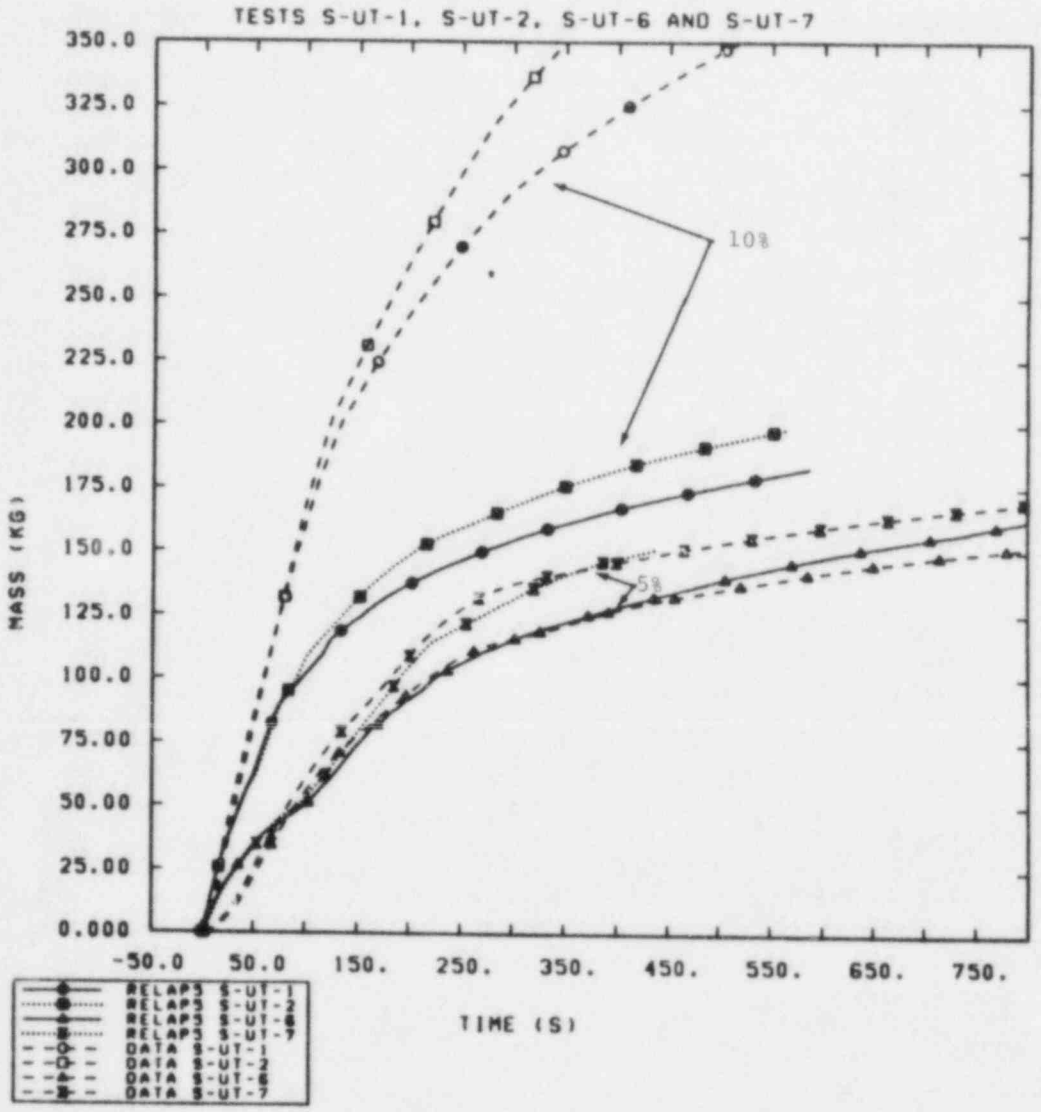

Figure 4.1.8 Effect of UHI on the Integrated Break Mass Flow for 10% and 5% Cold Leg Breaks

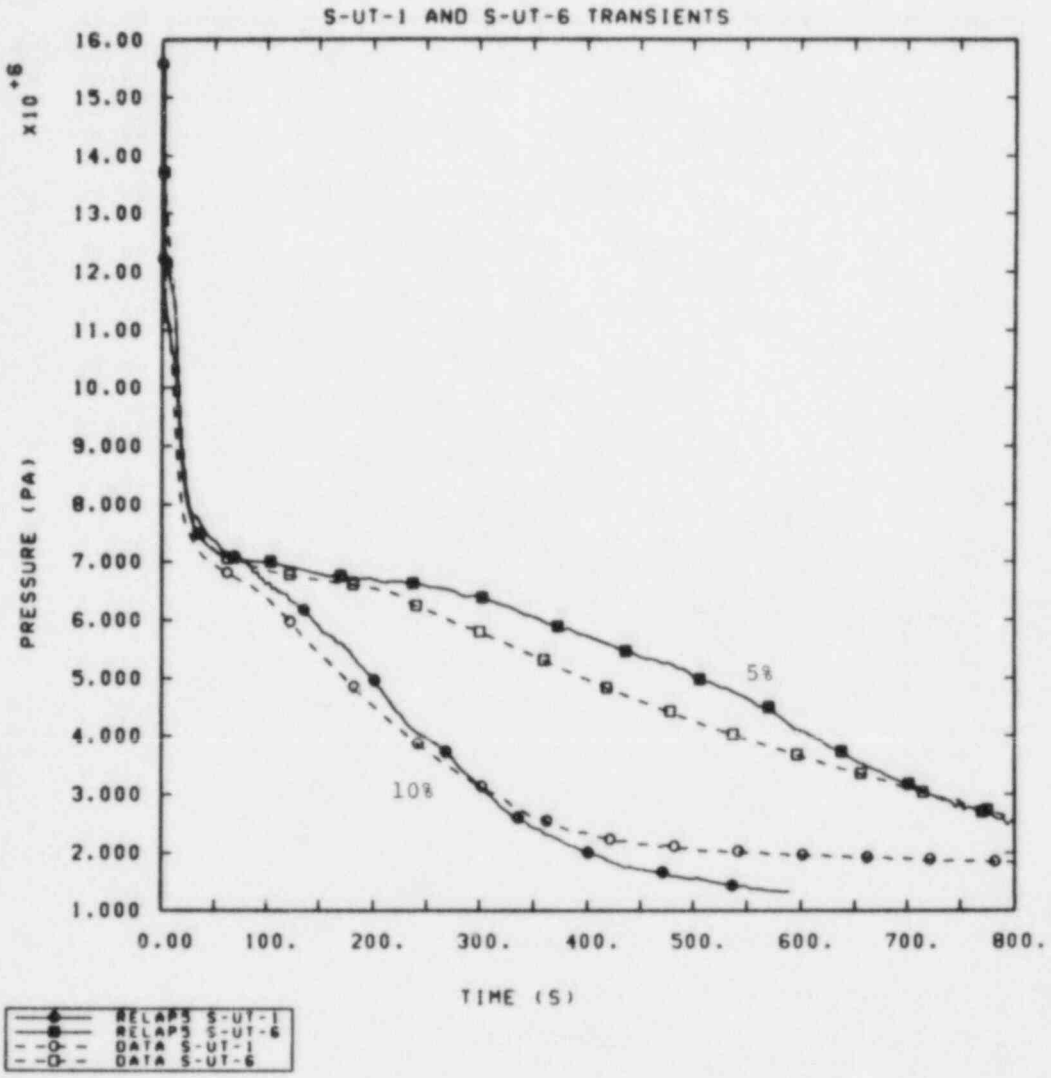

Figure 4.2.1 Effect of Break Size on the Primary System Pressure

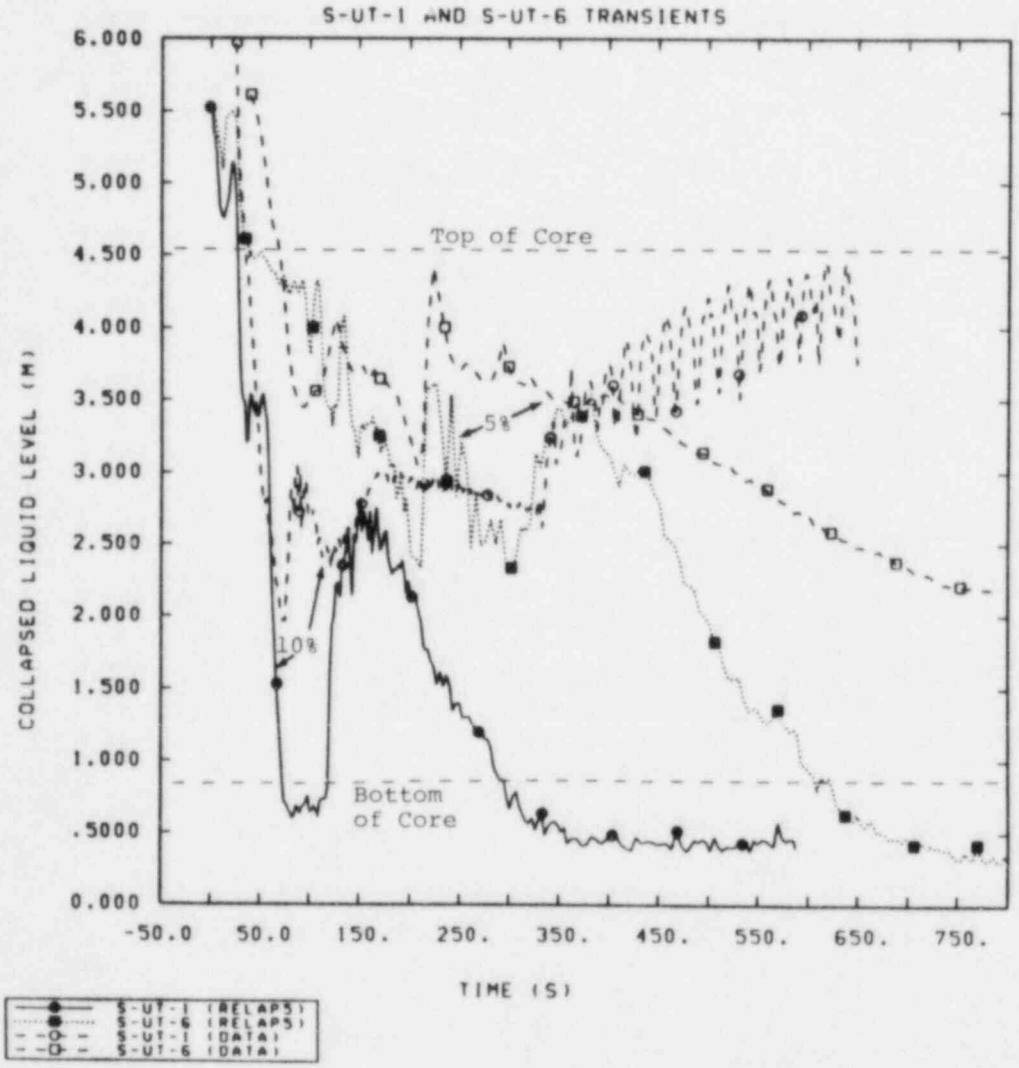

Figure 4.2.2 Effect of Break Size on the Vessel Collapsed Liquid Level

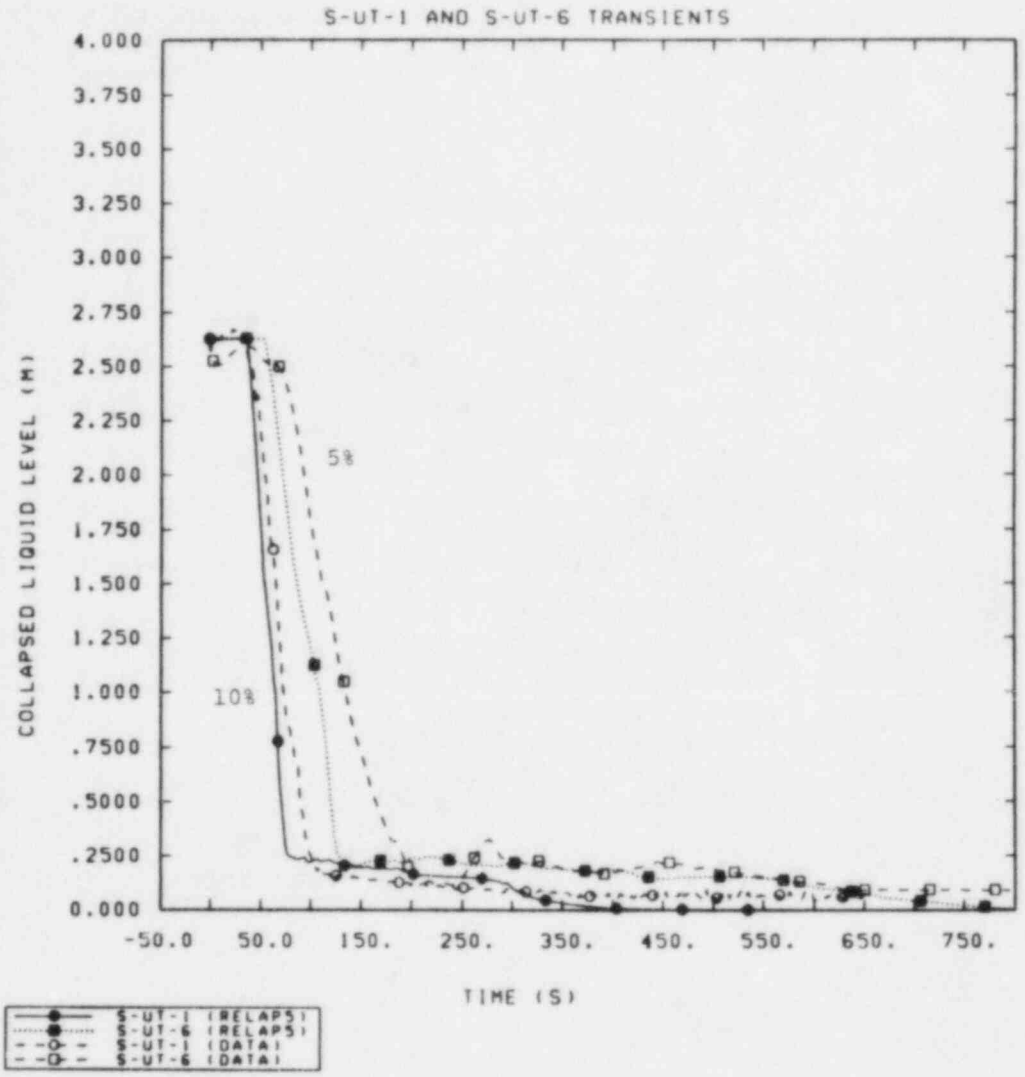

Figure 4.2.3 Effect of Break Size on the Upper Head Collapsed Liquid Level

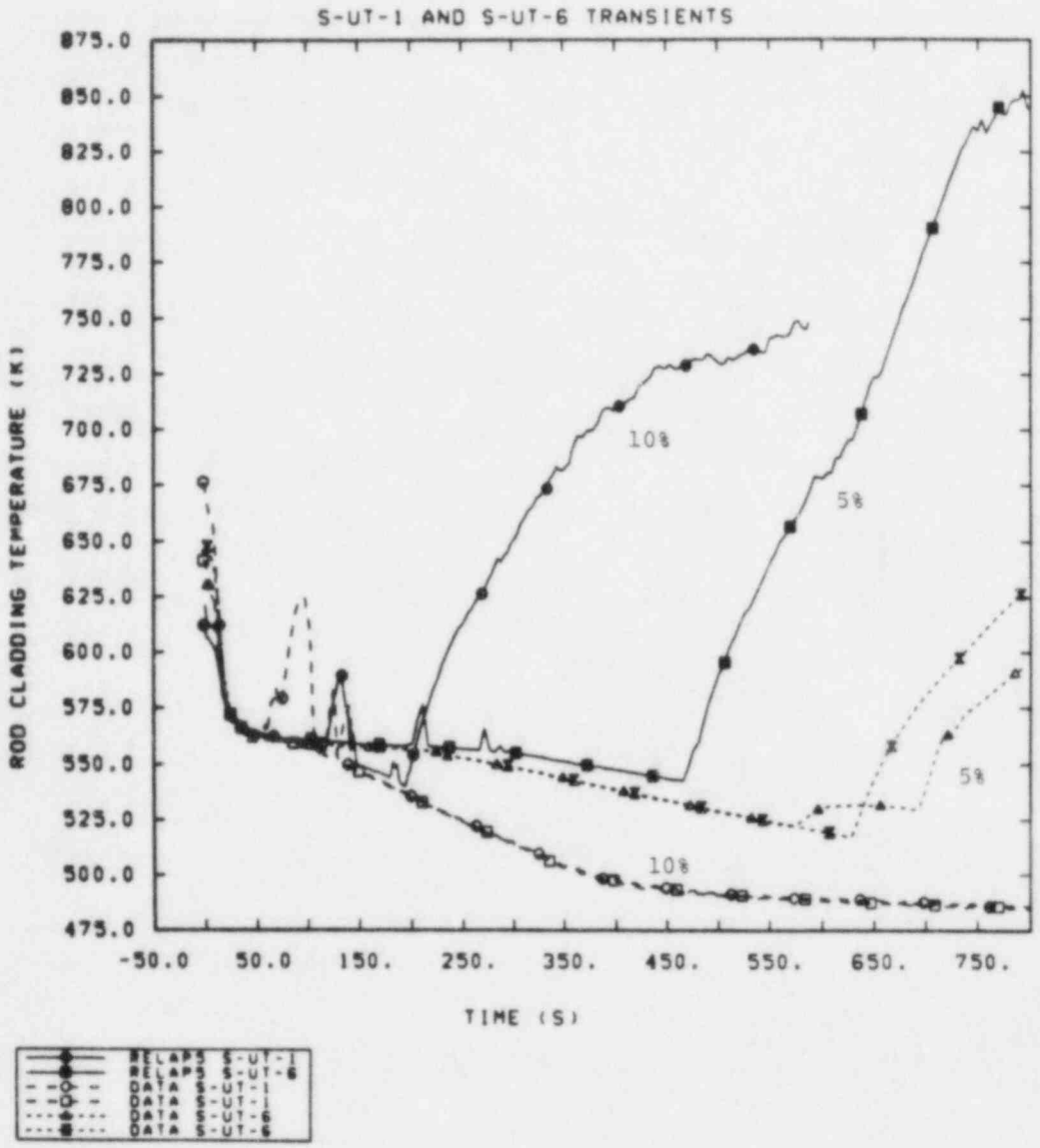

Figure 4.2.4 Effect of Break Size on the Rod Cladding Temperature Response at the 3.0 to 3.6 m Core Elevation

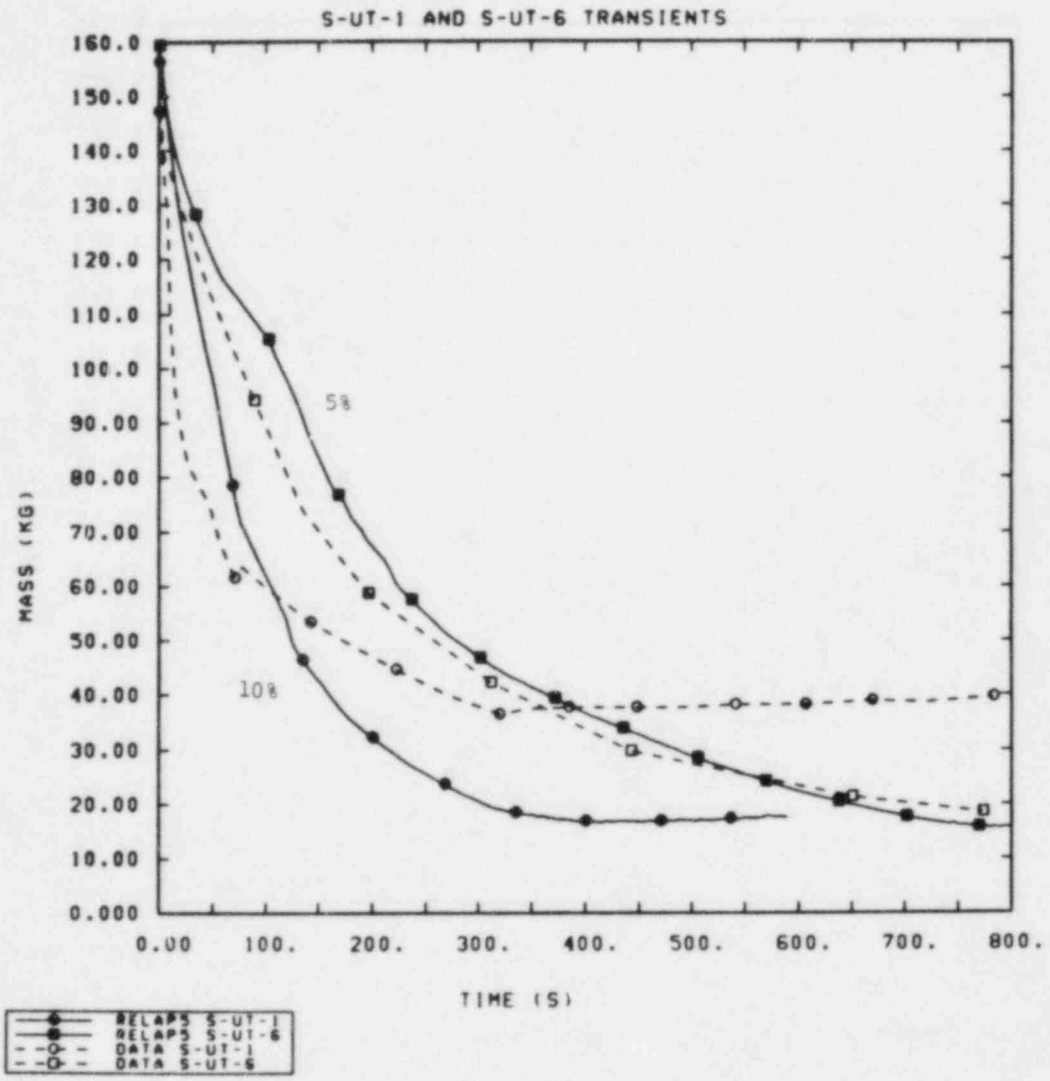

Figure 4.2.5 Effect of Break Size on the Primary System Mass

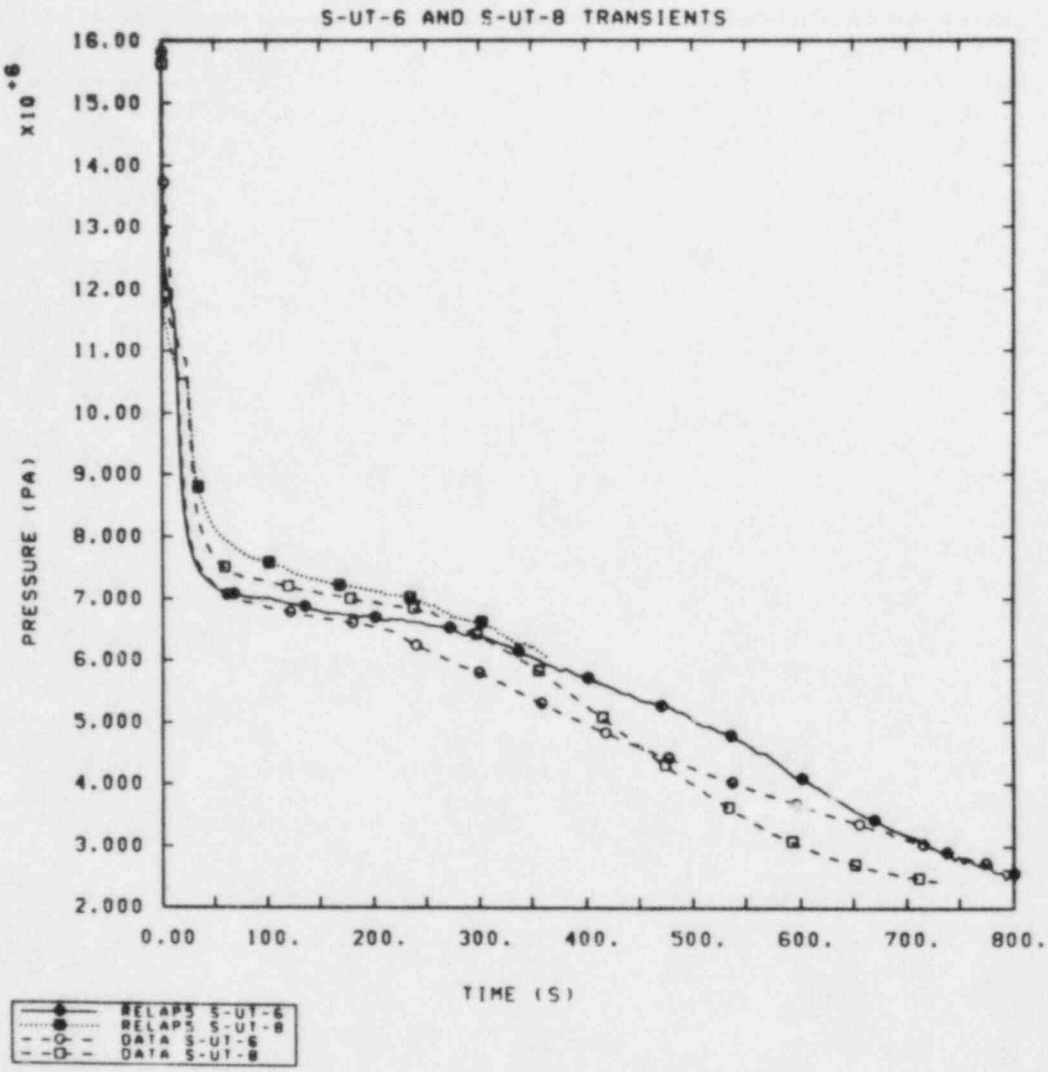

Figure 4.3.1 Effect of Upper Head Geometry on the Primary System Pressure

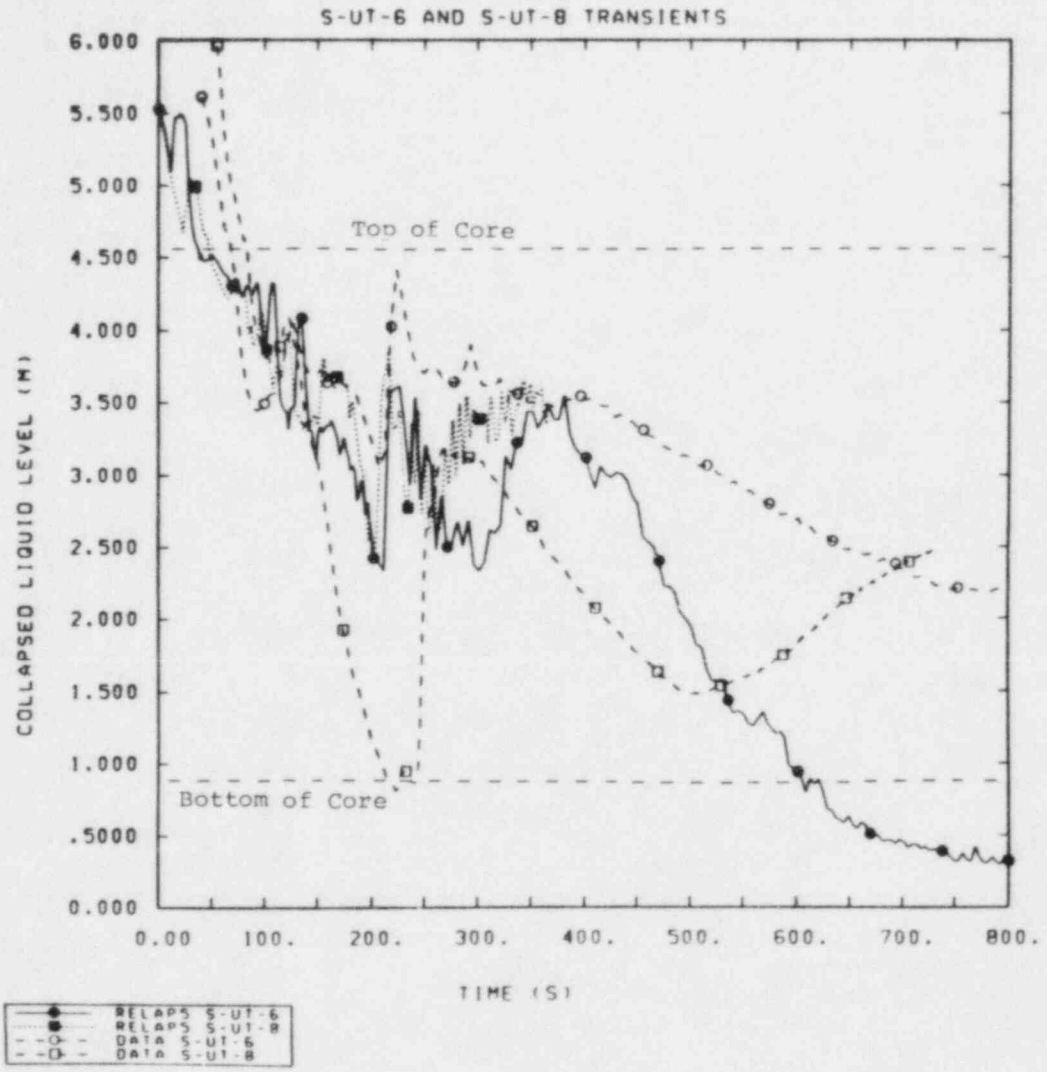

Figure 4.3.2 Effect of Upper Head Geometry on the Vessel Collapsed Liquid Level

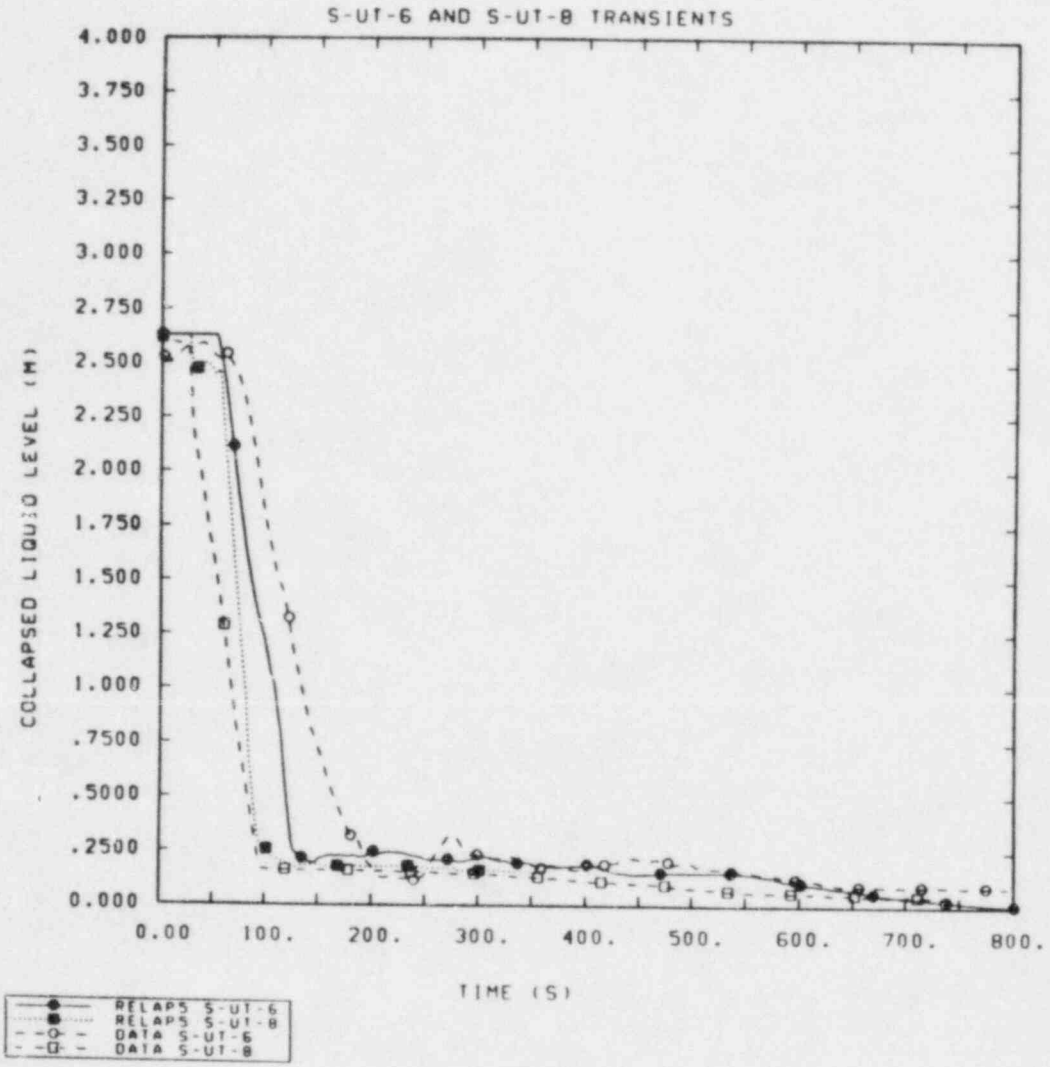

Figure 4.3.3 Effect of Upper Head Geometry on the Upper Head Collapsed Liquid Level

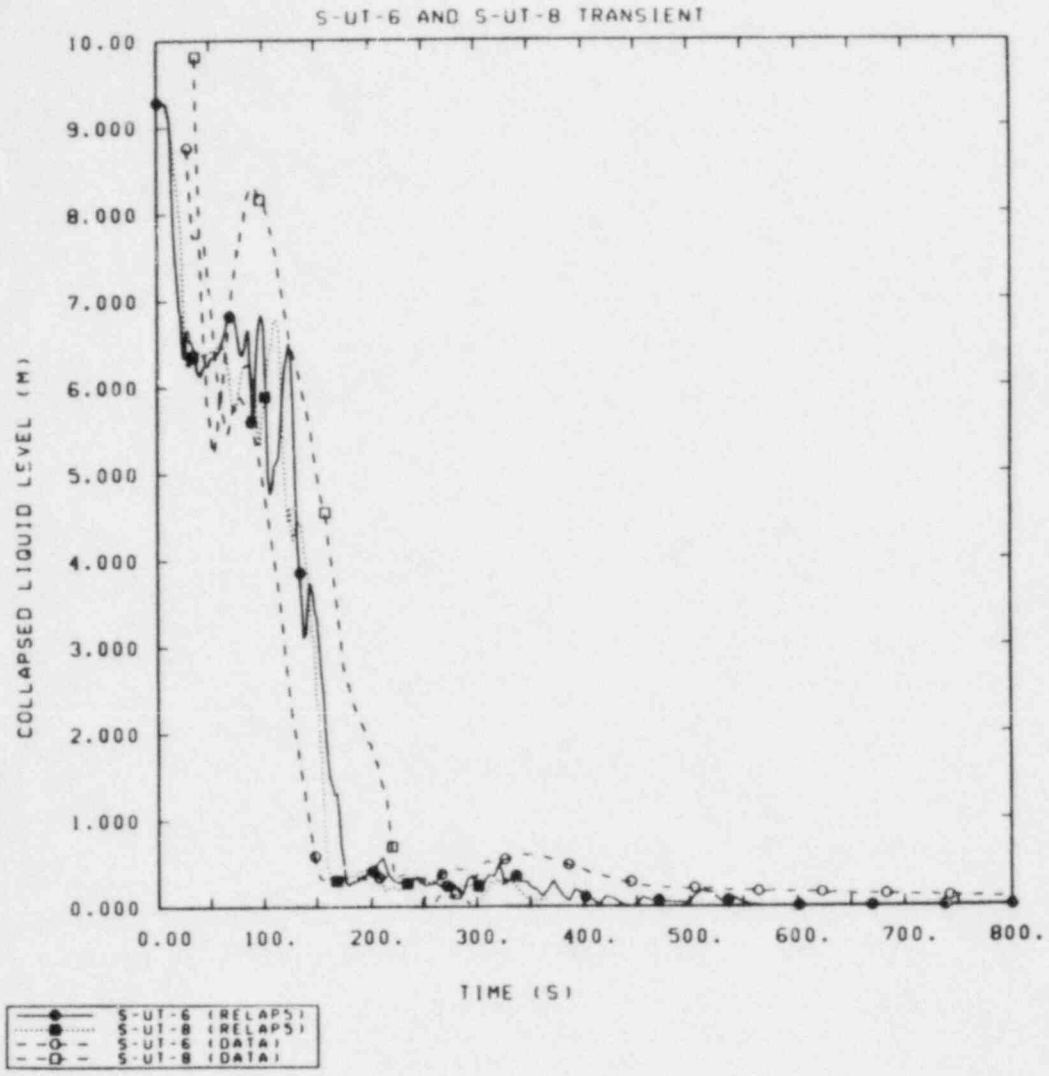

Figure 4.3.4 Effect of Upper Head Geometry on Intack Loop Steam Generator Primary Upflow Side Collapsed Liquid Level

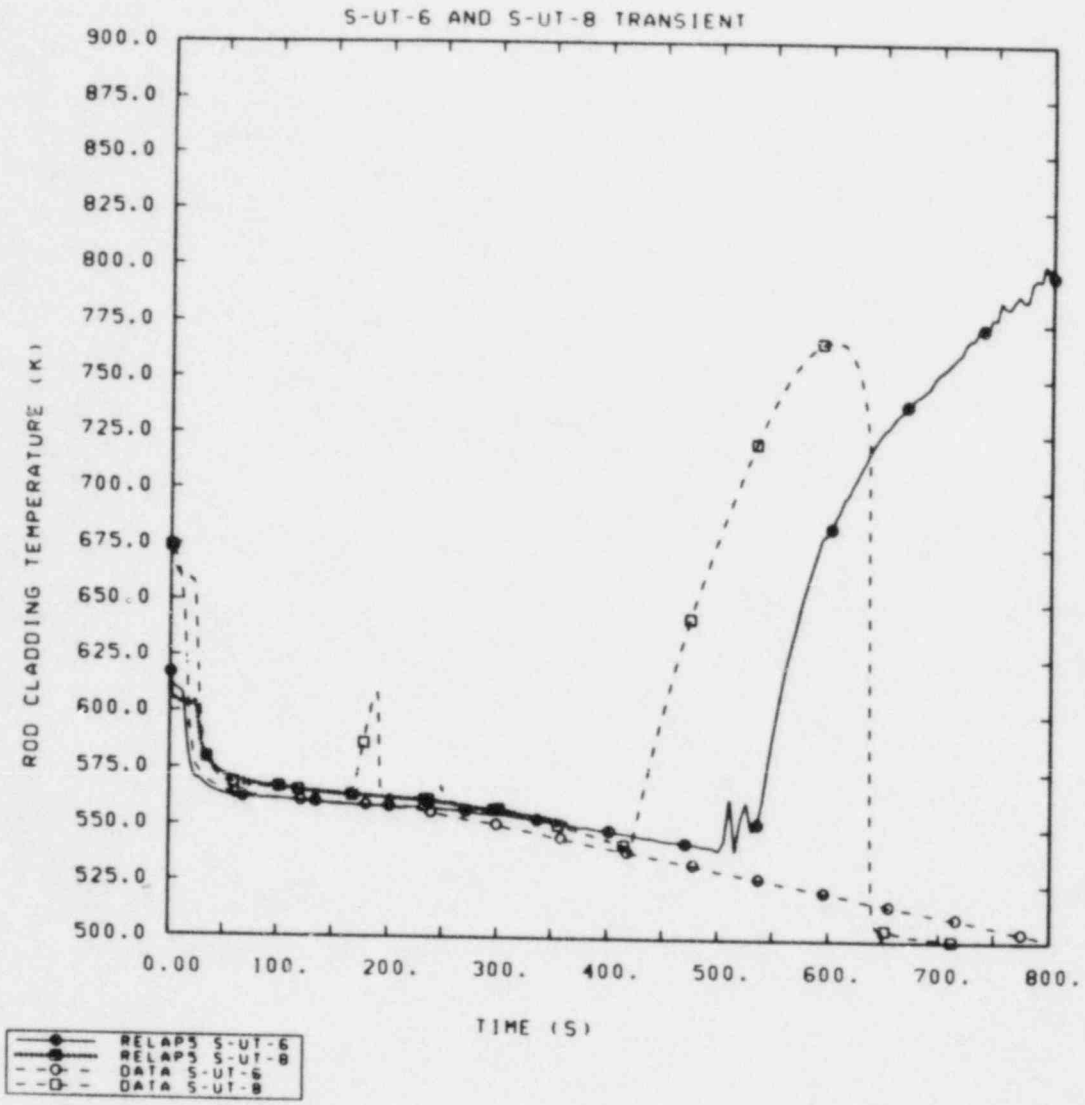

Figure 4.3.5 Effect of Upper Head Geometry on the Rod Cladding Temperature Response at the 1.5 to 1.8 m Core Elevation

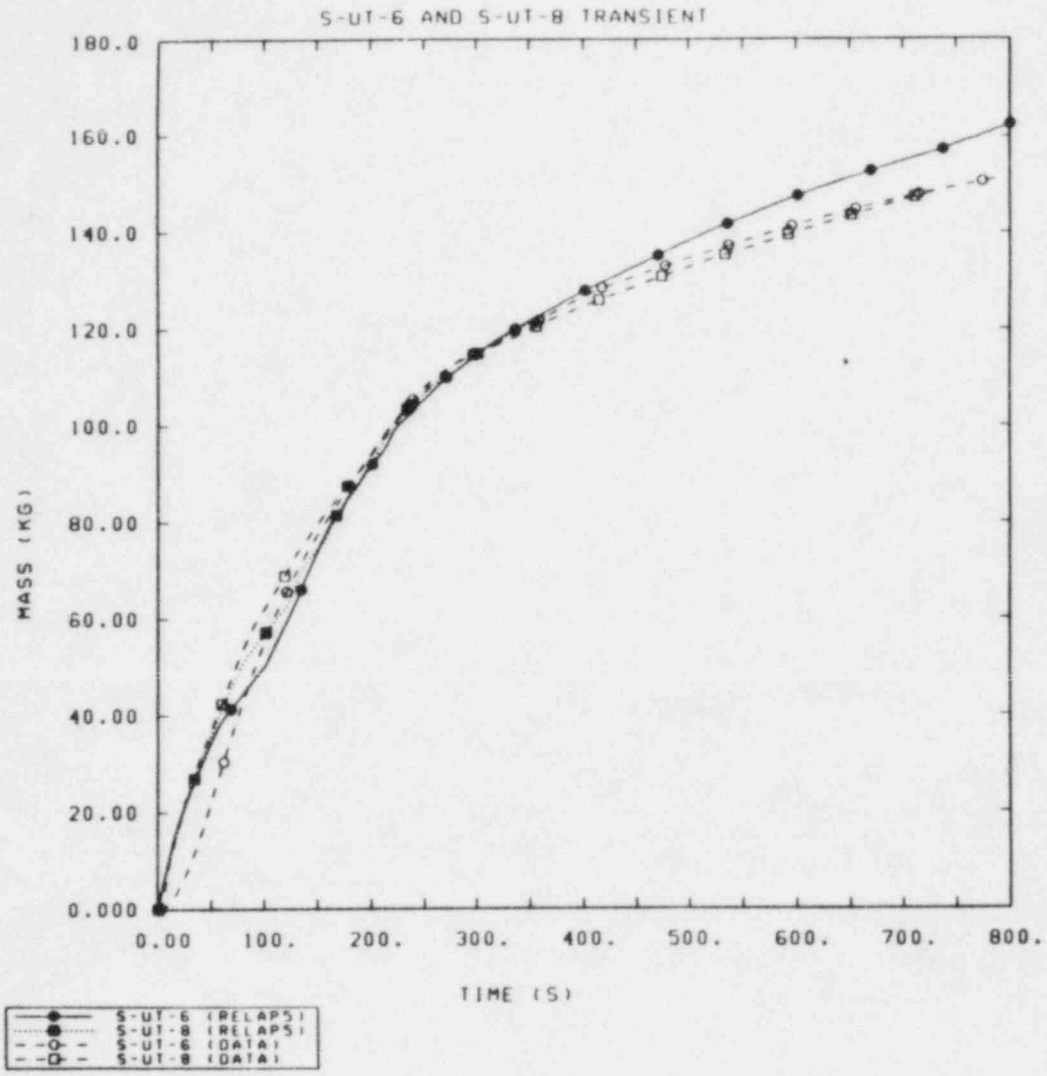

Figure 4.3.6 Effect of Upper Head Geometry on the Integrated Break Mass Flow

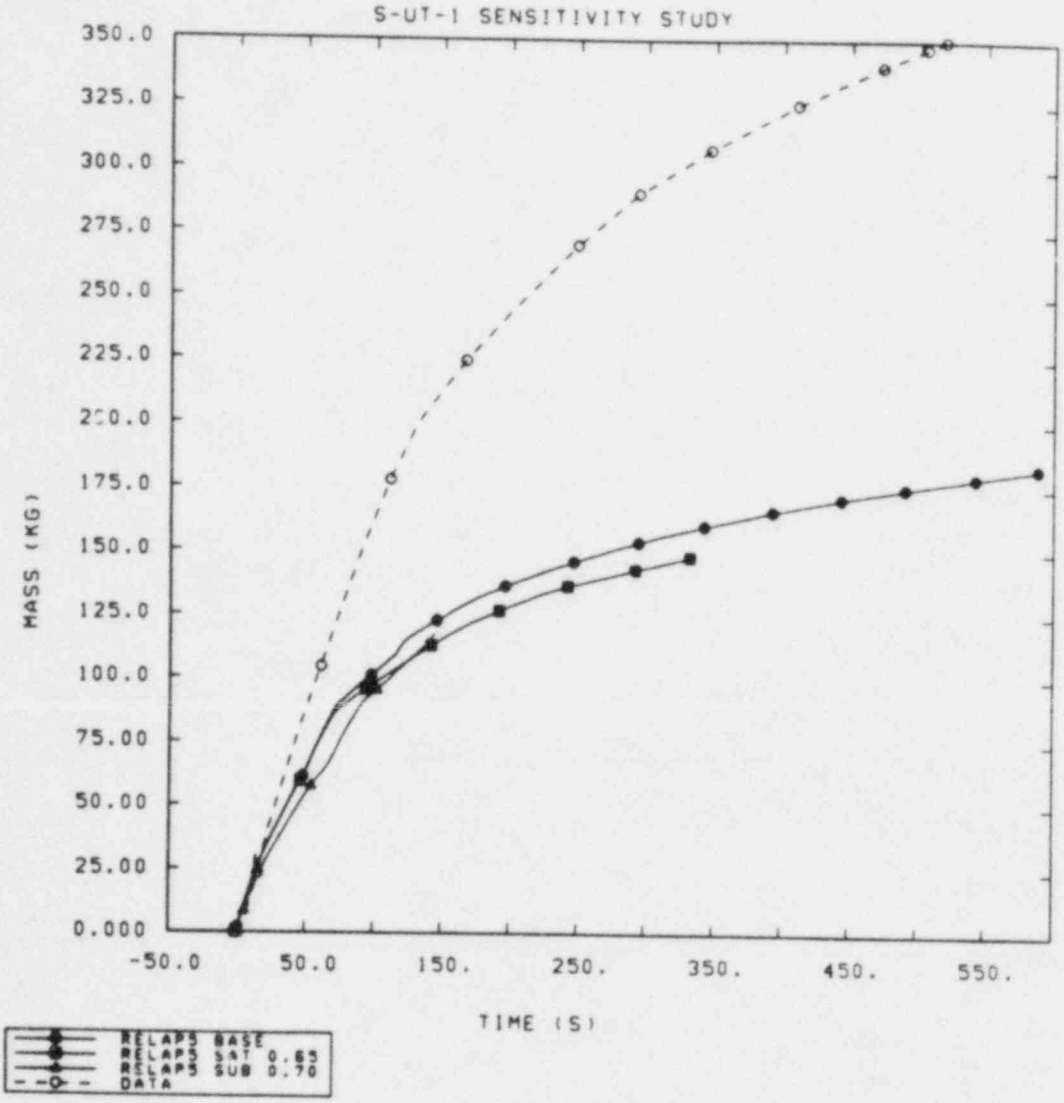

Figure 4.5.1 Effect of Discharge Coefficients on Integrated Break Mass Flow for Test S-UT-1

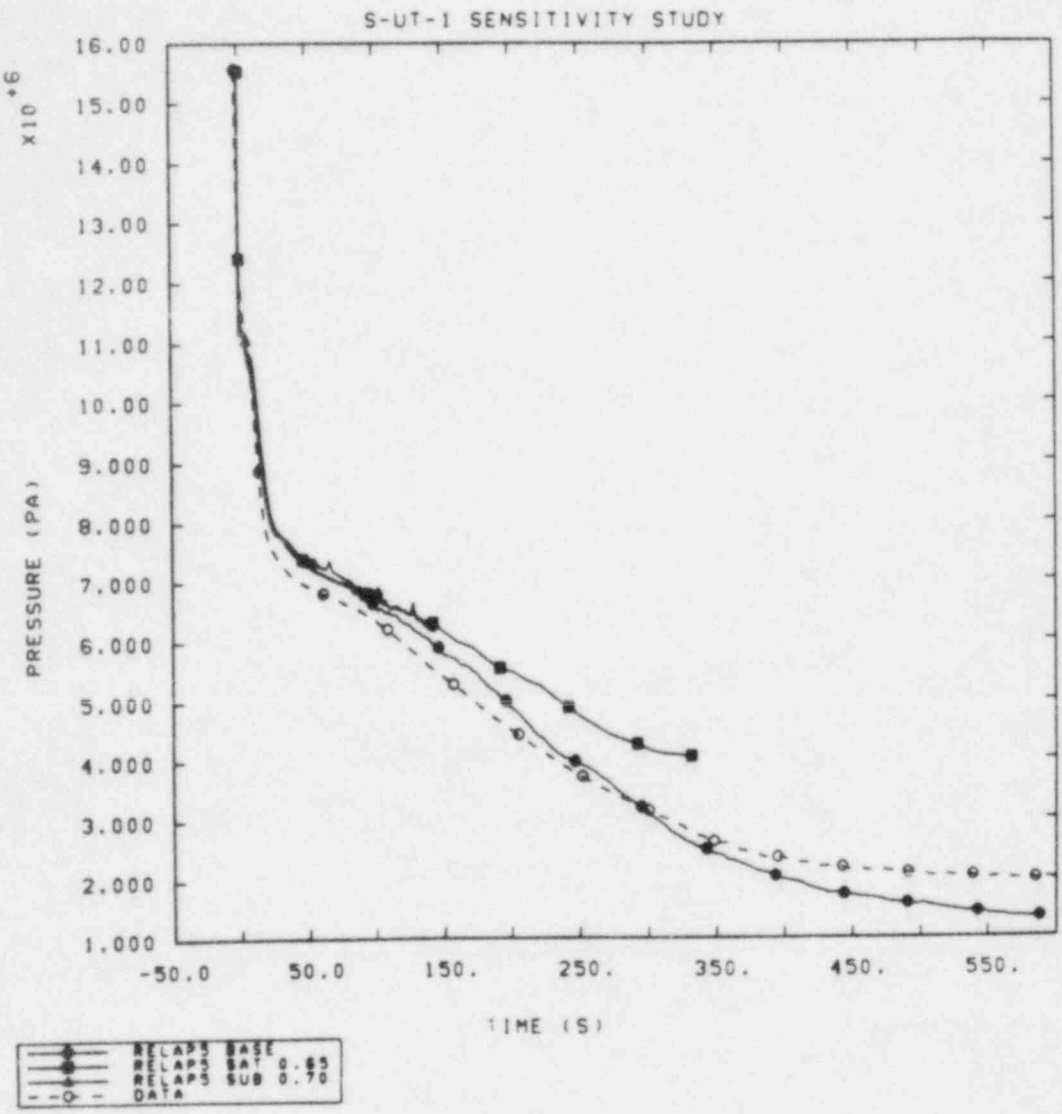

Figure 4.5.2 Effect of Discharge Coefficients on Primary System Pressure for Test S-UT-1

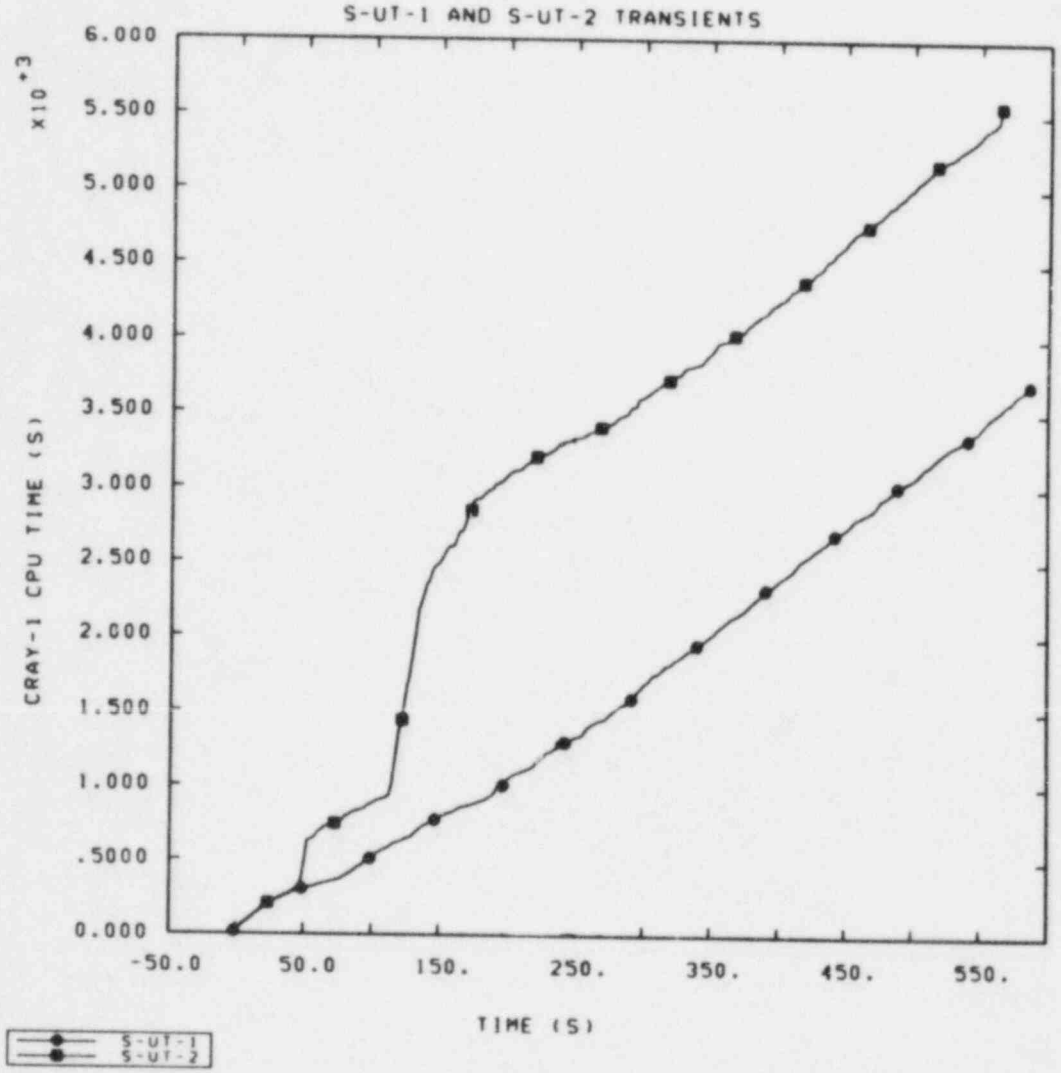

Figure 4.6.1 CPU Time Used for Tests S-UT-1 and S-UT-2

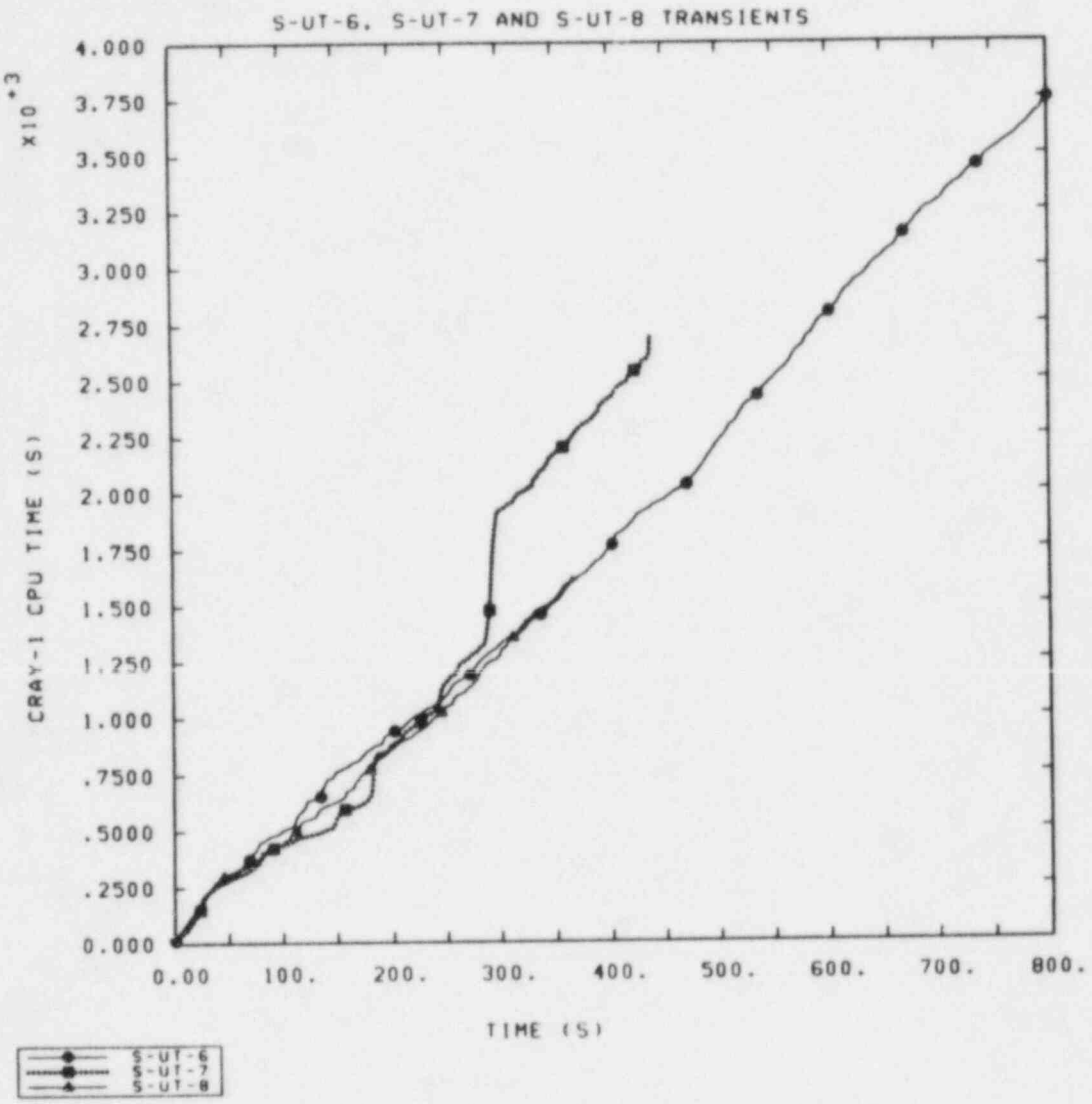

Figure 4.6.2 CPU Time Used for Tests S-UT-6, S-UT-7, and S-UT-8

5.0 CONCLUSIONS

The major conclusions from our analyses of tests from the Semiscale Mod-2A S-UT series are similar to the conclusions from our earlier analyses of small breaks in the Semiscale Mod-3 facility. [18] Some aspects of the important phenomena during small breaks both with and without UHI were calculated reasonably. The times for the system to depressurize to the UHI and/or loop accumulator flow initiation were calculated satisfactorily. The correct trends for the effects of break size and UHI on the system depressurization were calculated. As a result of oscillations in the flow from the UHI and loop accumulators, the calculated system response during accumulator flow was not correct. The times of loop seal clearing and the late-time mass inventories in the system were usually not calculated correctly, resulting in higher late-time core temperatures than measured. The pressures and temperatures in the secondary sides of the steam generators were not predicted accurately; higher pressures and temperatures were usually calculated.

The differences in the steam generator initial conditions, when the primary and secondary experimental conditions could not be matched simultaneously, and the uncertainty in the modeling of the break flow and environmental heat losses, may have contributed to the differences between the calculated and measured results. Since there are still uncertainties in the facility configuration for the S-UT test series that are being addressed, the results for these tests should be considered preliminary until the actual initial conditions are finally established.

Some specific conclusions from these assessment calculations are:

1. The flow from the accumulator component cycled with large spikes. The pressure in the accumulator decreased to below the system pressure and the flow stopped until the system depressurized below the accumulator pressure and the flow cycle started again, indicating deficiencies in the accumulator component model in RELAP5/MOD1. This type of oscillation in flow from the accumulator component also occurred in our assessment calculations in the LOFT and LOBI facilities. [20,25]

2. The break mass flow rate was higher than measured when the break was uncovered, with stratified liquid on the bottom of the pipe. The calculated void fraction at the break junction appeared to be lower than occurred in the tests when the break uncovered and high quality steam was discharged. Similar results occurred in our assessment calculations for the Semiscale Mod-3 small break pumps-off tests [18].

3. The densities in the upper plenum and at the top of the core were significantly higher than measured during UHI flow, indicating liquid was not properly draining down into the vessel. The higher densities affected the vessel mass distribution during UHI flow. This result indicates possible problems with the interfacial drag model.

4. Unexpected fluid behavior in the pump component occurred with the two-velocity hydrodynamic model. During high quality two-phase flow the liquid and vapor were not coupled, with the vapor flowing forward and the liquid flowing backwards. This result appeared to inhibit the clearing of the broken loop pump. The RELAP5 interphasic momentum transfer model in the pump component may have a deficiency and should be evaluated.

5. The boiloff of liquid from the core was more rapid in the calculation than was measured, resulting in a late-time core heatup. A more rapid boiloff of liquid from the core also occurred in our assessment calculations for small breaks in the Semiscale Mod-3 facility [18]. This result may also indicate a potential deficiency in the interfacial drag model, i.e. too large a drag which causes too much liquid to be carried out of the core region.

With regard to applications to PWR analysis, calculations with RELAP5/MOD1 would be expected to predict too high a break flow when the break uncovers, which may result in miscalculating the vessel mass and calculating too large a core heatup. Calculations for PWRs with UHI may result in the calculation of too severe a core liquid level depression during UHI flow. Due to the oscillations in the accumulator component flow, the correct ECC injection rate would probably not be calculated, which may also result in the calculation of rod temperatures that are too high.

6.0 REFERENCES

1. V. H. Ransom, et al., RELAP5/MOD1 Code Manual Volume 1: System Model and Numerical Methods; Volume 2: Users Guide and Input Requirements, NUREG/CR-1826, EGG-2070, Idaho National Engineering Laboratory, March 1982.

2. P. North letter to R. E. Tiller, PN-120-80, Experiment Operating Specification for Semiscale Mod-2A 10% Break Experiments (Tests S-UT-1 and S-UT-2), EG&G Idaho Inc., October 20, 1890.

3. J. E. Blakeley, R. G. Hanson, and D. J. Shimeck, Quick-Look Report for Semiscale Mod-2A Test S-UT-1, EGG-SEMI-5331, Idaho National Engineering Laboratory, January 1981.

4. J. E. Blakeley, R. G. Hanson, and D. J. Shimeck, Quick-Look Report for Semiscale Mod-2A Test S-UT-2, EGG-SEMI-5333, Idaho National Engineering Laboratory, January 1981.

5. K. E. Sackett and L. B. Clegg, Experiment Data Report for Semiscale Mod-2A small Break Test Series (Tests S-UT-1 and S-UT-2), NUREG/CR-2176, EGG-2108, Idaho National Engineering Laboratory, July 1981.

6. R. G. Hanson, Experiment Operating Specification for Semiscale Mod-2A 5% Break Experiments S-UT-6 and S-UT-7, EGG-SEMI-5421, Idaho National Engineering Laboratory, April 1981.

7. J. M. Cozzuol and C. M. Kullberg, Quick-Look Report for Semiscale Mod-2A Test S-UT-6, EGG-SEMI-5446, Idaho National Engineering Laboratory, May 1981.

8. R. G. Hanson, D. J. Shimeck, and J. L. Steiner, Quick-Look Report for Semiscale Mod-2A Test S-UT-7, EGG-SEMI-5442, Idaho National Engineering Laboratory, May 1981.

9. R. A. Larson and L. B. Clegg, Experiment Data Report for Semiscale Mod-2A Small Break Test Series (Tests S-UT-6 and S-UT-7), NUREG/CR-2355, EGG-2132, Idaho National Engineering Laboratory, November 1981.

10. W. W. Tingle, Experiment Operating Specification for Semiscale Mod-2A 5% Break Experiment S-UT-8, EGG-SEMI-5865, Idaho National Engineering Laboratory, December 1981.

11. G. W. Johnsen, Semiscale Sytem Description, Handout at Joint LOFT/Semiscale Modeling Workshop, August 18 19, 1981, at Idaho Falls, ID.

12. M. T. Leonard, RELAP5 Standard Model Description for the Semiscale Mod-2A System, EGG-SEMI-5692, Idaho National Engineering Laboratory, December 1981.

13. J. M. McGlaun and L. N. Kmetyk, RELAP5 Assessment: Semiscale Natural Circulation Tests S-NC-2 and S-NC-7, NUREG/CR-3258, SAND83-0833, Sandia National Laboratories, May 1983.

14. C. C. Wong and L. N. Kmetyk, RELAP5 Assessment: Semiscale Natural Circulation Tests S-NC-3, S-NC-4 and S-NC-8, Sandia National Laboratories, July 1984.

15. R. L. Benedetti Letter to J. E. Solecki, RLB-119-83, S-UT-8 Information, EG&G Idaho Inc., December 15,1983.

16. M. T. Leonard, Vessel Coolant Mass Depletion During a Small Break LOCA, EGG-SEMI-6013, Idaho National Engineering Laboratory, September 1982.

17. M. T. Leonard, Posttest RELAP5 Simulations of the Semiscale S-UT Series Experiments, EGG-SEMI-5622, Idaho National Engineering Laboratory, October 1981.

18. R. M. Summers, RELAP5 Assessment: Semiscale Mod-3 Small Break Tests, NUREG/CR-3277, SAND-1083, Sandia National Laboratories, July 1983.

19. S. L. Thompson and L. N. Kmetyk, RELAP5 Assessment: LOFT Large Break Test L2-5, NUREG/CR-3608, SAND83-2549, Sandia National Laboratories, February 1984.

20. J. L. Orman and L. N. Kmetyk, RELAP5 Assessment: LOFT Intermediate Breaks L5-1 and L8-2, NUREG/CR-3406, SAND83-1575, Sandia National Laboratories, August 1983.

21. L. N. Kmetyk, RELAP5 Assessment: LOFT Small Break L3-6/L8-1, NUREG/CR-3163, SAND83-0245, Sandia National Laboratories, March 1983.

22. C. B. Davis, RELAP5 Calculations of the Effect of Primary Coolant Pump Operation During Semiscale Small Break Experiments, EGG-CAAD-5531, Idaho National Engineering Laboratory, August 1981.

23. Personal Communication, A. C. Peterson with J. L. Perryman, INEL October 1983.

24. L. Lee, T. Ito, and P. B. Abramson, Sensitivity of SBLOCA Computations to Steam Generator Nodalization Selection, ANL/LWR/NRC 83-4, Argonne National Laboratory, February 1983.

25. L. N. Kmetyk, RELAP5 Assessment: LOBI Large Break Transients, NUREG/CR-3075, SAND82-2525, Sandia National Laboratories, March 1983.

26. Personal Communication, A. C. Peterson with D. M. Kiser, INEL February 1984.

APPENDIX I FACILITY DESCRIPTION

The standard Semiscale Mod-2A system [11,12], shown in Figure AI.1, consists of a vessel with its associated internals and an external downcomer, an intact loop and a broken loop both with active steam generators and pumps, a break effluent measuring system, and a steam generator secondary system. Other subsystems include the emergency core cooling system, external heat loss makeup system, leakage makeup system and a noncondensible gas injection system. The Semiscale system was scaled from a reference PWR system based on the core power ratio, 2/3411; component elevations, dynamic pressure heads and liquid distribution were maintained as similar as practical, most notably in the design of a full-length core, full-length upper plenum and upper head, and full-height steam generators. The major primary coolant system elevations are given in Table AI.1.

The intact loop consists of a steam generator, primary coolant pump, and pressurizer connected by piping. The intact loop piping itself is composed of individual pipe sections called spool pieces. These spool pieces and their relative locations in the intact loop are identified by spool numbers in Figure AI.2; the upper drawing unfolds the intact loop for easier viewing by preserving the orientation of the components in the vertical plane without regard to the actual horizontal orientation, which is shown in the lower drawing. The spool piece lengths and blueprint numbers are given in Table AI.2. The intact loop piping, other than the vertical spool pieces leading to the steam generator inlet and outlet (spools 4 through 12) and spool 3, are constructed of 3-in. Sch 160 Type 316 stainless steel pipe; spool pieces 3 through 12 are constructed of 2-1/2-in. Sch 160 pipe. The intact loop pump is a volute-type, heavy duty, horizontal, centrifugal pump. A venturi is installed in the pump discharge to give the properly scaled locked rotor hydraulic resistance.

The broken loop is designed to simulate a single loop of a four-loop PWR; in addition to a break assembly it also contains an active steam generator and pump. The spool pieces in the broken loop are constructed of 1-1/2-in. Sch 160 Type 316 stainless steel piping; these spool pieces and their relative locations in the broken loop are identified by spool numbers in Figure AI.3, and the corresponding spool piece lengths and blueprint numbers are given in Table AI.3. Figure AI.4 is a schematic drawing of the communicative small break assembly used in the S-UT tests. The areas of the break orifices used for the 10% and 5% breaks were 0.233 cm^2 and 0.1123 cm^2, respectively. The broken loop pump is a high-speed, vertical, centrifugal pump with a bottom suction and side discharge, similar to PWR pumps. A flow restriction is incorporated into the pump discharge.

The intact and broken loop steam generators, shown in Figure AI.5 and summarized in Table AI.4, consist of a two-pass tube and shell design with primary fluid flowing through vertical inverted U-shaped tubes and secondary coolant passing through the shell side. With the secondary side operating at saturation conditions, a centrifugal separator at the top of the riser (or boiler) section increases the exit quality of the steam rising through the steam dome and out a discharge line, while liquid separated from the steam falls down a downcomer outside the boiler shroud, creating a recirculation flow path. The intact loop steam generator has two short, two medium and two long tubes representative of the range of bend elevations in a PWR steam generator, while the broken loop steam generator contains just one short tube and one long tube. The same tube stock (2.22 cm OD, 0.124 cm wall) and tube spacing (3.175 cm triangular pitch) used for PWR U-tubes are used in this "Type II" steam generator. Since the heat transfer area is specified based on the ratio of PWR to Semiscale primary system volume, the number of tubes is thereby fixed by the specified tube diameter and lengths.

Fillers are installed on the shell side in both the boiler and downcomer regions to provide a more properly scaled secondary fluid volume. The addition of these filler pieces not only reduces the total secondary coolant volume, but also changes the flow geometry of the boiler and downcomer, as shown in the cross-sectional view in Figure AI.5. The boiler section filler pieces create a parallelogram-shaped flow channel along the length of the U-tubes, while the downcomer filler pieces reduce the downcomer annulus to a set of slotted flow channels. Baffle plates are located at several axial positions in the boiler section of the steam generator, creating a substantial flow restriction to the rising coolant. Feedwater enters the downcomer above the filler pieces at approximately the elevation of the top of the U-tubes; auxiliary feedwater is also added a this point. The elevations of the steam generator nozzles, plena and tubes are similar to those in a PWR; however, the steam dome is shorter than a PWR steam dome and the steam drying equipment is of a simpler and less efficient design. (As a result of these dissimilarities, the secondary fluid operating level at full power conditions is about 75% of the operating level in a PWR, with the lower level required to ensure stable steam generator operation.)

The pressurizer, which is connected to the intact loop hot leg, is shown in Figure AI.6. The pressurizer vessel is made of .0-in. Sch 160 Type 347 stainless steel pipe, is approximately 1.14 m high and has a total volume of 0.034 m^3. Heat is supplied by 24 0.05-kW vertically-oriented electric heater rods, which are inserted in 2.2 cm OD stainless steel tubes sealed at

the bottom. A pressurizer spray system is not included in the Mod-2A system. The pressurizer operates in a manner similar to its counterpart in a large PWR in that the vessel is partially filled with water and maintained at a saturation temperature corresponding to the desired system pressure. The pressurizer surge line and tubing (1.27 cm OD, 0.165 cm wall, ~2.7 m length and ~1.53 m total elevation drop from bottom of pressurizer vessel to hot leg centerline) is sized for a flow restriction that provides representative flow rates.

The Mod-2A vessel, shown in Figure AI.7, consists of a multi-section pressure vessel containing a lower plenum, heated core, upper plenum and upper head, and an external inlet annulus and downcomer. The pressure vessel is constructed primarily of 6-in. Sch XXS stainless steel pipe, with stainless steel Grayloc clamps used to connect the various vessel sections; the complete pressure vessel is approximately 10 m long.

The upper head region, shown in more detail in Figure AI.8, is contained within the top ~25% of the pressure vessel, and contains ports for upper head ECC injection, a filler to provide the proper upper head internal volume, an insulator designed to provide a steam gap between the filler ID and the insulator OD, and a simulated control rod guide tube. An upper core support plate simulator forms the boundary between the upper head and upper plenum regions; this upper core support plate provides support for the simulated guide tube and for the upper ends of the two simulated core support columns which extend down through the upper plenum region. Approximately 4% of the total primary coolant flow into the vessel bypasses the downcomer and core through an external upper head bypass line from the top of the downcomer inlet annulus to the upper head. The bypass coolant rejoins the heated coolant in the vessel upper plenum via the simulated control rod guide tube and core support columns. The exit of the upper head bypass line standpipe and the inlets of the control rod guide tube and core support columns are at different elevations within the upper head. The UHI accumulator flow is through a perforated pipe containing 50 uniformly spaced 0.356 cm diameter holes. The UHI pipe extends through the top of the upper head to 14.5 cm above the upper core support plate.

The upper plenum region, shown in more detail in Figure AI.9, extends from the upper core support plate to the top of the heated core region, and is approximately 2.5 m long. The upper and lower sections of the upper plenum contain fillers and insulators similar to those in the upper head. Two hot leg nozzles extend from the vessel upper plenum approximately 21.6 cm above the cold leg centerline to provide connections for the intact and broken loop hot leg piping. The flow path above the core to the hot leg nozzles is quite tortuous; in addition to a

core flow measurement assembly, a simulated control rod guide tube and two simulated core support columns obstruct the flow path, and a short set of vertical tubes creates a horizontal flow restriction across the vessel at the hot leg elevation. This flow restrictor assembly simulates the flow restriction in a PWR caused by control rod guide tubes and core support columns. Above the hot legs, the upper plenum contains a significant amount of fluid which is not involved in the main flow path. The simulated control rod guide tube and core support columns extend from the upper head through the upper plenum and terminate open-ended in the upper core plate located in the heater ground hub which forms the boundary between the upper plenum and the top of the active heated core region. The guide tube is slotted in the upper plenum region.

The 3.66 m heated length of the core, shown in Figure AI.10, extends downward from the heater rod ground hub to the top of the mixer box (approximately 4.96 m below the cold leg center-line), which separates the core and the lower plenum regions. This figure includes a cross-sectional view of the Mod-2A vessel over the core region. The 25-rod electrically-heated core is enclosed in a square housing with no coolant bypass. The heater rods, 1.07 cm in diameter, are positioned and held in the core with 10 grid spacers (at elevations shown in Figure AI.11) which maintain the heater rods on a typical PWR pitch of 1.43 cm. The 16 peripheral rods are powered separately from the 9 central rods, permitting a radial profile (although normally no radial peaking is simulated); two of the 16 peripheral rods, however, are not powered. The Semiscale Mod-2A heater rod design consists of a helically-wound constantan filament, electrically insulated from the dual-sheath stainless steel clad by compacted boron nitride powder. Chromel-alumel thermocouples are swaged between cladding sheaths in six symmetrical polar locations and ten axial elevations distributed along the rod. The heater rods have a symmetric chopped-cosine axial power distribution (shown in Figure AI.11); the peak-to-average power ratio is 1.55.

The lower plenum, shown in Figure AI.12, consists of an annular region between the flow mixer box and the pressure vessel, which serves to distribute flow from the downcomer pipe around the vessel periphery, and a lower head chamber region below the mixer box which approximates the scaled volume of a PWR lower plenum. (The lower plenum is the only part of the vessel which is not height-scaled.) Coolant flow from the downcomer distribution annulus changes direction within the lower head, turning up into the core housing. A simulated lower core plate at the entrance of the core housing provides a significant reduction in coolant flow area. The outer walls of the downcomer distribution annulus and the lower head are lined

with honeycomb insulation to reduce heat transfer between the outer vessel wall and the fluid in the lower plenum. The heater rods pass through the length of the lower plenum and penetrate the vessel through the bottom head.

The downcomer inlet annulus assembly contains the cold leg nozzles and is designed to provide an annular inlet geometry similar to that in a PWR. Both surfaces of the inlet annulus are covered with insulators that maintain a steam gap to isolate the fluid from the hot walls of the assembly. The lower end of the inlet annulus contains a transition section that funnels the flow into the downcomer pipe. The downcomer inlet annulus is connected to the vessel upper head with 1/2-in. tubing which simulates the bypass flow paths in a PWR; as already mentioned, about 4% of the total combined loop flows is normally routed through the bypass line into the upper head. Coolant enters the vessel through an external downcomer inlet annulus (shown in Figure AI.9). This annular entrance section reduces to an instrumented pipe over the major length of the lower vessel, until the bottom of the downcomer rejoins the vessel at the lower plenum through an annular distribution annulus, as shown in Figure AI.12. The downcomer pipe is fabricated from 3-in. Sch 160 pipe, and the inner wall of the downcomer pipe is lined with a honeycomb insulator to limit heat transfer between the pipe wall and the fluid. An instrumented spool piece provides the connection between the lower end of the downcomer pipe and the downcomer nozzle connecting to the downcomer distribution annulus.

The high pressure injection (HPI) systems, low pressure injection (LPI) systems, and the loop accumulators are connected to the cold legs between the pump and the vessel in the intact loop and between the pump and the break in the broken loop. Positive displacement pumps supply the HPI and LPI flows, which are scaled to represent PWR ECC systems. The UHI accumulator injects ECC into the upper head through a 2.54 cm OD by 8.3 m long pipe perforated with fifty 0.356 cm diameter holes, as already mentioned. The accumulators are partially filled with water and pressurized with nitrogen. The pressure of the nitrogen and the liquid and nitrogen volumes are scaled from PWR ECC systems. The total volumes of the accumulators are: $2.513 m^3$ for the intact loop, $1.182 m^3$ for the broken loop, and $2.992 m^3$ for the UHI.

Table AI.1

SEMISCALE PRIMARY COOLANT SYSTEM ELEVATIONS[a]

LOCATION	ELEVATION (IN.)
VESSEL	
TOP OF UPPER HEAD	+166.6
TOP OF GUIDE TUBE	+132.1
BOTTOM OF UHI INJECTION TUBE	+127.1
TOP OF CORE SUPPORT TUBES	+67.1
TOP OF UPPER SUPPORT PLATE	+61.4
BOTTOM OF UPPER SUPPORT PLATE	+53.4
HOT LEG NOZZLE CENTERLINE	+8.5
COLD LEG NOZZLE CENTERLINE	0.0
TOP OF HEATED CORE	-51.1
BOTTOM OF HEATED CORE	-191.1
TOP OF LOWER PLENUM	-215.0
BOTTOM OF LOWER PLENUM	-227.6
INTACT LOOP	
BOTTOM OF STEAM GENERATOR TUBE SHEET	+81.6
SHORT TUBE TOP, SPILLOVER	+436.9
MIDDLE TUBE TOP, SPILLOVER	+465.4
LONG TUBE TOP, SPILLOVER	+491.9
PUMP SUCTION CENTERLINE	-111.0
BOTTOM OF PRESSURIZER INTERNAL VOLUME	+68.8
TOP OF PRESSURIZER INTERNAL VOLUME	+117.3
BROKEN LOOP	
BOTTOM OF STEAM GENERATOR TUBE SHEET	+81.6
SHORT TUBE TOP, SPILLOVER	+436.9
LONG TUBE TOP, SPILLOVER	+491.9
PUMP SUCTION CENTERLINE	-110.3

[a] ELEVATIONS ARE RELATIVE TO COLD LEG CENTERLINE

Table AI.2

Intact Loop Spool Pieces

Spool Piece Number	Spool Piece Indent	Total Length (in)	Blueprint Number
H. L. Nozzle		8.65	407968
1	3-PC-1B	23.06	414684
2	3-PC-18	15.61	407346
3	2½-PC-2	52.51	415155
4	2½-PC-6	26.31	414431
5	2½-PC-7	13.995	414425
6	2½-PC-8	14.00	414426
7	2½-PC-9	19.195	414427
SG Inlet		6.32	414271
SG Outlet		6.32	414271
8	2½-PC-10	27.195	414428
9	2½-PC-11	13.995	414425
10	2½-PC-12	14.00	414426
11	2½-PC-13	14.00	414429
12	2½-PC-14A	19.41	414430
13	3-PC-20	85.25	409027
14	3-PC-20	20.638	409027
15	3-PC-20	60.00	409027
16	3-PC-20	23.06	414684
17	3-PC-9A	19.319	404749
18	3-PC-10A	20.53	408613
IL Pump			
19	3-PC-11A	17.00	412858
20	3-PC-12	17.25	404759
21	3-PC-13	23.06	404794
22	3-PC-19A	37.90	414684
C. L. Nozzle		7.15	407986

Table AI.3

Broken Loop Spool Pieces

Spool Piece Number	Spool Piece Indent	Total Length (in)	Blueprint Number
H. L. Nozzle	(3 in. Sch. 160)	16.07	407975
50	1½-ABL-1	24.01	407670
55	1½-ABL-14A	59.517	414670
56	1½-ABL-30	11.83	414671
57	1½-ABL-31	13.872	414672
58	1½-ABL-32	13.75	414673
59	1½-ABL-33	19.826	414674
SG Inlet		4.142	414272
SG Outlet		4.142	414272
60	1½-ABL-34	15.316	414675
61	1½-ABL-35	13.75	414676
62	1½-ABL-36	13.872	414672
63	1½-ABL-37	13.75	414673
64	1½-ABL-6A	109.17	414677
65	1½-ABL-7	33.834	407384
72	1½-ABL-9	61.82	407380
73	1½-ABL-11	27.56	407673
BL Pump			
74	1½-ABL-12	23.64	407674
76	1½-ABL-17	19.77	407875
79	1½-ABL-15	28.01	407675
CL Nozzle	(3 in. Sch 160)	15.314	407986

Table AI.4 Type II Steam Generator Data (Mod-2A)

	Intact Loop	Broken Loop
Number Tubes	6	2
Tube Dimensions	(0.875 in. OD x 0.049 in.	Wall x 1.25 in. Pitch
Tube Height(1)	2 @ 391 in. 2 @ 364.5 in. 2 @ 336 in.	1 @ 391 in. 1 @ 336 in.
Primary Volume, Bundle	1.27 ft^3	0.40 ft^3
Primary Plenum Volume	0.058 ft^3 each	0.042 ft^3 each
Secondary Volume(2)	4.27 ft^3	2.97 ft^3
Downcomer Volume	1.34 ft^3	1.13 ft^3
Total Secondary Volume(3)	11.0 ft^3	9.45 ft^3
Secondary Heat Transfer Area	83.3 ft^2	27.76 ft^2

(1) Above top of tube sheet
(2) Tube sheet to top of tubes
(3) Tube sheet to top of separators

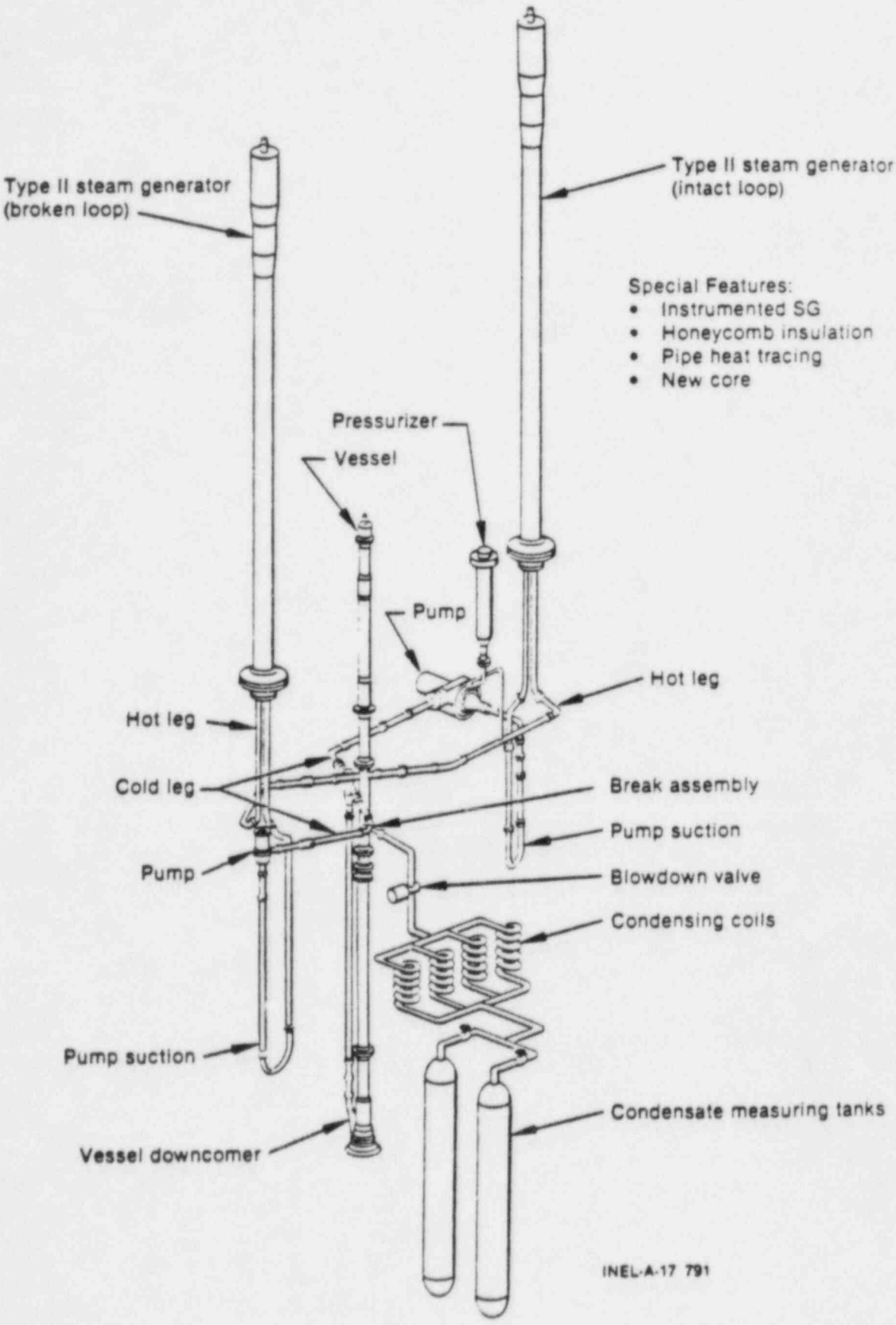

Figure AI.1 Isometric View of the Semiscale Mod-2A System

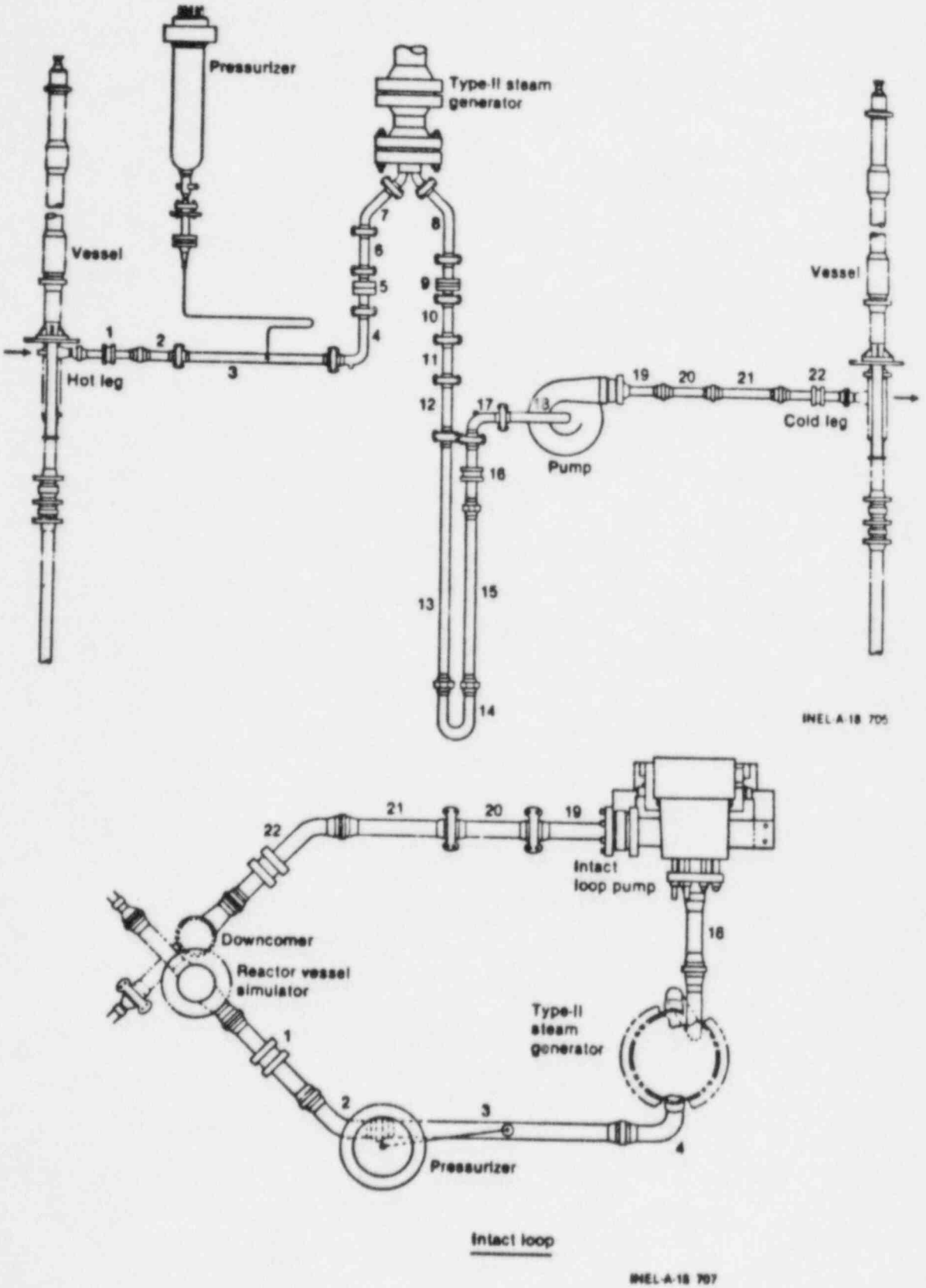

Figure AI.2 Intact Loop Spool Pieces

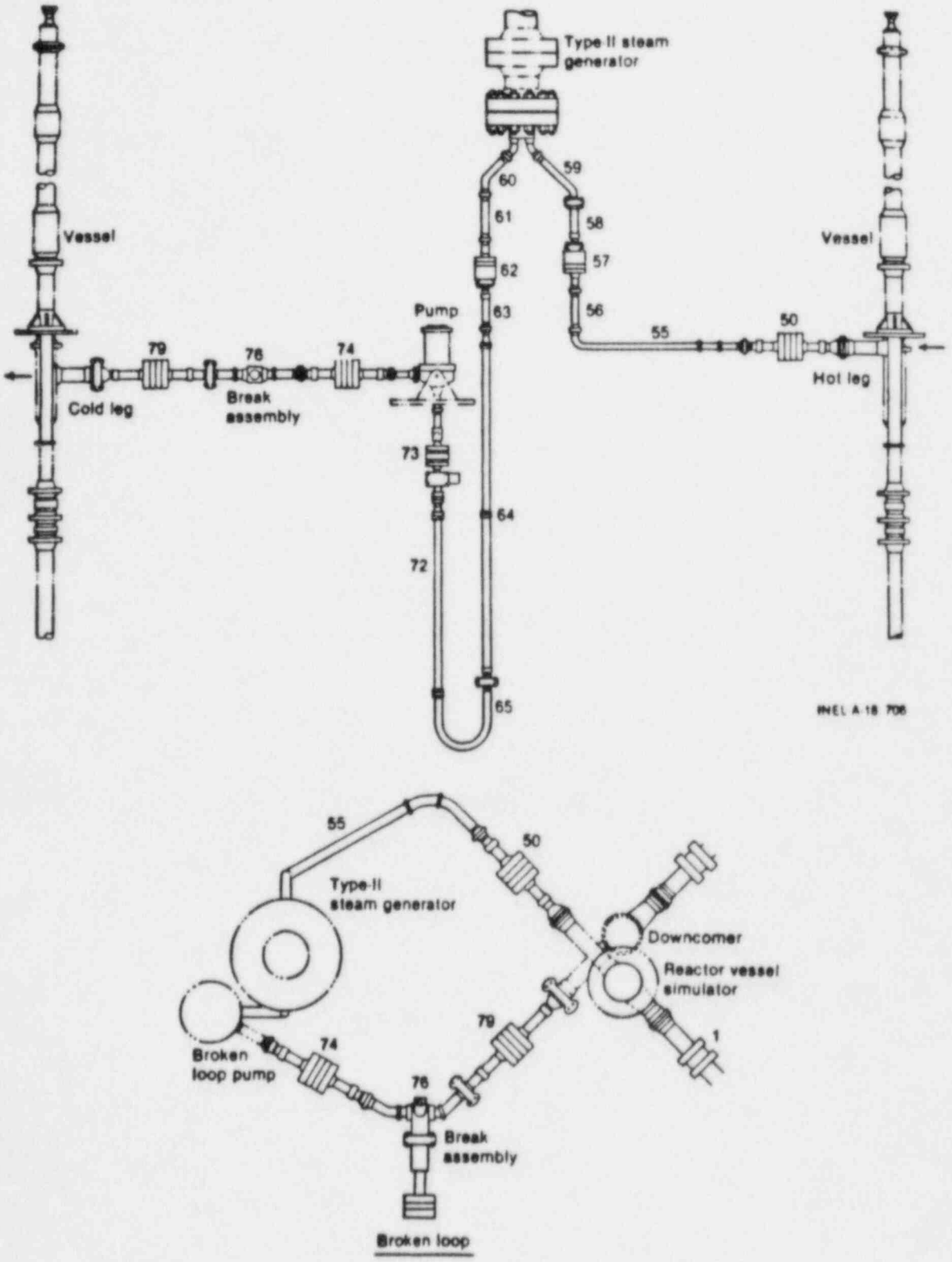

Figure AI.3 Broken Loop Spool Pieces

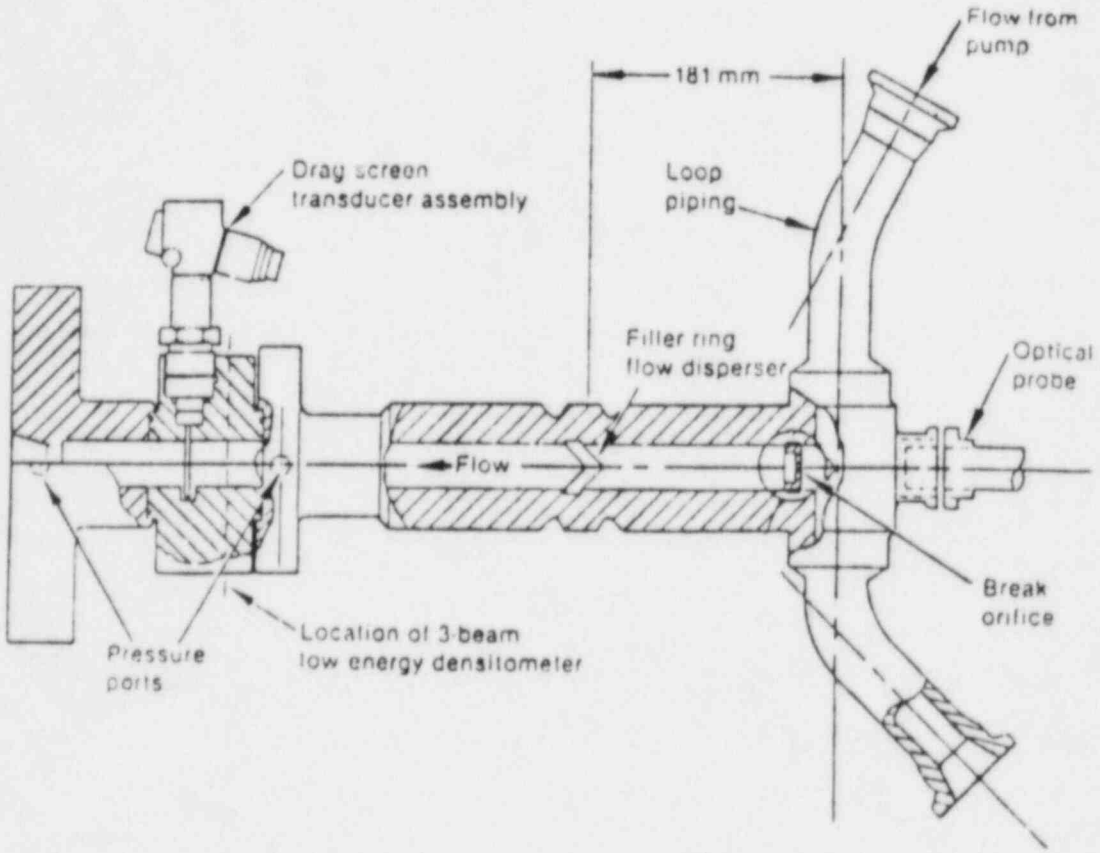

Figure AI.4 Communicative Small Break Assembly

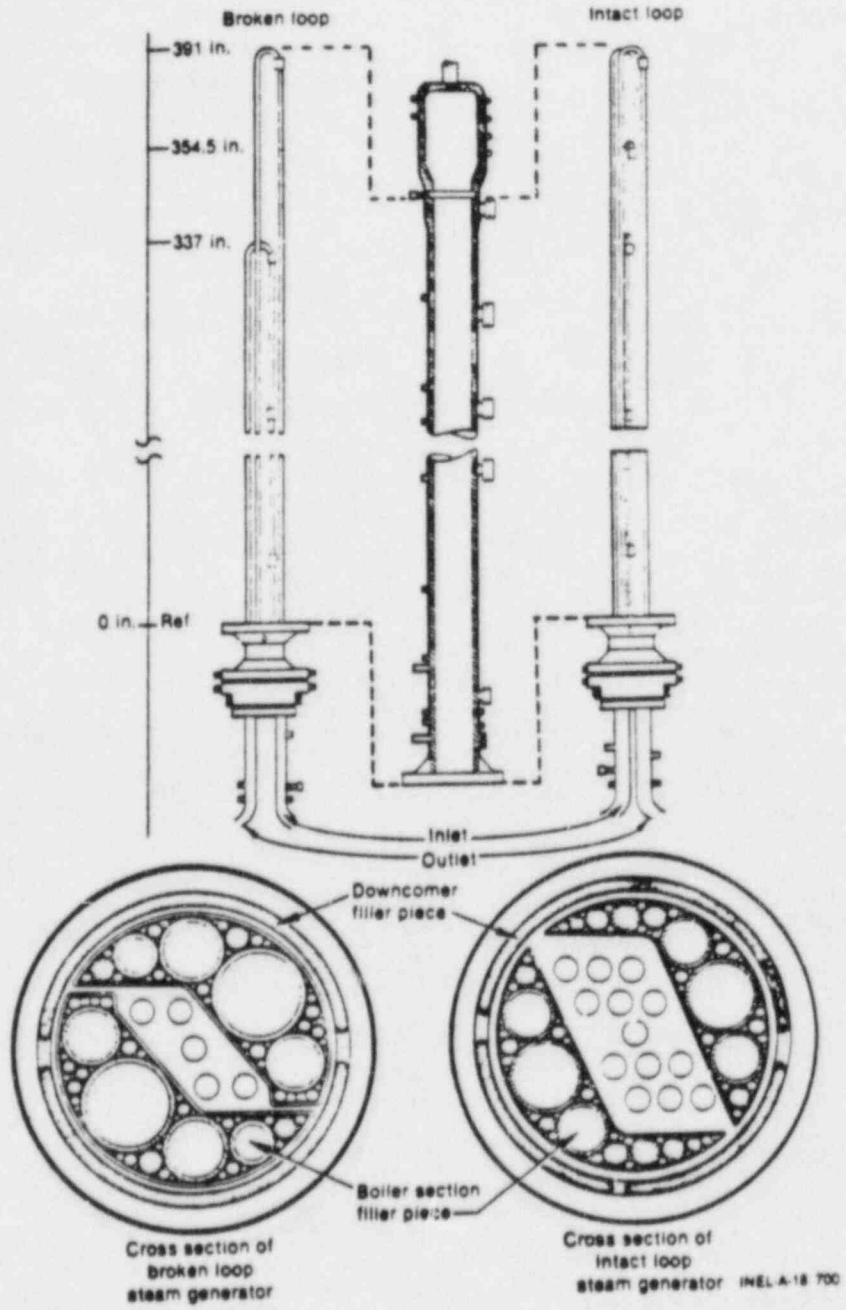

Figure AI.5 Steam Generator Assembly

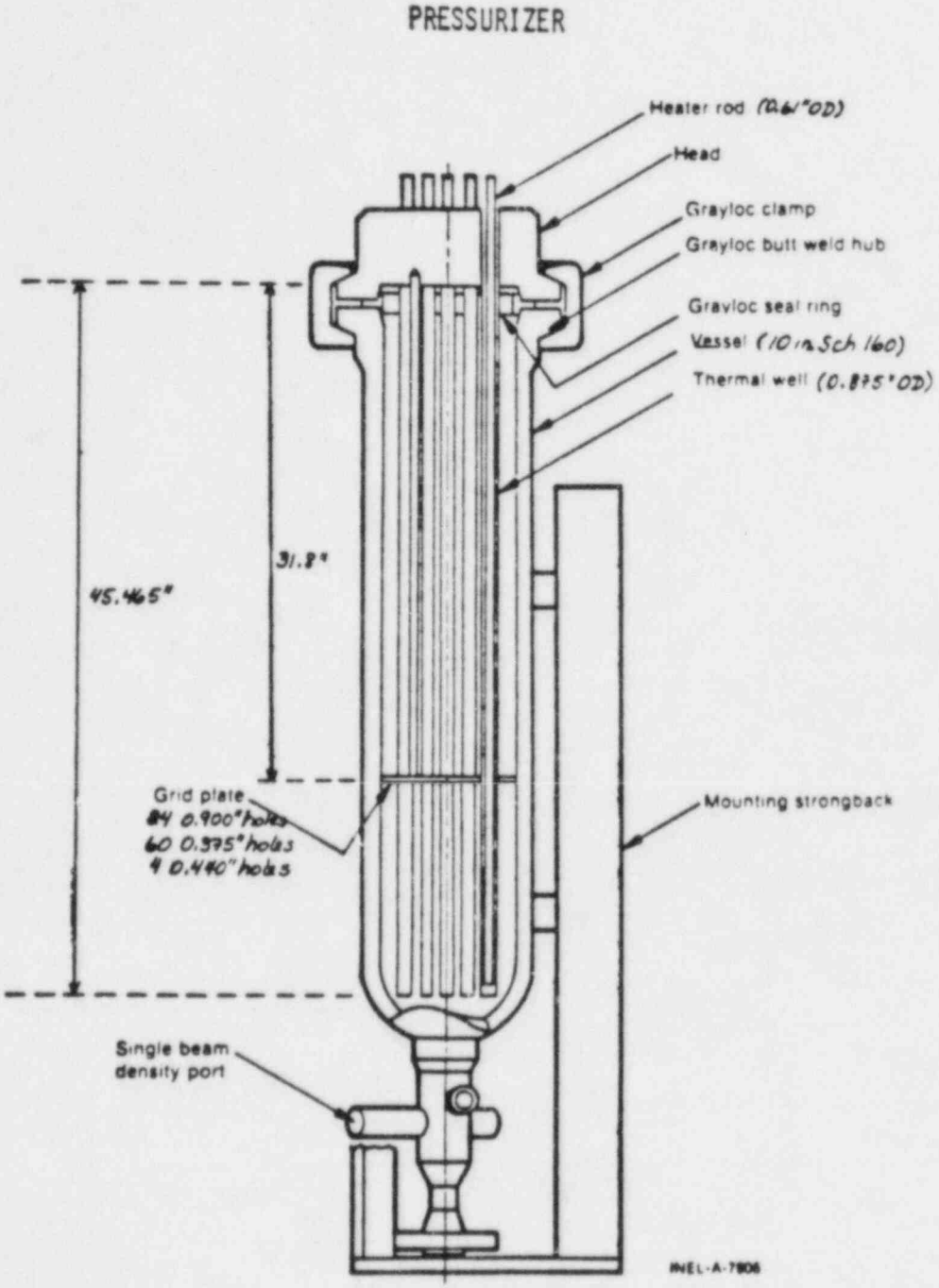

Figure AI.6 Pressurizer Vessel

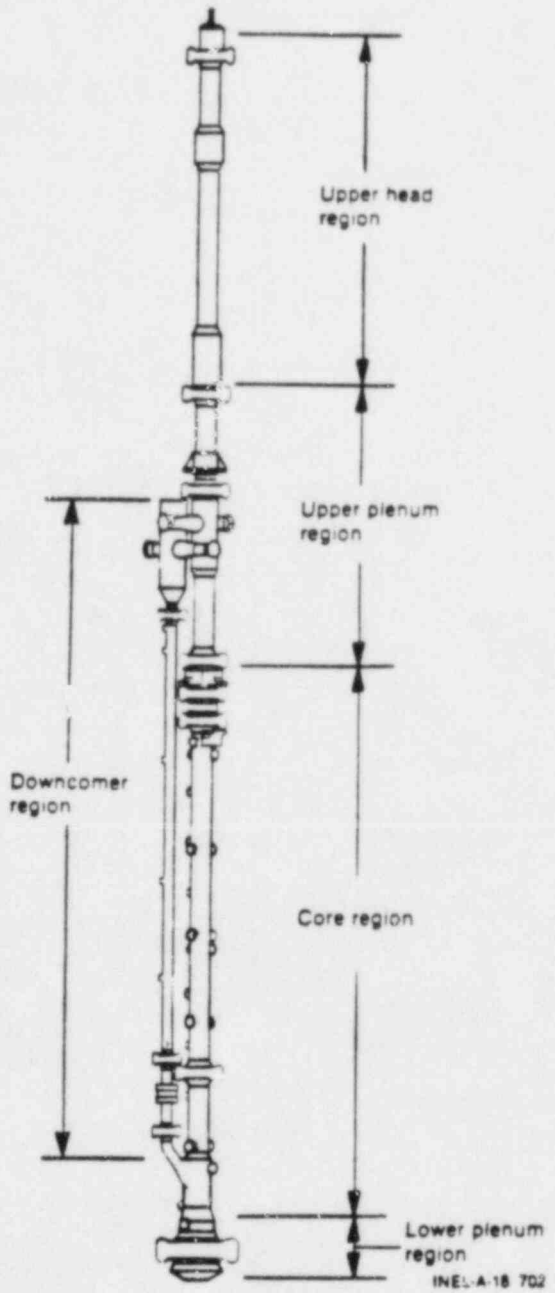

Figure AI.7 Semiscale Mod-2A Vessel Assembly

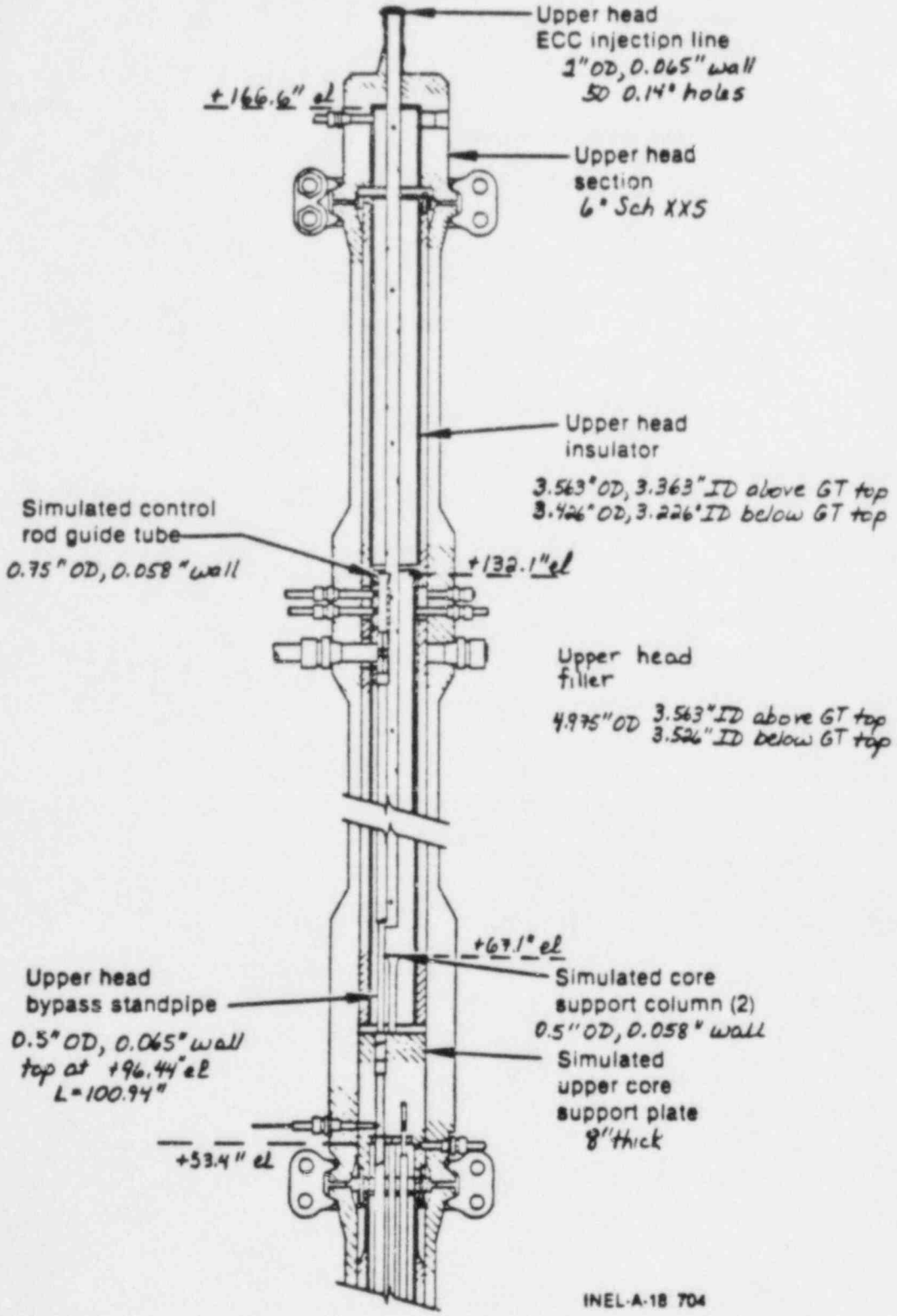

Figure AI.8 Semiscale Mod-2A Vessel Upper Head Region

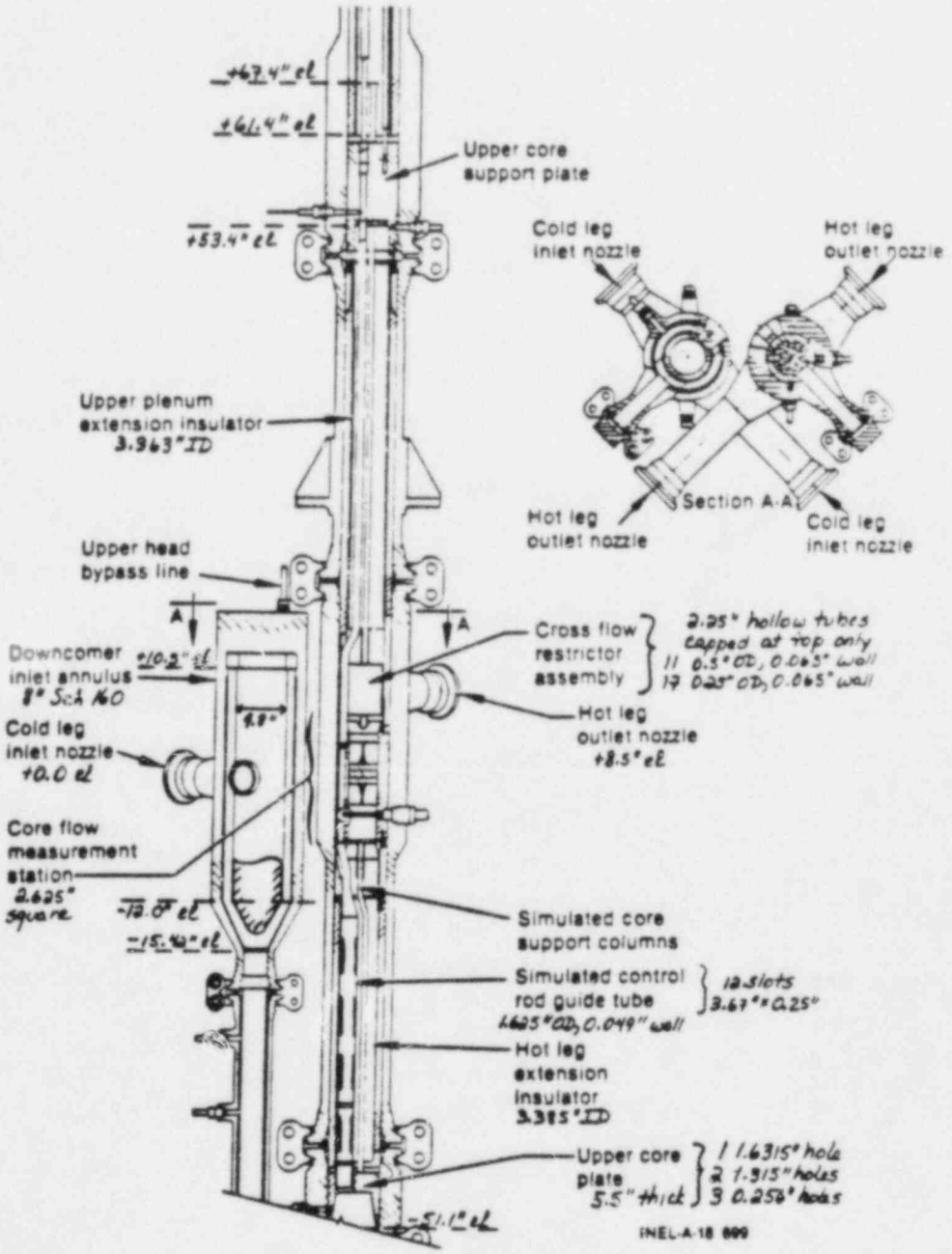

Figure AI.9 Semiscale Mod-2A Vessel Downcomer Inlet and Upper Plenum Region

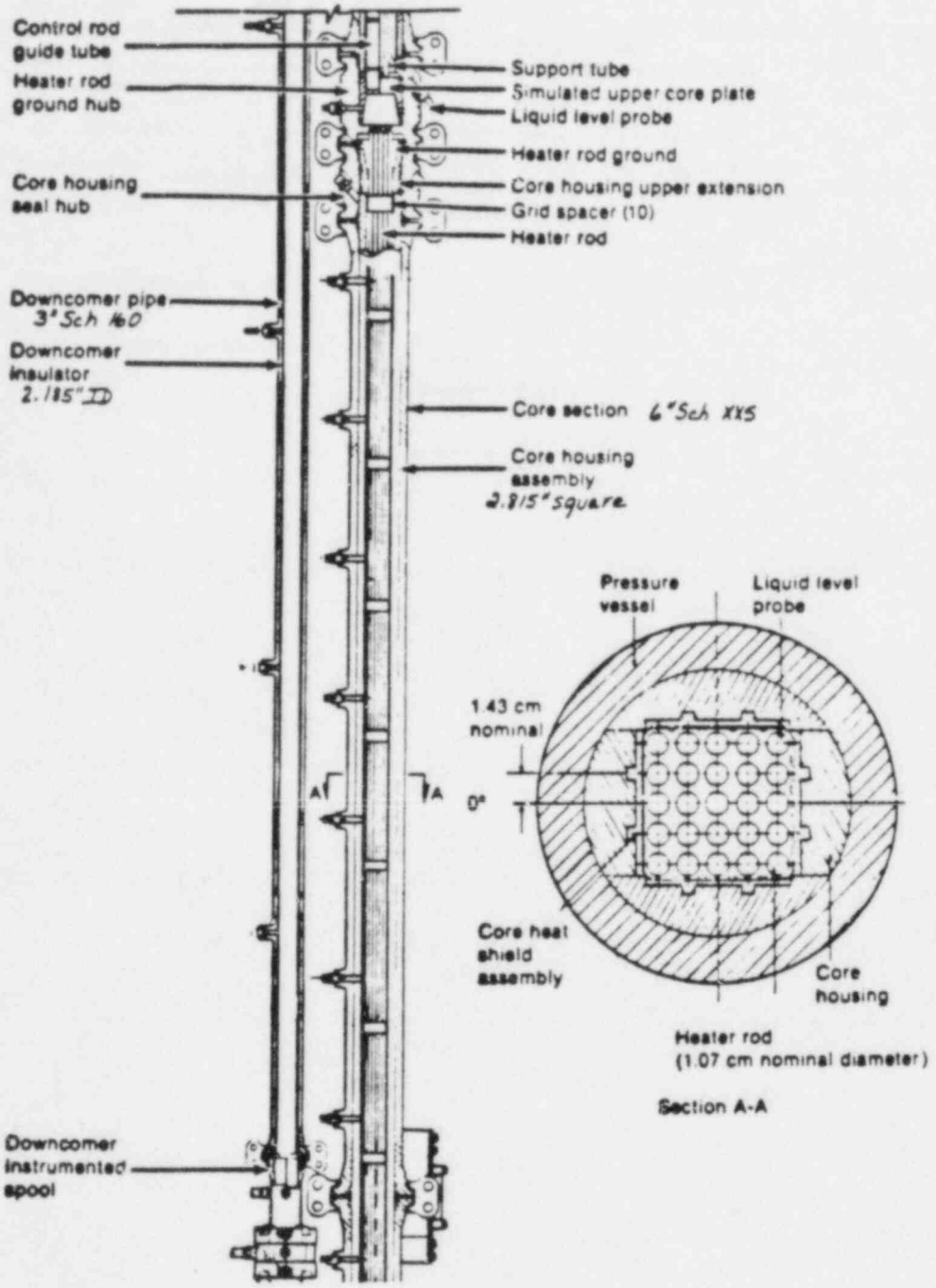

Figure AI.10 Semiscale Mod-2A Vessel Core Region

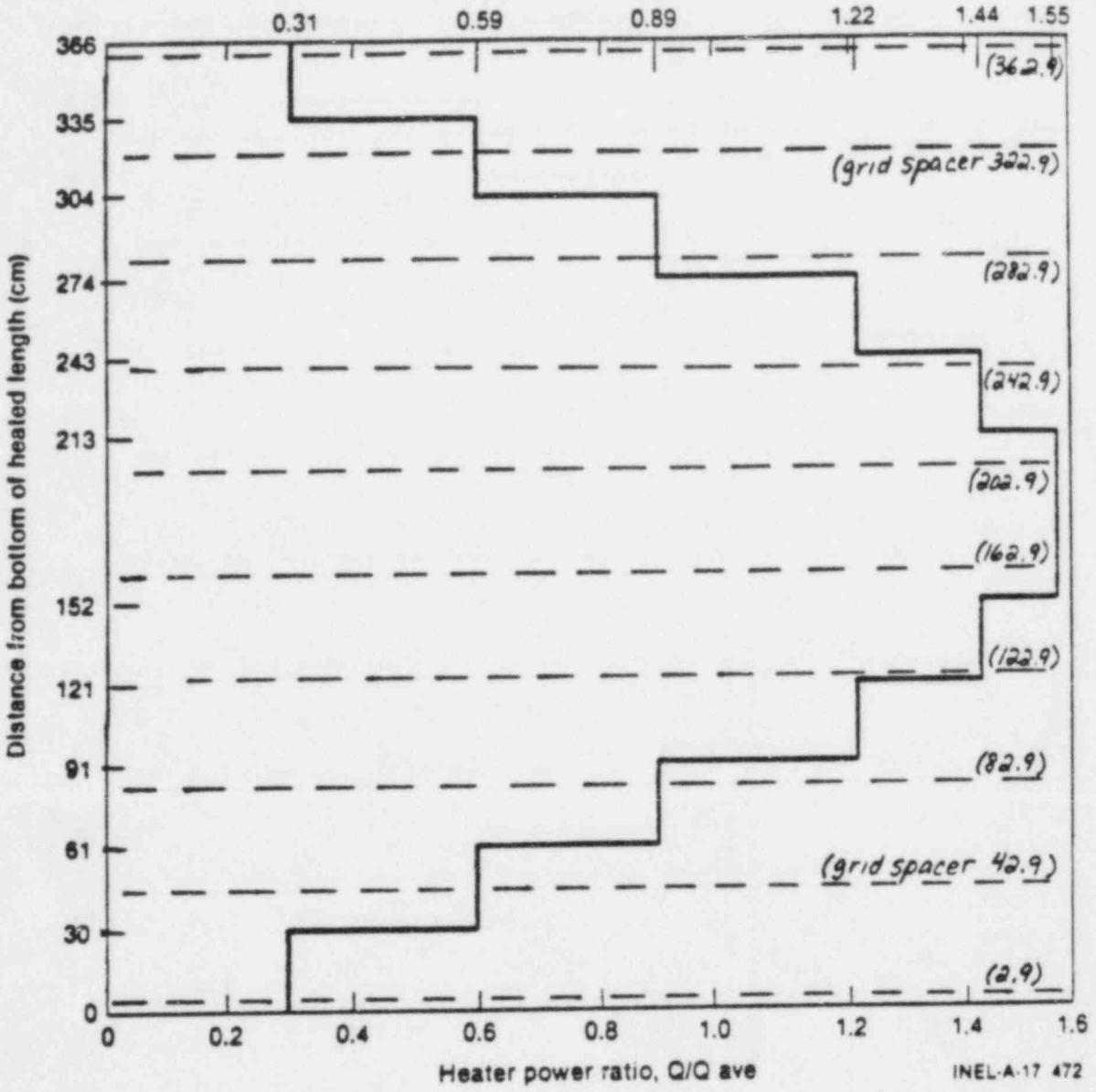

Figure AI.11 Core Axial Power Profile

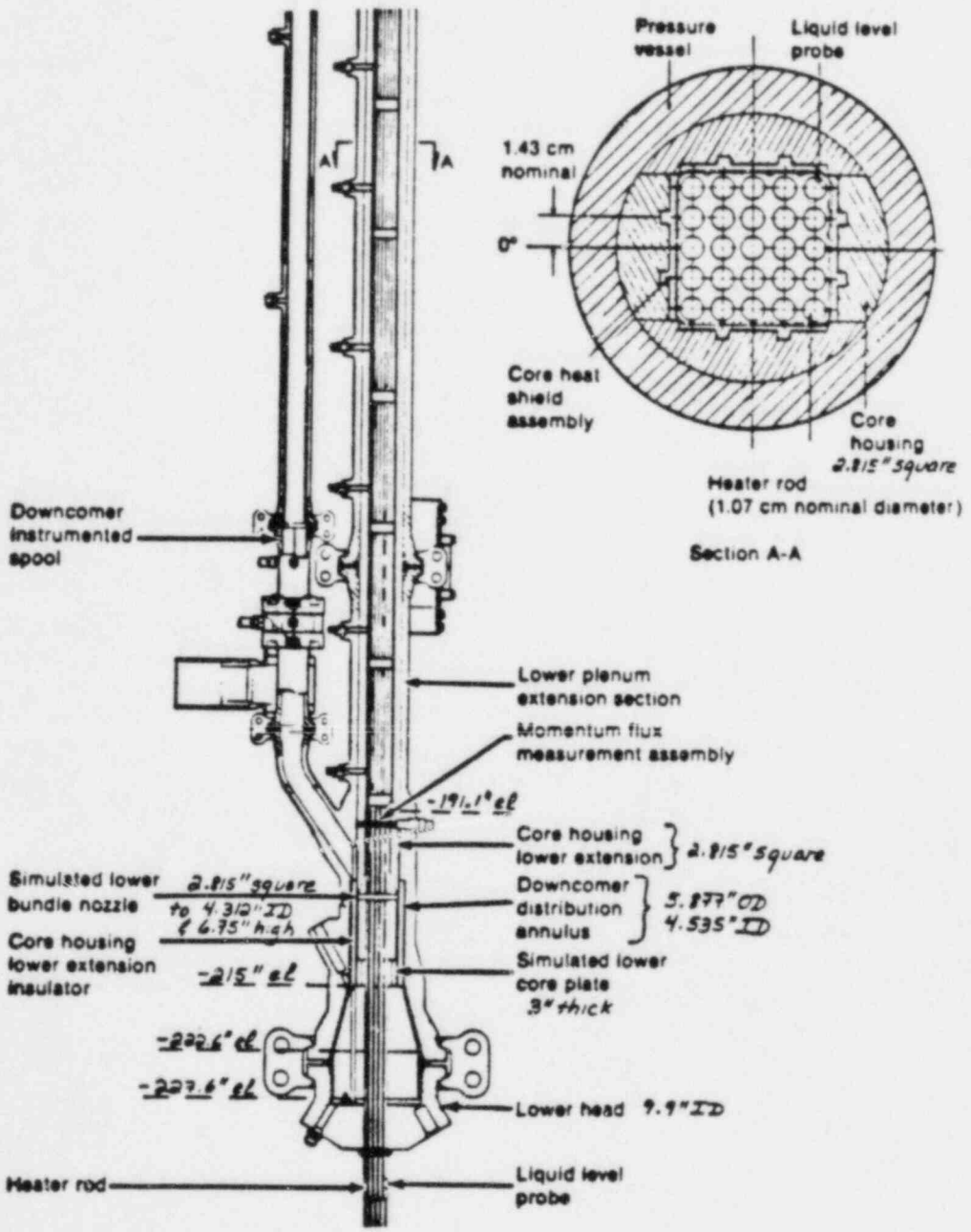

Figure AI.12 Semiscale Mod-2A Vessel Lower Plenum and Lower Downcomer Region

APPENDIX II INPUT LISTINGS

Input listings for each of the five transient calculations are given on attached microfiche.

APPENDIX III RELAP5 CALCULATIONS WITH DETAILED AND COARSE NODING OF THE STEAM GENERATORS

This sensitivity study was carried out at the specific request of the NRC because Argonne National Laboratory (ANL) had performed some RELAP5 calculations for a PWR [24] that showed the peak clad temperatures for small break LOCAs were higher with detailed noding than with coarse noding of the steam generators. The calculation of the higher clad temperatures was reported by ANL as being the result of more liquid holdup in the primary side of the steam generator tubes and lower core liquid levels with the more detailed noding. The holdup of liquid in the primary side of the steam generator tubes apparently caused a core level depression in test S-UT-8; therefore, test S-UT-8 was selected to investigate the effect of steam generator noding.

The initial information obtained from the Semiscale Program [23] identified the unplanned flow path during test S-UT-8, when the support column instrumentation was removed, as being from the bottom of the upper head to the top of the upper plenum. This flow path was modeled in these calculations as a short pipe from the upper head to the upper plenum. (Later documentation received from the Semiscale Program established that the actual leakage flow path was through the support columns from the upper head to the upper core.) The flow holes through the guide tube wall near the bottom of the upper head plate were also left out of this version of the model. Even though the geometry was not modeled correctly in the calculations discussed here, the results are nevertheless provided to give an indication of the effect of the steam generator noding on RELAP5 calculations for a small break LOCA.

Two calculations were performed before these errors in the geometry were identified. One calculation was performed using the base case detailed steam generator model discussed in Section 2.1, and a second calculation was performed using about half as many nodes in the steam generators, similar to the nodings used by Argonne. The coarse noding of the intact and broken loop steam generators used in the second calculation is shown in Figure AIII.1. Except for the changes in steam generator noding, the models were identical. The resistances of the support plates in the secondary side of the steam generators were modeled as user input form losses in both cases, rather than using the code's abrupt area change model, so that they could be combined to ensure the same total resistance was used in both calculations. The initial conditions for the start of each transient calculation are tabulated in Table AIII.1 and are nearly identical, except for the steam generator secondary pressures, which were about 0.1 MPa lower for the coarse node calculation than for the base calculation. Several attempts to identically match the secondary conditions were not successful.

The effect of the steam generator noding on the calculated primary pressure is shown in Figure AIII.2. The experimental data is also shown for reference. The initial difference in the calculated primary pressures was due to the small differences in the initial steam generator secondary pressures; as mentioned above, the conditions in the steam generator secondaries were not matched exactly with the two nodings. By the end of the transient there was no significant difference in the calculated pressures.

An important phenomenon in the Argonne calculations was the draining of the primary sides of the steam generator tubes. The collapsed liquid levels on the primary upside and downside of the intact loop steam generator tubes are shown in Figure AIII.3. In both calculations, the primary sides of the tubes start to drain at about 100 s and the downflow sides empty about 40 s before the upflow sides. There was essentially no difference in the time of draining between the calculations.

The effect of steam generator noding on the hydraulics in the vessel upper head is shown in Figure AIII.4, which compares the vessel upper head collapsed liquid levels. The upper head voided slightly earlier and drained slightly earlier with the coarse noding; however, the rate of draining was about the same for each model. This small difference in the time of draining of the upper head should not significantly affect the results and no such effect could be identified.

The voiding of the vessel is indicated by the vessel collapsed liquid levels shown in Figure AIII.5. For both calculations the vessel voided early in the transient and the level was depressed into the core, with the minimum level about 0.3 m lower with the coarse noding. From about 225 s to 350 s, the collapsed level was about 0.5 m lower for the coarse noding. The depth and duration of the core level depressions are also indicated from the core inlet densities, which are shown in Figure AIII.6. The decrease in the calculated densities at about 200 s indicates some voiding occurred for a few seconds in both calculations, with slightly more voids with the coarse noding. Since we did not plot every time step, some of these apparent differences could result simply from the frequency of plotting and we do not consider these to be significant differences.

The calculated and measured densities at the 1.7 m core elevation are shown in Figure AIII.7. In both calculations, this elevation was initially voided at about 190 s. For the coarse noding, this elevation remained almost totally voided until 340 s when it was refilled, whereas with the base noding large oscillations in the density occurred. Both calculations indicated the liquid level dropped below this elevation again later in the transient. The later decrease in density occurred at 440 s for the base noding and 500 s for the coarse noding.

The effect of the core densities on the rod temperatures at the 1.2 m to 1.8 m core elevation is shown in Figure AIII.8. In both calculations, dryouts and rewets occurred early in the transient when the densities were low. The peak rod temperature during this period was slightly higher with the coarse noding. When the liquid level dropped in the core and the densities decreased again later in the transient, a sustained heatup of the rods occurred. At the termination of the calculations, the peak rod temperatures were nearly equal.

The intact loop pump suction collapsed liquid levels are shown in Figure AIII.9. The intact loop pump suction downside cleared a few seconds earlier in the coarse node calculation; however, after downside clearing, slightly more liquid remained for a longer period of time in the upflow side during the base calculation.

The results were considerably different in the broken loop pump suction. The broken loop pump suction collapsed liquid levels are shown in Figure AIII.10. With the coarse noding both the upside and the downside of the pump suction cleared, whereas neither side cleared for the detailed noding; the downside started to clear at about 375 s, but then refilled. The reasons for the difference in the broken loop pump suction behavior could not be identified. (The results for the calculation of the broken loop pump suction with the detailed noding were similar to the results for tests S-UT-1 and S-UT-6, discussed in Sections 3.1 and 3.3.)

In summary, there were several differences in the calculated loop and vessel hydraulics, depending on the number of volumes used to model the steam generators. Part of the cause of these differences may have been small differences in the initial steam generator secondary side conditions at the beginning of the two calculations. The differences in the system hydraulics did not have a large effect on the core liquid level depression or the peak rod temperatures. Overall, there was not a significant effect of steam generator noding on the calculated results.

Table AIII.1 Initial Conditions for Base and Coarse Node Steam Generator Calculations

	S-UT-8	RELAP (Base)	RELAP (Coarse)
Core Power (MW)	1.95	1.95	1.95
System Pressure (MPa)	15.6	15.5	15.5
Intact Loop Cold Leg Temperature (K)	559.5	559.5	559.5
Intact Loop ΔT (K)	35.1	35.2	35.2
Intact Loop Flow (ℓ/s)	10.3	10.0	10.0
Intact Loop Steam Generator Pressure (MPa)	5.71	5.75	5.66
Intact Loop Pump Speed (rad/s)	244.0	226.9	226.8
Broken Loop Cold Leg Temperature (K)	561.4	561.4	561.4
Broken Loop ΔT (K)	33.8	33.3	33.3
Broken Loop Flow (ℓ/s)	3.7	3.3	3.3
Broken Loop Steam Generator Pressure (MPa)	6.11	6.00	5.90
Broken Loop Pump Speed (rad/s)	1192	1491	1489
Bypass Flow (ℓ/s)	NM*	0.09	0.09
Support Column Flow (ℓ/s)	NM*	0.0	0.0
Guide Tube Flow (ℓ/s)	0.09	0.09	0.09

*Not Measured

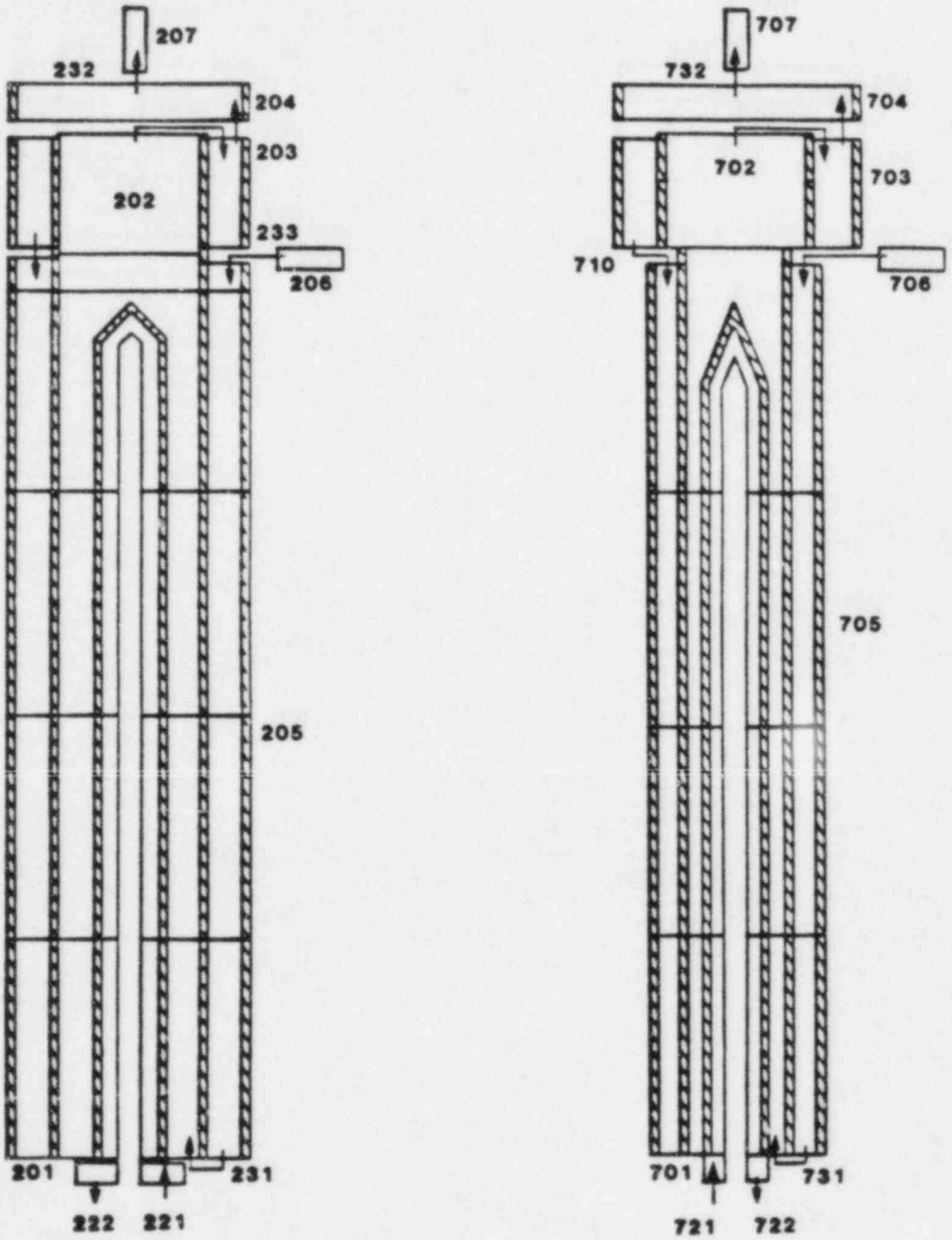

Figure AIII.1 RELAP5 Coarse Nodalization of the Steam Generators

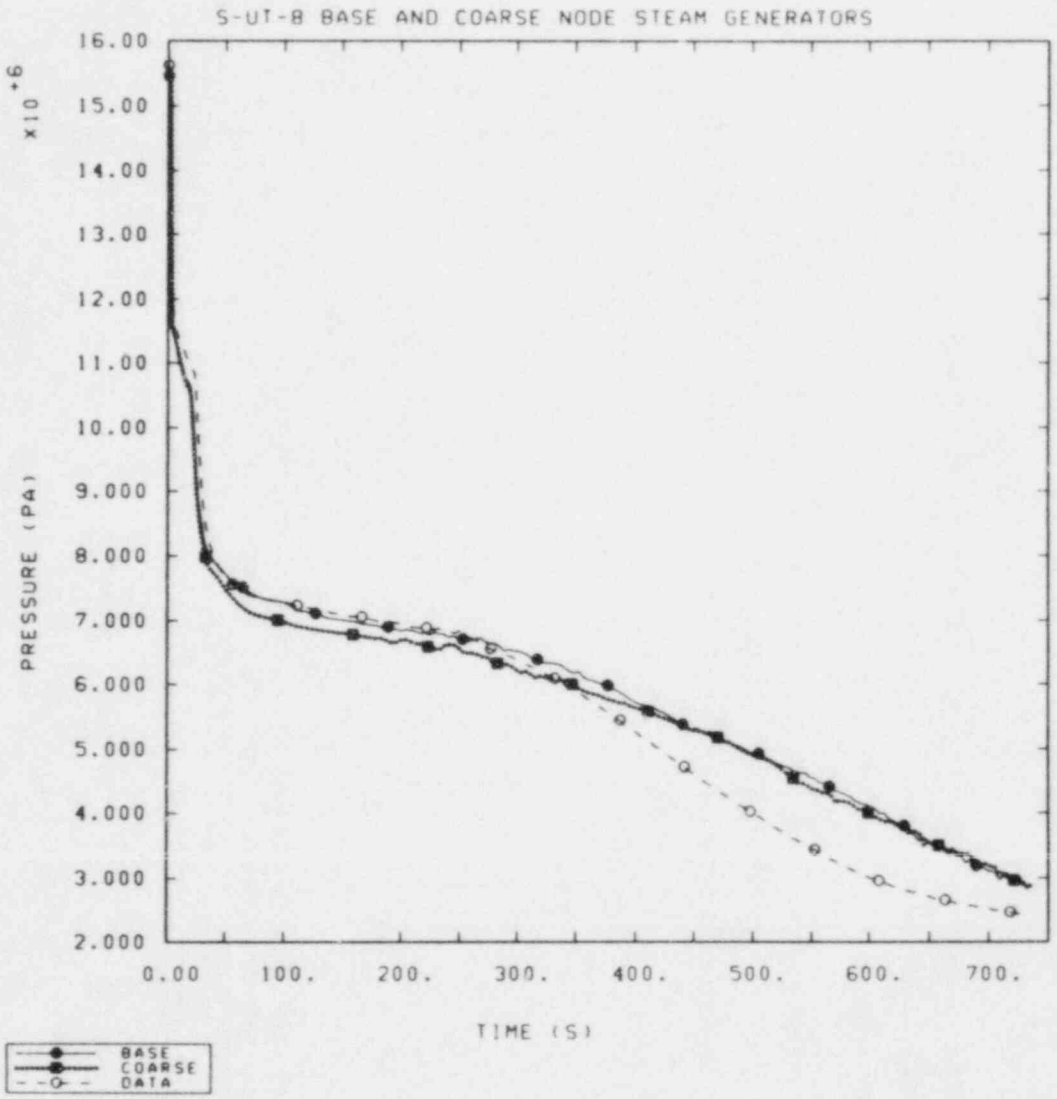

Figure AIII.2 Effect of Steam Generator Nodalization on the Primary Pressure

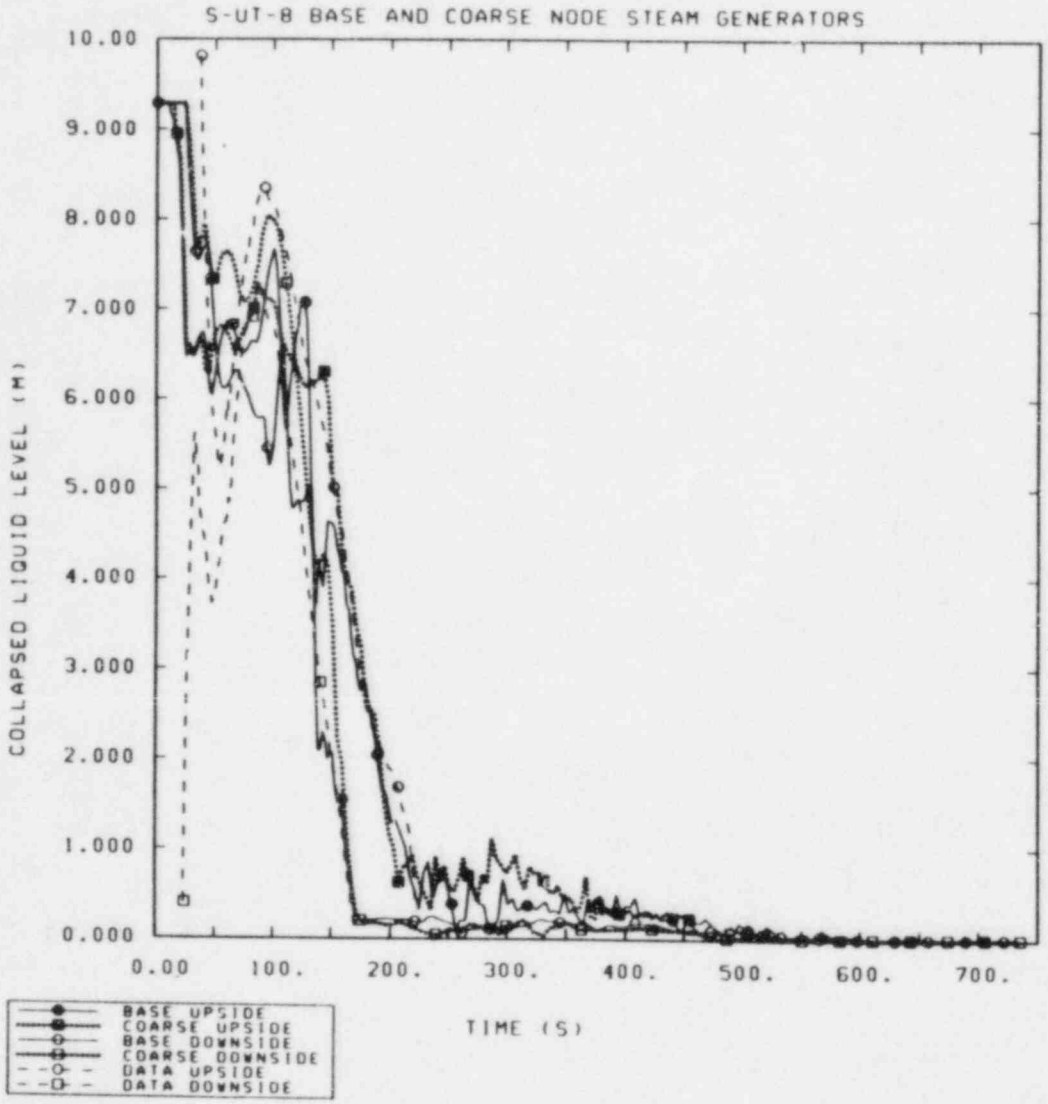

Figure AIII.3 Effect of Steam Generator Nodalization on the Collapsed Liquid Levels in the Primary Side of the Intact Loop Steam Generator Tubes

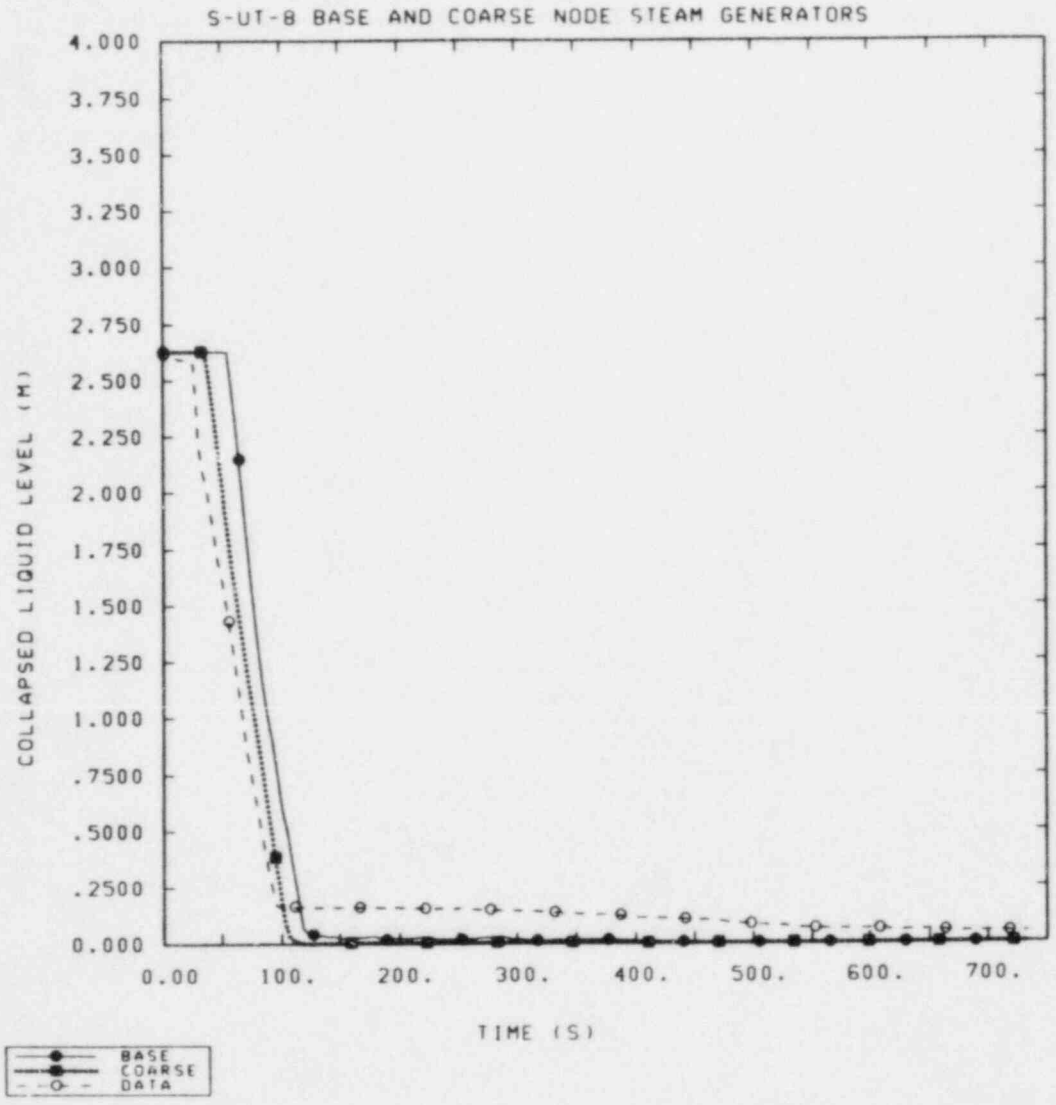

Figure AIII.4 Effect of Steam Generator Nodalization on the Upper Head Liquid Levels

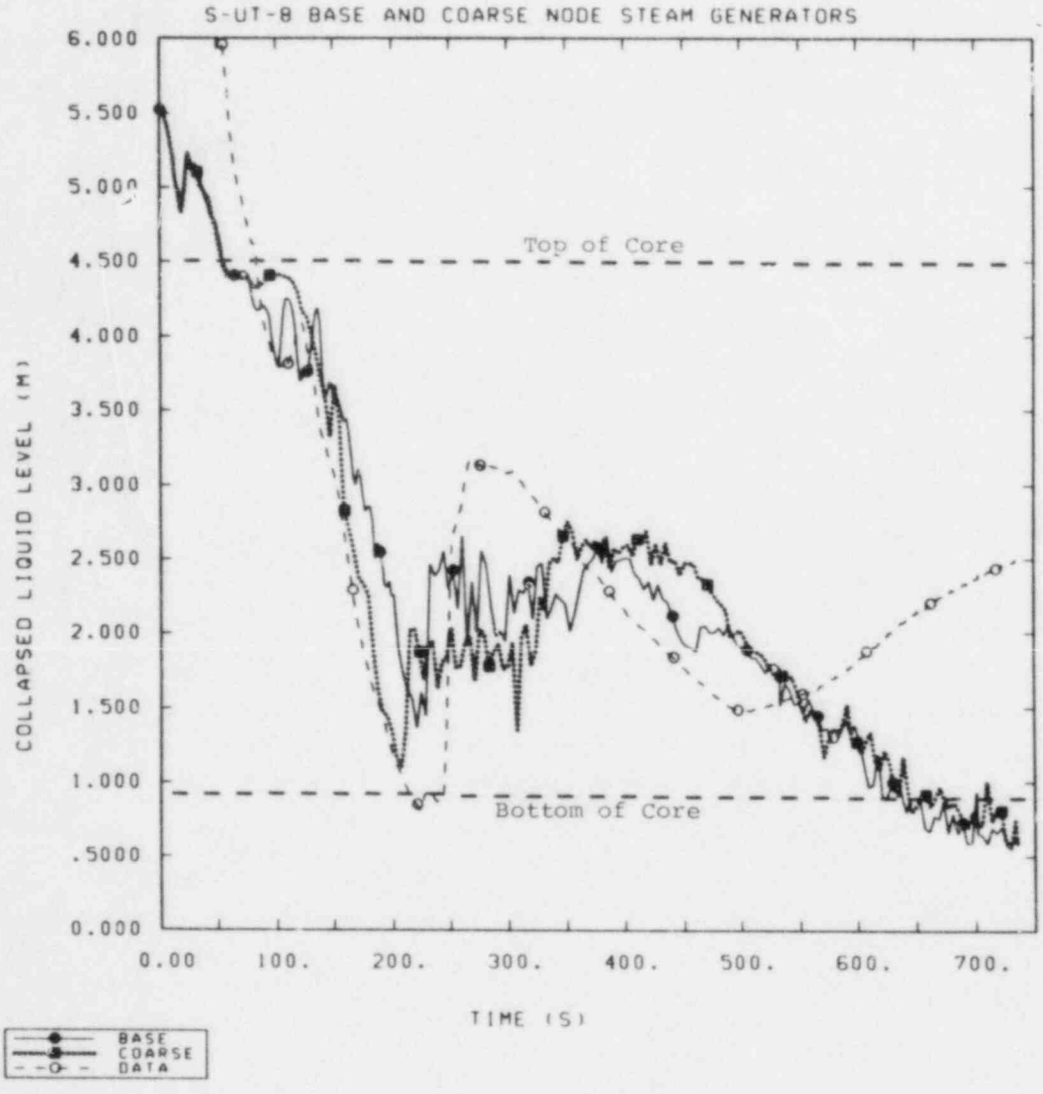

Figure AIII.5 Effect of Steam Generator Nodalization on the Vessel Collapsed Liquid Level

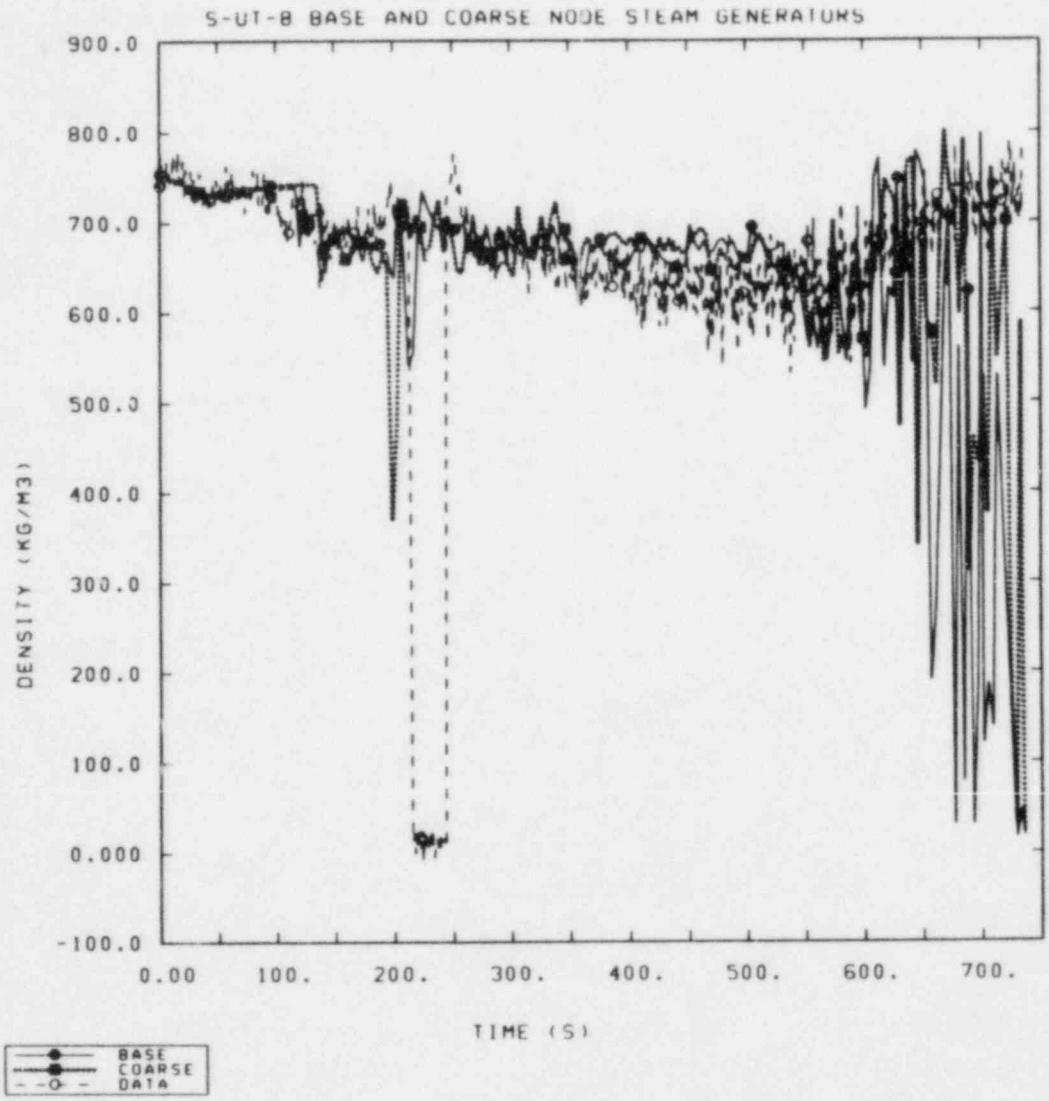

Figure AIII.6 Effect of Steam Generator Nodalization on the Core Inlet Density

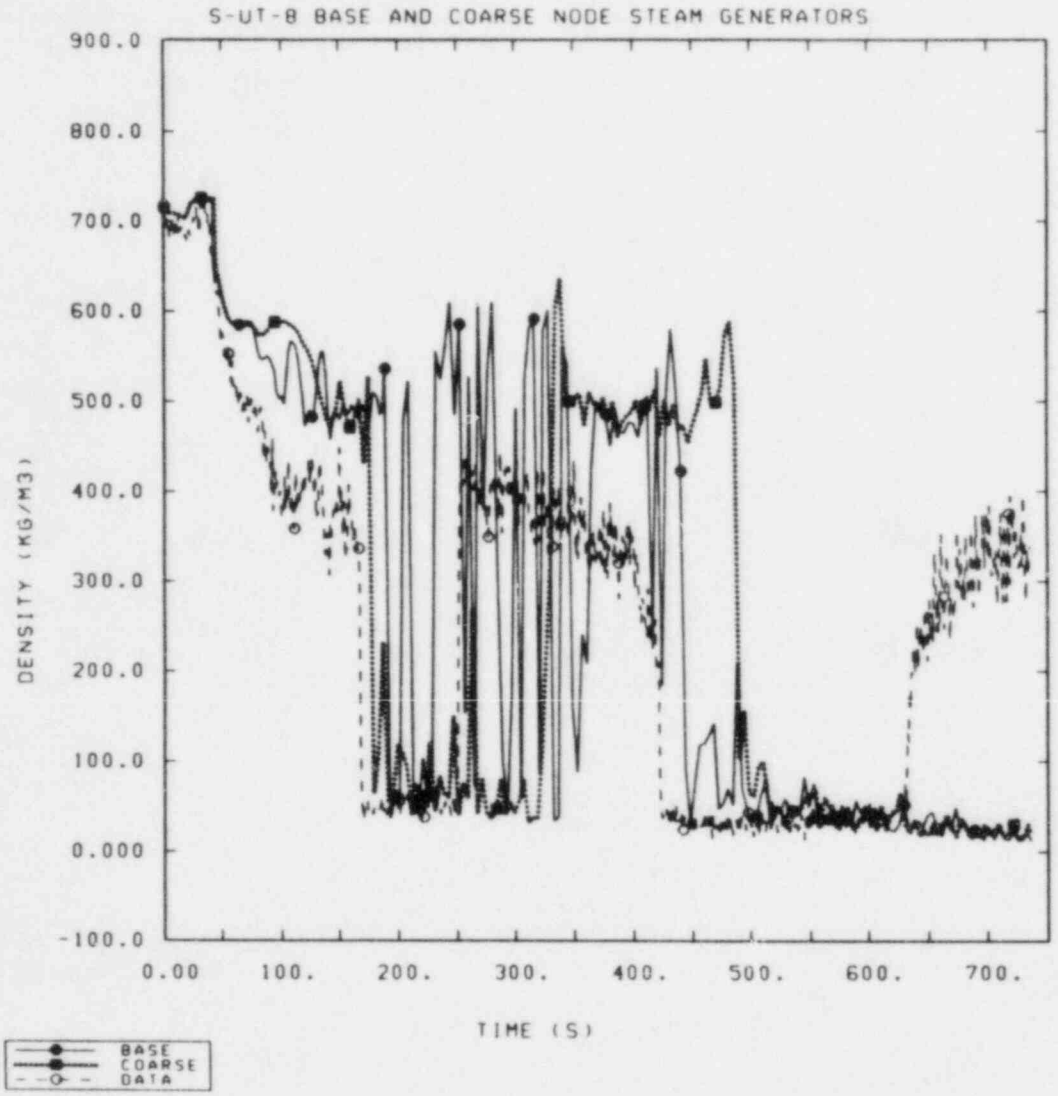

Figure AIII.7 Effect of Steam Generator Nodalization on the Density at the 1.7 m Core Elevation

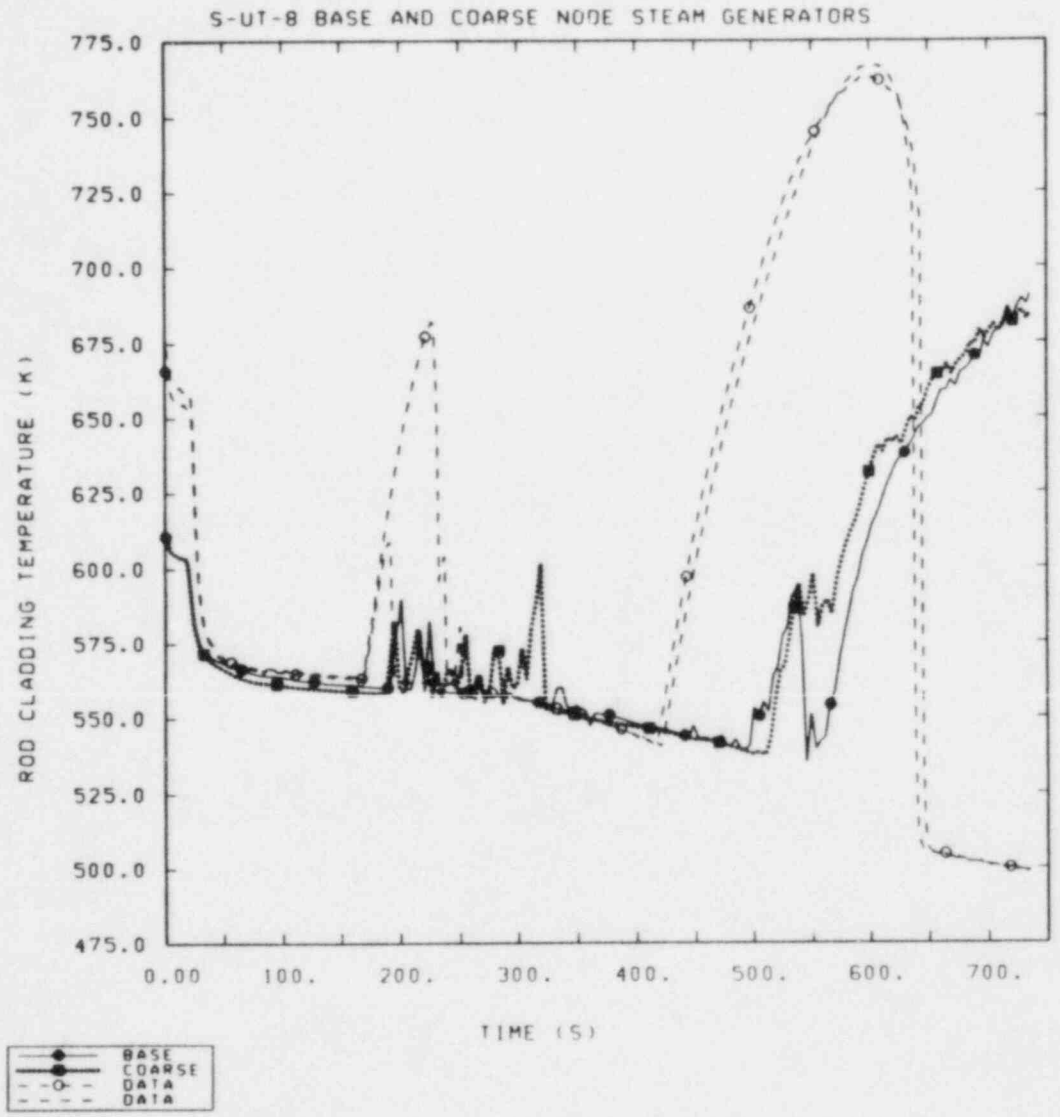

Figure AIII.8 Effect of Steam Generator Nodalization on the Rod Cladding Temperature at the 1.2 m to 1.8 m Core Elevation

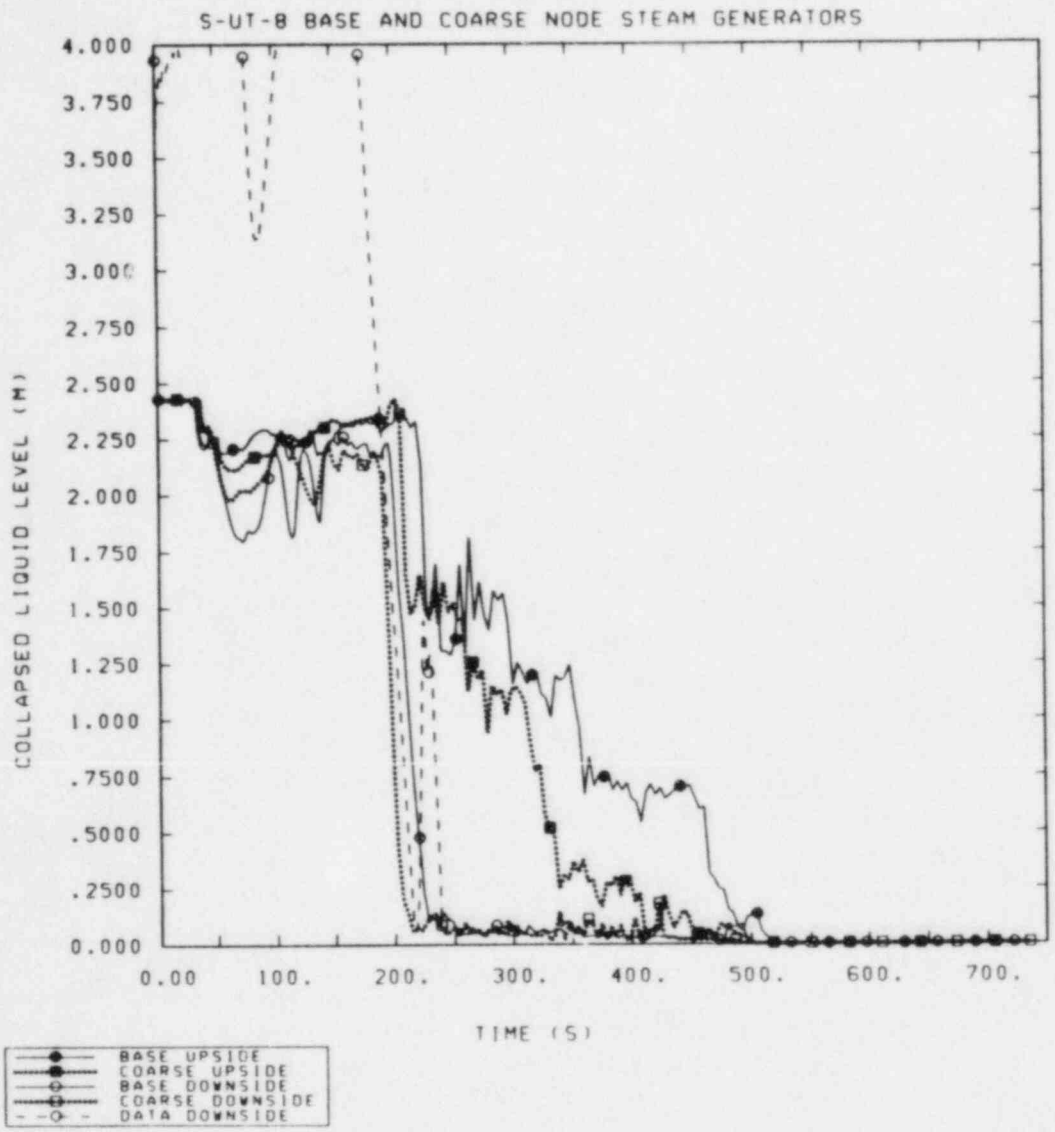

Figure AIII.9 Effect of Steam Generator Nodalization on the Intact Loop Pump Suction Collapsed Liquid Levels

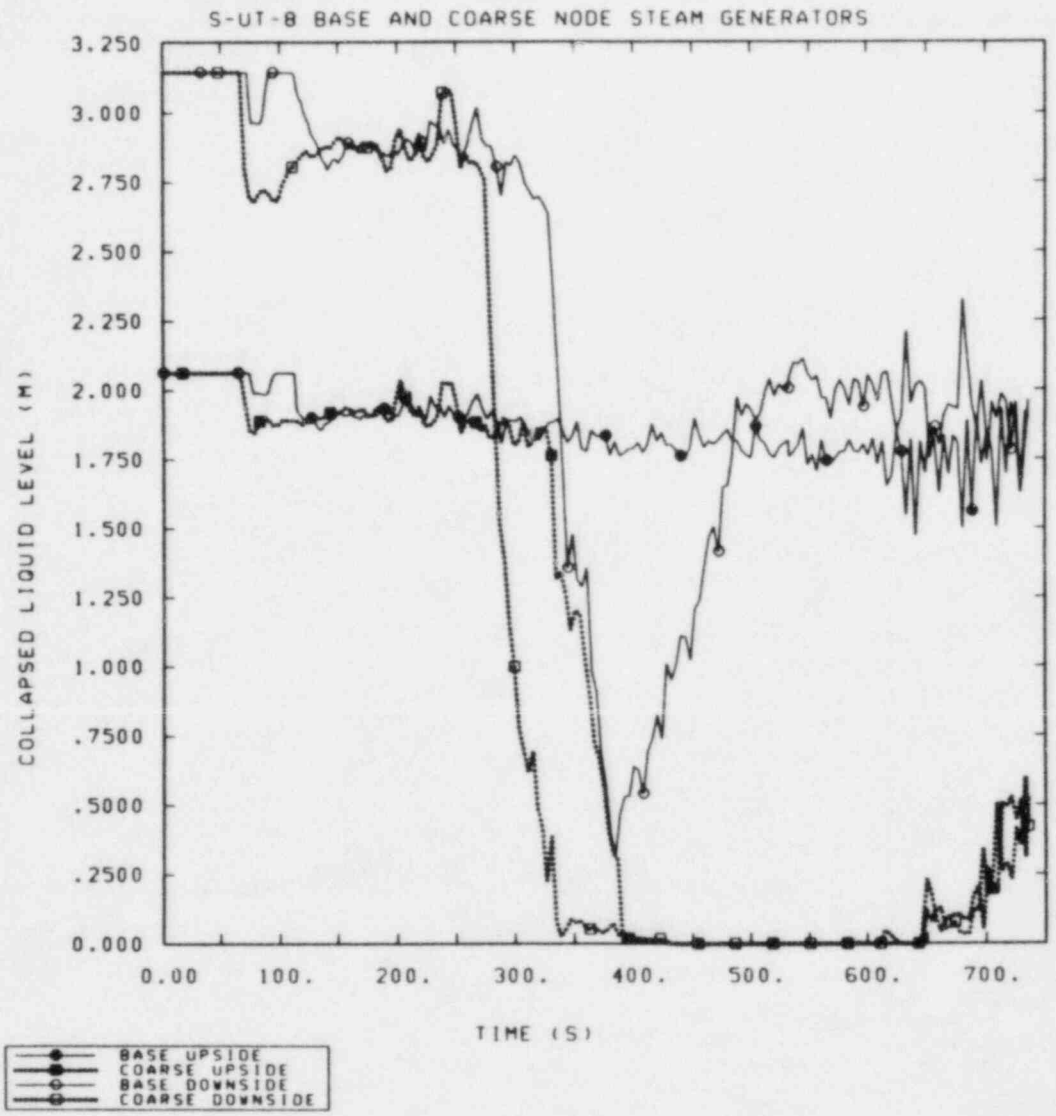

Figure AIII.10 Effect of Steam Generator Nodalization on the Broken Loop Pump Suction Collapsed Liquid Levels

APPENDIX IV RELAP5 UPDATES FOR CYCLE 18+

In June 1982, updates to bring RELAP5/MOD1 to the cycle 18 level were received from INEL. Also added to our version of cycle 18 were some other recommended updates from INEL. These additional updates are listed below by their identifier names for reference.

KERR015: This update adds a subroutine to check elevation changes around piping loops. The check is done during input processing.

DEBUG: Adds diagnostic printout during computation of junction properties.

DMKTIM: Adds mass error debug printout during computation of equation of state variables.

BRFIX: Attempts to fix a branching problem by multiplying viscous terms in momentum equation by the square of the ratio of the junction area to the volume flow area.

Also included in INEL's June 1982 recommended updates was a new interfacial drag model (identifier HXCRXXX). That update was not implemented in our version of RELAP5/MOD1/CYCLE 18.

DISTRIBUTION:

Division of Technical Information
and Document Control
NRC Distribution Contractor
U. S. Nuclear Regulatory Commission
15700 Crabbs Branch Way
Rockville, MD 20850
300 copies for R4

U. S. Nuclear Regulatory Commission (4)
Reactor Systems Research Branch
Division of Accident Evaluation
Office of Nuclear Regulatory Research
7915 Eastern Avenue
Silver Spring, MD 20910
Attn: Louis M. Shotkin
Fuat Odar
R. Lee
H. S. Tovmassian

EG&G Idaho (6)
Idaho National Engineering Laboratory
P. O. Box 1625
Idaho Falls, ID 83415
Attn: T. R. Charlton
G. W. Johnsen
Edna Johnson
L. Feinauer
V. H. Ransom
R. J. Wagner

Thad D. Knight
Dennis R. Liles
Los Alamos National Laboratory (2)
K553 Q-9
Los Alamos, NM 87545

P. Saha, 130
Department of Nuclear Energy
Brookhaven National Laboratory
Associated Universities, Inc.
Upton, New York 11973

N. H. Shah
Babcock & Wilcox Co. (NPGD)
P. O. Box 1260
Lynchburg, VA 24505

Jesse Fell (5)
Deputy Director, Water Reactor Programs
Atomic Energy Establishment
Winfrith
Dorchester, Dorset DT28DH
ENGLAND

6400 A. W. Snyder
6410 J. W. Hickman
6411 A. C. Peterson
6417 D. C. Carlson
6420 J. V. Walker
6421 T. R. Schmidt
6422 D. A. Powers
6423 P. S. Pickard
6425 W. J. Camp
6427 M. Berman
6440 D. A. Dahlgren
6442 W. A. von Riesemann
6444 D. A. Dahlgren, Actg (17)
6444 L. D. Buxton
6444 R. K. Byers
6444 R. K. Cole, Jr.
6444 P. N. Demmie
6444 D. Dobranich
6444 M. G. Elrick
6444 L. N. Kmetyk
6444 R. Knight
6444 J. M. McGlaun
6444 J. Orman
6444 W. H. Schmidt
6444 R. M. Summers
6444 S. W. Webb
6449 K. D. Bergeron
3141 C. M. Ostrander (5)
3151 W. L. Garner
8024 M. A. Pound

NRC FORM 335 (2-84) NRCM 1102, 3201, 3202

U.S. NUCLEAR REGULATORY COMMISSION

BIBLIOGRAPHIC DATA SHEET

SEE INSTRUCTIONS ON THE REVERSE

1 REPORT NUMBER (Assigned by TIDC, add Vol. No., if any)

NUREG/CR-3772
SAND84-0884

2 TITLE AND SUBTITLE

RELAP5 Assessment: Semiscale S-UT Series Tests S-UT-1, S-UT-2, S-UT-6, S-UT-7 and S-UT-8

3 LEAVE BLANK

4 DATE REPORT COMPLETED

MONTH: November YEAR: 1984

5 AUTHOR(S)

A. C. Peterson

6 DATE REPORT ISSUED

MONTH: November YEAR: 1984

7 PERFORMING ORGANIZATION NAME AND MAILING ADDRESS (Include Zip Code)

Division 6444
Sandia National Laboratories
P. O. Box 5800
Albuquerque, NM 87185

8 PROJECT/TASK/WORK UNIT NUMBER

9 FIN OR GRANT NUMBER

FIN Nos. A-1205 & A-1374

10 SPONSORING ORGANIZATION NAME AND MAILING ADDRESS (Include Zip Code)

Reactor Systems Research Branch
Division of Accident Evaluation
Office of Nuclear Regulatory Research
U. S. Nuclear Regulatory Commission
Washington, DC 20555

11a TYPE OF REPORT

Technical

b PERIOD COVERED (Inclusive dates)

12 SUPPLEMENTARY NOTES

13 ABSTRACT (200 words or less)

The RELAP5 independent assessment project at Sandia National Laboratories in Albuquerque (SNLA) is part of an overall effort funded by the NRC to evaluate the capability of various system codes to calculate the detailed thermal/hydraulic response of LWRs during accident and off-normal conditions. The RELAP5 computer code is being assessed at SNLA against test data from various integral and separate effects test facilities. As part of the assessment effort, several small break tests with and without upper head injection (UHI) of emergency core coolant (ECC), performed in the Semiscale Mod-2A facility, have been analyzed.

The results show that RELAP5/MOD1 is capable of calculating some aspects of the important phenomena during small breaks both with and without UHI. The times for the system to depressurize to the UHI and/or loop accumulator flow initiation were calculated satisfactorily. The correct trends of the effects of break size and of UHI on the system pressure response were also calculated. The injection rate from the UHI and loop accumulators was not always calculated correctly; the flows cycled on and off because large flow surges caused the accumulator pressures to temporarily decrease below the system pressure. This cycling of the flow had a significant effect on the system response during UHI accumulator flow. When the upper head was liquid-filled from UHI flow, a core liquid level depression was calculated, but not measured, that resulted in a dryout of the core. During UHI flow the calculated densities in the upper plenum and near the top of the core were too high, which also affected the vessel mass distribution. The calculated break flow rates were too large, when the break uncovered later in the transients, contributing to a low liquid level in the vessel and late-time core heatup. Higher late-time core temperatures were calculated than measured both with and without UHI.

Some of the differences between the calculated and measured results can be attributed to uncertainties in the boundary conditions (i.e., break mass flow rate, pump curves, environmental heat losses, bypass flow rate); these uncertainties are large and can significantly affect the results. Since there are also uncertainties in the facility configuration for the S-UT series of tests that are still being addressed, any results for this test series should be considered preliminary until the actual conditions are finally established.

14 DOCUMENT ANALYSIS - a KEYWORDS/DESCRIPTORS

b IDENTIFIERS/OPEN ENDED TERMS

15 AVAILABILITY STATEMENT

16 SECURITY CLASSIFICATION

(This page) Uncl

(This report) Uncl

17 NUMBER OF PAGES

210

18 PRICE

*U.S. GOVERNMENT PRINTING OFFICE: 1984-0-576-035/4403

120555078877 1 1AN1R4
US NRC
ADM-DIV OF TIDC
POLICY & PUB MGT BR-PDR NUREG
W-501
WASHINGTON DC 20555